Kinetics of Methylcyclohexane Dehydrogenation and Reactor Simulation for "On-board" Hydrogen Storage

A thesis submitted to The University of Manchester for the degree of
Doctor of Philosophy
in the Faculty of Engineering and Physical Sciences

2010

by

Muhammad Rashid Usman

under the supervision of

Dr. David L. Cresswell
Dr. Arthur A. Garforth

School of Chemical Engineering and Analytical Science

Table of Contents

List of Tables

List of Figures

Abstract

Today's transportation system is contributing to increasing air pollution and lack of future fuel for a growing number of vehicles. Over the years, many alternate solutions have been proposed to replace or to assist conventional fuels in order to alleviate the environmental damage and future fuel shortage. One such solution is to use hydrogen gas as fuel in an internal combustion engine or a fuel cell. Hydrogen being light, flammable and having very low critical temperature has associated problems of storage, transportation and utilisation. The methylcyclohexane-toluene-hydrogen (MTH)-system is a safe and economical way of storage and "on-board" hydrogen generation. The dehydrogenation reaction of MCH is highly endothermic and suffers from equilibrium limitations. Therefore, success of the MTH-system for "on-board" applications lies in the development of a highly active, selective and stable catalyst as well as a reactor supplying high rates of heat transfer to the catalytic bed. A review of the literature has shown that there is a huge disagreement in describing the kinetic mechanism of the dehydrogenation reaction of MCH. There is no consensus on the rate-determining step and the inhibition offered by the products. Moreover, there is no detailed kinetic investigation over a wide range of operating conditions including experiments without H_2 in the feed and under integral conditions.

The present study is designed to conduct a detailed kinetic investigation over a wide range of operating conditions including experiments without hydrogen in the feed for the most promising catalyst developed to date. The reaction kinetics are incorporated into a two-dimensional pseudo-homogeneous model to predict observed longitudinal temperature profiles. Alternative configurations and schemes for "on-board" hydrogen generation based on the MTH-system are compared and a prototype reactor, suitable for "on-board" hydrogen generation, is designed and simulated in detail, exchanging heat with the engine exhaust gas.

Kinetic experiments were performed in a laboratory fixed bed tubular reactor under integral conditions. A 1.0 wt% Pt/Al_2O_3 catalyst was prepared and a wide range of experimental conditions were studied. A number of kinetic models were applied based on the power law, Langmuir-Hinshelwood-Hougen-Watson (LHHW) and Horiuti-Polanyi (HP) mechanisms. A kinetic model based on LHHW single-site mechanism with loss of the first H_2 molecule the rate rate-controlling step was found to best fit the data.

Analyses of the products show that the dehydrogenation of MCH is very selective towards toluene. As well as the main product toluene, a number of condensable by-products were also identified. Benzene, cyclohexane and ring-closed products (ethylcyclopentane and dimethylcyclopentanes) are the major by-products.

Laboratory experimental data for the 12 experimental runs made under varying conditions of pressure, space velocity and feed composition were simulated and good agreement between predicted and observed centreline temperatures was found.

A hybrid MTH-gasoline-system is a viable option. Using titanium aluminide as the material of construction, the dynamic (start up) time requirement for the prototype reactor may be halved over that required for a stainless steel construction.

Declaration

No portion of the work referred to in the thesis has been submitted in support of an application for another degree or qualification of this or any other university or other institute of learning.

Copyright Statement

i. The author of this thesis (including any appendices and/or schedules to this thesis) owns certain copyright or related rights in it (the "Copyright") and he has given The University of Manchester certain rights to use such Copyright, including for administrative purposes.

ii. Copies of this thesis, either in full or in extracts and whether in hard or electronic copy, may be made **only** in accordance with the Copyright, Designs and Patents Act 1988 (as amended) and regulations issued under it or, where appropriate, in accordance with licensing agreements which the University has from time to time. This page must form part of any such copies made.

iii. The ownership of certain Copyright, patents, designs, trade marks and other intellectual property (the "Intellectual Property") and any reproductions of copyright works in the thesis, for example graphs and tables ("Reproductions"), which may be described in this thesis, may not be owned by the author and may be owned by third parties. Such Intellectual Property and Reproductions cannot and must not be made available for use without the prior written permission of the owner(s) of the relevant Intellectual Property and/or Reproductions.

iv. Further information on the conditions under which disclosure, publication and commercialisation of this thesis, the Copyright and any Intellectual Property and/or Reproductions described in it may take place is available in the University IP Policy (see http://www.campus.manchester.ac.uk/medialibrary/policies/intellectualproperty-.pdf), in any relevant Thesis restriction declarations deposited in the University Library, The University Library's regulations (see http://www.manchester.ac.uk-/library/aboutus/regulations) and in The University's policy on presentation of Theses.

To my parents
Muhammad Karamat Ullah and Amtullah
To my brothers and only sister
Shahid, Zahid, Aamer, Faisal and Chanda

Acknowledgements

List of Abbreviations

AES	Augur electron spectroscopy
BET	Brunauer-Emmett-Teller
BZN	Benzene
cw	Cooling water
CHN	Cyclohexane
C.I.	Confidence interval
COSHH	Control of substances hazardous to health
CSTR	Continuous stirred tank reactor
DFT	Density functional theory
ECP	Ethylcyclopentane
ECPe	Ethylcyclopentene
DMBPh	Dimethylbiphenyl
DMCP	Dimethylcyclopentane
DMCPe	Dimethylcyclopentene
DOE	Department of energy
DS	Dual-site
FID	Flame ionisation detector
FTMS	Fourier transform mass spectrometry
GC	Gas chromatograph or Gas chromatography
GC-MS	Gas chromatograph-mass spectrometer or Gas chromatography-mass spectrometry
GPSA	Gas processers suppliers association
HP	Horiuti-Polanyi
HPLC	High performance liquid chromatograph
HSC	High surface coverage
HTN	Heptane
IC	Internal combustion
I.D.	Internal diameter
IEP	Isoelectric point
LEED	Low-energy electron diffraction
LHHW	Langmuir-Hinshelwood-Hougen-Watson
LHSV	Liquid hourly space velocity
LITD	Laser-induced thermal desorption
MCH	Methylcyclohexane
MCHde	Methylcyclohexadiene
MCHe	Methylcyclohexene
MHN	methylhexane
ML	Monolayer
MoC	Material of construction
MPR	Micropulse reactor

MTH	Methylcyclohexane-toluene-hydrogen
NCV	Net calorific value
NIOSH	National institute of occupational safety and health
O.D.	Outer diameter
PDE	Partial differential equation
PDNC	Partially dehydrogenated naphthenic compounds
PFD	Process flow diagram
Ph.D.	Doctor of philosophy
PR	Peng-Robinson
QMS	Quadruple mass spectrometry
RCP	Ring-closed product
RDS	Rate-determining step
Ri	*ith* experimental Run
RON	Research octane number
SET	Series of experimental targets
SI	Spark ignition
SOFC	Solid oxide fuel cell
SS	Single-site
SS	Stainless steel
TDS	Thermal desorption mass spectroscopy
Tol	Toluene
TLV	Threshold limit value
TWA	Time weighted average
UOP	Universal oil products
wt	Weight
XLN	Xylene
XPS	X-ray photoelectron spectroscopy
ZPC	Zero point of charge

Nomenclature

a_0 initial activity of catalyst

A_b surface area of the bare surface (between the fins), m^2

A_e effective external heat transfer area of the finned surface, m^2

A_f surface area of the fins, m^2

A_T total surface area, m^2

B dimensionless activation energy

Bi_b Biot number defined for inner wall of the reactor tube defined in Eq. 6.34

B_{Cr} dimensionless heat of adsorption for K_{Cr} defined at T_r

Bi_h Biot number for heat transfer

B' dimensionless heat of adsorption for lumped equilibrium constant defined in Eq. 4.21

c exponent in Eq. 2.20 and Eq. 4.25

c_p constant pressure specific heat capacity of a gas at, $J \cdot kg^{-1} \cdot K^{-1}$

$(c_{p,A})_L$ constant pressure specific heat capacity of liquid MCH, $J \cdot kg^{-1} \cdot K^{-1}$

$c_{p,A}$ constant pressure specific heat capacity of gaseous MCH, $J \cdot kg^{-1} \cdot K^{-1}$

$c_{p,B}$ constant pressure specific heat capacity of gaseous toluene, $J \cdot kg^{-1} \cdot K^{-1}$

$c_{p,C}$ constant pressure specific heat capacity of gaseous hydrogen, $J \cdot kg^{-1} \cdot K^{-1}$

$c_{p,eg}$ constant pressure specific heat capacity of exhaust gas, $J \cdot kg^{-1} \cdot K^{-1}$

$c_{p,I}$ constant pressure specific heat capacity of gaseous inert, $J \cdot kg^{-1} \cdot K^{-1}$

$c_{p,lr}$ constant pressure specific heat capacity of the "lumped reactor", $J \cdot kg^{-1} \cdot K^{-1}$

C_A concentration of MCH, mol/m^3

C_{A0} initial concentration of MCH, mol/m^3

$C_{A \cdot s}$ concentration of adsorbed MCH, mol/kg-cat

$C_{A,s}$ concentration of MCH at catalyst surface, mol/kg-cat

$C_{B \cdot s}$ concentration of adsorbed toluene, mol/kg-cat

$C_{C \cdot s}$ concentration of adsorbed hydrogen, mol/kg-cat

$C_{D \cdot s}$ concentration of adsorbed MCHe, mol/kg-cat

$C_{E \cdot s}$ concentration of adsorbed MCHde, mol/kg-cat

C_s concentration of empty active sites, mol/kg-cat

C_T total concentration of active sites, mol/kg-cat

d_p particle diameter, m

D_{AC} binary molecular diffusion coefficient of MCH in hydrogen, $\mathrm{m^2/s}$

D_e equivalent diameter, m

D_{eff} effective mass diffusivity for catalyst particle defined in Eq. H.3, $\mathrm{m^2/s}$

D_i inside diameter of the reactor tube, m

D_{is} inside diameter of the shroud tube, m

$D_{K,eff}$ effective Knudsen diffusivity, $\mathrm{m^2/s}$

D_o outside diameter of the reactor tube, m

D_r effective radial mass diffusivity, $\mathrm{m^2/s}$

D_{tw} outside diameter of thermowell, m

e equilibrium approach factor

E activation energy, J/mol

F_A molar flowrate of MCH, mol/s

F_{A0} initial molar flowrate of MCH, mol/s

F_{HC0} initial molar flowrate of hydrocarbon (MCH or MCHe), mol/s

G superficial gas mass velocity, $\mathrm{kg \cdot m^{-2} \cdot s^{-1}}$

h_i inside surface heat transfer coefficient, $\mathrm{W \cdot m^{-2} \cdot K^{-1}}$

h_o outside surface heat transfer coefficient, $\mathrm{W \cdot m^{-2} \cdot K^{-1}}$

h_w wall heat transfer coefficient, $\mathrm{W \cdot m^{-2} \cdot K^{-1}}$

$\Delta h^\circ_{f,A}$	standard heat of formation of MCH, Table L.1, J/mol
$\Delta h^\circ_{f,B}$	standard heat of formation of toluene, Table L.1, J/mol
$\Delta h^\circ_{f,C}$	standard heat of formation of hydrogen, Table L.1, J/mol
$\Delta h^\circ_{f,i}$	standard heat of formation of *ith* species, J/mol
Δh°_{rxn}	standard heat of reaction, J/mol
$\Delta h_{v,A}$	latent heat of vaporisation of MCH, J/mol
$\Delta h'$	lumped heat of adsorption defined in Chapter 4, J/mol
H	rate of enthalpy flow, J/s
H_f	height of fin, m
ΔH	rate of change in enthalpy, J/s
j_H	*j*-factor for heat transfer
k	rate constant for the MCH dehydrogenation reaction
k_d	apparent short term deactivation constant, s^{-1}
k_{eg}	thermal conductivity of exhaust gas, $W{\cdot}m^{-1}{\cdot}K^{-1}$
k_f	thermal conductivity of fin material, $W{\cdot}m^{-1}{\cdot}K^{-1}$
k_g	thermal conductivity of a gas, $W{\cdot}m^{-1}{\cdot}K^{-1}$
$k_{g,i}$	thermal conductivity of *ith* gaseous species, $W{\cdot}m^{-1}{\cdot}K^{-1}$
k_i	rate constant for *ith* step
k_{-i}	rate constant for reversible *ith* step
k_r	rate constant at the reference temperature
k_r	effective radial thermal conductivity, $W{\cdot}m^{-1}{\cdot}K^{-1}$ (Chapters 6 and 7)
k_r^o	stagnant radial thermal conductivity, $W{\cdot}m^{-1}{\cdot}K^{-1}$
k_s	thermal conductivity of a porous catalyst, $W{\cdot}m^{-1}{\cdot}K^{-1}$
k_s'	thermal conductivity of the microspheres of a porous catalyst, $W{\cdot}m^{-1}{\cdot}K^{-1}$
k_w	wall thermal conductivity, $W{\cdot}m^{-1}{\cdot}K^{-1}$
k_0	frequency factor in Arrhenius equation

K	equilibrium constant of MCH dehydrogenation reaction, Pa^3
K_A	adsorption equilibrium constant of methylcyclohexane, Pa^{-1}
K_B	adsorption equilibrium constant of toluene, Pa^{-1}
K_B'	ratio of K_B to K_A defined in Eq. 4.24
K_C	adsorption equilibrium constant of hydrogen, Pa^{-1}
K_{Cr}	adsorption equilibrium constant of hydrogen at T_r, Pa^{-1}
K_C^*	adsorption equilibrium constant of hydrogen adsorbed on $s*$ site, Pa^{-1}
K_{Cr}^*	constant in Eq. 4.26, Pa^{-3}
K_D	surface equilibrium constant of methylcyclohexene, Pa^{-1}
K_E	surface equilibrium constant of methylcyclohexadiene, Pa^{-1}
K_H	adsorption equilibrium constant of n-heptane, Pa^{-1}
K_i	surface equilibrium constant of ith step in a reaction sequence, Pa^{-1}
K_r'	lumped adsorption equilibrium constant defined at T_r
K'	lumped equilibrium constant
K''	lumped equilibrium constant
K'''	lumped equilibrium constant
L	length of the reactor tube, m
L_b	length of catalyst bed, m
L_f	length of fin, m
m	number of parameters
m	horizontal position in finite grid, m
m	parameter in Eq. 7.10
m_{lr}	total mass of the "lumped reactor", kg
$\dot{m}_A$	mass flowrate of MCH, kg/s
$\dot{m}_{eg}$	mass flowrate of exhaust gas, kg/s
$\dot{m}_P$	mass flowrate of the reaction products leaving the "lumped reactor", kg/s
M	dimensionless quantity defined in Eq. 7.6

M	dimensionless number defined in Eq. K.12
M_{ave}	average molecular weight, kg/mol
M_A	molecular weight of MCH, kg/mol
M_B	molecular weight of toluene, kg/mol
M_C	molecular weight of hydrogen, kg/mol
M_F	molecular weight of the feed, kg/mol
M_i	molecular weight of *ith* species, kg/mol
M_I	molecular weight of inert, kg/mol
M_j	molecular weight of *jth* species, kg/mol
M'	dimensionless number defined in Eq. K.17
Ma	Mach number
n	order of the reaction
n	axial position in finite grid, m
N	number of data points
N_A	number of moles of MCH, mol
N_f	number of fins
N_t	number of tubes
Nu	Nusselt number
p	pressure, Pa
p_A	partial pressure of methylcyclohexane, Pa
p_B	partial pressure of toluene, Pa
p_C	partial pressure of hydrogen, Pa
p_H	partial pressure of n-heptane, Pa
P	dimensionless number defined in Eq. K.13
$Pe_{r,h}$	radial heat transfer Peclet number
$Pe_{r,m}$	radial mass transfer Peclet number
Pr	Prandtl number
Q	rate of heat transfer, J/s

Q	dimensionless number defined in Eq. K.18
Q_{max}	maximum rate of heat transfer, J/s
Q_T	total heat transfer rate, J/s
r	position in radial direction, m
$(-r)$	rate of the dehydrogenation reaction, mol·kg^{-1}·s^{-1}
$(-r)_0$	initial rate of the dehydrogenation reaction, mol·kg^{-1}·s^{-1}
(r_B)	rate of production of toluene, mol·kg^{-1}·s^{-1}
$(r_B)_0$	initial rate of production of toluene, mol·kg^{-1}·s^{-1}
Δr	thickness of differential element taken in catalyst bed (Fig. K.1), m
R	universal gas constant, J·mol^{-1}·K^{-1}
R_i	inside radius of the reactor tube, m
R_o	outside radius of the reactor tube or the long rod, m
R_{si}	inside radius of the shroud tube (outer tube), m
Re	Reynolds number
Re_p	particle Reynolds number
s	active or empty site
$s*$	hydrogen only active or empty site
S_g	surface area of catalyst, m^2/kg
t	time, s
t_d	online reaction deactivation time, s
T	temperature, K
T_{ave}	local average temperature defined in Section 4.2.4, K
$T_{A,in}$	temperature of methylcyclohexane entering into the "lumped reactor", K
T_b	temperature of catalyst bed, K
T_{calc}	calculated temperature, K
T_{eg}	exhaust gas temperature, K
$T_{eg,in}$	temperature of the exhaust gas entering into the "lumped reactor", K

$T_{eg,o}$	temperature of the exhaust gas leaving the "lumped reactor", K
$T_{m,n}$	temperature defined at the position m and n in the finite grid (Fig. K.2), K
T_o	temperature of the reaction products leaving the lumped reactor, K
T_{obs}	observed or measured temperature, K
T_r	reference temperature, K
$T_{r=Ri}$	temperature at the inner surface of the reactor tube, K
$T_{sl,A}$	temperature of saturated liquid MCH, K
$T_{sv,A}$	temperature of saturated vapour MCH, K
T_w	reactor wall temperature, K
T_{w0}	temperature of the outside surface of the reactor tube, K
T_z	temperature at any position in the axial direction, K
T_0	initial or inlet temperature, K
$T_{0,0}$	temperature at inlet and centre of the finite grid (Fig. K.2), K
T_∞	surrounding temperature, K
T^*	dimensionless temperature defined in Eq. 6.32
u'	superficial velocity, m/s
U_i	overall heat transfer coefficient based on inside wall surface, $\text{W·m}^{-2}\text{·K}^{-1}$
U_{lr}	overall heat transfer coefficient for the "lumped reactor", $\text{W·m}^{-2}\text{·K}^{-1}$
v_P	pore volume of material, m^3/kg
V_c	volume of catalyst, m^3
W	weight of catalyst, kg
W_f	width of fin, m
W_{fr}	width of fin root, m
x	position along the height of the fin, m
Δx	height of an element taken in fin's body (Fig. M.2), m
X	conversion (fractional conversion) of MCH
X_{mod}	model or calculated conversion of MCH

X_{obs}	observed or measured conversion of MCH
y_A	mole fraction of MCH in the vapour phase
y_{A0}	initial mole fraction of MCH in the vapour phase
y_B	mole fraction of toluene in the vapour phase
y_{B0}	initial mole fraction of toluene in the vapour phase
y_C	mole fraction of hydrogen in the vapour phase
y_{C0}	initial mole fraction of hydrogen in the vapour phase
y_i	mole fraction of ith component in the vapour phase
y_{i0}	mole fraction of ith component in the vapour phase
y_I	mole fraction of inert in the vapour phase
y_{I0}	initial mole fraction of inert in the vapour phase
y_j	mole fraction of jth component in the vapour phase
Y_{BZN}	yield of benzene, mol/100 mol of MCH fed
Y_{CHN}	yield of cyclohexane, mol/100 mol of MCH fed
Y_{MCHes}	yield of methylcyclohexenes, mol/100 mol of MCH fed
Y_{RCPs}	yield of ring closed products, mol/100 mol of MCH fed
Y_{Tol}	yield of toluene, mol/100 mol of MCH fed
Y_{XLNs}	yield of xylenes, mol/100 mol of MCH fed
z	position in axial direction, m
Δz	height of differential element taken in a catalyst bed (Fig. K.1), m
α	thermal diffusivity, m^2/s
β	parameter in Kunii-Smith formula (Eq. 6.17) defined in Eq. 6.19
β	heat generation factor defined in Eq. H.5
β'	parameter used in equation Eq. 6.26 and defined in Eq. 6.27
γ	parameter in Kunii-Smith formula (Eq. 6.17) defined in Eq. 6.20
ε_b	fractional voidage of a catalyst bed
ε_A	characteristic energy of MCH molecules, J

ε_C	characteristic energy of hydrogen molecules, J
ε_{AC}	combined characteristic energy of MCH-hydrogen molecules, J
η	effectiveness factor
η_f	fin efficiency
$\theta_{o,1}$	angle corresponding to boundary of heat flow area for one contact point for most open packing, rad
$\theta_{o,2}$	angle corresponding to boundary of heat flow area for one contact point for closest packing, rad
κ	ratio of k_s to k_g
μ	viscosity of a gas, Pa.s
μ_i	viscosity of *ith* species, Pa.s
μ_j	viscosity of *jth* species, Pa.s
μ_w	viscosity of a gas at wall temperature, Pa.s
ρ	density of a gas, kg/m^3
ρ_b	density of catalyst bed, kg/m^3
ρ_p	particle density of a material, kg/m^3
ρ_s	skeletal density of a material, kg/m^3
σ	one of the Lennard-Jones parameters, Table 6.3, collision diameter, m
σ_A	collision diameter for MCH, m
σ_C	collision diameter for hydrogen, m
σ_{AC}	combined collision diameter of MCH and hydrogen defined in Eq. 6.30, m
τ_m	modified tortuosity factor
ϕ	parameter in Kunii-Smith formula (Eq. 6.17) defined in Eq. 6.18
ϕ_{ij}	factor in Wilke's equation, Eq. L.11, defined in Eq. L.12
ϕ_1	ϕ-value corresponding to loose or most open packing defined in Eq. 6.21
ϕ_2	ϕ-value corresponding to closest packing defined in Eq. 6.22

ϕ' volume fraction of the dispersed microspheres in catalyst particles defined in Eq. 6.28

Φ_s modified Thiele modulus, defined in Eq. H.1

$\Omega_{D,AC}$ collision integral for diffusivity of MCH in H_2

$\dfrac{K}{\varepsilon}$ one of the Lennard-Jones parameters, Table 6.3, K^{-1}

$\dfrac{K}{\varepsilon_{AC}}$ one of the combined Lennard-Jones parameters, Eq. 6.32, K^{-1}

Chapter 1
Introduction

1.1 Introduction to the hydrogen economy

Today's transportation system is contributing to increasing air pollution and lack of future fuel for our growing number of vehicles. Over the years, many alternate solutions have been proposed to replace or to assist the conventional fuels in order to alleviate the environmental damage and future fuel shortage. One such solution is to use hydrogen gas as fuel in an internal combustion (IC) engine or a fuel cell. Hydrogen as a fuel is considered not only sustainable but benign to the environment. Hydrogen is a very clean fuel. When burnt in a fuel cell or an IC engine it produces nothing other than water and 242 kJ/mol of net heat energy at 25 °C. A hydrogen based transportation system then has potential to be more sustainable and less polluting to the environment than the current fossil fuel system. However, hydrogen is not freely available, it is available in forms chemically bound to other elements, especially oxygen in the form of water. So unlike fossil fuels, hydrogen is not a fuel but, like electricity, it is a carrier of energy [Hoffmann, 2001; Keith and Farrell, 2003; Shinnar, 2003]. To use hydrogen as an energy source requires some methodology for its generation. Also extremely light and gaseous in nature and with extremely low critical temperature (the temperature above which a gas cannot be liquefied), −240 °C [Lide, 2007], hydrogen presents challenging problems of storage and transportation. A sustainable hydrogen economy is thus dependent entirely upon successful and economical production, storage and transportation of hydrogen and its appropriate utilisation to produce the required power.

1.1.1 Production of hydrogen

To generate hydrogen from its combined form, some kind of physical, chemical or biological process is required. It is important to note that none of these production processes is 100 percent environmentally friendly [Ragwitz et al., 2003]. The following are the principal hydrogen production methods that may be employed:

- Steam reforming of natural gas (methane)
- Partial oxidation of heavy hydrocarbons
- Coal gasification
- Biomass gasification
- Bio-inspired processes
- Splitting the water molecule
    - Electrochemical (Electrolysis)
    - Photochemical
    - Thermochemical

Steam reforming of methane is a well established method and it is currently carried out all around the world to produce the synthesis gas for the production of methanol, liquid fuels (Fischer-Tropsch) and ammonia leading to urea, a fertiliser. The advantages of using steam reforming is that it is cheaper and well developed commercial process and most of the world's hydrogen comes from this process [Turner, 2004], but the real essence of the hydrogen economy is not fulfilled here. We are not by-passing the use of fossil fuels and also we are not free of carbon dioxide and carbon monoxide production. Partial oxidation of hydrocarbons and gasification processes are also accompanied with the release of oxides of carbon. Crops that are of low economic value can be transformed into hydrogen [Wald, 2004]. Also, scientists are thinking about developing bio-catalysts that work in algae and other micro-organisms producing hydrogen most efficiently at room temperatures [Crabtree et al., 2004]. These bio-inspired processes look promising but the technology is far from being commercialised [Wald, 2004]. Splitting water into

hydrogen and oxygen is probably the best way of producing hydrogen. However, the splitting of the water molecule requires much energy (286 kJ/mol at 25 °C) which has to be provided from another primary energy source. There are three ways, namely electrochemical, photochemical and thermochemical [Steinfeld and Meier, 2004] that the water molecule can be split into hydrogen and oxygen. The electrochemical method is a well developed process in which some primary energy such as solar or wind is first converted into electricity and then this electricity is utilised in the electrolysis of water. In a photochemical process, however, hydrogen is directly produced from absorption of sun light without first converting the energy into electricity. Thermochemical cycles utilise a heat source from solar collectors or nuclear reactors [Crabtree et al., 2004] and generate hydrogen gas in a series of chemical reactions taking place at temperatures much less than the temperatures required for direct thermal decomposition of the water molecule (thermolysis) [Sherif et al., 2005]. Sulphur-iodine and calcium-bromine-iron cycles are some of the examples. Solar radiation, nuclear energy, tidal-power, wind energy and geothermal energy, when utilised and combined efficiently, can really economise and fulfil the spirit of the hydrogen economy. The combination is entirely sustainable and generous for the environment and humans themselves.

1.1.2 Hydrogen storage and transportation

The efficient storage of hydrogen is probably the greatest hurdle to the success of the hydrogen economy. Hydrogen, being the lightest element and highly inflammable with extremely low critical temperature, renders difficult its safe and economic storage especially for "on-board" applications. It has the highest energy per unit mass, NCV (net calorific value), for any fuel [Pant and Gupta, 2009] i.e. 119.3 kJ/g at 1 bar and 25 °C [Hsiung, 2001] which is about three times the gasoline energy content. However, its volumetric energy density (NCV) is quite low, which is, only 10.1 kJ/L at 1 bar and 15 °C [Hsiung, 2001] (see Table 1.1 for comparison of energy values with gasoline and MCH). Such properties of hydrogen offer a great challenge

to its storage in a confined space especially in mobile applications where volume is largely an issue.

Table 1.1 Comparative properties of MCH, toluene, typical gasoline and molecular hydrogen [Lide, 2007; DOE, 2009; GPSA, 1997; Sonntag et al., 2003; NIOSH, 2009; Hsiung, 2001; Dancuart et al., 2004]

Property	Units	MCH	Toluene	Gasoline	Hydrogen
Chemical formula	–	(C_7H_{14})	(C_7H_8)	$(C_4–C_{12})$	(H_2)
Carbon (C)	wt%	85.63	91.25	85–88	0
Hydrogen (H)		14.37	8.75	12–15	100
Molecular weight	$kg \cdot kmol^{-1}$	98.19	92.14	100–105	2.016
Physical state at room conditions	–	liquid	liquid	liquid	gas
Density at 20 °C	$kg \cdot m^{-3}$	769.4	866.8	720–780*	0.084§
Boiling point at 1 bar	°C	100.93	110.63	27–225	−252.76
Melting point at 1 bar	°C	−126.60	−94.95	−40	−259.34
Lower heating value	$kJ \cdot kg^{-1}$	43357	40921	43440	119.93%
Upper heating value	$kJ \cdot kg^{-1}$	46525	42450	46529	141.86%
Latent heat of vaporisation at 25 °C	$kJ \cdot kg^{-1}$	360.12	412.52	~348.9*	441.99
Specific heat	$kJ \cdot kg^{-1} \cdot °C^{-1}$	1.88	1.71	2.01	14.29
Flash point (closed cup)	°C	−4.0	4.0	−42.8	<−253
Auto ignition temperature	°C	250	480	257.2	585
Flammability range in air	vol%	1.2–6.7	1.1–7.1	1.4–7.6	4.0–75
Octane rating	RON	75	120	88–98	130+ (lean burn)
Viscosity at 25°C	mPa·s (cP)	0.679	0.56	0.38–0.45	0.009‡
Stoichiometric air-fuel ratio	wt%/wt%	14.75	13.47	14.7	68.98
CO_2 emissions	$kg \cdot L^{-1}$	2.41	2.90	2.34–2.42	0
Threshold limit value (TWA)	ppm	400	100	300	–

* at 15.5 °C
§ at 1 bar under ideal conditions
‡ at 27 °C

The following is a list of the methods by which hydrogen can be stored:

- Compressed gaseous hydrogen
- Liquid hydrogen in tanks
- Physically adsorbed hydrogen
- Metal hydride method
- Complex hydride method
- Organic hydride method

Hydrogen can be compressed and stored in high pressure cylinders at 200 to 700 bar [Züttel, 2004]. Even at 700 bar pressure the volumetric energy density of hydrogen is around 7 times less than that of gasoline. Moreover, at high pressure, a heavier storage cylinder is required which will affect the overall gravimetric energy density of hydrogen [Züttel, 2004]. As mentioned earlier the critical temperature of hydrogen is −240 °C, there is thus a lot of energy required to liquefy hydrogen below that temperature. The energy density of liquid hydrogen is just twice as high as gaseous hydrogen at 700 bar. It is important to note that liquid hydrogen can only be stored in an open system [Züttel, 2004] and a relatively open area is required for vehicles to park so that the leakage can safely diffuse into the atmosphere. Hydrogen can also be stored by physically adsorbing (physisorption) the hydrogen on some solid materials such as carbon. Hydrogen in the form of metal hydrides and metal complexes provides another means of storage. These hydrides are formed by the absorption of hydrogen in metals and alloys [Zhou, 2005]. The two hydrides are different in that the transition of metals occurs to ionic or covalent compounds for the complex hydrides [Zhou, 2005]. $LaNi_5H_6$ and $LiBH_4$ are the examples of metal and complex hydrides, respectively. Physisorption and metal hydrides are attributed to the low gravimetric hydrogen densities [Züttel, 2004]. Complex hydrides, with high gravimetric densities, raise issues of stability, sorption kinetics and reversibility [Züttel, 2004]. For transport purposes, where weight and dimensions of the vehicle are important and sufficient fuel is required for vehicles to travel significant distances in one charge [Crabtree et al., 2004], all of the above methods seem un-suitable and impractical. Moreover, unlike gasoline and diesel fuels, no infrastructure for fuel supply and its dispensation on the filling station is available for the above mentioned hydrogen storage techniques. Liquid organic hydrides, such as cyclohexane, methylcyclohexane and decalin are considered a more suitable source for "on-board" hydrogen generation, storage, transportation and utilisation. They contain sufficiently high hydrogen mass in their molecule and are stable, relatively less volatile and easy to transport. For detail, see Section 1.2 of this chapter. Keeping in view the potential advantages of the liquid organic hydride system, scientists are searching further for

molecules that have lower release temperatures and lower heat of the endothermic reaction (dehydrogenation) compared to cyclohexanes [Clot et al., 2007].

1.1.3 Hydrogen utilisation

Hydrogen can be utilised for power production in the following two ways:

- Using hydrogen in a fuel cell
- Using conventional combustion of the hydrogen gas in an IC engine

The combustion of hydrogen and oxygen (from air) in a fuel cell is considered twice as efficient as that of hydrogen combustion in an IC engine [Schlapbach and Züttel, 2001]. However, the fuel cell technology is not developed enough to produce the cells that are affordable and competitive in cost with the conventional technology of the IC engine. The internal combustion engine can work nearly 25% more efficiently when hydrogen is used as a fuel instead of gasoline [Crabtree et al., 2004]. Not only this, a blend of hydrogen and gasoline claims a better thermal efficiency of the engine and reduction in harmful pollutants. Comparing fuel cells and IC engines, for vehicle applications, at least for the interim period (from now until the fuel cells are fully commercialised) the use of hydrogen in an IC engine is considered the more practical and viable. It is taken up as a part of the hydrogen economy to be used for hydrogen end use in the present work.

1.2 The MTH-system

A complete system that includes hydrogen production, its storage and utilisation can be viewed in the so called MTH-system. The MTH-system stands for methylcyclohexane-toluene-hydrogen-system and operates on reversible dehydrogenation/hydrogenation of methylcyclohexane/toluene i.e. in the forward reaction (Eq. 1.1) MCH is dehydrogenated to toluene and hydrogen and toluene is hydrogenated back to MCH in the reverse reaction (Eq. 1.2). Fig. 1.1 shows the

concept and essential parts of the MTH-system. In the above paragraphs, cyclohexanes have been presented as one of the potential tools for hydrogen storage. Among the cyclohexanes, methylcyclohexane is preferred to cyclohexane since benzene is a carcinogen. Decalin, on the other hand, produces the solid product naphthalene, which may lead to handling difficulties. Table 1.2 depicts a brief comparison of the three hydrides.

Table 1.2 Comparison of the three potential organic hydrides

Organic hydride (*product*)	Reaction	H_2* (wt%)	Δh_{rxn}° ‡ (kJ/mol)	*VHED*** (kJ/L-hydride)	Comments
Cyclohexane (*Benzene*)	$C_6H_{12} \rightleftharpoons C_6H_6 + 3H_2$	7.2	+206.3	6670.3	Product benzene is a carcinogen and has very low TLV 0.1 ppm [NIOSH, 2009]
MCH (*Toluene*)	$C_7H_{14} \rightleftharpoons C_7H_8 + 3H_2$	6.2	+205.2	5684.1	—
Decalin (*Naphthalene*)	$C_{10}H_{18} \rightleftharpoons C_{10}H_8 + 5H_2$	7.3	+332.7	7572.1	Product naphthalene is a solid and is difficult to transport

* representing wt% H_2 produced during dehydrogenation not present per molecule.
** representing volumetric hydrogen energy density. Hydrogen is the hydrogen produced during dehydrogenation.
‡ calculated from heats of formation of gaseous species [Lide, 2007].

On inspection the MTH-system appears a complete cycle, but actually it is not. The hydrogen produced during the dehydrogenation of MCH (forward reaction, Eq. 1.1) disappears from the cycle as it is consumed during the generation of required power. Therefore, hydrogen for the hydrogenation of toluene (reverse reaction, Eq. 1.2) has to be provided from the external source such as the electrolysis of water (Eq. 1.3). For the description below, hydrogen is generated from electrolysis of water (assuming electrochemical decomposition of water is the cheapest practice in the future) using any sustainable and eco-friendly energy such as solar energy or wind energy. The selection of solar energy and wind energy is entirely based on their sustainability, amiability to the environment and their presence all around the world and especially in the author's country, Pakistan, in immeasurable amounts.

$$\text{Forward Reaction: } C_7H_{14} \longrightarrow C_7H_8 + 3\,H_2 \qquad\qquad (1.1)$$
$$\underset{MCH}{} \qquad\qquad \underset{Toluene}{}$$

$$\text{Reverse Reaction: } C_7H_8 + 3\,H_2 \longrightarrow C_7H_{14} \qquad\qquad (1.2)$$
$$\underset{Toluene}{} \qquad\qquad \underset{MCH}{}$$

Electrolysis of water: $2H_2O \xrightarrow{\text{Solar/Wind Energy}} 2H_2 + O_2$ (1.3)
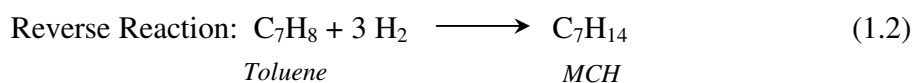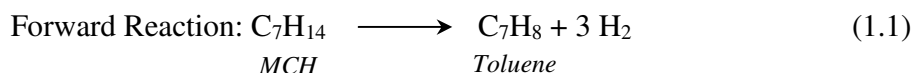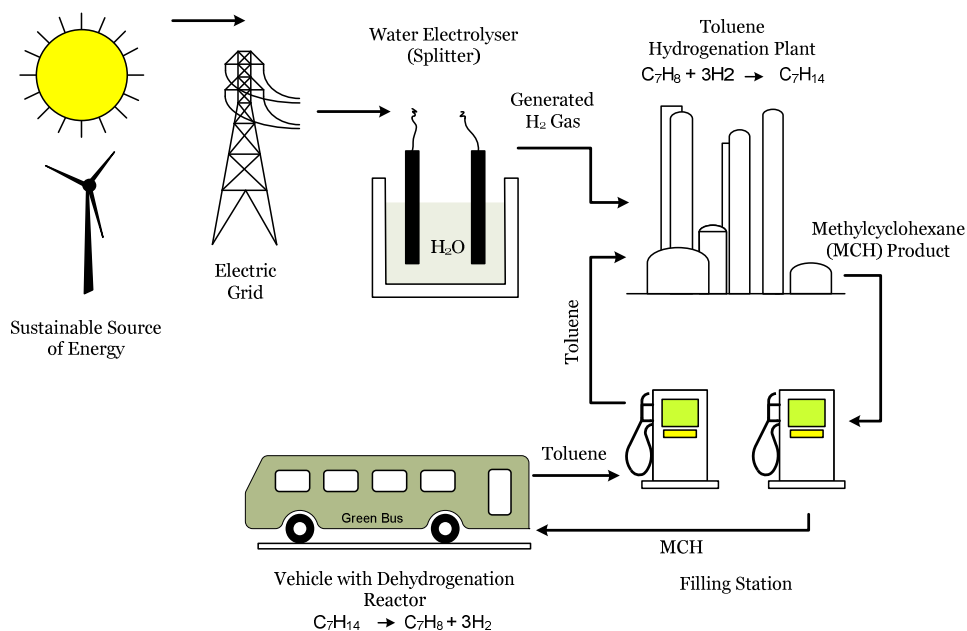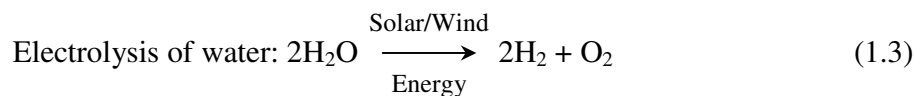
Fig. 1.1 Concept of MTH-system.

1.2.1 Components of MTH-system

The following are the principal steps that encompass a complete MTH-system:

- Production of hydrogen from the decomposition (electrolysis) of water using a sustainable and environmentally friendly energy source (solar or wind energy)
- Hydrogenation of aromatic toluene to produce methylcyclohexane (MCH)
- Transportation of MCH from hydrogenation plant to the existing fuel filling station for loading MCH onto the vehicle
- Production of "on-board" hydrogen by dehydrogenating MCH in a dehydrogenation reactor installed within the vehicle
- On-board storage of toluene, the by-product of dehydrogenation reaction, and dispensation of the toluene at the filling station

- Transportation of toluene back to the hydrogenation plant, where it can be re-hydrogenated to produce MCH again.

1.2.2 Factors that suggest the use of the MTH-system

Using methylcyclohexane for hydrogen storage and hydrogen generation has a number of advantages that are outlined below:

- MCH and its product of dehydrogenation (toluene) are stable and non-carcinogen and have relatively high TLV values, see Table 1.1 for their properties
- Properties of MCH are very similar to those of gasoline, see Table 1.1
- The current gasoline infrastructure can effectively be applied for the transportation, distribution and dispensation of the liquid MCH at the consumer level
- Hydrogen is produced in a single step without any associated non-condensables
- Catalysts with high selectivity, activity and relatively long life are commercially available, though none meet the required targets
- Low pressures (1−10 bar) are involved so safer and lower cost equipment is possible. The thermodynamics of MCH dehydrogenation are favoured by low pressure.
- A satisfactory amount (6.2 wt% H_2 or 47.4 g H_2/L MCH) of hydrogen is contained in a molecule of methylcyclohexane
- The reversible reaction is commercial and requires mild reaction conditions.

1.2.3 Factors that repress the use of the MTH-system

In spite of the many encouraging factors outlined above, there are some factors that deter the acceptable and successful implementation of MTH-technology on a commercial scale. The following is a list of such factors

- The dehydrogenation reaction is highly endothermic

$$C_7H_{14} + 205 \text{ kJ/mol} \longrightarrow C_7H_8 + 3\,H_2 \qquad\qquad (1.4)$$
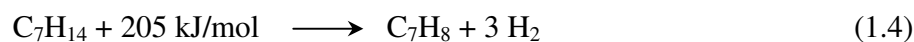
- Dehydrogenation requires high reaction temperatures (300–400 °C)
- No commercial methylcyclohexane dehydrogenation catalyst meets the required targets of selectivity, activity and stability for a MCH feed not containing added hydrogen.

1.2.4   History of the MTH-system

Sultan and Shaw [1975] were the first to propose the idea of using methylcyclohexane as a recyclable liquid carrier in automotive applications and concluded, at that time the method was not favourable compared to gasoline systems. In their calculations, the dehydrogenation reactor pressure was kept at 1 bar and the kinetic data of Faith et al. [1971, 1972] was employed [Manser Sonderer, 1992]. The requirement of around 16 times more volume of MCH compared to gasoline, the time required to heat up the catalyst to the reaction temperature, excessive weight, high cost and less operating flexibility were the factors that made that MTH-system unsuitable for vehicular applications [Sultan and Shaw, 1975] in their study.

Taube and Taube [1980] picked upon the idea of Sultan and Shaw [1975] and set forth a new idea of seasonal storage of electricity. The surplus electricity (in the summer) was proposed to produce electrolytic hydrogen that could be used to hydrogenate toluene to produce MCH [Manser Sonderer, 1992]. The MCH later (in winter) could be dehydrogenated to produce hydrogen which could be utilised for power generation. In a continuing effort, Taube et al. [1983] taking a reference lorry of 17 ton and 150 kW power operating for 250 km/day and 250 days in a year analysed the complete MTH-system. Economic considerations based on surplus energy produced during nights, weekends and summer were used to provide the feasibility. In the same group of researchers, Cresswell et al. [1984], in an effort to

produce a suitable catalytic material and to address the endothermicity associated with the reaction, performed a number of catalytic experiments and carried out the heat integration study for an average 100 kW IC engine. In the heat integration study, the isothermal reactor employed was a simple hair-pin exchanger which exchanged heat with the exhaust gases. The temperature and pressure conditions of the reactor were 400 °C and 10 bar respectively with 90% conversion of methylcyclohexane. It was concluded that the heat content of the exhaust gases was insufficient to dehydrogenate MCH due to the high endothermicity of the dehydrogenation reaction. Thus, in addition to exhaust gas thermal content, 20 kW of thermal power had to be added by combusting some of the hydrogen gas to provide the necessary heat for carrying out the dehydrogenation reaction. Alternatively, they proposed a little air addition to the reactor and found empirically that air addition caused a decrease in the yield of the product toluene, possibly due to the combustion of toluene. However, the deactivation characteristics of the catalyst were greatly enhanced. It was concluded that if the combustion of hydrocarbons could be controlled, the air addition would be beneficial in overcoming the thermal shortage and to maintain the activity of the catalyst. Later, Taube et al. [1985] developed a first ever prototype, a 17 ton, and 6 cylinders with ca.150 kW power truck. The engine was a hydrogen internal combustion engine operating at 10 bar pressure with an efficiency of 32%. The exhaust gas temperature was reported to be 700 °C. The methylcyclohexane fixed bed multitubular reactor, used for hydrogen production was operated at 400 °C and 10 bar, where the catalyst used was 0.25 wt% Pt, 0.25 wt% Re on alumina. The "on-board" dehydrogenation plant developed was called MTH-1 and is shown in Fig. 1.2.

Further, in their work, a complete MTH-system starting from the electrical grid (grid electricity required for electrolysis of water) to produce hydrogen for toluene hydrogenation, was analysed and compared with a similar diesel based system. At least for Switzerland where the work was carried out, it was proposed that the MTH based system would be competitive to the Diesel based fuel technology.
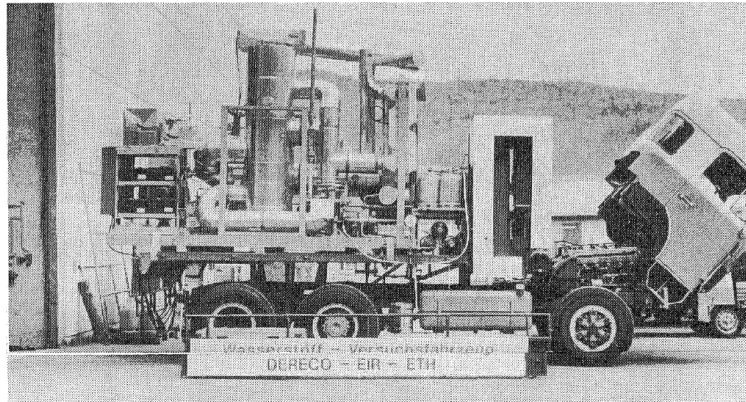
Fig. 1.2 First ever prototype "on-board" dehydrogenation plant,
MTH-1. *Source*: [Tages-Anzeiger, 1984].

The success of the MTH-1 led the workers, Grünenfelder and Schucan [1989] to test the second improved kind of "on-board" dehydrogenation plant called MTH-2. A heat exchanger network was installed to have better heat recovery from the exhaust gases. The internal combustion engine was operated at an inlet pressure of 10 bar hydrogen with a compression ratio of 8.5, the same as that used with MTH-1. The dehydrogenation reactor was operated in the range of 12 to 16 bar and 340 to 480 °C with a bimetallic commercial UOP catalyst. Under these conditions, the maximum power for the MTH-2 could reach 110 kW. In pursuit of further improvement in MTH-1 and to follow MTH-3, Manser Sonderer [1992] modelled and simulated the "on-board" dehydrogenation reactor under the conditions expected in the actual MTH-3. Unfortunately, the MTH-3 system was not taken further.

In addition to the above Swiss, a parallel group of researchers continued their efforts in Canada. They carried out their experimental and simulation studies to improve the catalyst and to understand and solve the problems of high endothermicity associated with the reaction. In their group, Touzani et al. [1987], using a Pt-Sn/Al_2O_3 catalyst, developed a mathematical model based on some experimental results and simulated for axial and radial temperatures distributions and conversions. Klvana et al. [1991] empirically coupled the dehydrogenation reactor directly to the engine cylinder. This was done to utilise heat that otherwise a cooling system had to remove for engine cooling. Experimental data obtained at 400°C was satisfactorily simulated. Their study suggested that the MTH-system had potential to be used in

vehicles, especially those that require a low fuel quantity. Finally, Chaouki and Klvana [1994] successfully produced a global reactor model combining the kinetic model equation of Chaouki et al. [1988] and deactivation model of Chaouki et al. [1991] together with the concept of directly utilising the engine heat. On the basis of the modelling results they suggested the use of a hydrogen permselective membrane similar to that of Itoh et al. [1988] for cyclohexane dehydrogenation. As an alternative, however, they suggested the use of partial recycling of the hydrogen to increase the life of the catalyst. Other workers, such as Ali and Baiker [1997], Ferreira-Aparicio et al. [2002] and Gora et al. [2006], applied the concept of membrane-assisted dehydrogenation to shift the equilibrium and to increase the conversion at low temperature. The cost, complexity, temperature limitations and life of the multifunction catalytic reactor are the principal hindrances in following this route.

Scherer [1997] studied the MTH-system for a stationary application. Three systems, namely integrated gas and steam turbines, molten carbonate and solid oxide fuel cells (SOFC) were compared for the MTH-system. The cheapest source of electricity was for the SOFC. However, the estimated cost was 2.6 to 5.2 times higher than current conventional energy costs. Newson et al. [1998] argued that for stationary applications and seasonal storage of electricity, the MTH-system was equivalent in cost to other carbon-free alternatives and better than the battery storage option. Tschudin [1997] and Tschudin et al. [1999] worked on the catalyst coated wall reactor with the aim of developing seasonal storage of electricity using methylcyclohexane as the liquid organic hydride. One monometallic Pt on alumina catalyst and two bimetallic Pt-Re and Pt-Sn on alumina catalysts were tested. A tube of Fecralloy® was coated from the inside with the monometallic and bimetallic catalysts. A two-dimensional reactor model was developed which considered the transport resistances between the bulk gas phase and the coated wall catalyst and within the coating itself. The results were in good agreement with the experimental data, and showed a high catalyst efficiency of such wall-coated reactors. Unfortunately, for a practical production of hydrogen, such a reactor system would be excessively large because of the low volumetric rate. Schildhauer et al. [2001]

experimentally revised the equilibrium constant for the dehydrogenation of methylcyclohexane and Schildhauer [2001], in his Ph.D. thesis, developed a unique structured catalytic reactor designed to direct the flow towards the outer wall of the reactor assembly in order to minimise the film resistance responsible for the unwanted radial temperature distribution in the catalyst bed. Due to the low catalyst to packing ratio, their efforts were not very successful.

Bustamente et al. [2005] proposed a multitubular reactor with the outside wall of the tubes wash-coated with catalyst. This was done to keep the catalyst temperature as isothermal as possible. The hydrogen produced was to be purified by adsorbents to feed to a fuel cell stack.

Cresswell and Metcalfe [2006] carried out a heat integration study on a range-extender system of electrical vehicles based on the MTH-SOFC-system. In their study, a three stage adiabatic flow reactor was assumed and the heat necessary for the interstage heating was provided by the exhaust stream issued from the SOFC operated between 900 and 1000 °C. In conclusion, they integrated the system successfully with a high temperature SOFC.

Hrein Energy, Inc., in August 2007 [Hrein Energy, 2008], with the cooperation of Fatuba Industrial Co. Ltd., Ito Racing Co., Ltd. and Prof. Masaru Ichikawa of Hokkaido University, Japan, successfully demonstrated a test drive of a 50 cc MTH-based cart. The reactor was made of aluminium and was coated with a thin layer of alumina in which platinum was impregnated. The reactor was 45 cm in length and 15 cm in diameter [Green Car Congress, 2008]. The same group produced even better results in February 2008, when they produced the world's first car, based on the MTH-system. Actually the vehicle was partially based on the MTH-system which basically assisted gasoline combustion by blending gasoline with hydrogen in the fuel system [Hrein, 2008]. The prototype car was fitted with a dehydrogenation reactor that was placed inline to the exhaust pipe as shown in Fig. 1.3 [Silobreaker, 2008]. The dehydrogenation reactor was a spray pulse type in which atomised methylcyclohexane was fed to the catalyst surface. The exhaust gases were used to heat the catalytic bed. The reactor worked at $\geq 85\%$ conversion with a hydrogen production rate of 3 Nm^3/h [Silobreaker, 2008]. The supplement hydrogen, only three

to five volume percent of the intake air [Tech-On, 2008], proved useful towards lean-burn and improved efficiency of the 1200 cc car by 30% [Hrein Energy, 2008]. In the test drive at 50 to 60 km/h, the mileage covered was ca. 30% higher than could be done with the gasoline alone [Tech-On, 2008]. Moreover, the emission of CO_2 was also reduced by 30% and other harmful gases were also reduced [Hrein Energy, 2008].

Dehydrogenation reactor
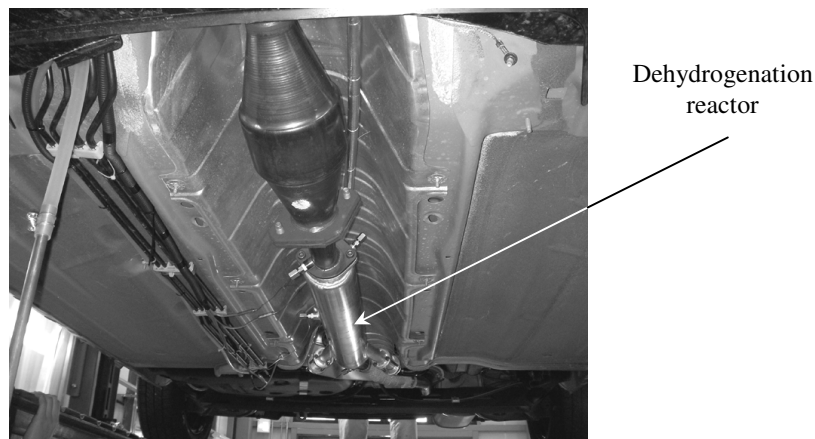
Fig. 1.3 Dehydrogenation reactor fitted inline to the exhaust pipe in the 1200 cc MTH-system based car developed by Hrein Energy, Inc.
Source: [Silobreaker, 2008].

In the research group of Garforth and Cresswell (one of the pioneers of the MTH-technology, an important part of Taube's research group), Tsakiris [2007] and Alhumaidan [2008] tested a number of commercial catalysts as well preparing their own mono-metallic and bi-metallic versions in an effort to find a catalyst with a suitable combination of activity, selectivity and stability.

This literature review has attempted to cover both theoretical and practical aspects of the MTH-system. Attempts for developing kinetic models for the dehydrogenation reaction of methylcyclohexane will be reviewed in the following chapter.

1.3   Problem statement

The objectives of the present work are to take the best catalyst tested to date and study it more fundamentally and even over a wider experimental range.

An important goal is to develop a robust kinetic model which can be reliably extrapolated to explore new reactor designs (Chapter 4).

Following the experimental testing of the model (Chapter 6) it is applied to the design of suitable "on-board" reactor to generate a hydrogen feed to be mixed with a conventional gasoline/air feed fed to the IC engine, the objective being to raise overall combustion efficiency and lower CO_2 emissions (Chapter 7).

Chapter 2
Literature Review of the Mechanisms and the Kinetics of Methylcyclohexane Dehydrogenation

The catalytic dehydrogenation of methylcyclohexane over supported Pt metal catalysts has remained of interest to a whole host of investigators. Exploiting MCH as a fuel, taking MCH dehydrogenation as the model reforming reaction and considering MCH as a hydrogen energy storage material appear to be the three most important reasons behind studying the dehydrogenation reaction [Schildhauer, 2001]. Zelinskii [1911, 1912 in Sinfelt, 2000], Haensel and Donaldson [1951], Hettinger et al. [1955], Keulemans and Voge [1959], Sinfelt et al. [1960], Myers et al. [1961], Rohrer and Sinfelt [1962], Ritchie et al. [1965], Ritchie and Nixon [1966], Hawthorn et al. [1968], Zengel [1968], Nixon et al. [1967, 1968, 1970], Ackerman et al. [1970], Lander et al. [1971], Faith et al. [1971, 1972], Akyurtlu and Stewart [1978], Wolf and Petersen [1977], Corma et al. [1979, 1981], Jossens and Petersen [1982a, 1982b, 1982c], Cresswell et al. [1984], Coughlin et al. [1984a, 1984b], Touzani et al. [1984], Pacheco and Petersen [1984, 1985], Jothimurugesan et al. [1985a, 1985b], Van Trimpont et al. [1985, 1986], Pal et al. [1986], García de la Banda et al. [1986], Rimensberger [1987], Chaouki et al. [1988, 1991], El-Sawi et al. [1989], Chai and Kawakami [1990], Garland et al. [1991], Manser Sonderer [1992], Müller [1995], Maria et al. [1995], Fung et al. [1997], Tschudin [1997], Schildhauer [2001], Schildhauer et al. [2001], Aberuagba and Susu [2004], Bustamante et al. [2005], Okada et al. [2006], Tsakiris [2008], Yolcular and Olgun [2008], Xiaoyun et al. [2008] and Alhumaidan [2008] all exploited supported Pt-containing catalysts and studied the dehydrogenation reaction of MCH. However, only a few workers attempted to understand and to develop the kinetic mechanism and analyse the experimental data to produce an appropriate kinetic model. In the following sections, firstly an overview of the fundamental studies on single-crystal surfaces and a "first-principles based" kinetic study, using density functional theory (DFT) calculations for the dehydrogenation of cyclohexane (a model for methylcyclohexane), is outlined. This

brief discussion is followed by a comprehensive account of the efforts made on supported and structured catalysts that have been undertaken to uncover the mechanism of the main dehydrogenation reaction and to develop a suitable kinetic rate expression.

2.1 Single-crystal surface studies relevant to methylcyclohexane dehydrogenation

The study of the chemisorption and reactivities of hydrocarbons on single-crystal surfaces is important in understanding the fundamentals of a particular reaction such as the dehydrogenation of cyclohexane. In the following discussion a concise and relevant review of the cyclohexane dehydrogenation over single-crystal Pt surfaces is provided. A quite handsome and brief introduction to the related surface chemistry and the nomenclature used in the following discussion is provided by Tsakiris [2007].

Somorjai and his coworkers, namely Gland et al. [1975], Blakely and Somorjai [1975], Smith et al. [1979] and Herz et al. [1981], profoundly studied the dehydrogenation of cyclohexane both on clean and pre-oxidised Pt single-crystal surfaces under varying conditions of pressure (ultrahigh vacuum to atmospheric).

Gland et al. [1975] studied the dehydrogenation of cyclohexane, cyclohexene, and 1,3-cyclohexadiene on a clean Pt(111) single-crystal. The experiments were performed at low pressures of 5×10^{-7} mmHg in the presence of H_2 with a H_2 to cyclohexane molar ratio of 5:1, and at 423 K. Auger electron spectroscopy (AES) and low-energy electron diffraction (LEED) were employed to measure the composition on the Pt surface and to find the structure and the degree of the clean surface and the adsorbed layers. Quadrapole mass spectrometry (QMS) was used to analyse the gas phase composition. It was found that Pt(111) catalyses the dehydrogenation of cyclohexane to cyclohexene but the reaction is not completed at 423 K. On the other hand, 1,3-cyclohexadiene rapidly and completely converts to benzene. The cyclohexene was, therefore, regarded as an intermediate and dehydrogenation of cyclohexene as the rate-limiting step. The adsorption of 1,3-cyclohexadiene on the

Pt(111) surface in a different orientation to that of cyclohexane was put forward as the reason behind the complete conversion of cyclohexadiene.

Blakely and Somorjai [1975] studied the dehydrogenation of cyclohexane and cyclohexene on a number of Pt single-crystal surfaces having varying Miller indices. The experiments were carried out at the pressures of 10^{-7}–10^{-6} mmHg and temperatures of 300–725 K and in the presence of excess hydrogen. The authors identified two different kinds of sites on the crystal surfaces responsible for different types of reaction. They proposed that H–H and C–H bonds break at one site while C–C, H–H and C–H bonds break at the other type of site. Moreover, they proposed the significance of the carbonaceous layer, deposited on the Pt surface, in changing the rate and selectivity of the dehydrogenation reaction. It was observed that the surface planes with higher concentrations of atomic steps than Pt(111) dehydrogenate the precursor molecules effectively and are responsible for the breaking of H–H and C–H bonds. The breaking of the C–C bond along with C–H and H–H bonds were observed to take place on the kinks in the steps. They concluded that the dehydrogenation of cyclohexane to cyclohexene is structure insensitive, while dehydrogenation of cyclohexene is structure sensitive.

Smith et al. [1979] studied the dehydrogenation of cyclohexane and cyclohexene and the hydrogenation of cyclohexene on both clean and pre-oxidised Pt single-crystal surfaces, such as Pt(111), a stepped Pt(755) and a kinked Pt(10,8,7) surface. Experiments were performed at pressures of 10^{-6}–10^{-5} mmHg, slightly higher than Blakely and Somorjai [1975] and at a single temperature of 423 K, the same as that of Gland et al. [1975]. On clean Pt surfaces, they found dehydrogenation of cyclohexane to be structure insensitive while dehydrogenation of cyclohexene to benzene was structure sensitive. The latter results are in agreement with the results of Blakely and Somorjai [1975]. For pre-oxidised surfaces, they observed improvements in the rates and selectivity of the dehydrogenation and the hydrogenation reactions at low coverages of strongly bound oxygen. The pre-oxidation introduced the structure sensitivity to the catalytic rates and the selectivity. It was found that "kink" sites were particularly important in increasing the dehydrogenation and hydrogenation rates. The change in the electronic structure of the Pt-surface by oxidation provided the

reason behind these observations. It was concluded that the additive such as oxygen could be applied to enhance the rate and alter the selectivity of the hydrocarbon reactions over Pt catalysts even on supported Pt catalysts.

Herz et al. [1981] studied in detail the dehydrogenation of cyclohexane on Pt single-crystal surfaces. The investigation was carried out at temperatures of 503−573 K and much higher pressures (115−760 mmHg) than the previous studies in the same group [Gland et al., 1975; Blakely and Somorjai, 1975; Smith et al., 1979]. The hydrogen to cyclohexane molar ratio ranged between 6 and 50. Three different types of clean and pre-oxidised crystal surfaces were used, namely flat Pt(111), stepped Pt(557) and kinked Pt(25,10,7) and Pt(10,8,7). The high pressures used in their study made it possible for the workers to compare the results obtained at low pressures in the earlier works of their group. Moreover, experiments at atmospheric pressure made it possible for them to compare the results with a conventional supported Pt-metal catalyst. Some experiments were performed with the addition of toluene to study the inhibition effect of the product benzene.

Under these high pressure conditions, benzene was the major product and the rate of formation of benzene was several orders of magnitude higher than the rate of formation of cyclohexene. The experiments performed with the addition of toluene exhibited inhibition in the rate of formation of benzene. The dehydrogenation to benzene was found approximately first order in cyclohexane and positive fractional order with hydrogen partial pressures. Comparing results at low and high pressures [Smith et al., 1979], it was observed that at high pressure the initial rate of formation of benzene depends significantly on the surface structure. These observations suggested the dehydrogenation reaction to be structure sensitive on the clean surfaces, in contrast to the work of Smith et al. [1979] on single-crystal surfaces and Cusumano et al. [1966], Mitrofanova et al. [1966], Kraft and Spindler [1968] and Maatman et al. [1971] on supported Pt catalysts. The apparent activation energy (71.1 kJ/mol) at high pressures was observed to be more than four times the activation energy at low pressures. The reason for the difference in the structure sensitivity of dehydrogenation at high and low pressures was related to the difference in the concentrations of the adsorbed carbonaceous deposits (adsorbed reactants, reaction

intermediates, reaction products and irreversibly adsorbed carbonaceous species) at these two different pressures. At high pressures, the "step" and "kink" sites might have a tendency to provide resistance to be blocked by these carbonaceous deposits. Moreover, it was suggested that the different structure sensitivity might be due to the different rate-determining steps prevailing in the two pressure regimes. The difference in apparent activation energies at the two different pressures was thought to be the result of different reaction mechanism occurring at the two pressures.

When comparing the results with a supported Pt catalyst, the rate of benzene formation was found much faster than that on the supported catalyst. Also, as discussed earlier, the reaction was found structure sensitive on the single-crystal surfaces but structure insensitive on the supported Pt catalyst.

Campbell and his co-workers in a series of articles [Campbell et al., 1989a; Campbell et al., 1989b; Rodriguez and Campbell, 1989; Henn et al., 1989] studied the chemisorption and dehydrogenation reactions to fundamentally understand the ensemble effects and the ensemble size of atoms required for cyclic hydrocarbon dehydrogenation on Pt single-crystal surfaces using bismuth site blocking. Rodriguez and Campbell [1989] thoroughly studied the adsorption of cyclohexane on clean and bismuth-covered Pt(111) crystal surfaces. They applied thermal desorption mass spectroscopy (TDS), deuterium labelling, Auger electron spectroscopy (AES) and X-ray photoelectron spectroscopy (XPS) to study the adsorption and dehydrogenation of cyclohexane. It was found that the dehydrogenation of cyclohexane to benzene occurs at ~236 K on a clean Pt(111) surface. Analysis of XPS data and bismuth-poisoning show that an ensemble of nearly five Pt-atoms is required to chemisorb cyclohexane. Moreover, the results of kinetic analysis show that an ensemble of a minimum of eight free Pt-atoms, in addition to the above five required for chemisorption, is needed for the dehydrogenation of adsorbed cyclohexane. For methylcyclohexane, an even greater ensemble size of atoms may be required.

Pettiette-Hall et al. [1991] and Parker et al. [1992] in the same group, studied the initial dehydrogenation of cyclohexane to benzene on a clean Pt(111) single-crystal using laser-induced thermal desorption (LITD) and Fourier transform mass spectrometry (FTMS). They observed that the dehydrogenation starts at ~180 K, but

significant rates of formation of benzene are not obtained below ~280 K. Between 180–270 K, a stable surface intermediate was observed. The stoichiometry of the stable intermediate was proposed to be C_6H_9. Moreover, the dehydrogenation reaction was studied for varying initial cyclohexane coverage. It was observed that the dehydrogenation reaction is first order with respect to cyclohexane coverage for all the initial cyclohexane coverages studied. However, the activation energy and pre-exponential factors increased with an increase in the starting coverage. The activation energies of 39.7 kJ/mol and 56.5 kJ/mol were obtained at low (0.05 ML) and high coverage (~0.30 ML), respectively.

Saeys et al. [2005a, 2005b] applied density functional theory (DFT) calculations to propose the mechanism of benzene hydrogenation over a single-crystal of Pt(111) based on first-principles. In doing so, they outlined all the possible reaction schemes for the hydrogenation of benzene and, applying DFT calculations, the activation energy in each path was calculated, as shown in Fig. 2.1. The dominant reaction mechanistic path was chosen as the one having least sum of the activation energies and proposed as the reaction mechanism for the hydrogenation of benzene. The proposed reaction mechanism is shown in Fig 2.1 with the bold reaction symbols. The reaction step with the highest activation energy (104.0 kJ/mol), atomic hydrogenation of 1, 2, 3, 5-tetrahydrobenzene (1235THB) to cyclohexyl (c-hexyl), in the overall hydrogenation of benzene to cyclohexane was proposed as the rate-determining step.

For the proposed reaction mechanism, taking hydrogen adsorption-desorption as an additional step in the mechanism and using Langmuir-Hinshelwood-Hougen-Watson (LHHW) kinetics, a kinetic rate expression was developed. The kinetic parameters for the rate equations were determined using DFT calculations and a simulated model equation was proposed. The experimental rate values of toluene hydrogenation over 0.5 wt% Pt/ZSM-22 catalyst were compared with the rates obtained from the simulated model equation. Experimental and simulated rates, though different in magnitude, showed similar trends with the change in temperature and the reactor space velocity. However, the data shown for comparison was

insufficient to allow any detailed conclusion from the study. A more extensive and rigorous experimental study is required to test such ab initio calculations.
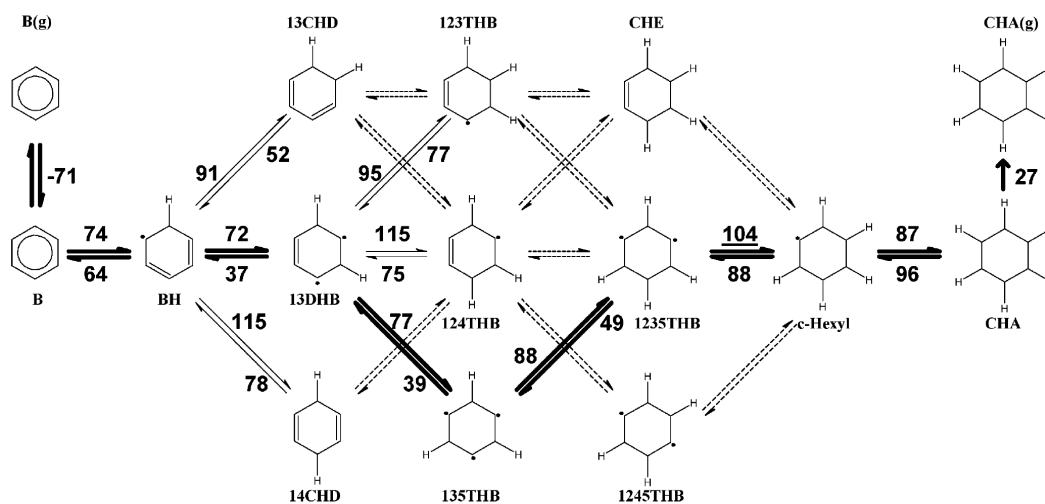
Fig 2.1 Possible reaction pathways and the activation energies for hydrogenation of benzene to cyclohexane measured by DFT. Nomenclature: B (benzene); CHD (cyclohexadiene); CHE (cyclohexene); DHB (dihydrobenzene); THB (trihydrobenzene and tetrahydrobenzene); CHA (cyclohexane); c-Hexyl (cyclohexyl). Units of activation energies are kJ/mol.
Source: [Saeys et al., 2005a].

Following the same procedure, the mechanism for the reverse reaction (dehydrogenation of cyclohexane) may also be worked out. For cyclohexane dehydrogenation, using Fig. 2.1 (although information is not complete), loss of the first atomic hydrogen may be proposed as the rate-determining step. The same reaction mechanism may also be adopted for the dehydrogenation of methylcyclohexane.

No doubt the study on the single-crystal surface is helpful in identifying the reaction intermediates and somehow the reaction mechanism. However, the understanding developed by single-crystal surfaces is difficult to relate to the supported-metal catalysts (most real-life catalysts) due to the metal-support interactions and the multifaceted exposed crystal planes. Therefore, for any particular supported-metal catalyst, such as Pt/Al_2O_3, the classical procedure of developing a mechanism and kinetic rate model is preferred and a review of such attempts for the

dehydrogenation of MCH is outlined below, while a summary of the important kinetic models is provided in Table 2.1.

2.2 Supported Pt-containing catalysts

The kinetics and supporting mechanisms on supported platinum containing catalysts derived from applied kinetic studies are reviewed in the following sections. The kinetics of the MCH dehydrogenation are mostly studied on alumina-supported catalysts. However, a few studies have also been carried out on Pt supported on NaY-zeolite.

2.2.1 Alumina supported Pt-containing catalysts

A kinetic study of the dehydrogenation reaction of MCH was pioneered by Sinfelt et al. [1960], although some experimental studies [Zelinskii, 1911, 1912 in Sinfelt, 2000; Haensal and Donaldson, 1951; Hettinger et al., 1955; Keulemans and Voge et al., 1959] were undertaken before. Sinfelt et al. [1960] utilised a 1.27 cm I.D. (internal diameter) stainless steel reactor and a 0.3 wt% Pt/Al_2O_3 catalyst, made by impregnating 155 m^2/g Al_2O_3, to study the dehydrogenation reaction of MCH. The temperatures used were 315 to 372 °C and the total pressure was varied between 1.42 and 6.38 bar. H_2/MCH ratios were 2–20, while molal space velocity was in the range of 3.60×10^3 to 1.80×10^4 s·g-cat /mol-MCH. In some of the experiments benzene and meta-xylene (aromatics) were mixed with the MCH feed to observe the effect of product (toluene) inhibition.

Table 2.1 Summary of the important kinetic models

Investigator/s	Catalyst	Kinetic equation (Page no.)	Rate-controlling step	Product inhibition	E (kJ/mol)
Sinfelt et al. [1960]	Pt/Al$_2$O$_3$ (0.3 wt% Pt)	Eq. 2.1 (p. 56)	Desorption of toluene	Toluene	138.1
Corma et al. [1979]	Pt/NaY-zeolite (0.5 wt% Pt)	Eq. 2.16 (p. 68)	Dual-site surface reaction (Loss of first hydrogen)	Toluene Hydrogen	—
Touzani et al. [1984]	Commercial Pt-Sn/Al$_2$O$_3$	Eq. 2.1 (p. 56)	Single-site surface reaction	N.A.	118.3
Pacheco and Petersen [1985]	Commercial pre-sulphided Pt-Re/γ-Al$_2$O$_3$ (0.3 wt% Pt, 0.3 wt% Re, 0.6 wt% Cl)	Eq. 2.6 (p. 60)	Adsorption of MCH	N.A.	58.6
Jothimurugesan et al. [1985a]	Pt-Re/γ-Al$_2$O$_3$ (0.3 wt% Pt and 0.3 wt% Re)	Eq. 2.8 (p. 61)	Adsorption of MCH	Toluene	51.9
Van Trimpont et al. [1986]	Commercial sulfided Pt/Al$_2$O$_3$ catalyst (0.59 wt% Pt, 0.67 wt% Cl)	Eq. 2.12 (p. 64)	Dual-site surface reaction (Loss of third hydrogen)	Hydrogen n-heptane	121.7
Van Trimpont et al. [1986]	Commercial pre-sulfided Pt-Re/Al$_2$O$_3$ (0.3 wt% Pt, 0.31 wt% Re, 0.95 wt% Cl)	Eq. 2.13 (p. 65)	Single-site surface reaction (Loss of first hydrogen)	Toluene n-heptane	181.4
Chai and Kawakami [1990]	Commercial Pt/γ-Al$_2$O$_3$ (0.375 wt% Pt, ~1.0 wt% Cl) Commercial Pt-Re/γ-Al$_2$O$_3$ (0.375 wt% Pt, 0.375 wt% Re, ~1.0 wt% Cl) pre-sulphided Pt-Re/γ-Al$_2$O$_3$ (0.375 wt% Pt, 0.375 wt% Re, ~1.0 wt% Cl)	Eq. 2.14 (p. 66)	Single-site surface reaction (Loss of second hydrogen)	Hydrogen	—
Maria et al. [1996]	Commercial sulphided Pt/Al$_2$O$_3$	Eq. 2.15 (p. 67)	Single-site surface reaction	Hydrogen	220.7
Tsakiris [2007]	Commercial Pt/γ-Al$_2$O$_3$ (0.5 wt% Pt)	Eq. 2.17 (p. 71)	Dual-site surface reaction (Loss of first hydrogen)	Hydrogen Toluene	50.3
Alhumaidan [2008]	Commercial Pt/Al$_2$O$_3$ (1.0 wt% Pt)	Eq. 2.19 (p. 72)	Non-Langmurian-non-competitive-Horiuti-Polanyi surface reaction (Loss of first hydrogen)	Hydrogen	55.4

The experiments were conducted under differential conditions with conversion-levels in the range 4 to 12%. Initial rates of reaction were applicable under these conditions and the kinetics of the reverse reactions were ignored. The dehydrogenation reaction was found to be very selective (negligible side reactions) and zero order with respect to hydrogen and nearly zero order with respect to methylcyclohexane. The activation energy of the reaction was found to be 138.1 kJ/mol. The nearly zero order behaviour was assumed to be affected by the following Langmuir-Hinshelwood-Hougen-Watson (LHHW) type expression

$$(-r) = \frac{k \cdot K_A \cdot p_A}{1 + K_A \cdot p_A} \qquad (2.1)$$

Eq. (2.1) assumes that methylcyclohexane is in adsorptive equilibrium with the surface and the near zero order behaviour of the dehydrogenation reaction shows that the active sites are almost fully covered. Applying Eq. (2.1) to the experimental rate data, the heat of adsorption of methylcyclohexane was found to be 125.5 kJ/mol. Sinfelt et al. [1960] argued that such a high value for methylcyclohexane adsorption was highly unlikely and experiments with addition of aromatics showed the rate to be decreased by 20%, which could not be explained on the basis of highly covered surfaces. Above findings led the investigators to a two step non-equilibrium adsorption mechanism, according to which methylcyclohexane adsorbed and converted to toluene on the surface in the first step and the toluene formed was desorbed from the surface in the following step as shown below

$$MCH \xrightarrow{k_1} Tol \cdot s \xrightarrow{k_2} Tol \qquad (2.2)$$

where, MCH and Tol stand for gas phase methylcyclohexane and toluene, respectively, while Tol·s stands for toluene adsorbed. The adsorbed toluene mechanism proposed by the authors assumed that the adsorption equilibria had not been developed and only a very small fraction of active sites was covered by

components that were not toluene. For the two step reaction the rate equation can be written as

$$(-r) = \frac{k_2 \cdot \left(\dfrac{k_1}{k_2}\right) \cdot p_A}{1 + \left(\dfrac{k_1}{k_2}\right) \cdot p_A} \qquad (2.3)$$

where, k_i = rate constant of an *ith* reaction step.

The activation energy, 138.1 kJ/mol, of the reaction was then regarded as the activation energy of desorption of the toluene from the surface and by difference the heat of adsorption of MCH might be 138.1 − 125.5 = 12.6 kJ/mol, which was considered by the workers more realistic. In the same paper, Sinfelt et al. [1960] questioned Balandin's multiplet theory of catalysis (single step simultaneous removal of all hydrogen atoms) [Trapnell, 1951] and suggested the formation of toluene as a result of series of dehydrogenation steps, which were adopted by later investigators, as will be apparent in the following discussion.

One way to provide a heat sink in high speed aircraft ($Ma \geq 3.0$) is to use a fuel that can undergo a highly endothermic dehydrogenation reaction. Ritchie and Nixon [1966] utilised the idea and studied MCH dehydrogenation with and without catalyst (quartz chips) in the reactor. One laboratory prepared 1.0 wt% Pt/Al_2O_3 (surface area 91 m^2/g and without halogen) and the other commercial UOP-R8 platforming catalyst with 0.76 wt% Pt with 0.70 wt% halogen. The reaction was carried out at 1.013, 10.13, 20.27 and 30.40 bar in a temperature range of 433.0 °C to 700.6 °C. LHSV of 5 to 150 h^{-1} were employed. No hydrogen was added in any of the experiments. First order kinetics were evaluated for some of the data with 1.0 wt% Pt/Al_2O_3 catalyst and apparent activation energy of 48.9 kJ/mol was reported between 450 °C and 550°C at 10.13 bar. In order to improve the radial temperature distribution some experiments were done by diluting the catalyst bed with similar size copper granules or by reducing the catalyst bed thickness. In both cases an enhancement in conversion was reported but was not elaborated and quantified.

In the same group as Ritchie and Nixon [1966], Hawthorn et al. [1968] worked with the same commercial catalyst, 3.20 mm UOP-R8 (Pt/Al$_2$O$_3$ in two 9.53 mm O.D. and 19.05 mm O.D. fixed bed tubular reactors. The pressure (inlet) and temperature (fluid temperature at reactor centre line) ranges were 34.5–62.0 bar and 365.6–476.7 °C respectively. A mathematical model for the heat-exchanger reactor was developed and tested for the axial temperature and concentration distributions as well as for the radial temperature distribution in the packed bed. Both first order irreversible as well as reversible kinetics, as proposed by Ritchie and Nixon [1966], were found inappropriate in the models to represent the axial temperature distribution accurately. A kinetic model based on the work of Sinfelt et al. [1960], with the modification of the reversible kinetics and the rate constants as a function of temperature was employed and successfully fitted the observed results. Later, Nixon [1968], Ackerman et al. [1970] and Faith et al. [1971, 1972], working in the same group as that of Hawthorn et al. [1968] used the same rate expression in their work.

Kluksdahl [1968] introduced Re to monometallic Pt-supported catalyst. He obtained a high yield of high octane reformate for a longer period than with Pt alone. It was then widely thought that the addition of a second metal such as Ir, Sn or Re would be beneficial for the catalyst activity and selectivity over a longer time. Moreover, the beneficial effects of poisoning the catalyst with a small amount of sulphur [Sterba and Haensel, 1976; Menon and Prasad, 1977] were also generally recognised. Jossens and Petersen [1982a, 1982b, 1982c] realised the importance of the above mentioned observation and compared the dehydrogenation of methylcyclohexane over monometallic Pt/Al$_2$O$_3$ and bimetallic Pt-Re/Al$_2$O$_3$ with and without pre-sulphiding the catalysts. For monometallic Pt/Al$_2$O$_3$ catalyst, the reaction was carried out at slightly above atmospheric pressure in an external recycle differential reactor. The catalyst used was chlorinated 0.3 wt% Pt/Al$_2$O$_3$. The reaction conditions employed were 350–400 °C, 0.27 and 0.80 bar hydrogen pressure, 0.013 and 0.04 bar MCH and 0.0027 and 0.016 bar toluene. Analyses of their results showed a shift in order of the reaction with respect to MCH with variation in MCH concentration in the feed. The dehydrogenation reaction was found first order in MCH at low concentrations of MCH while the order decreased and approached zero

order at higher concentrations of MCH. Experiments performed in the presence of toluene showed toluene to be an inhibitor. The same observation was also made by Sinfelt et al. [1960] and Corma et al. [1979] who found that inhibition increased with increasing temperature, but strongly decreased with an increase in hydrogen pressure in the feed. Between 0.80 bar and 1.33 bar hydrogen pressure, a zero order rate was observed with respect to hydrogen pressure. However, below 0.80 bar hydrogen, the initial reaction rate increased with hydrogen pressure. The activation energy was found to be 71.1 kJ/mol between 200 °C and 350 °C and fell above 370 °C. The authors noticed similar kinetic behaviour for Pt-Re/Al$_2$O$_3$. However, an enhancement in selectivity was observed with Pt-Re/Al$_2$O$_3$ over Pt/Al$_2$O$_3$ catalyst. Sulphiding was found to decrease the initial rate of the dehydrogenation reaction.

Touzani et al. [1984] employed a Pt-Sn/Al$_2$O$_3$ catalyst in a U-shaped tubular reactor under integral conditions at temperatures of 300−450 °C with hydrogen in the feed. The partial pressures of MCH, hydrogen and toluene were varied within the ranges 0−0.65, 0.31−0.93 and 0−0.23 bar, respectively. Based upon the kinetic results, the following two step mechanism, similar to that of Sinfelt et al. [1960] was proposed.

$$\text{MCH} + \text{s} \xrightarrow{\ k_1\ } \text{MCH·s} \qquad\qquad (2.4)$$

$$\text{MCH·s} \xrightarrow{\ k_2\ } \qquad\qquad\qquad (2.5)$$

Several other rapid equilibrated steps followed the second step to produce toluene. Toluene inhibition was ignored and the rate of surface reaction was taken as the rate-controlling step. The rate expression was identical to Sinfelt et al. [1960] as shown in Eq. 2.1. The activation energy of 118.3 kJ/mol was calculated for the surface reaction.

In the same group of Jossens and Petersen [1982a, 1982b, 1982c], Pacheco and Petersen [1985] extended the study on the dehydrogenation of MCH over pre-sulphided bimetallic catalyst with an external recycle reactor for which the recycle ratio was over 10:1. The particle size used of the sulphided Pt-Re/Al$_2$O$_3$ was 80 μm. The catalyst employed was a pre-sulphided 0.3 wt% Pt, 0.3 wt% Re and 0.6 wt% Cl on γ-Al$_2$O$_3$ (surface area 200 m^2/g). For the main reaction on "un-fouled" catalyst

they observed several kinetic regimes over the range of variables studied and found, in contrast to Jossens and Petersen [1982a, 1982b, 1982c], the rate of the methylcyclohexane dehydrogenation was not affected by toluene. The isothermal data was best fitted with the following rate expression

$$(r_B) = \frac{k \cdot p_A}{1 + K_A \cdot \left(\dfrac{p_A}{\sqrt{p_C}} \right)}$$

(2.6)

Similar to Corma et al. [1979] discussed below in Section 2.1.2, they observed methylcyclohexene (MCHe), all three isomers, in the reaction products and suggested it might be a gas phase intermediate. Thus the dehydrogenation reaction was thought to be a two step consecutive irreversible reaction with the following possible chemistry

$$\text{MCH} \longrightarrow \text{MCHe} \longrightarrow \text{Tol}$$

(2.7)

It was observed that the reaction was controlled by adsorption of the reactant and above 360 °C, an activation energy of 58.6 kJ/mol was reported.

At this point no systematic and detailed kinetic study, over an extensive range of operating conditions had been undertaken over a Pt-containing catalyst. This was taken up by Jothimurugesan et al. [1985a]. The authors applied both single-site and dual-site LHHW mechanisms and rigorously studied the kinetics of the MCH dehydrogenation reaction. They employed a stainless steel 2.54 cm I.D. differential fixed bed reactor. The catalyst, 1.5×3.0 mm in size, was Pt-Re over γ-Al_2O_3 with 0.3 wt% Pt and 0.3 wt% Re. The γ-Al_2O_3 support used had a BET surface area of 220 m^2/g. For comparison purposes, individual monometallic catalysts of Pt/γ-Al_2O_3 and Re/γ-Al_2O_3 were also prepared. However, the detailed kinetics were studied only for the Pt-Re/γ-Al_2O_3 catalyst. The kinetic experiments were performed in the presence of hydrogen with a feed H_2/MCH ratio of 5:1. A space-time W/F_{A0} of 2.16×10^4 s·g-cat/mol-MCH was used at atmospheric pressure and temperatures of 325, 350, 375

and 425 °C. Nitrogen gas was used as a diluent and in some cases toluene was added to the feed to study the inhibition effect. Toluene and hydrogen were observed to be the only reaction products. The activity of the Pt/Al_2O_3 and Pt-Re/Al_2O_3 catalysts were comparable and the Re/Al_2O_3 catalyst showed no activity. No appreciable effect of hydrogen was observed on the catalyst activity. However, toluene showed an inhibiting effect. Using linear and non-linear regression, Jothimurugesan et al. [1985a] tested 11 alternate models based upon Langmuir-Hinshelwood-Hougen-Watson (LHHW) concepts for both single- and dual-site surface reaction mechanisms. The models were kinetically and statistically analysed and the rate expression based on the adsorption of MCH as the rate-controlling step was found most appropriate. The same rate-controlling step was also proposed by Lander [1970 in Jothimurugesan, 1985a] and Pacheco and Petersen [1985]. The final model equation in which only the toluene adsorption term was retained is shown below

$$(-r) = \frac{k \cdot p_A}{1 + K_B \cdot p_B} \cdot \left(1 - \frac{p_B \cdot p_C^3}{K \cdot p_A} \right) \tag{2.8}$$

Based on the kinetic results, a reaction mechanism was proposed that constituted the following three mechanistic steps

- MCH adsorption on the surface of the catalyst

$$\text{MCH} + \text{s} \rightleftharpoons \text{MCH·s} \tag{2.9}$$

- Dehydrogenation of the adsorbed MCH (could probably be taken as a series of steps from adsorbed methylcyclohexane to adsorbed methylcyclohexene to methylcyclohexadiene and finally to adsorbed toluene along with three hydrogen molecules as below)

$$\text{MCH} \rightleftharpoons \text{Tol·s} + 3\,H_2 \tag{2.10}$$

- Desorption of toluene

$$\text{Tol·s} \quad \rightleftharpoons \quad \text{Tol} + \text{s} \tag{2.11}$$
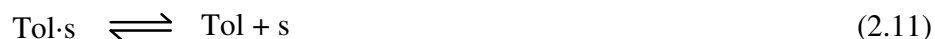
In order to avoid the confusion when interpreting the form of the equation, Eq. 2.8, it is important to mention that the third step, Eq. 2.11 — desorption of the toluene — was not proposed as the rate-controlling step. The activation energy was found to be 51.9 kJ/mol. The lower apparent value of activation energy was postulated to be the result of increased toluene inhibition with increasing temperature. This kind of inhibition was also observed by Jossens and Petersen [1982a, 1982b, 1982c]. However, as it was assumed that external and internal diffusion resistances had no effect on the reaction rate, it is worth noting that particle size was large and that diffusion could affect the rate and might well be the reason for the low value of the activation energy [Manser Sonderer, 1992].

In the same group of Jothimurugesan et al. [1985a], Pal et al. [1986] studied the kinetics of MCH dehydrogenation in the same reactor with the same catalyst, however, under integral conditions. The experiments were performed in the temperature range of 325–400 °C, W/F_{A0} of 1.8×10^4–9.0×10^4 s·g-cat/mol-MCH, H_2/MCH ratio of 3.0 and at 1.013 bar. Initial rates of the reaction were used to analyse the kinetics of the main reaction. Similar to Jothimurugesan et al. [1985a], the kinetic data was subjected to LHHW single- and dual-sites surface mechanisms and the same kinetic expression was found appropriate in their work. The energy of activation was found to be 56.4 kJ/mol compared with 51.9 kJ/mol for Jothimurugesan et al. [1985a].

Another detailed kinetic studied was carried out by Van Trimpont et al. [1986] at higher pressures compared to Jothimurugesan et al. [1985a] who worked at atmospheric pressure. They studied two commercial catalysts, one monometallic sulphided Pt/Al$_2$O$_3$ catalyst with 0.59 wt% Pt and 0.67 wt% Cl contents and the other a bimetallic pre-sulphided Pt-Re/Al$_2$O$_3$ catalyst with 0.3 wt% Pt, 0.31 wt% Re and 0.95 wt% Cl. The catalyst particle sizes were remained less than 0.4 mm. The experiments were performed in a tubular reactor in the temperature range of 309–446

°C, hydrogen partial pressure of 4.0−20 bar and MCH partial pressure of 0.15−1.5 bar. Some experiments were performed with the addition of toluene and n-heptane in the feed to investigate their competing effects. In most of the experiments, conversions were limited to less than 15%. The study revealed in the case of the Pt/Al$_2$O$_3$ catalyst, an increase in hydrogen partial pressure decreased the rate of dehydrogenation. However, for the Pt-Re/Al$_2$O$_3$ catalyst at 0.5 bar MCH pressure, an increase in the partial pressure of hydrogen had no effect on the dehydrogenation rate. A shift of the rate-determining step was put forward as the reason for the different responses to the hydrogen partial pressure. In contrast to Jothimurugesan et al. [1985a], an improved rate of dehydrogenation was observed on the Pt/Al$_2$O$_3$ catalyst compared with the Pt-Re/Al$_2$O$_3$ catalyst. For Pt/Al$_2$O$_3$, n-heptane and not toluene was found to compete for the reaction sites, whereas with Pt-Re/Al$_2$O$_3$ competitive adsorption was observed for both toluene and n-heptane. Greater than 99% selectivity was achieved under most of the reaction conditions. Both power law and LHHW kinetics were fitted to the rate data. Three kinetic schemes were proposed and for each reaction step (rate-controlling), separate rate equations based on LHHW theory were developed and discriminated on the basis of thermodynamics, kinetics and statistical information. Table 2.2 shows the kinetic schemes used in the work of Van Trimpont et al. [1986].

The Scheme-I was based on the elementary steps proposed by Horiuti and Polanyi [1934] for the hydrogenation of ethylene over Ni-containing catalysts. Rather simplified sequences based on dual-site and single-site surface reactions were put forward in the other two kinetic schemes, Scheme-II and Scheme-III, respectively.

For the Pt/Al$_2$O$_3$ catalyst, the following rate expression, based on the second sequence in which conversion of adsorbed methylcyclohexadiene (MCHde) to adsorbed toluene i.e. step-IV of Scheme-II was taken the rate-determining step, was found the most appropriate

$$(-r) = \frac{k \cdot p_A \cdot \left(1 - \dfrac{p_B \cdot p_C^3}{K \cdot p_A}\right)}{p_C^2 \cdot \left(1 + K_A \cdot p_A + K_E \cdot \left(\dfrac{p_A}{p_C^2}\right)\right)^2} \qquad (2.12)$$

63

where, K_E is the surface equilibrium constant for MCHde.

Table 2.2 Kinetic schemes proposed by Van Trimpont et al. [1986]

Scheme-I: Based on Horiuti-Polanyi [1934]	
MCH + s $\rightleftharpoons$ MCH·s	(I)
MCH·s + s $\rightleftharpoons$ MCH1·s + H·s	(II)
MCH1·s + s $\rightleftharpoons$ MCHe·s + H·s	(III)
MCHe·s + s $\rightleftharpoons$ MCH2·s + H·s	(IV)
MCH2·s + s $\rightleftharpoons$ MCHde·s + H·s	(V)
MCHde·s + s $\rightleftharpoons$ MCH3·s + H·s	(VI)
MCH3·s + s $\rightleftharpoons$ Tol·s + H·s	(VIII)
Tol·s $\rightleftharpoons$ Tol + s	(IX)
2 H·s $\rightleftharpoons$ H_2 + 2 s	(X)
Scheme-II: Based on dual-site surface reaction	
MCH + s $\rightleftharpoons$ MCH·s	(I)
MCH·s + s $\rightleftharpoons$ MCHe·s + H_2·s	(II)
MCHe·s + s $\rightleftharpoons$ MCHde·s + H_2·s	(III)
MCHde·s + s $\rightleftharpoons$ Tol·s + H_2·s	(IV)
Tol·s $\rightleftharpoons$ Tol + s	(V)
H_2·s $\rightleftharpoons$ H_2 + s	(VI)
Scheme-III: Based on single-site surface reaction	
MCH + s $\rightleftharpoons$ MCH·s	(I)
MCH·s $\rightleftharpoons$ MCHe·s + H_2	(II)
MCHe·s $\rightleftharpoons$ MCHde·s + H_2	(III)
MCHde·s $\rightleftharpoons$ Tol·s + H_2	(IV)
Tol·s $\rightleftharpoons$ Tol + s	(V)

For the Pt-Re/Al_2O_3 catalyst, however, the rate expression (Eq. 2.13) was proposed. This is based on the third sequence, in which the formation of adsorbed methylcyclohexene from adsorbed methylcyclohexane (i.e. step-II of the Scheme-III), was the rate-determining step.

$$(-r) = \frac{k \cdot p_A \cdot \left(1 - \dfrac{p_B \cdot p_C^3}{K \cdot p_A}\right)}{1 + K_A \cdot p_A + K_B \cdot p_B + K_H \cdot p_H} \qquad (2.13)$$

where, K_H and p_H are the adsorption equilibrium constant and partial pressure of the n-heptane, respectively.

For the Pt-Re/Al$_2$O$_3$ catalyst the reported activation energy was 181.4 kJ/mol, whereas for the Pt/Al$_2$O$_3$ catalyst, the value was 121.7 kJ/mol which is ~60 kJ/mol less than that of the Pt-Re/Al$_2$O$_3$ catalyst.

Rimensberger [1987] studied the dehydrogenation of methylcyclohexane in a microcontinuous reactor. Two catalysts were employed. One commercial UOP 0.5 wt% (total metal) Pt-Re/γ-Al$_2$O$_3$ (BET surface = 218 m^2/g) and other a 0.66 wt% Pt/graphite (BET surface = 60 m^2/g). Experiments were carried out at 2−10 bar pressure, 277−442 °C and liquid hourly space velocity (LHSV) in the range 1−10 h^{-1} with H$_2$/MCH molar ratio in the range of 10–20. Similar LHHW-type kinetic model as that was proposed by Jothimurugesan et al. [1985a] was considered and, where necessary, was integrated into a mathematical model that included both interphase and intra-particle gradients for both concentration and temperature. Higher activation energy and higher rates were found with the Pt/graphite catalyst. However, commercial catalyst was more stable. Activation energies of 184.3 and 115.6 kJ/mol were found for Pt/graphite and Pt-Re/Al$_2$O$_3$, respectively.

In the same group of Touzani et al. [1984], Chaouki et al. [4] modified the catalyst used by Touzani et al. [1984] to make it more effective towards deactivation. The kinetic model used was the same as that of Touzani et al. [1984] and a comparable activation energy of 116.2 kJ/mol was obtained.

El-Sawi et al. [1989] used crushed honeycomb Pt/Al$_2$O$_3$ catalyst with 0.7 wt% Pt and 0.9 wt% Cl to study the kinetics in a fixed bed reactor at 300−350 °C and atmospheric pressure. The experiments were performed with addition of toluene to the feed. A sequential experimental methodology was applied for model discrimination and improvement of the kinetic parameters. The same kinetic model as that of Jothimurugesan et al. [1985a] was proposed. However, the apparent activation energy of 17.9 kJ/mol was much lower.

Chai and Kawakami [1990] employed three commercial catalysts viz. 0.375 wt% Pt and sulphided and un-sulphided 0.375 wt% Pt-0.375 wt% Re, on γ-Al$_2$O$_3$. The chloride content of the catalysts was reported to be 0.95−1.02 wt%. The

experiments were carried out in a differential fixed bed reactor at atmospheric pressure. Nitrogen was used as a diluent to adjust the molar ratios of the reactants. For all the catalyst the rate of dehydrogenation decreased with an increase in hydrogen partial pressure and increased with an increase in the partial pressure of methylcyclohexane. Unlike Jothimurugesan et al. [1985a], who found no effect of Re, the presence of Re lowered the rate of reaction. A small amount of methylcyclohexene was found in the reaction products. A single-site mechanism, similar to that proposed by Van Trimpont et al. [1986] (Scheme-III in Table 2.1) was put forward. The dehydrogenation of methylcyclohexene to methylcyclohexadiene was proposed as the rate-controlling step.

$$(r_B)_0 = \frac{k \cdot K_A \cdot K_D \cdot p_A}{p_C \cdot \left(1 + K_A \cdot p_A + \dfrac{K_A \cdot K_D \cdot p_A}{p_C} + \dfrac{K_A \cdot K_D \cdot K_E \cdot p_A}{p_C^2}\right)} \qquad (2.14)$$

where, K_D is the surface equilibrium constant for MCHe.

Manser Sonderer [1992] studied the two commercial catalysts, namely Pt-Re/Al$_2$O$_3$ and Pt-S/Al$_2$O$_3$. The activation energy was found to be 116.0 and 200.0 kJ/mol, respectively, for the above catalysts. Two kinetic models were observed to fit the experimental data with similar accuracy. One was based on a power law model including reversibility terms and the other was a Langmuir-Hinshelwood-Hougen-Watson model similar to that employed by Jothimurugesan et al. [1985a] and Rimensberger [1987].

Müller [1995] applied mono- and bi-metallic platinum-(0)-cluster catalysts supported on alumina, titania and graphite to study the dehydrogenation of methylcyclohexane. The N$_2$-BET surface areas for alumina, titania and graphite were 193, 55, and 100 m^2/g, respectively. The series of the catalysts were screened in a micropulse reactor (MPR) at 2 bar and 7 bar pressures and two most effective catalysts, one a commercial sulphided mono-metallic catalyst and the other a monometallic 0.8 wt% Pt over alumina were chosen for further work in a microcontinuous reactor. The monometallic catalyst (0.8 wt% Pt over alumina)

proved to be the most active and selective and the activity decreased in the order alumina > titania >> graphite. First order kinetics were reported.

Maria et al. [1996] used a commercial sulphided Pt-Al$_2$O$_3$ reforming catalyst at two scales of a laboratory set up. The operating variables studied in the reactors were in the range of 3–20 h^{-1} LHSV, 0–10 H$_2$/MCH ratio, 0–3.3 He/MCH ratio, 6.08−16.21 bar overall pressure and 250 °C to 550 °C reaction temperature. The initial kinetic study was undertaken using a differential microreactor and two kinetic models were proposed. First, a two parameter model (Eq. 2.15) using a LHHW single-site surface reaction in which toluene and MCH inhibition were found insignificant and in the second, a reduced form of the above model, in which the hydrogen inhibition term was also discarded and the model reduced to first order kinetics with reversibility. The parameters in both models were found to be Arrhenius temperature dependent and the activation energy in both cases was reported to be 220.7 kJ/mol. To verify the main reaction kinetics, further experiments were performed on a much larger scale (840 times larger in volume) in two fixed bed integral reactors in series. The two-parameter kinetic model developed with the microreactor was combined with a one-dimensional pseudo-homogeneous model considering variations of temperature and composition only in the axial direction. The results of the simulation were found to be in good agreement with the experimental data validating the extended model of the main reaction on the larger scale as well. The reduced model, however, was also found reliable and was preferred in simulation studies. Finally experiments were performed in the same integral reactors in series with severe temperature conditions to study the deactivation levels of the catalyst.

$$(-r) = \frac{k \cdot p_A}{1 + K_C \cdot p_C} \cdot \left(1 - \frac{p_B \cdot p_C^3}{K \cdot p_A}\right) \tag{2.15}$$

Yolcular and Olgun [2008] used a glass tube fixed bed reactor of 2.0 cm diameter. The catalyst used was UOP R-50 commercial sulphided catalyst with 0.25 wt% Pt, 0.25 wt% Re and 0.9 to 1.0 wt% Cl. Experiments were performed at 380 °C, 400 °C, 420 °C and 440 °C and atmospheric pressure under differential conditions. A

simple power law model was fitted to the experimental data. Under all conditions of temperature and MCH partial pressures, the order of the reaction with respect to MCH was negative, which showed that the rate actually decreased with increasing partial pressure of MCH. The results appear anomalous. They might be explained as a result of catalyst deactivation.

The work of Tsakiris [2007] and Alhumaidan [2008] is given in Section 2.4.

2.2.2 Zeolite supported Pt-containing catalysts

In all the above works, alumina was the favoured support for Pt metal catalysts, Corma et al. [1979, 1981], however, studied the dehydrogenation of MCH with a zeolite as the catalyst support, though more cracked products and less dehydrogenation would be expected on zeolites, as a result of the increased acidity. Reactions were carried out over 0.5 wt% Pt over NaY-zeolite. Zeolites are microporous crystalline aluminosilicates and NaY is a sodium form of zeolite-Y (faujasite structure). A typical NaY zeolite contains nearly 13 wt% Na_2O [Sadeghbeigi, 2000]. The reaction was studied in a conventional fixed bed reactor and in the temperature range of 350−390 °C, MCH partial pressures of 0.04 to 1.42 bar and hydrogen partial pressures of 0.72 to 6.87 bar with W/F_{A0} in the range of $5.96 \times 10^2 - 1.57 \times 10^4$ s·g-cat/mol MCH. The liquid products obtained included toluene, methylcyclohexene (MCHe), methylcyclohexadiene (MCHde), dimethylcyclopentane (DMCP) and xylenes. Initial results of kinetic measurements showed the data to follow a surface reaction rate-controlling mechanism of the LHHW type. Both toluene and hydrogen were found to inhibit the reaction rate. Under the conditions of their experimentation, where high hydrogen to MCH ratios were maintained in the feed, the following dual-site surface reaction model was found to fit the data

$$(-r) = \frac{k \cdot K_A \cdot p_A}{(1 + K_C \cdot p_C)^2} \qquad (2.16)$$

The fact that MCHe and traces of MCHde were found in the reaction products led these authors to propose a mechanism that consisted of a series of dehydrogenation steps, as pointed out by Sinfelt et al. [1960], and shown in Fig. 2.2.
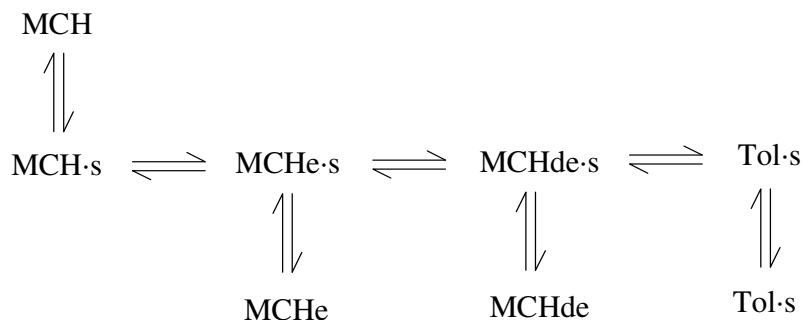
Fig. 2.2 Corma et al.'s [1979] mechanism for the dehydrogenation of MCH.

To check this hypothesis, Corma et al. [1979] carried out experiments with MCHe as the reactant. Upon comparing the initial rates of dehydrogenation of MCH and MCHe it was found that the rate of formation of toluene was 10 times faster when MCHe was the reactant. Combining these observations and the kinetic equation developed earlier (surface reaction rate-controlling), it was concluded that the first dehydrogenation step i.e. formation of MCHe from the adsorbed MCH was the rate-controlling step. Later in the same group, Garcia de la Banda et al. [1986] confirmed the same kinetics while working on the same catalyst, again by comparing the dehydrogenation of MCH and MCHe.

2.3   Structured Pt-containing catalysts

Owing to the highly endothermic nature of the MCH dehydrogenation reaction, large temperature gradients result in the conventional fixed bed reactor. As a result, low average temperatures are achieved and both activity and selectivity may adversely be affected [Tschudin et al., 1999]. In such situations wall-coated catalytic reactors may be used to enhance the heat transfer and to improve the reactor performance [Dalai and Bakhshi, 1992]. Tschudin [1997] utilised such a reactor in which the inside wall of a Fecralloy® tube was coated with $Pt/\gamma-Al_2O_3$. A simple first

order rate law (with respect to MCH), including the reversibility term, was employed and the apparent activation energy was found to be 79.0 kJ/mol.

In the same group of Tschudin [1997], Schildhaur et al. [2001] utilised three reactor tubes in series. The reactor tubes were coated with catalyst on their inside wall surface. The catalyst used was 2.75 wt% Pt/Al$_2$O$_3$. First order kinetics were employed to revise the equilibrium constant experimentally measured by Akyurtlu and Stewart [1978]. The equilibrium constant expression is provided in Section 4.2.3 of Chapter 4. Moreover, Schildhaur [2001] devised a new type of structured metal packing coated with Pt/Al$_2$O$_3$ catalyst. Again, a first order kinetics was presented to represent the experimental data with an activation energy of 149.3 kJ/mol at 300 °C.

In contrast to Tschudin [1997] and Schildhaur [2001], Bustamante et al. [2005] employed an outside coated-catalytic-wall reactor (catalyst coated on the outside of the reactor tube) to study the dehydrogenation reaction on Pt/γ-Al$_2$O$_3$ catalyst with 0.25 wt% Pt loadings. The O.D. of the stainless steel reactor tube was 0.6 cm and its length was 50 cm. The kinetic study was performed at 2 bar and 4 bar pressures and temperatures were maintained at 325 °C and 375 °C. No effect of partial pressure of MCH was observed on the rate of reaction and the order of reaction was proposed to be zero order with respect to methylcyclohexane. An activation energy of 77.5 kJ/mol was found.

2.4   Study at The University of Manchester

Tsakiris [2007] employed five Pt-catalysts, some commercial, to dehydrogenate MCH in a fixed bed 1.12 cm diameter glass reactor under integral conditions. Two internal catalysts were 0.3 wt% and 1.0 wt% Pt over α-Al$_2$O$_3$, while three commercial catalysts were Pt on γ-Al$_2$O$_3$ with 0.1wt%, 0.5 wt% and 1.0wt% Pt content. Experiments were conducted with and without hydrogen in the feed at atmospheric pressure and 340 °C, 360 °C and 380 °C reactor wall temperatures. Comparing two catalysts with the same Pt loading but different alumina supports, the catalyst with γ-Al$_2$O$_3$ as its support was found more active. Out of all the catalysts used, 1.0 wt% Pt/γ-Al$_2$O$_3$ was found most active. The selectivity to toluene was

reported greater than 99.8% for all the above catalysts. The kinetics of the reaction followed a LHHW dual-site surface reaction model, in which the surface reaction (adsorbed MCH to adsorbed toluene) itself was considered as the rate-controlling. Including high surface coverage limits and neglecting reversibility (due to high conversions at atmospheric pressure), the following rate equation was found appropriate for all the catalysts studied

$$(-r) = \frac{k' \cdot p_A}{(p_A + K'_B \cdot p_B + K'_C \cdot p_C)^2} \qquad (2.17)$$

where,

$$k' = \frac{k}{K_A}, \qquad K'_B = \frac{K_B}{K_A}, \qquad K'_C = \frac{K_C}{K_A} \qquad (2.18)$$

An apparent activation energy of ~50.0 kJ/mol was calculated for all the catalysts. This led Tsakiris [2007] to propose the catalytic dehydrogenation to be structure independent. However, the best fit results of the kinetic modelling were obtained with a commercial 0.5 wt% Pt/Al$_2$O$_3$ catalyst with an activation energy of 50.3 kJ/mol.

The results of Tsakiris [2007] with γ-Al$_2$O$_3$ encouraged Alhumaidan [2008] to study both commercial and development catalysts of mono and bimetallic type over γ-Al$_2$O$_3$ support. The commercial catalysts used were 1.0 wt% Pt/γ-Al$_2$O$_3$ and 0.5 wt% Pt/γ-Al$_2$O$_3$, while development catalysts were 0.3 wt% Pt/γ-Al$_2$O$_3$, 1.0 wt% Pt/γ-Al$_2$O$_3$, 0.3 wt% Pt-0.3 wt% Re/γ-Al$_2$O$_3$ (co-impregnation), 0.3 wt% Pt-0.3 wt% Re/γ-Al$_2$O$_3$ (sequential-impregnation) and 0.3 wt% Pt-0.3 wt% Pd/γ-Al$_2$O$_3$ (co-impregnation). Experiments were conducted in a tubular reactor of 1.02 cm I.D. under integral conditions. The temperature, pressure, feed composition and W/F_{A0} were varied between 340–450 °C, 1–9 bar, 0–9 H$_2$/MCH ratio and 3.10×10^4–1.22×10^5 s·g-cat/mol-MCH respectively. A development 0.3 wt% Pt/γ-Al$_2$O$_3$ catalyst showed the highest initial activity, while a commercial 0.5 wt% Pt/γ-Al$_2$O$_3$ showed lowest activity. Most of the experiments were performed using a commercial 1.0 wt% Pt/γ-Al$_2$O$_3$ catalyst and the same catalyst was chosen for kinetic

analysis. Initial rates of reaction were employed to study the kinetics of dehydrogenation. Model equations based on power law kinetics, LHHW dual-site surface reaction and non-competitive Horiuti-Polanyi surface reaction were applied and found un-satisfactory for correlating the entire data. An empirical modification was made by incorporating a total pressure dependence to the hydrogen adsorption equilibrium constant, as shown in Eq. 2.20. This non-Langmuirian-non-competitive-Horiuti-Polanyi model was found to give an excellent fit across a wide range of experimental variables with the minimum number of adjustable parameters.

$$(-r) = \frac{k}{1 + \sqrt{K_C \cdot p_C}} \tag{2.19}$$

$$K_C = K_{Cr} \cdot \left(\frac{p}{9} \right)^c \cdot \exp\left(B_{Cr} \cdot \left(1 - \frac{T_r}{T} \right) \right) \tag{2.20}$$

where, K_{Cr} and B_{Cr} are constants at reference temperature, T_r. The same kinetic equation was applied for all the catalysts and the energy of activation of 55.4 kJ/mol was taken in each fit.

It is important to mention here that both Tsakiris [2007] and Alhumaidan [2008] studied the long term deactivation (up to 600 h) for the catalysts tested in their studies. The 1.0 wt% Pt/γ-Al_2O_3 development catalyst in Alhumaidan's study [2008] showed exceptionally stable characteristics with very high activity and acceptable selectivity.

2.5   Relevance to the present study

The review of the literature has shown that there is a huge disagreement in describing the kinetic mechanism of the dehydrogenation reaction of methylcyclohexane. There is no consensus on the rate-determining step and the inhibition offered by the products. Table 2.2 shows the results of the kinetic treatments undertaken by the different researchers and points out the controversy among their work. In the literature, only Jothimurugesan et al. [1985a] and Van Trimpont et al. [1986] have carried out systematic and detailed kinetic analyses of the dehydrogenation reaction on relatively abundant and wide-ranging experimental data. However, Jothimurugesan et al. [1985a] applied the kinetic analysis to the data only at atmospheric pressure while Van Trimpont et al. [1986] worked at higher pressures, but not at 1 bar. Also, both researchers carried out their experiments under differential conditions and in the presence of hydrogen. For the "on-board" MTH-system, it is expedient to have no hydrogen in the feed and also high conversions (> 80%) are desirable. The present study is designed therefore to conduct a detailed kinetic investigation over a wide range of operating conditions including experiments without hydrogen in the feed for the most promising catalyst developed to date [Alhumaidan, 2008], as mentioned earlier. The kinetic model will be tested in Chapter 6 to predict observed longitudinal temperature profiles (i.e. under non-isothermal, non-adiabatic conditions found in practice). Then, in Chapter 7, a prototype reactor, suitable for "on-board" hydrogen generation, will be designed in detail, incorporating the kinetic model. This reactor model will be used to compare alternative configurations and schemes for "on-board" hydrogen generation.

Chapter 3
Experimental Details

Kinetic experiments for the catalytic dehydrogenation of methylcyclohexane (MCH) and 1-methylcyclohexene (MCHe) were carried out in a vertical fixed bed tubular reactor. 1.0 wt% Pt/Al_2O_3 catalyst was prepared and employed for the kinetic measurements. In the following sections details of the experimental system and methods are provided, together with the catalyst preparation.

3.1 Experimental setup

The dehydrogenation rig was designed and built in the laboratory [Alhumaidan, 2008] and is capable of operating under a wide range of conditions. Table 3.1 indicates the safe ranges for the equipment and Fig. 3.1 shows an actual photograph of the experimental facility. A detailed piping and instrumentation diagram of the unit is, however, shown in Fig. 3.2. The experimental facility may be divided into five main sections for better understanding: the feed section, reactor section, separation section, pressure-controlling section and safety measures.

Table 3.1 Design specifications of the experimental rig

Parameter	Design specifications
Pressure	30 bar
Temperature	650 °C
Liquid flowrate	0−1 ml/min
H_2 flowrate	0−1000 ml/min
N_2 flowrate	0−1000 ml/min
Air flowrate	0−200 ml/min

Fig. 3.1 Actual photograph of the experimental facility.

3.1.1 Feed section

The main parts of the feed section are a liquid feed reservoir, an HPLC pump for injecting the liquid feed, high pressure gas cylinders fitted with pressure regulators and an electronic flowmeter assembly for accurate gas supplies.

Gases to the high pressure unit were provided through high pressure gas cylinders (~180 bar max.). Hydrogen, nitrogen and air were the three gases used in the present work. Each gas cylinder was fitted with pressure regulators that could easily be manipulated to the desired pressure. The necessary flowrate required for each gas was controlled by Brooks electronic flowmeters. The flowmeters were calibrated using a bubble flow meter. At the downstream of the flowmeters, check valves were installed to avoid any flowback that could contaminate the devices. The HPLC (high performance/pressure liquid chromatograph) pump, a pulsating metering pump, was used to pump liquid methylcyclohexane (and in some cases liquid 1-

methylcyclohexene) into the reaction zone. The HPLC pump was calibrated against the absolute difference in weight measured by the digital mass balance. At the suction end of the HPLC pump, there was a feed reservoir placed on a digital balance with sensitivity of 0.01 g. Again a check valve was there at the discharge end of the pump to protect the equipment.
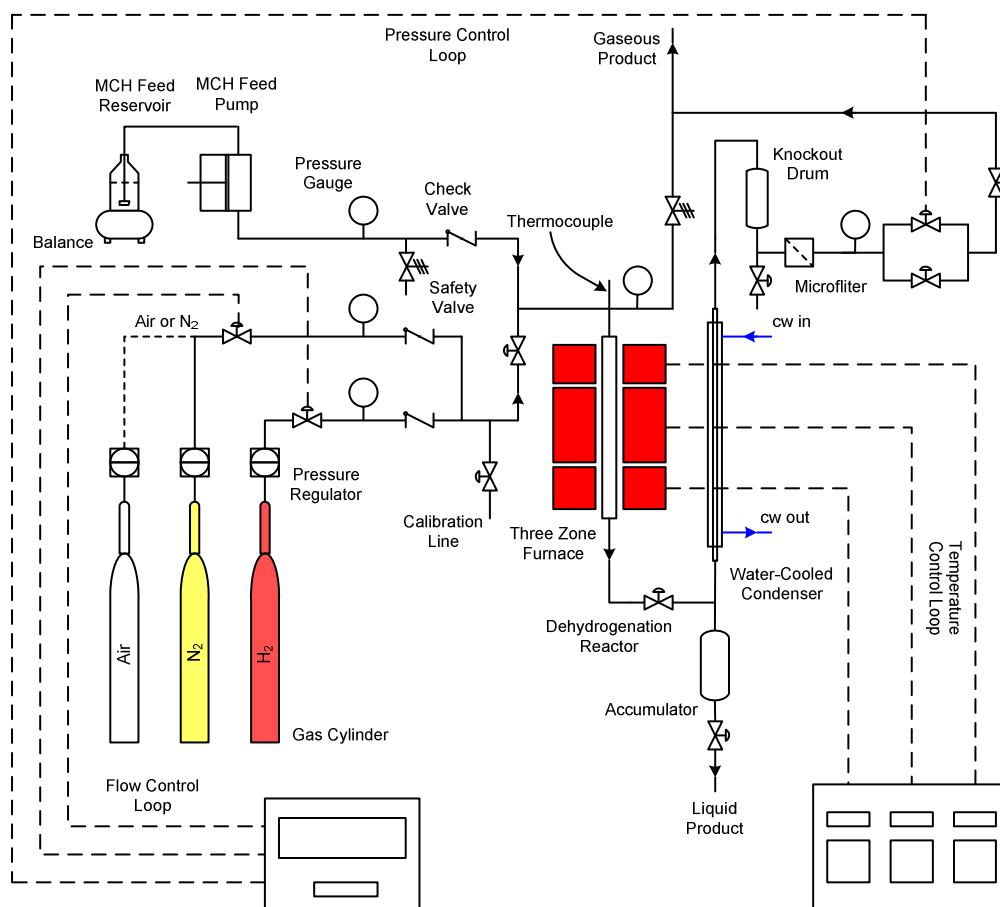
Fig. 3.2 Detailed configuration of the experimental rig.

3.1.2 Reactor section

The heart of the dehydrogenation apparatus was the reactor section. The reactor was designed to operate as a fixed bed reactor with reactants flowing from the top to the bottom. It comprised of a stainless steel tube of 1.02 cm I.D. A concentric ceramic thermowell was installed in the reactor through which a K-type thermocouple was located to measure the axial temperature distribution. The relevant information of the reactor assembly is shown in Table 3.2. The whole reactor assembly was placed within a three zone tubular furnace Carbolite® in order to maintain the required temperatures. Three zones were used to provide better heat distribution along the length of the reactor. Each zone had its own K-type thermocouple and independent separate control panel. However, only the middle zone was programmable, the other two zones being manually controlled. The settings were adjusted so as to obtain an approximately isothermal zone containing the catalyst bed. Quartz wool insulation was used to fill the spaces between the reactor and furnace wall at the top and bottom of the furnace-reactor assembly. The contents of the reactor are described in Section 3.2.1 under the heading "Catalyst loading".

Table 3.2 Reactor specifications for the experimental rig

Description	Specification
Body material	SS-316
Reactor tube length (cm)	66
Reactor bed length (cm)	55
Tube outside diameter (cm)	1.27
Tube inside diameter (cm)	1.02
Tube wall thickness (cm)	0.1245
Thermowell material	Al_2O_3
Thermowell outside diameter (cm)	0.2880–0.3175

3.1.3 Separation section

The condensable organic products leaving the reactor were recovered in a surface condenser of simple double-tube heat exchanger. The hot product gases

passed through the inner metal tube, while cooling water flowed counter-currently through the annulus of the double-tube heat exchanger.

3.1.4 Pressure-controlling section

The products leaving the condenser were passed through a knock-out drum and fine wire-mesh micro-filter (7.0 μm) to avoid any liquid slippage to the pressure control valve. The Brooks pressure control system was employed to maintain the required pressure in the apparatus.

3.1.5 Safety measures

COSHH (control of substances hazardous to health) and risk management forms were prepared and pasted close to the apparatus in order to identify the hazards caused by operating the high pressure rig and the associated chemicals used in the study. The whole rig was placed within a fume-cupboard fitted with a safety glass visor so that product gases and any leakage as a result of malfunction or accident were safely vented. Two pressure relief valves, adjusted to 30 bar, provided additional protection to personnel and equipment in case of excessive pressure build up.

3.2 Experimental method

The experimental method can be categorised into three major operations: loading the catalyst, operating the rig and analyses of the products.

3.2.1 Catalyst loading

The first concern before conducting the actual dehydrogenation reactions was loading of the catalyst particles. The hollow reactor tube was dismantled from the main frame and loaded with catalyst particles and the glass beads. The size of the

glass beads used was 1.0–1.2 mm. Three separate zones of particles were distinguishable, each separated by a thin layer of glass wool. The purpose of the glass wool was to avoid slippage and mixing of the catalyst particles with glass beads. Catalyst was placed in the middle zone in the reactor tube while above and below were the zones of glass beads. The upper zone of glass beads acted not only as a calming zone for uniform mixing and distribution of the reactants but it also worked as a heater-vaporiser-superheater. The bottom zone was employed to reduce the empty volume of the reactor to support the catalyst bed and to retain any fine particles of coke. Fig. 3.3 illustrates the setup of the three zones found in the reactor tubing.
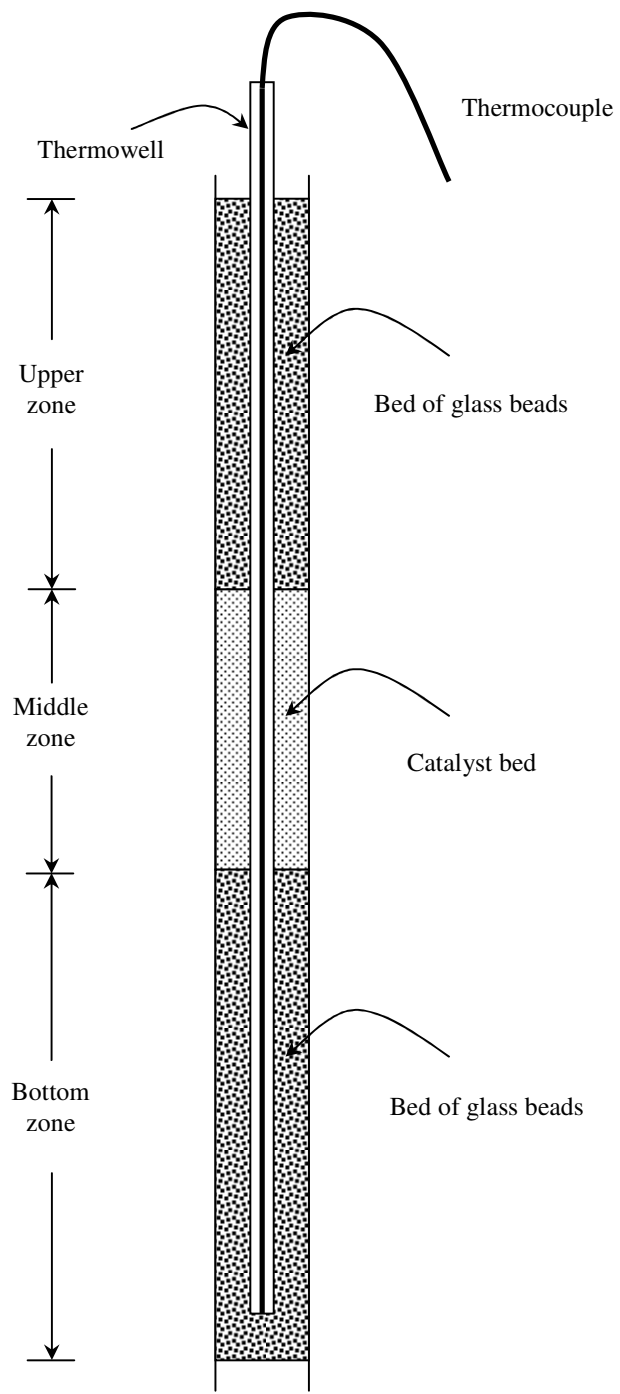
Fig. 3.3 Cross-section of the reactor tube loaded with catalyst particles.

3.2.2 Running the experiments

After successful loading of the catalyst, the experimental system was tested for leaks. The reactor furnace was turned on and the catalyst was calcined in air and reduced under a hydrogen atmosphere. For details of the calcination and reduction methods, see Section 3.3.1.2. The desired temperature, pressure and feed composition were set and the dehydrogenation reaction was initiated. Typically, on a single day, four experimental runs were conducted that constituted a SET (series of experimental targets).The sequence of experimental runs is depicted in Table 3.3. The sequence started with the middle flowrate of reactant (say) MCH (0.25 ml/min) and after the first 30 min of operation the liquid product was collected and sent to waste. In the next 30 min, the axial temperature profile was recorded and at the end of 60 min, the first sample was collected for analysis. The dehydrogenation reaction was continued for the same conditions and again the axial temperature profile was taken and a second sample was collected after a total of 90 min of operation. At this point the MCH flowrate was changed to the lowest value (0.125 ml/min). The same procedure was followed for the next 90 min and then conditions were changed to the highest flowrate (0.50 ml/min) of MCH. The third run finished at the end of a total of 270 min of operation. At the end of the third run the flowrate of MCH was changed back to middle value (0.25 ml/min). This was done to investigate the short term deactivation that occurred during the total time of operation. The last run lasted only for 45 min and the complete SET was ended after a total time of 315 min. At the completion of a SET, the temperature was raised to 450 °C and the catalyst was reduced overnight under a hydrogen flowrate of 100 ml/min in order to recover the activity of the catalyst for the next SET.

Table 3.3 Typical sequence of experiments for one day operation

Status	Start	Waste	Sample	Sample	Waste	Sample	Sample	Waste	Sample	Sample	Waste	Sample (End)	Reduction overnight
Run	R2-30	R2-30	R2-60	R2-90	R1-30	R1-60	R1-90	R3-30	R3-60	R3-90	R2-285	R2-315	
MCH (ml/min)	0.25	0.25	0.25	0.25	0.125	0.125	0.125	0.50	0.50	0.50	0.25	0.25	0
Time (min)	0	30	60	90	120	150	180	210	240	270	285	315	1275

A few experiments deviated from the above sequence, but the procedure for any particular run remained the same, product wastage after 30 min, measuring the axial temperature profile and the sample collection for analysis.

3.2.3   Analyses of the products

The products of reaction were analysed by GC (gas chromatography) and GC-MS (gas chromatography-mass spectrometry). The major products of dehydrogenation were quantified by the Varian 3400 GC containing non-polar capillary column (BP-5: 5% phenyl and 95% dimethylpolysiloxane) equipped with an FID (flame ionisation detector). The by-products of the dehydrogenation reaction were first subjected to qualitative analyses in a GC-MS and then quantified in a GC-FID system. The GC-MS (model-6890N) was from Agilent technologies and contained a non-polar capillary column (HP-5 MS: 5% phenyl and 95% dimethylpolysiloxane). For quantitative analysis of the by-products the above mentioned capillary columns were unable to separate some of the important peaks, so a new fused silica column (CP-Sil PONA CB: 100% dimethylpolysiloxane) was employed with the GC-FID system. Samples with known compositions were prepared and calibration curves were developed to check the GC-system response. Those standards were run time to time to check the variation in the response of the machine.

3.3   Materials used

Methylcyclohexane (MCH) from Sigma-Aldrich (purity 99.0 wt%) was the major liquid chemical (reactant) used. However, some dehydrogenation reactions were carried out using 1-methylcyclohexene (MCHe) of Sigma-Aldrich (purity 97.0 wt%) as the reactant. The physical properties of pure MCH and MCHe are listed in Appendix A. Hydrogen and nitrogen were the gases employed as carriers. Air was used in the catalyst calcination. All the gases were provided by BOC and exceeded the purity of 99.9 mol%.

3.3.1 The dehydrogenation catalyst

1.0 wt% Pt/Al_2O_3 was prepared in the laboratory and employed for carrying out the dehydrogenation reaction. The physical information of the catalyst is provided in Table 3.4.

Table 3.4 Physical information of the catalyst

Catalyst	Development catalyst
Contents	1.0 wt% Pt over Al_2O_3
Type	homogeneous
Shape	broken
Particle size (mm)	0.57

γ-Al_2O_3 extrudates provided by Alfa-Aesar (Johnson-Matthey) were employed as a support material for the preparation of the catalyst. The properties of the support are provided by the supplier and listed in Table 3.5. The extrudates were crushed and then impregnated, with 1.0 wt% Pt from a solution of chloroplatinic acid ($H_2PtCl_6.6H_2O$). Chloroplatinic acid was supplied by Sigma-Aldrich. The Pt-loaded catalyst was then calcined and reduced in-situ prior to carrying out the dehydrogenation reactions. The detailed procedure for the catalyst preparation is given below, followed by the calcination and reduction techniques used in the experimentation.

Table 3.5 Properties of the alumina support

Property	Description
Physical form	extrudates
Extrudates size	1/8 in (3.175 mm)
N_2-BET surface	208 m^2/g
Pore volume	0.58 cm^3/g
Median pore diameter	69 Å

3.3.1.1 Catalyst preparation

The following method of catalyst preparation is based on the work of Alhumaidan [2008], where the detailed discussion on the catalyst preparation may be found. The block diagram in Fig. 3.4 shows the steps that were followed in the preparation of the catalyst. The γ-Al$_2$O$_3$ support was crushed and sieved to 425−710 μm (average 567.5 μm) of random shaped particles. The size of the catalyst so selected was based on an effort to find the intrinsic reaction rate data and in compliance to the findings of the research group (in which the present study is performed) over the years. The ratio of diameter of the reactor to the diameter of the catalyst particle is important. On the one hand, larger diameter particles cause an improper loading, which results in by-passing and channelling of the reactant gases. Also the reaction may become internally "diffusion-limited", which makes the study of the intrinsic reaction kinetics much more difficult. On the other hand, smaller diameter particles, although having no diffusion related problems, are a prime factor in causing intolerable pressure drop in the catalyst bed. Separately, 5.13×10^{-3} mol/L solution of chloroplatinic acid, H$_2$PtCl$_6$.6H$_2$O, was prepared using de-ionised water. 5.0 g of the crushed γ-Al$_2$O$_3$ particles were added to the 50 ml of acid solution and the system was stirred for 15 min. The pH value of the mixture formed was monitored and observed to be equal to 4.2. It is important to mention here that all the catalyst preparation procedure was undertaken in virtual darkness as the concentration of the solution was known to be affected by light [Heise and Schwarz, 1985]. A few drops of 1.0 M HCl solution were added to the mixture and the pH was adjusted to be equal to 2.0. The contents were stirred for 30 min and the pH was again recorded. The reported pH was slightly higher than 4.0. The mixture was left in darkness overnight (~16 h). The mixture was then heated to 70 °C, while gently stirring, allowing the water to evaporate. The remaining wet particles were placed in an oven at 105 °C and left overnight to dry completely. The dried catalyst was pale yellow in colour (due to adsorbed palatinate ions [Heise and Schwarz, 1985]). The catalyst so obtained was screened and if required pelleted to produce the desired size of 425−710 μm (average 567.5 μm).

The zero point of charge (ZPC) or isoelectric point (IEP, the pH value at which the surface electrical charge of Al_2O_3 is null and no Pt metal adsorption takes place [Brunelle, 1978]) of γ-Al_2O_3 is ~8.0 [Heise and Schwarz, 1985; Pinna, 1998]. Below this point γ-Al_2O_3 takes up anion complexes, while above this value it only adsorbs cationic species [Brunelle, 1978; Pinna, 1998]. Moreover, the maximum uptake of Pt metal over γ-Al_2O_3 takes place around pH equal to 4.0 [Burnelle, 1978; Mang et al., 1993]. In the absence of any co-ingredient, such as HCl, the adsorption of Pt is restricted to the external part of the Al_2O_3 and an "egg-shell" catalyst results [Maatman and Prater, 1957; Shyr and Ernst, 1980]. Adding HCl [Pinna, 1998; Maatman, 1959] and decreasing the pH of the solution [Olsbye et al., 1997] is helpful in reducing the rate of approach to the equilibrium, thereby facilitating the deep penetration of the Pt solution into Al_2O_3, producing more uniform Pt distribution.

3.3.1.2 Calcination and reduction

The freshly prepared catalyst, as discussed in the above procedure, was not yet ready for the dehydrogenation study and it was first calcined and then reduced. Both calcination and reduction were done in-situ i.e. within the reactor itself. Calcination was the first step for which 100 ml/min of air was passed over the catalyst and the temperature of the catalyst was raised to 500 °C with a 3.0 °C rise per min. When the temperature reached 500 °C, it was maintained there for 5.0 h. The temperature was then lowered to 450 °C at which the reduction was carried out. The air flow was stopped at that stage and the hydrogen flow was established at 100 ml/min. The reduction of the catalyst was carried out for 16 h at a constant temperature of 450 °C. The temperature of the reactor was then lowered to the reaction temperature and the experimental dehydrogenation study was initiated.

Few drops
of HCl

γ-Al$_2$O$_3$ support → **Mixing** ← H$_2$PtCl$_6$·6H$_2$O solution

Equilibration
(16 h)

Drying
(70 °C)

Oven Drying
(16 h)
T = 105 °C

Pelleting and Sieving
(425–710 µm)

Calcination
(500 °C, 5.0 h)
Air = 100 ml/min

Reduction
(450 °C, 16 h)
H$_2$ = 100 ml/min

Dehydrogenation reaction
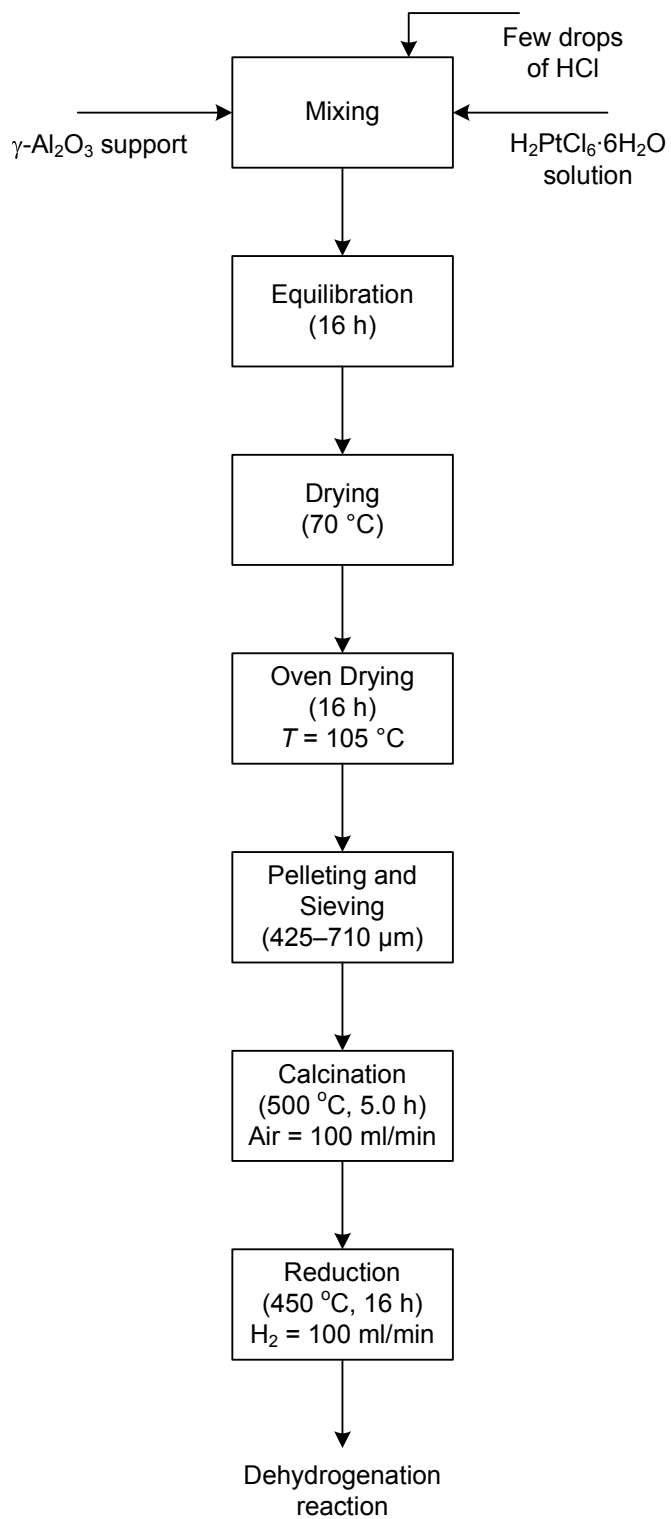
Fig. 3.4 Block diagram for the development catalyst
preparation procedure.

Chapter 4
Kinetic Analysis and Modelling of the Methylcyclohexane Dehydrogenation Reaction

Kinetic modelling of the experimental data is an important tool in understanding the reaction mechanism and developing a model equation that may be applied in the design of a commercial chemical reactor. Knowledge of the reaction mechanism in describing what actually is occurring during the course of a chemical reaction, allows safe extrapolation and optimisation of the reaction variables and helps in the better development and design of a new catalyst and catalytic system [Levenspiel, 1999]. Moreover, if the intrinsic reaction rate model is known any type of reactor may be designed in principle [Smith, 1981]. As mentioned earlier in Chapter 1 and Chapter 2, there is a lot of conflict and disagreement as to the kinetic mechanism proposed in the literature for MCH dehydrogenation. Therefore there arises a need for a detailed and rigorous kinetic analysis of the extensive experimental data. In this chapter, an effort is made to search for the appropriate intrinsic rate model which best describes the extensive data based upon a plausible mechanism of the dehydrogenation reaction. It is later applied to the simulation of the laboratory setup (Chapter 6) and the commercial MTH-reactor (Chapter 7). The model rate expressions based on simple power law kinetics, single-site and dual-site Langmuir-Hinshelwood-Hougen-Watson and competitive and non-competitive Horiuti-Polanyi mechanisms are developed and analysed kinetically and statistically against the laboratory experimental data.

4.1 Grouping of data

The experimental data obtained over the 1.0 wt% Pt/γ-Al$_2$O$_3$ catalyst may be grouped according to the feed composition, pressure and temperature. Table 4.1 shows the manner in which the experimental data is grouped. The data collection in groups is carried out in order to highlight trends in the parameter values and to see the

effects of feed composition on the particular fit for a specified pressure and to signify the effects of pressure itself. Experimental data obtained at relatively high temperature and high flowrates is collected in Group-5159 and was not subjected to the usual procedure of kinetic treatment of the data carried out in the present study. All the inlet mole fractions are specified at 1.013 bar and 298.15 K and the mole fraction of the inert, y_{I0}, is a sum of the mole fractions of N_2 gas in the feed and the 1.0 wt% impurity present in the feed MCH.

Table 4.1 Groups formation for the experimental rate data obtained for the dehydrogenation of MCH over 1.0 wt% Pt/γ-Al$_2$O$_3$ catalyst

Group	N	Feed composition			T_w (K)	p (bar)	$W/F_{A0} \times 10^{-4}$ s.g-cat-/mol
		y_{A0}	y_{C0}	y_{I0}			
11	21	0.106	0.893	0.001	614.2, 634.2, 653.2	1.013	3.11, 6.22, 12.44
21	21	0.485	0.511	0.005	614.2, 634.2, 653.2	1.013	3.11, 6.22, 12.44
31	21	0.990	0	0.010	614.2, 634.2, 653.2	1.013	3.11, 6.22, 12.44
41	21	0.485	0	0.515	614.2, 634.2, 653.2	1.013	3.11, 6.22, 12.44
15	21	0.106	0.893	0.001	614.2, 634.2, 653.2	5.0	3.11, 6.22, 12.44
25	21	0.485	0.511	0.005	614.2, 634.2, 653.2	5.0	3.11, 6.22, 12.44
45	21	0.485	0	0.515	614.2, 634.2, 653.2	5.0	3.11, 6.22, 12.44
19	21	0.106	0.893	0.001	614.2, 634.2, 653.2	9.0	3.11, 6.22, 12.44
29	21	0.485	0.511	0.005	614.2, 634.2, 653.2	9.0	3.11, 6.22, 12.44
49	21	0.485	0	0.515	614.2, 634.2, 653.2	9.0	3.11, 6.22, 12.44
5159	29	0.785, 0.876, 0.990	0	0.010, 0.124, 0.215	653.2, 673.2, 693.2, 713.2, 733.2	1.013, 5.0, 9	1.55, 2.22, 3.11

4.2 Basic expressions applied in kinetic modelling

Below are the basic expressions that were employed in carrying out the kinetic analysis of the experimental data.

4.2.1 Mole balance, the reactor performance equation

A mole balance for MCH over a differential mass of catalyst bed dW gives

$$\frac{F_{A0} \cdot dX}{dW} = (-r) \tag{4.1}$$

or $\quad \dfrac{dX}{d\left(\dfrac{W}{F_{A0}}\right)} = (-r)$ \hfill (4.2)

Eq. (4.2) is a differential form of the one-dimensional pseudo-homogeneous model for the catalytic plug flow reactor.

Upon integrating between limits when $X = 0$ at $\dfrac{W}{F_{A0}} = 0$ and $X = X$ at $\dfrac{W}{F_{A0}} = \dfrac{W}{F_{A0}}$, it

may be shown that

$$\frac{W}{F_{A0}} = \int_{0}^{X} \frac{dX}{(-r)} \tag{4.3}$$

Eq. 4.2 and Eq. 4.3 may be applied to calculate the values of X at any given values of $\dfrac{W}{F_{A0}}$ or vice-versa, provided the quantity $(-r)$ is available in terms of X and the integral on the right hand side of Eq. 4.3 is executable.

4.2.2   Stoichiometric mole fractions

The dehydrogenation reaction was found highly selective (selectivity generally greater than 98.2 %) with toluene and hydrogen as the only main dehydrogenated products. In the light of the above statement, the kinetic modelling was performed for the principal reaction, Eq. 4.4, only. From the overall stoichiometry of the principal reaction and assuming ideal gas behaviour, the mole fraction of components may be expressed in terms of the MCH conversion, X, as given in Table 4.2.

$$\text{MCH} \quad \rightleftharpoons \quad \text{Tol} + 3\text{H}_2 \tag{4.4}$$

Table 4.2 Mole fractions in the vapour at conversion X

Component	Representation	Mole fraction
MCH	A	$\dfrac{y_{A0} \cdot (1-X)}{1 + 3 \cdot y_{A0} \cdot X}$
Tol	B	$\dfrac{y_{B0} + y_{A0} \cdot X}{1 + 3 \cdot y_{A0} \cdot X}$
H_2	C	$\dfrac{y_{C0} + 3 \cdot y_{A0} \cdot X}{1 + 3 \cdot y_{A0} \cdot X}$
Inert	I	$\dfrac{y_{I0}}{1 + 3 \cdot y_{A0} \cdot X}$

Again in Table 4.2, the mole fraction y_{I0} includes both the MCH impurities and N_2 gas in the feed.

4.2.3 Equilibrium constant and equilibrium approach factor

The value of K was recently revised by Schildhauer and co-workers [2001] to

$$K = 3600 \cdot \exp\left(\frac{-217650}{R}\left(\frac{1}{T} - \frac{1}{650}\right)\right) \tag{4.5}$$

with K in bar^3, R in J·mol^{-1}·K^{-1}, and T in K.

The data obtained in the present study was obtained under integral conditions and necessitated introduction of the reaction reversibility expressed by the equilibrium approach factor, e, in the kinetic models proposed. The reversibility may be written as

$$e = 1 - \frac{p_B \cdot p_C^3}{K \cdot p_A} \tag{4.6}$$

For an essentially irreversible process the equilibrium approach factor must have a value equal to unity.

4.2.4 Rate constant and dimensionless activation energy

The rate constant k is assumed to follow the Arrhenius temperature dependency and may be written as follows

$$k = k_0 \cdot \exp\left(\frac{-E}{R \cdot T}\right) \tag{4.7}$$

However, reparameterising the rate constant in terms of k_r (k at the reference temperature, T_r), to reduce the correlation among the parameters and to converge the solution more rapidly as proposed by Kittrell [1970], Eq. 4.7 may be written as

$$k = k_r \cdot \exp\left(B \cdot \left(1 - \frac{T_r}{T}\right)\right) \tag{4.8}$$

The reference temperature, T_r, is the temperature at the centre of the experimental temperatures obtained in this study and is equal to 617.2 K.

The term B in Eq. 4.8 is called the dimensionless activation energy and is given by the expression

$$B = \frac{E}{R \cdot T_r} \tag{4.9}$$

k_r and B are therefore among the kinetic parameters that are to be fitted.

It is important to mention here the calculation of the average bed temperatures used in ensuing kinetic analyses. Owing to the endothermic nature of the reaction and due to the thermal resistance in the catalyst bed, the centre-line temperatures as measured by the vertically sliding thermocouple were different from the reactor wall temperatures (temperatures measured under no reaction conditions) maintained by the three zone electric furnace. For the purpose of kinetic analysis, the average bed

temperatures were calculated using the following formula assuming a parabolic temperature distribution in the radial direction

$$T = \frac{1}{N} \cdot \sum_{i=1}^{i=N} \left(\frac{T_{z,i} + T_w}{2} \right)$$ (4.10)

where, $T_{z,i}$ is the temperature at the *ith* axial position at the centreline in the catalyst bed, T_w is the reactor wall temperature and N is the number of axial temperature measurements. Fig. 4.1 shows the reactor wall temperature, measured reactor centreline temperatures, local average temperatures, T_{ave}, of the above two values and the overall average catalyst bed temperature, T, calculated using Eq. 4.10 for a specified set of reaction conditions.
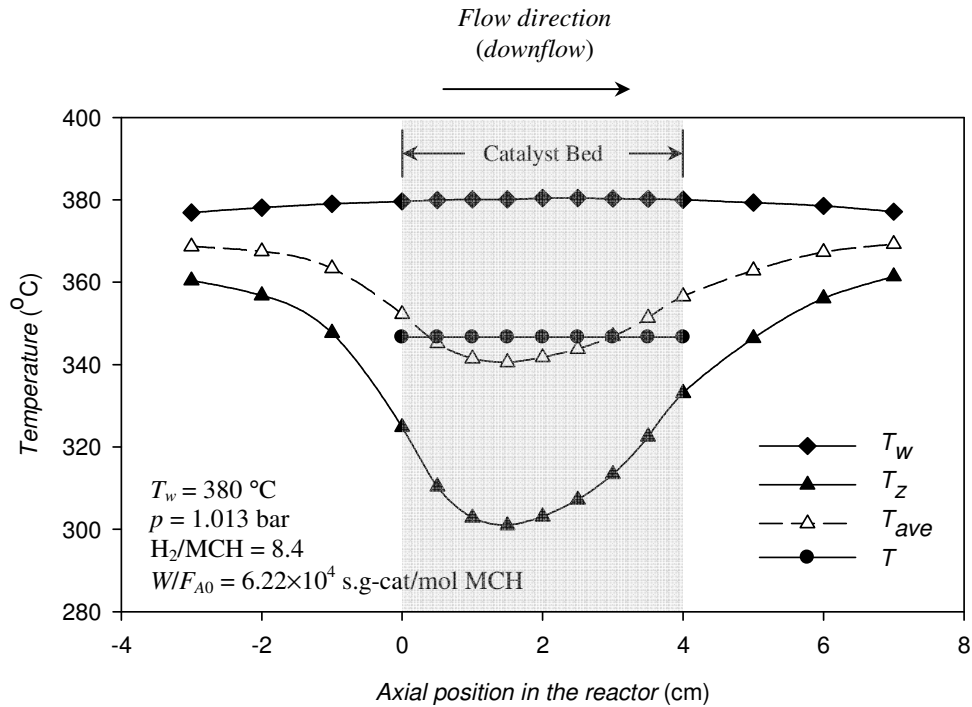
Fig. 4.1 A typical set of temperature profiles in the dehydrogenation reactor, T_w = reactor wall temperature; T_z = measured centerline temperatures in the reactor; T_{ave} = local average temperatures between the above two values and T = overall average catalyst bed temperature.

4.2.5   Catalyst deactivation constant

As mentioned in Section 2.2.2, Run R2-315 is a repeat of earlier Runs R2-60 and R2-90. Inspection shows a loss in conversion over the intervening period. However, this "short term" catalyst deactivation may be reversed overnight by exposing the catalyst to a stream of hydrogen at an elevated temperature. To account for such reversible deactivation, it is suggested that the rate of reaction falls linearly with the daily time "online" (t_d). See Section 7.8.3.5. Thus,

$$(-r) = (-r)_0 \cdot (1 - k_d \cdot t_d) \tag{4.11}$$

where, k_d is an apparent "short term" deactivation rate constant. One might expect k_d to depend upon temperature, pressure and composition and k_d becomes an additional fitting parameter.

4.3   Regression procedure and parameter estimation

The regression of the kinetic data for any particular kinetic model was carried out using a FORTRAN code named RKPES. The RKPES routine was based on the modified Marquardt algorithm and applied the 4th order Runge-Kutta method to solve the integral in Eq. 4.3. Further details on the software along with a simple illustration are provided in Appendix B. However, an interested reader is advised to follow the detailed manual of the RKPES code [Klaus, 1981b]. The kinetic model equation and the experimental kinetic data were fed to the RKPES solver and the initial values of the parameters were provided. During the execution of the program the program tried to minimise the following objective function, the sum of squares of the errors (SSE)

$$Obj. fn. = \text{SSE} = \sum_{i=1}^{i=N} (X_{obs,i} - X_{mod,i})^2 \tag{4.12}$$

where, $X_{obs,i}$ is the *ith* measured or observed value of conversion, $X_{mod,i}$ is the corresponding value calculated from the particular kinetic model and *N* is the total number of data points. At the end of the execution, the program generated two files namely FORT.3 and FORT.4, the contents of which were able to be exported to the Microsoft® Excel worksheet. The former contained the best-fit values of the parameters of the model, the standard deviations of the parameters, the parameter t-values and 95% confidence limits of each parameter. Moreover, it contained the correlation matrix of the parameters and the plot of residuals (the difference between the observed and actual values of conversion). The latter file contained the values of both observed and model conversions. Once the program output appeared, the parameters were assessed for their significance. The t-values, the ratio of the parameter value to the standard deviation were expected to be greater than 3.0 [Manser Sonderer, 1992]. If the 95% confidence interval of any parameter included zero, that parameter was set zero in the kinetic equation for the next regression. The model Adj(R^2) and F-statistics were not part of the program output and were calculated separately. The statistical equations applied for the determination of model Adj(R^2) and F-value are provided in Appendix C. The model F-value was made the base criterion for comparison of the significance of the different kinetic equations.

4.4 Power law kinetics

For heterogeneous catalytic reactions, the empirical power law model may be a useful tool in providing clues that lead to a more appropriate model. However, it should not be extrapolated beyond the experimental range of the data [Hill, 1977].

A simple power law model may be written as

$$(-r) = k \cdot \left(p_A - \frac{p_B \cdot p_C^3}{K} \right)^n \tag{4.13}$$

Introducing deactivation kinetics from Eq. 4.11

$$(-r) = k \cdot \left(p_A - \frac{p_B \cdot p_C^3}{K} \right)^n \cdot (1 - k_d \cdot t_d) \qquad (4.14)$$

where,

$$k = k_r \cdot \exp\left(B \cdot \left(1 - \frac{T_r}{T} \right) \right), \text{ and} \qquad (4.8)$$

$$B = \frac{E}{R \cdot T_r} \qquad (4.9)$$

Substituting Eq. 4.13 into the performance equation, Eq. 4.2, it may be shown that

$$\frac{dX}{dY} = (-r) \times 10^5 = k \times 10^5 \cdot \left(p_A - \frac{p_B \cdot p_C^3}{K} \right)^n \cdot (1 - k_d \cdot t_d) \qquad (4.15)$$

where,

$$Y = 10^{-5} \times \frac{W}{F_{A0}} \qquad (4.16)$$

The equation 4.15 was used with the RKPES solver and was fitted against the experimental kinetic data. Four kinetic variables n, k_r, B and k_d were jointly estimated.

4.4.1 Discussion of the power law model

For the power law model both the experimental data in the individual groups as shown in Table 4.1, and the overall experimental data were subjected to regression for the best-fit kinetic parameters. Table 4.3 provides the parameter values and overall statistics obtained during the regression of the data in the individual groups. Detailed regression results for the individual groups are, however, provided in Table D.1 to Table D.3 in Appendix D. Fig. 4.2 to Fig. 4.4, on the other hand, are scatter diagrams to provide a relationship between the measured values of conversion, X_{obs}, and model values, X_{mod}, to visualise the goodness of the fit. A graphical version of the effect of pressure and composition on the parameters obtained is depicted in Fig. 4.5

to Fig. 4.7. The results of power law regression for the overall data are presented in Table 4.4 and Fig. 4.8.

4.4.1.1   1.013 bar pressure

It is obvious that each individual group is relatively better fitted at 1 bar by the simple power law model giving SSE values always less than 0.00989 and the corresponding values of $Adj(R^2)$ not less than 0.983. Moreover, the residuals obtained are also randomly distributed and no specific trend is found in the scatter plots as shown in Fig 4.2 (a–d).

Table 4.3 Results of power law regression for the data in individual groups

Group	n $-$	E (kJ·mol^{-1})	$(-r)_0 \times 10^5$ (mol MCH·g-cat^{-1}·s^{-1})	k_d day^{-1}	SSE	$Adj(R^2)$	F
11	0.99	54.55	4.14	1.35	0.00519	0.992	834.16
21	0.78	58.83	8.00	1.68	0.00989	0.983	401.26
31	0.71	54.55	8.29	1.75	0.00831	0.986	507.20
41	0.69	53.37	4.09	1.67	0.00648	0.991	810.32
15	1.51	138.66	0.30	0.69	0.00545	0.992	866.48
25	1.21	117.15	0.76	1.21	0.00682	0.989	636.61
45	0.98	83.04	1.27	1.67	0.00247	0.996	1840.93
19	1.30	93.70	0.08	0.81	0.00213	0.995	1482.03
29	1.29	119.52	0.15	0.99	0.00255	0.995	1317.22
49	1.20	85.39	0.38	2.01	0.00378	0.992	922.44
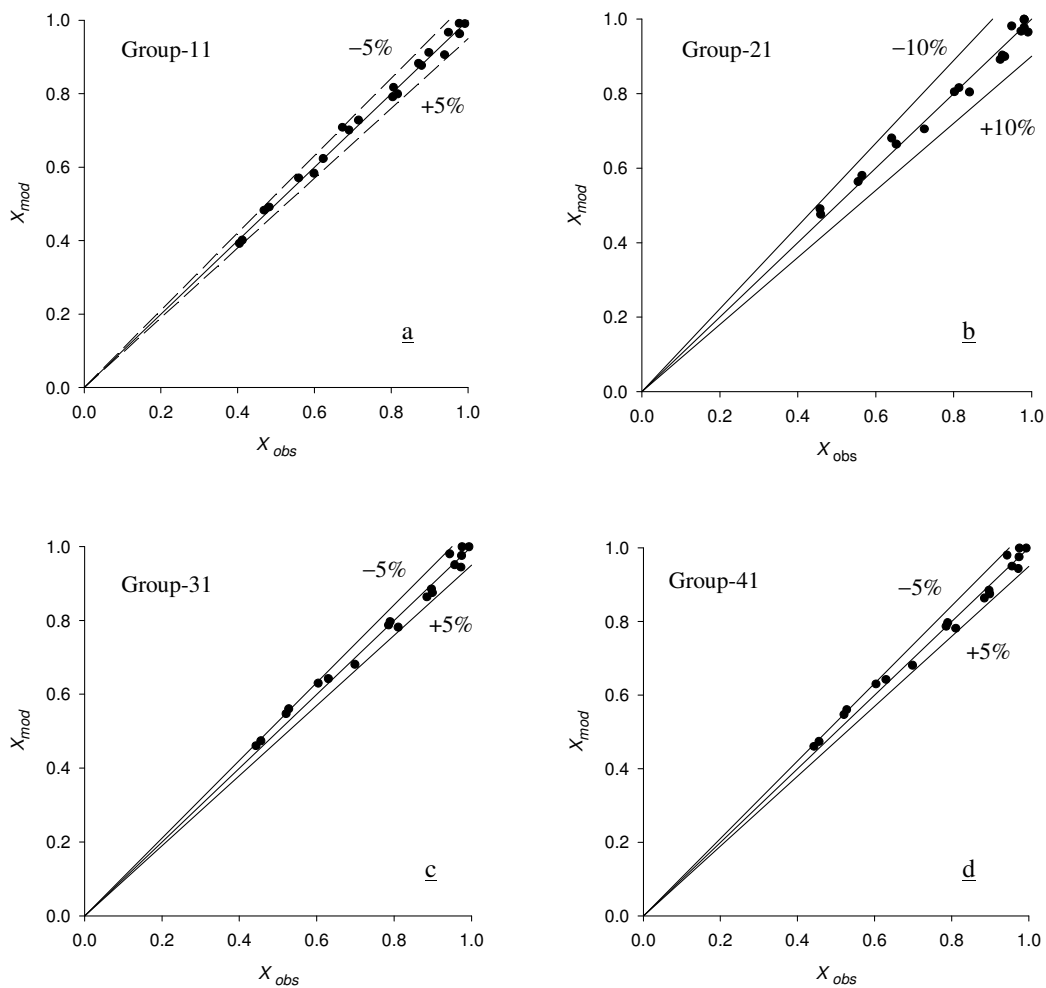
Fig. 4.2 (a–d) Scatter diagrams for the power law model relating observed and model values of conversions at 1.013 bar.

Inspecting orders of the reaction for the individual groups fitted, it is apparent that the order of the reaction decreases from Group-11 to Group-21 and then remains virtually the same for Group-31 and Group-41. This observation is crucial in explaining the fact that the concentration of hydrogen and not the MCH concentration in the feed is responsible for change in the order of the reaction. The highest value of the order of the reaction occurs is the result for Group-11 in which the concentration of hydrogen is the maximum, that is almost 89 mol% in the feed. A comparison of the results for Group-21 and Group-41 allows a direct assessment of the effects of replacing H_2 with N_2 in the feed, while maintaining a constant partial pressure of

MCH. Calculating initial rates at $T = T_r = 617.2$ K, the initial rate of the reaction decreases from 8.0×10^{-5} to 4.09×10^{-5} mol·g-cat^{-1}·s^{-1} on replacing H_2 by N_2. This observation should not be a result of irreversible loss of activity, since the periodic activity test showed no long term activity loss. These observations suggest that H_2, a product of the reaction, appears to act as a promoter, and has a positive effect towards the kinetics of the reaction, at least at 1 bar. The observation may be explained on the basis of relatively higher toluene inhibition under the conditions when no hydrogen is in the feed. This same promotion in the presence of H_2 and toluene inhibition at 1 bar was also observed by other researchers in the field [Jossens and Petersen, 1982b; Rohrer and Sinfelt, 1962]. A reaction order close to unity for Group-11 suggests a low MCH coverage. However, a decrease in the order of the reaction with decreasing H_2 in the feed suggests an increase in coverage of MCH. Combining the above statements it is concluded that the presence of H_2 may be helpful in replacing the strongly adsorbed products species, which otherwise cover the active surface. The activation energy parameter, B, remains more or less the same, and the apparent activation energy lies within 53.4 to 58.8 kJ/mol. A wide range of apparent activation energies is reported in the literature (see the review in Chapter 2). The values given above tend to be towards the bottom of the range. The deactivation rate constant, k_d, was always significant, confirming the importance of including the short term deactivation.

4.4.1.2   5 bar pressure

Also at $p = 5$ bar, individual groups are fitted very well. It is apparent for Groups-15 and -25 in Table 4.3 that $n > 1$. This seems unlikely on physical grounds. However, the manifestation of an apparent order $n > 1$ can be reconciled with strong chemisorption of one or both of the reaction products toluene or hydrogen, or of reaction intermediates, such as methylcyclohexenes or methylcyclohexadienes. The former intermediate, methylcyclohexene, was observed in low concentrations in the condensate, corresponding to intermediate levels of conversion of methylcyclohexane. Methylcyclohexadienes, on the other hand, have never been observed. This is not to

say, however, that they are not formed on the catalyst surface. It is obvious that the apparent order n is significantly greater at 5 bar than at 1 bar, when hydrogen is in the feed. LHHW postulates, on the other hand, predict a decreasing apparent order n with increasing pressure, consistent with an increasing surface coverage of methylcyclohexane.

The values of the activation energy are considerably higher for Group-15 and Group-25. This shows that pressure has a significant effect on the activation energy of the reaction when H_2 is present in the feed. Comparing Group-25 and Group-45, in contrast to 1 bar results, no promotion of hydrogen is observed. The initial rate of reaction, $(-r_0) \times 10^5$, is reduced by up to an order of magnitude on increasing the pressure from 1 bar to 5 bar, which suggests strong product retarding effects. On average, the value of the deactivation constant, k_d, is less than that for 1 bar and especially for Group-15 (highest hydrogen feed concentration) where, as shown in Table D.3 the 95% confidence interval involves zero suggesting the parameter k_d becomes insignificant.
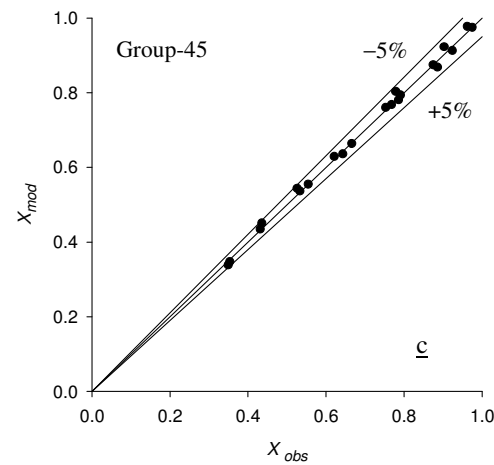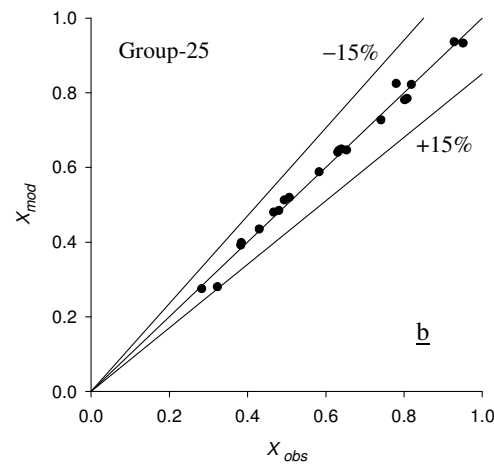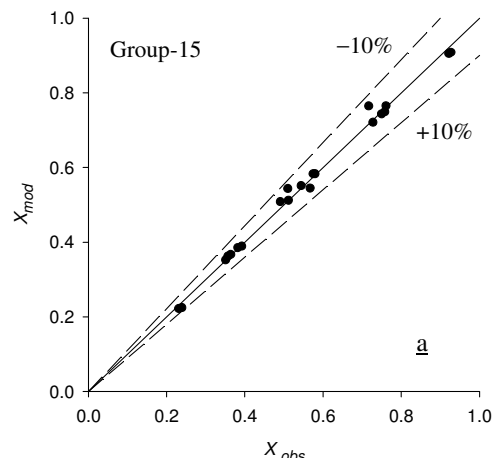
Fig. 4.3 (a–c) Scatter diagrams for power law
model relating observed and model values of
conversions at 5 bar.

4.4.1.3   9 bar Pressure

In all the cases at 9 bar, an extremely good individual group fit of the data is found with $Adj(R^2) > 0.99$. Similar to the results at 1 bar and 5 bar, the power law model parameters appear to be group dependent. The value of n remains virtually the same in Group-19, -29, and -49; a slight increase, however, is noticeable in the groups containing H_2. The same observation is observed at 5 bar, however, with a greater variation. The order of the reaction $n > 1.0$ can be described in the same as explained previously. The activation energy is found to be quite high, greater than 85 kJ/mol in all the individual group listings. Comparing, Group-29 and -49, an increased initial rate and lower activation energy is observed for Group-49. Similarly a low value of the deactivation constant (k_d) is observed when hydrogen is in the feed, which confirms the beneficial effects of hydrogen in maintaining the catalyst activity. A high value of the deactivation constant (k_d) in the absence of hydrogen may be explained on the basis of the formation of unsaturated intermediates which act as coke-precursors.

In conclusion, at each pressure, parameters are found group dependent. This is summarised graphically in Fig. 4.5 to Fig. 4.7. When H_2 is in the feed both apparent order of the reaction and apparent activation energy have increased values at high pressures. Actually for higher concentration of hydrogen in the feed these pass through a maximum and then fall back, while for lower hydrogen feed concentration the values increase and then remain almost same. An increased value of activation energy provides the clue of some strongly adsorbed components that require higher activation energies of desorption to desorb into the gas phase. A higher order of the reaction, greater than unity, at increased pressure somewhat confirms this hypothesis. The initial rates of reaction at $T = T_r = 617.2$ K tend to decrease with pressure for all the groups. This kind of behaviour is less common, though it is compatible with an LHHW dual-site kinetic model. The effect of hydrogen at higher pressures, (say) 9 bar, seems to be vanishing as values of parameters somehow approach each other.
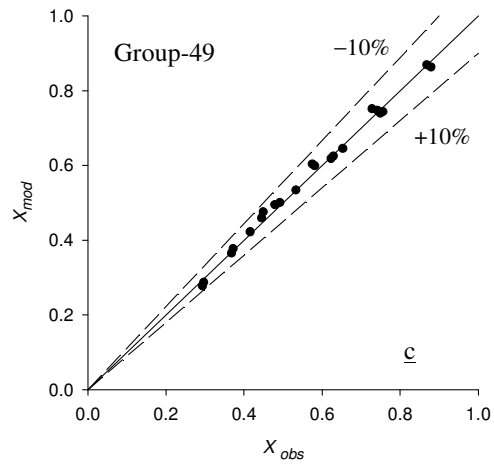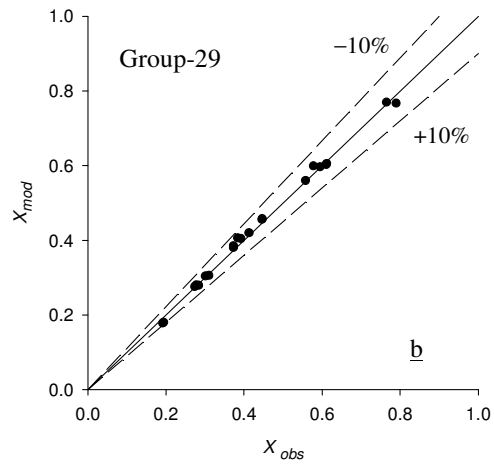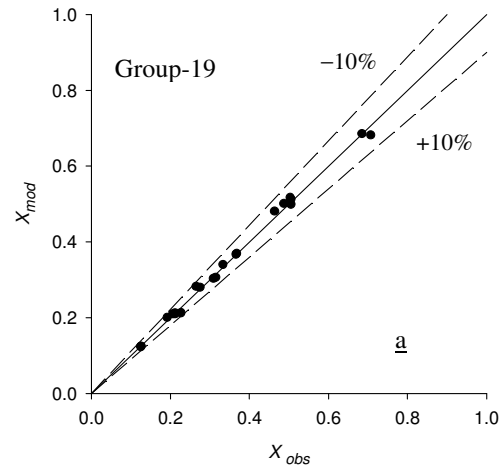
Fig. 4.4 (a–c) Scatter diagrams for power law model relating observed and model values of conversions at 9 bar.

Comparing, Group-2 at different pressures, it is observed that at low pressures, a promotion of H_2 is observed as mentioned earlier, however, at increased pressure values, in fact, H_2 adversely effects the rate which may be manifested that reversible reaction is important at higher pressures than at 1 bar or the excess H_2 in the feed may be involved in the associative adsorption of some products species which otherwise are gaseous products. Another possibility that at high pressures hydrogen may be competing for the active adsorption sites and therefore lowering the rates of the reaction may not be ruled out. This effect of hydrogen observed to be more pronounced at 5 bar than at 9 bar.

In the overall discussion, the partial pressures of hydrogen and MCH and adsorption of MCH are found important contributors at low pressures (1 bar), while partial pressures of H_2 and adsorption of hydrogen and other major product (toluene) are found important at higher pressures with adsorption of hydrogen less pronounced. This suggests a kinetic equation that includes the effects of partial pressure of MCH and hydrogen and adsorption kinetics of MCH, hydrogen and toluene. As with pressures, the initial rates are decreased non-linearly, so need is there for a term in the denominator that constitutes product of square or cube of the partial pressure of hydrogen (non-linear dependence of hydrogen partial pressure) and some parameter representing adsorption kinetics of at least one of the major products other than hydrogen, i.e. toluene.
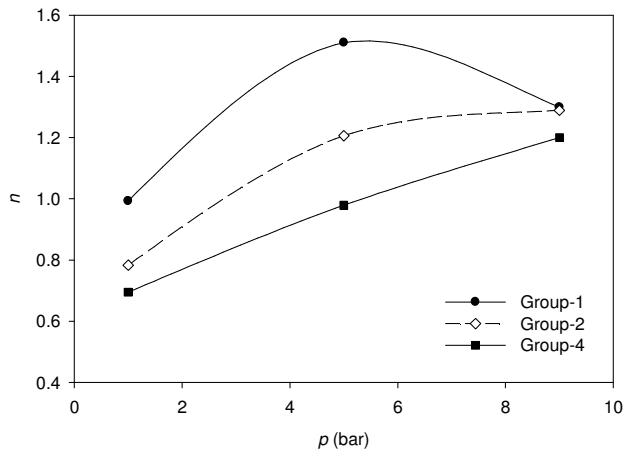
Fig 4.5 Effect of pressure on the order of the reaction for
the power law model kinetics.
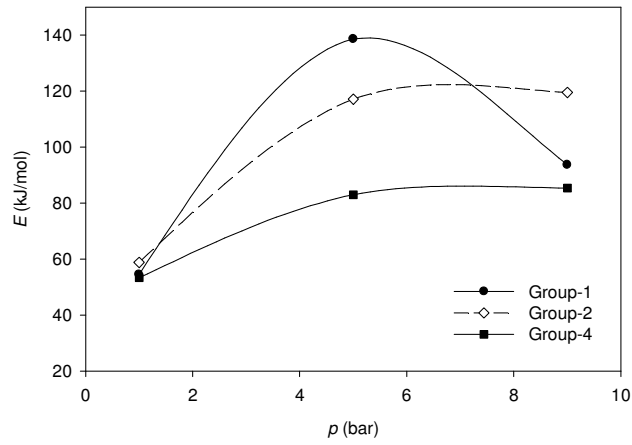
Fig 4.6 Effect of pressure on the activation energy of the
reaction for the power law model kinetics.
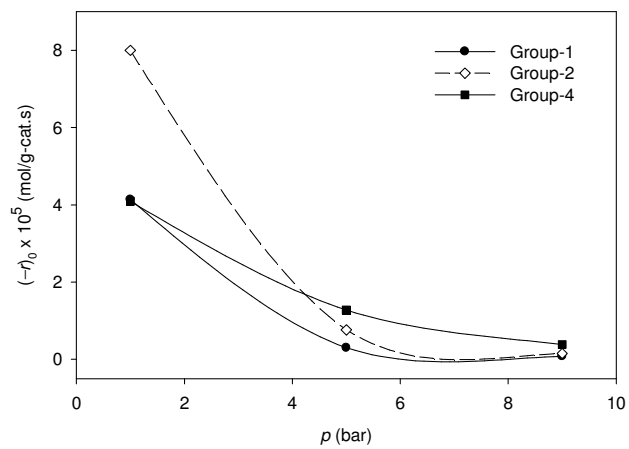
Fig 4.7 Effect of pressure on the initial rate of the
reaction for the power law model kinetics.

105

4.4.1.4 Overall Data

All the data at 1.013 bar, 5 bar and 9 bar, except the data in Group-5159, was pooled and fitted by the power law model. Table 4.4 and Fig. 4.8 show the results. Poor fitting results were obtained, as shown by a very high value of SSE and a large deviation of the model conversion values from the observed values of conversion in Fig. 4.8.

For power law model to be practically useful the values of the parameters k_r, B and n should not vary from group to group i.e. should not be composition dependent. This is clearly not the case here. However, the exercise has been useful in providing clues as to a more formal kinetic treatment based upon LHHW (Langmuir-Hinshelwood-Hougen-Watson) mechanistic models in which reaction products such as toluene and hydrogen or intermediates, such as methylcyclohexenes or methylcyclohexadienes, may be acting as inhibitor.

Table 4.4 Results of regression for the power law with overall data

Kinetic model

$$(-r) = k \cdot \left(p_A - \frac{p_B \cdot p_C^3}{K} \right)^n \cdot (1 - k_d \cdot t_d) \qquad (4.14)$$

$$k = k_r \cdot \exp\left(B \cdot \left(1 - \frac{T_r}{T} \right) \right) \qquad (4.8)$$

$$B = \frac{E}{R \cdot T_r} \qquad (4.9)$$

Kinetic parameters with parameters statistics					
Parameter	Values	Units	t-values	95% confidence intervals	
				Lower	Upper
$k_r \times 10^5$	1.487±0.01	mol·g-cat^{-1}·s^{-1}·bar$^{-0.52}$	160.1	1.469	1.505
n	0.515±0.01	—	74.59	0.502	0.529
B	3.045±1.28	—	2.37	0.526	5.563
(E)	(15.63)	(kJ·mol^{-1})			
k_d	1.980±0.31	day^{-1}	6.43	1.376	2.583

Overall statistics				
N	m	Adj(R^2)	SSE	F
210	4	−0.938	22.359	−32.544

Correlation matrix
of parameters

1			
0.151	1		
−0.480	−0.744	1	
0.704	−0.246	−0.355	1
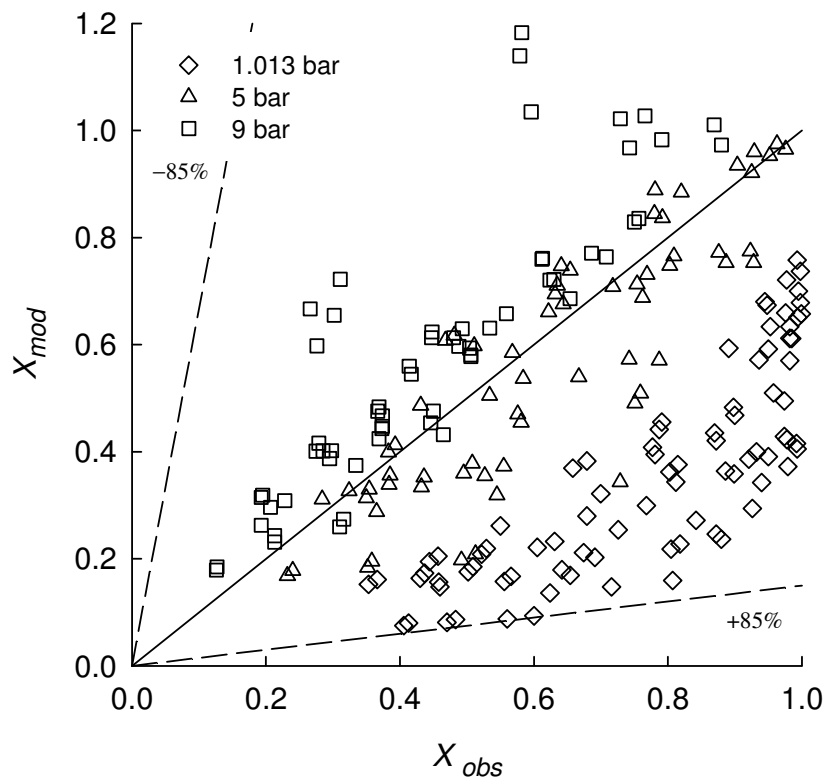
Fig. 4.8 Scatter diagram for power law model relating observed and model values of conversions for overall data.

4.5 Langmuir-Hinshelwood-Hougen-Watson (LHHW) kinetics

The Langmuir-Hinshelwood-Hougen-Watson (LHHW) approach accounts for the surface concentrations of the species taking part in the reaction. Relating surface species to the observed species partial pressures in the gas phase provides equations that can be fitted to the kinetic data. Based on the Langmuir adsorption isotherm, the approach was first developed by Hinshelwood and therefore sometimes termed as Langmuir-Hinshelwood kinetics [Carberry, 2001]. Hougen and Watson [1943] developed a similar approach. Throughout the following discussion, the term Langmuir-Hinshelwood-Hougen-Watson (LHHW) is employed to give credit to both groups [Carberry, 2001]. The LHHW approach assumes that all active sites are energetically uniform and, upon adsorption, adsorbed species do not interact with species already adsorbed [Carberry, 2001]. Active sites have similar kinetic and

108

thermodynamic characteristics and the entropy and enthalpy of adsorption are constant and not functions of the adsorbed amount [Rase, 1977]. The species adsorption restricts itself to only monolayer coverage [Froment and Bischoff, 1979] and the rate of adsorption is proportional to the concentration of the active sites not occupied (empty) and the partial pressure of the component in the gas phase.

A kinetic equation based on LHHW kinetics can generally be represented in the following form [Rase, 1990]

$$(-r) = \frac{kinetic\ term \times potential\ term}{adsorption\ term} \qquad (4.17)$$

For intrinsic kinetics, the *kinetic term* contains the reaction velocity constant and may or may not contain adsorption constants. The *potential term* is the simple driving potential and for an essentially irreversible reaction should be equal to unity. The *adsorption term* contains the adsorption coefficients and partial pressures of species and provides a means of quantifying the competition among the species to occupy the active centres. This is useful in the sense that it helps in interpreting the effect of partial pressures of reaction species and even inert and poisons on the rate of reaction [Rase, 1977].

4.5.1 Kinetic schemes

Two kinetic schemes based on the work of Van Trimpont et al. [1986] were proposed and subjected to the LHHW kinetics. Scheme-I shown below in Fig. 4.9 is based on a dual-site surface reaction of the adsorbed species. It starts with the molecular adsorption of MCH on the empty active centres of the Pt catalyst. The adsorbed MCH further seeks an empty site to undergo a surface heterogeneous reaction to form an adsorbed hydrogen deficient species, methylcyclohexene (MCHe), accompanied by an adsorbed molecular hydrogen. The further dual-site abstractions of H_2 in the successive steps lead to the formation of adsorbed methylcyclohexadiene

(MCHde) and toluene respectively. The adsorbed toluene is then desorbed from the surface into the gas phase. Finally, desorption of hydrogen closes the sequence.

$$MCH + s \rightleftharpoons MCH \cdot s \qquad (I)$$
$$MCH \cdot s + s \rightleftharpoons MCHe \cdot s + H_2 \cdot s \qquad (II)$$
$$MCHe \cdot s + s \rightleftharpoons MCHde \cdot s + H_2 \cdot s \qquad (III)$$
$$MCHde \cdot s + s \rightleftharpoons Tol \cdot s + H_2 \cdot s \qquad (IV)$$
$$Tol \cdot s \rightleftharpoons Tol + s \qquad (V)$$
$$H_2 \cdot s \rightleftharpoons H_2 + s \qquad (VI)$$
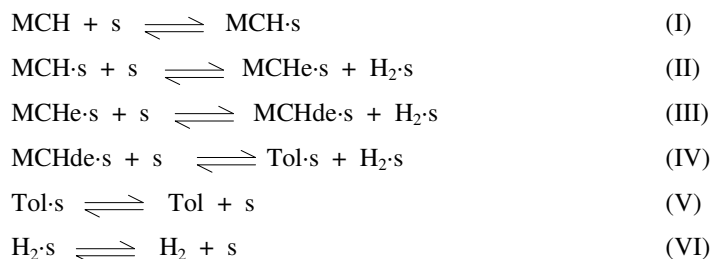
Fig 4.9 Scheme-I, dual-site surface reaction.

The second reaction scheme, Scheme-II, shown below in Fig 4.10 is based on single-site surface reaction of adsorbed species. The reaction mechanism opens with the same first step as that of scheme-I, adsorption of molecular MCH. The adsorbed reactant dehydrogenates in a single-site fashion to form adsorbed MCHe and gaseous hydrogen in the molecular form. Further dehydrogenation of the intermediate forms the adsorbed MCHde, which dehydrogenates in the step following to adsorbed toluene. Finally adsorbed toluene is desorbed into the gas phase. Adsorption or desorption of H_2 is not considered in this scheme.

$$MCH + s \rightleftharpoons MCH \cdot s \qquad (I)$$
$$MCH \cdot s \rightleftharpoons MCHe \cdot s + H_2 \qquad (II)$$
$$MCHe \cdot s \rightleftharpoons MCHde \cdot s + H_2 \qquad (III)$$
$$MCHde \cdot s \rightleftharpoons Tol \cdot s + H_2 \qquad (IV)$$
$$Tol \cdot s \rightleftharpoons Tol + s \qquad (V)$$
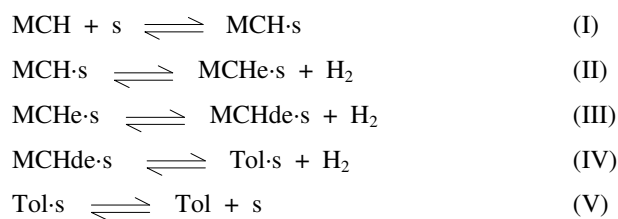
Fig 4.10 Scheme-II, single-site surface reaction.

4.5.2 Development of rate equations

Each mechanistic step in the above sequences was assumed the rate-controlling step (RDS) and a rate equation was developed for the proposed controlling step based on the LHHW theory. However, step-VI of the Scheme-I — hydrogen desorption — not considered as the rate controlling step, because it was considered highly unlikely. Hydrogen adsorption-desorption is considered so fast that an equilibrium is always assumed to exist between the adsorbed and desorbed H_2 in the gas phase over the Pt metal surface. In the derivation of a rate equation assuming a particular rate-controlling step, all of the other steps of the corresponding mechanism are considered in equilibrium [Rase, 1977]. Applying the simple theory of law of mass action, based on the controlling-step in the mechanism, a kinetic equation was derived in terms of the concentrations of the adsorbed species. From the remaining steps of the reaction mechanism the quantities of the adsorbed concentrations were replaced by the measurable quantities i.e. species partial pressures. Table 4.5 summarises all such rate equations developed and a sample derivation procedure for one of the rate equations is illustrated in Appendix E.

Table 4.5a Model equations developed for Scheme-I (dual-site surface reaction)

Step	Rate equations
DS-I	$$(-r) = \dfrac{k \cdot p_A \left(1 - \dfrac{p_B \cdot p_C^3}{K \cdot p_A}\right)}{1 + K_C \cdot p_C + K_B \cdot p_B + \dfrac{K_B \cdot K_C \cdot p_B \cdot p_C}{K_4} + \dfrac{K_B \cdot K_C^2 \cdot p_B \cdot p_C^2}{K_3 \cdot K_4} + \dfrac{K_B \cdot K_C^3 \cdot p_B \cdot p_C^3}{K_2 \cdot K_3 \cdot K_4}}$$
DS-II	$$(-r) = \dfrac{k \cdot K_A \cdot p_A \cdot \left(1 - \dfrac{p_B \cdot p_C^3}{K \cdot p_A}\right)}{\left(1 + K_A \cdot p_A + K_C \cdot p_C + K_B \cdot p_B + \dfrac{K_B \cdot K_C^2 \cdot p_B \cdot p_C^2}{K_4 \cdot K_3} + \dfrac{K_B \cdot p_B \cdot K_C \cdot p_C}{K_4}\right)^2}$$
DS-III	$$(-r) = \dfrac{k \cdot K_A \cdot K_2 \cdot p_A \cdot \left(1 - \dfrac{p_B \cdot p_C^3}{K \cdot p_A}\right)}{K_C \cdot p_C \cdot \left(1 + K_A \cdot p_A + K_C \cdot p_C + K_B \cdot p_B + \dfrac{K_B \cdot K_C \cdot p_B \cdot p_C}{K_4} + \dfrac{K_A \cdot K_2 \cdot p_A}{K_C \cdot p_C}\right)^2}$$
DS-IV	$$(-r) = \dfrac{k \cdot K_A \cdot K_2 \cdot K_3 \cdot p_A \cdot \left(1 - \dfrac{p_B \cdot p_C^3}{K \cdot p_A}\right)}{K_C^2 \cdot p_C^2 \cdot \left(1 + K_B \cdot p_B + K_C \cdot p_C + K_A \cdot p_A + \dfrac{K_A \cdot K_2 \cdot p_A}{K_C \cdot p_C} + \dfrac{K_A \cdot K_2 \cdot K_3 \cdot p_A}{K_C^2 \cdot p_C^2}\right)^2}$$
DS-V	$$(-r) = \dfrac{k \cdot K_4 \cdot K_3 \cdot K_2 \cdot K_A \cdot p_A \cdot \left(1 - \dfrac{p_B \cdot p_C^3}{K \cdot p_A}\right)}{K_C^3 \cdot p_C^3 \cdot \left(1 + K_C \cdot p_C + K_A \cdot p_A + \dfrac{K_4 \cdot K_3 \cdot K_2 \cdot K_A \cdot p_A}{K_C^3 \cdot p_C^3} + \dfrac{K_2 \cdot K_A \cdot p_A}{K_C \cdot p_C} + \dfrac{K_A \cdot K_2 \cdot K_3 \cdot p_A}{K_C^2 \cdot p_C^2}\right)}$$

Table 4.5b Model equations developed for Scheme-II (single-site surface reaction)

Step	Rate equations
SS-I	$$(-r) = \frac{k \cdot p_A \cdot \left(1 - \dfrac{p_B \cdot p_C^3}{K \cdot p_A}\right)}{1 + \dfrac{K_B \cdot p_B \cdot p_C^2}{K_2 \cdot K_3 \cdot K_4} + K_B \cdot p_B + \dfrac{K_B \cdot p_B \cdot p_C^2}{K_3 \cdot K_4} + \dfrac{K_B \cdot p_B \cdot p_C}{K_4}}$$
SS-II	$$(-r) = \frac{k \cdot K_A \cdot p_A \cdot \left(1 - \dfrac{p_B \cdot p_C^3}{K \cdot p_A}\right)}{1 + K_A \cdot p_A + K_B \cdot p_B + \dfrac{K_B \cdot p_B \cdot p_C^2}{K_3 \cdot K_4} + \dfrac{K_B \cdot p_B \cdot p_C}{K_4}}$$
SS-III	$$(-r) = \frac{k \cdot K_A \cdot K_2 \cdot p_A \cdot \left(1 - \dfrac{p_B \cdot p_C^3}{K \cdot p_A}\right)}{p_C + K_A \cdot p_A \cdot p_C + K_A \cdot K_2 \cdot p_A + K_B \cdot p_B \cdot p_C + \dfrac{K_B \cdot p_B \cdot p_C^2}{K_4}}$$
SS-IV	$$(-r) = \frac{k \cdot K_A \cdot K_2 \cdot K_3 \cdot p_A \cdot \left(1 - \dfrac{p_B \cdot p_C^3}{K \cdot p_A}\right)}{p_C^2 \cdot \left(1 + K_B \cdot p_B + K_A \cdot p_A + \dfrac{K_A \cdot K_2 \cdot p_A}{p_C} + \dfrac{p_A \cdot K_A \cdot K_2 \cdot K_3}{p_C^2}\right)}$$
SS-V	$$(-r) = \frac{k \cdot K_A \cdot K_2 \cdot K_3 \cdot K_4 \cdot p_A \cdot \left(1 - \dfrac{p_B \cdot p_C^3}{K \cdot p_A}\right)}{p_C^3 \cdot \left(1 + K_A \cdot p_A + \dfrac{K_A \cdot K_2 \cdot K_3 \cdot K_4 \cdot p_A}{p_C^3} + \dfrac{K_A \cdot K_2 \cdot p_A}{p_C} + \dfrac{K_A \cdot K_2 \cdot K_3 \cdot p_A}{p_C^2}\right)}$$

4.5.3   Kinetic treatment of the rate equations

Table 4.5 shows 10 kinetic model equations. However, each of the 10 equations was simplified based on the assumption that one or more of the terms in the denominator are insignificant i.e. which species involved had negligible coverage. All these simplified kinetic equations were fitted to the kinetic data and their fit and the physical significance of the parameters examined. As an illustration, for the model equation DS-I (based on the dual-site and methylcyclohexane adsorption) that has five denominator terms other than "1" can lead to 31 model equations while retaining "1" in the denominator of all of the kinetic equations. Appendix F includes all such equations and shows how the addition of a new term and varying assumptions of species coverage affect the statistics i.e. F-value and SSE of the corresponding model.

Discrimination among the rival kinetic models was performed on the basis of model F-values. The model equations with negative parameters or with low values of the F-statistic were discarded and a set of model equations with significant F-values was assembled. Table G.1 in Appendix G shows the list of kinetic equations, along with their model SSE, $Adj(R^2)$ and model F-values, that fulfilled the above criteria. As proposed by Van Trimpont et al. [1986] further discrimination was made by considering the Arrhenius temperature dependency of the adsorption equilibrium constants. Also it is evident from the power law results that parameters are group dependent, so one or more of the adsorption coefficients are temperature dependent. Table 4.6 shows the best three kinetic models selected after statistical discrimination and considerations of the temperature dependency of the adsorption coefficients. Clearly, model M-10 in Table 4.6, based on the model M-1 in Table G.1, shows the highest F-value, and the lowest SSE value. This model was derived on the basis of a single-site surface reaction mechanism with loss of the first hydrogen molecule as the rate-controlling step. The surface concentration of MCHde was considered negligible and the combined equilibrium constant was assumed to be temperature dependent. Table 4.6 shows the successful kinetic model along with the parameter values and the statistics associated with them. Fig. 4.11 is the scatter diagram representing the relationship between observed conversion and the model conversion values.

Table 4.6 List of kinetic models after second discrimination

Model	Model type	Kinetic equation	m	Adj(R^2)	SSE	F
M-10	SS-II (Loss of 1st hydrogen) Negligible coverage of MCHde including temperature dependency of adsorption terms	$$(-r) = \frac{k \cdot K_A \cdot \left(p_A - \dfrac{p_B \cdot p_C^3}{K} \right)}{1 + K_A \cdot p_A + K_B \cdot p_B + K' \cdot p_B \cdot p_C^2}$$ $$K' = \frac{K_B}{K_3 \cdot K_4}$$ $$K' = f(T)$$	7	0.964	0.412	932.74
M-11	SS-II (Loss of 1st hydrogen) Negligible coverage of MCHde including temperature dependency of adsorption terms	$$(-r) = \frac{k \cdot K_A \cdot \left(p_A - \dfrac{p_B \cdot p_C^3}{K} \right)}{1 + K_A \cdot p_A + K_B \cdot p_B + K' \cdot p_B \cdot p_C^2}$$ $$K' = \frac{K_B}{K_3 \cdot K_4}$$ $$K_A = f(T)$$	7	0.959	0.463	825.10
M-12	DS-I (Adsorption of MCH) Negligible coverages of both MCHe and MCHde including temperature dependency of adsorption terms	$$(-r) = \frac{k \cdot \left(p_A - \dfrac{p_B \cdot p_C^3}{K} \right)}{1 + K_B \cdot p_B + K' \cdot p_B \cdot p_C^3}$$ $$K' = \frac{K_B \cdot K_C^3}{K_2 \cdot K_3 \cdot K_4}$$ $$K' = f(T)$$	6	0.950	0.574	795.63

4.5.4   Discussion of the preferred model

4.5.4.1   Regression

In the first discrimination step for the model equation M-1, as shown in Table G.1, the F-statistic of 801.92 came out to be fairly high with a corresponding low magnitude of SSE of 0.569. The parameters values appear reasonable kinetically and an activation energy of 59.8 kJ/mol was obtained. No parameter had a 95% confidence interval that included zero. All the parameters were well defined with t-values greater than 3.0 except for the parameter K_B which had a t-value close to 3.0. Since the results for the power law model suggested, a variation of adsorption equilibrium constants with temperature, the temperature dependency according to Arrhenius equation was incorporated. The best values of the SSE and F-statistics were obtained while taking K', a composite constant, as a function of temperature. Not only a higher value of F was obtained i.e. from 801.9 to 932.7 but also the SSE decreased. The higher value of F justified retaining the additional parameter. The new set of kinetic parameters were even better determined. No parameter 95% confidence interval included zero and all the t-values were greater than 3.0. Even the t-value of K_B was found to be greater than 3.0. The correlation matrix showed no high correlation among the parameter values. All correlation coefficients are $< |0.9|$. The model residuals were randomly distributed and no specific trend was visible in the residual plot (RKPES output not shown here).

Table 4.7 Results of regression for the best model based on single-site LHHW when loss of first H_2 controls the rate

Kinetic model

$$(-r) = \frac{k \cdot K_A \cdot p_A \cdot \left(1 - \dfrac{p_B \cdot p_C^3}{K \cdot p_A}\right)}{1 + K_A \cdot p_A + K_B \cdot p_B + K' \cdot p_B \cdot p_C^2} \cdot (1 - k_d \cdot t_d) \tag{4.18}$$

$$K' = \frac{K_B}{K_3 \cdot K_4} \tag{4.19}$$

$$k = k_r \cdot \exp\left(B \cdot \left(1 - \frac{T_r}{T}\right)\right) \tag{4.8}$$

$$B = \frac{E}{R \cdot T_r} \tag{4.9}$$

$$K' = K_r' \cdot \exp\left(B' \cdot \left(1 - \frac{T_r}{T}\right)\right) \tag{4.20}$$

$$B' = \frac{\Delta h'}{R \cdot T_r} \tag{4.21}$$

Kinetic parameters with parameters statistics					
Parameter	Values	Units	t-values	95% confidence intervals	
				Lower	Upper
$k_r \times 10^5$	4.064±0.44	mol·g-cat^{-1}·s^{-1}	9.24	3.202	4.925
B	7.652±0.10	—	7.69	5.700	9.603
(E)	(39.27)	(kJ·mol^{-1})	—	—	—
K_A	40.91±10.5	—	3.89	20.28	61.53
K_B	22.19±7.05	bar^{-1}	3.15	8.371	36.02
K_r'	6.688±1.43	bar^{-3}	4.66	3.877	9.499
B'	−24.04±3.14	—	7.66	−30.19	−17.89
$(\Delta h')$	(−123.36)	(kJ·mol^{-1})	—	—	—
k_d	1.471±0.17	day^{-1}	8.60	1.136	1.806

Overall statistics				
N	m	Adj(R^2)	SSE	F
210	7	0.964	0.412	932.742

Correlation matrix of parameters

1						
0.616	1					
−0.516	−0.281	1				
0.128	9.6×10^{-5}	0.724	1			
−0.055	0.072	0.849	0.857	1		
0.290	0.704	−0.150	−0.028	0.045	1	
0.744	0.284	−0.257	0.136	0.027	0.092	1
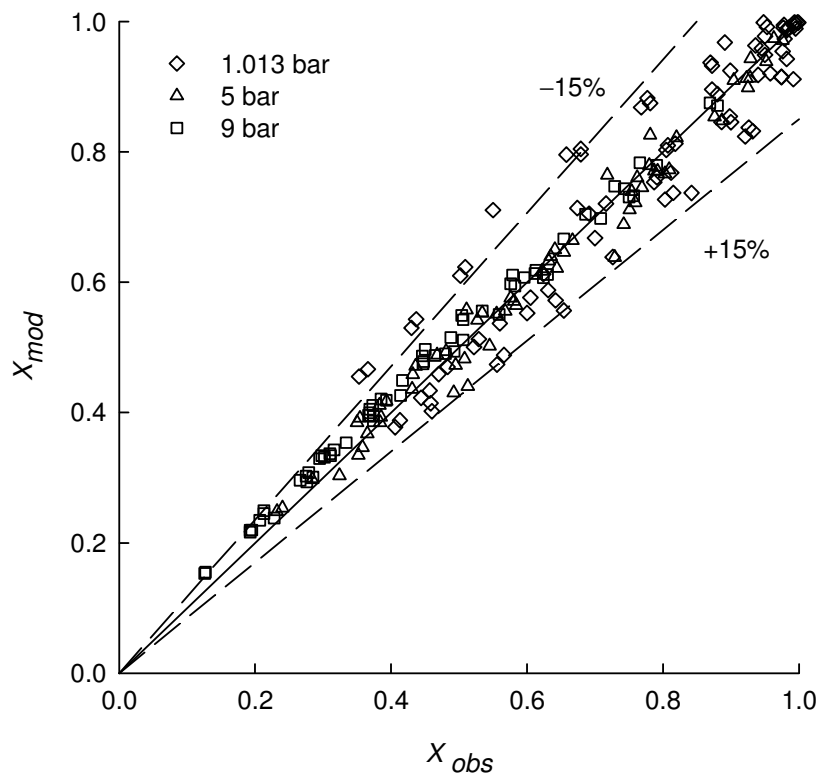
Fig 4.11 Scatter diagram for the best fitting model (M-10) based on single-site
LHHW kinetics when loss of first H_2 controls the rate.

4.5.4.2 Mechanism and the rate-determining step

As mentioned in Chapter 2, there exists significant controversy in the literature on the mechanism and the rate determining step. In the present study, loss of the first hydrogen molecule in the single-site surface reaction mechanism is considered the rate-determining step. Moreover, the surface coverage by the second intermediate (MCHde) is neglected. Close inspection of all the three kinetic equations in Table 4.6, shows that each contains a non-linear term with respect to hydrogen pressure in the denominator as suggested earlier in the discussion of the power law model. Although, a stronger non-linearity is present in M-12, which is based on a dual-site mechanism and adsorption of MCH rate-controlling, coverage effect of

MCH is absent. In the remaining two models, taking account of the temperature dependence of the "lumped" constant K' gives results those found for the power law kinetics. Further, as MCHde has never been reported in the reaction products, the assumption of negligible coverage by MCHde may be justified. It could also be that MCHde is present on the catalyst surface but not in equilibrium with the gas phase. Rather, it is strongly adsorbed but is rapidly dehydrogenated to toluene before it can be desorbed. In the literature, Zengel [1967] proposed the single-site mechanism with a surface reaction as the rate-controlling step. Touzani et al. [1984], Van Trimpont et al. [1986], Chaouki et al. [1988] and Chai and Kawakami [1990] also considered a single-site surface reaction to control the dehydrogenation reaction. Taking into account the surface reaction intermediates, Touzani et al. [1984] and Chaouki et al. [1988] concluded that the loss of first hydrogen molecule i.e. dehydrogenation of adsorbed MCH to adsorbed MCHe was the rate controlling step. Van-Trimpont et al. applied both the LHHW single-site and dual-site mechanisms and reported loss of the first H_2 molecule in the single-site mechanism as the rate controlling step. Corma et al. [1979], García de la Banda et al. [1986], Tsakiris [2007] and Alhumaidan [2008] also found the rate-controlling step involving loss of the first hydrogen molecule supplied by their experimental data. However, they adopted a dual-site surface reaction. Further, for the dehydrogenation of cyclohexane, Maatman et al. [1971]. suggested that the dehydrogenation reaction of cyclohexane on Pt/Al_2O_3 may be controlled by a surface reaction involving reaction intermediates such as cyclohexene or cyclohexadiene. Moreover, Blakely and Somorjai [1976], have concluded that for cyclohexane dehydrogenation reaction on a platinum single crystal surface, loss of the first hydrogen molecule is the rate-determining step. As mentioned in Chapter 2, some support may also be found from the work of Saeys et al. [2005] on cyclohexane dehydrogenation using DFT calculations for a single Pt crystal.

4.5.4.3 Parameters

The apparent activation energy: In the literature for supported Pt-containing catalysts, there is no consensus on the value of the activation energy. There exists a large range

of apparent activation energies and quite a varying number of values of E are reported. The values range from 17.90 kJ/mol by El-Sawi [1989] to 220.67 kJ/mol by Maria et al. [1996]. As shown in Table 4.7, for the present study, the apparent activation energy of 39.3 kJ/mol was obtained. Other studies in the literature found the values close to the above. Ritchie and Nixon [1966] reported 48.9 kJ/mol for their 1.0 wt% Pt/Al$_2$O$_3$, Pacheco and Petersen [1985], while studying the dehydrogenation of MCH over pre-sulfided bimetallic Pt-Re over alumina catalyst, found the activation energy as 58.6 kJ/mol for T > 360 °C. Jothimurugesan et al. [1985a] reported a value of 51.9 kJ/mol on their Pt-Re-alumina catalyst and Pal et al. [ref] obtained an activation energy of 56.4 kJ/mol on the same catalyst as that of Jothimurugesan et al. [1985a]. Tsakiris [2007] for his Pt over α- and γ-alumina catalysts reported apparent activation energy values in the range of 44.1−60.0 kJ/mol and for his 0.3 wt% Pt/α-Al$_2$O$_3$ and 1.0 wt% Pt/γ-Al$_2$O$_3$, activation energies were 45.7 and 49.8 kJ/mol respectively. Alhumaidan [2008] obtained a value of 55.4 kJ/mol for the activation energy for commercial and development Pt/Al$_2$O$_3$ catalysts. It is important to mention here that the low value of activation energy is not the result of diffusion limitations as the factor was ruled out by selecting the appropriate catalyst particle size. The calculations for the diffusion limitations to confirm the said statement are given in Appendix H. However, a relatively low value of the apparent activation energy might be attributed to the fact that the major temperature dependence lies in the denominator term and the inhibition term K' (K_B) is a strong inverse function of temperature. This can easily be seen by a high value of the combined apparent heat of adsorption of K', which is −123.37 kJ/mol. In the above discussion, Ritchie and Nixon [1966] had no temperature dependency term in the denominator.

The adsorption equilibrium constants: The model value of the MCH adsorption coefficient (K_A) was found to be 40.9 bar^{-1}, higher than that of the toluene (K_B) of 22.2 bar^{-1}. Toluene, being aromatic in nature, adsorbs more strongly to the platinum as compared to the naphthenic MCH. However, the current observation may be explained in a different way. As suggested by Boudart [1956] in his famous manuscript in response to Weller's [1956] argument of using power law kinetics, that

the denominator constants in the LHHW type kinetics usually do not equate to the adsorption constants derived independently, the coefficients obtained, here, are not the true adsorption coefficients but "lumped" empirical apparent coefficients.

4.5.5 Supporting data for the model using experiments with MCHe (methylcyclohexene)

In the above kinetic schemes the dehydrogenation is assumed to occur in a series of dehydrogenation steps and MCHe and MCHde are considered as the reaction intermediates in the overall dehydrogenation reaction of MCH to toluene.

With this in mind, it was thought that dehydrogenation experiments starting with an intermediate as feed would be valuable in contributing to a better understanding of the reaction mechanism. Thus, experiments were carried out with pure 1-methylcyclohexene as the feed reactant rather than methylcyclohexane. Under virtually the same conditions as maintained for methylcyclohexane, experiments were carried out under hydrogen pressure at 5 bar total pressure and reactor wall temperatures of 340 °C and 380 °C.

Fig. 4.12 shows the results and a comparison between MCH and MCHe dehydrogenation. As methylcyclohexene contains one unsaturated bond, it was expected that it would undergo both hydrogenation and dehydrogenation reactions. If the rate-determining step lies after loss of the first hydrogen molecule i.e. downstream from the formation of methylcyclohexene intermediate then a toluene yield comparable to that obtained with MCH was expected. However, as shown in Fig. 4.12, that under all the conditions studied, the toluene yield was always higher when MCHe was the feed. This tends to support the hypothesis that either the rate-controlling step in the dehydrogenation of MCH lies in the loss of the first hydrogen molecule or the adsorption of MCH. The same procedure was followed by Corma et al. [1979] to discriminate among the possible rate-controlling steps. They reached the same conclusion.
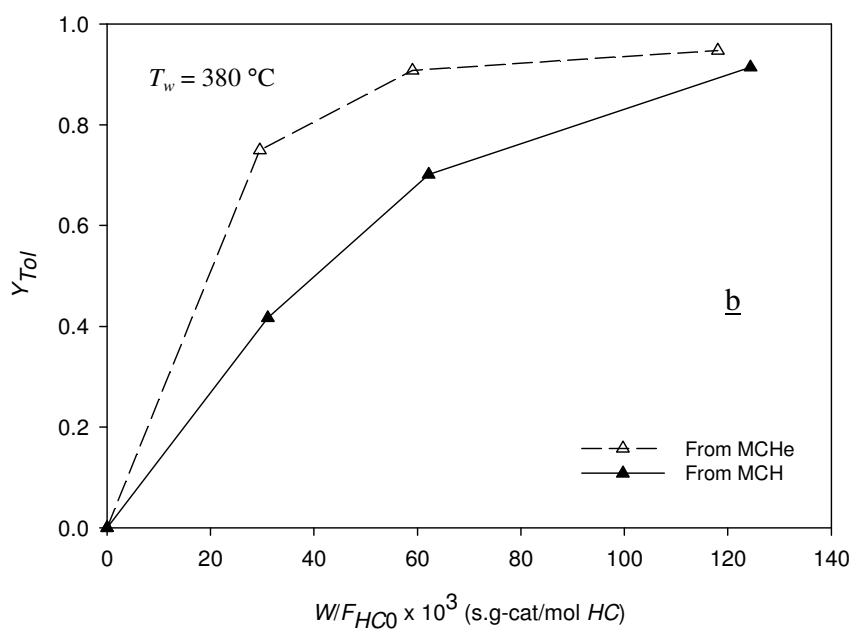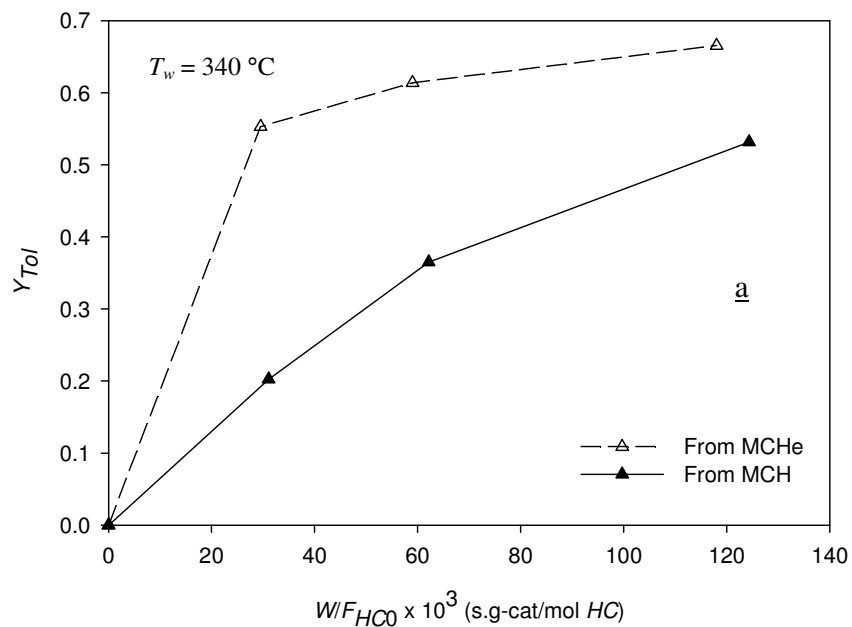
Fig. 4.12 Yields of toluene at p = 5 bar pressure, H_2/HC ratio of 8:1 and reactor wall temperature of (a) 340 °C and (b) 380 °C; HC stands for hydrocarbon i.e. MCH or MCHe.

4.5.6 The confirmation and validity of the model using high temperature and high flow conditions i.e. Group-5159

Experiments were performed with no hydrogen in the feed as anticipated in the "on-board" MTH-system and at 1.013 to 9 bar and under temperatures range between 380 °C and 460 °C with low W/F_{A0} in the range of 1.55×10^4–3.11×10^4 s·g-cat/mol MCH. Group-5159 in Table 4.2 represents the data at high temperatures and high MCH flowrates. The best form of kinetic equation obtained in the preceding discussion was fitted to the data in Group-5159. This was done to check the robustness of the model to apply under the more extreme conditions in which the MTH-system might find its applications. Table 4.8 and Fig. 4.13 show the results obtained when the kinetic model was applied to 29 data points under varying conditions of temperature, pressure and MCH flows. A very low value of SSE of 0.00397 and a high value of Adj(R^2) i.e. 0.993 were obtained and the scatter diagram shown in Fig. 4.13 shows an excellent fit to the experimental data. Table I.1 in Appendix I shows the parameter values for Group-5159. Confidence intervals of parameter K_B includes zero suggesting one less parameter in the model for Group-5159. The results for the new regression conditions are shown in Table I.2 in Appendix I.

The parameter values were found moderately different but clearly the data points are well fitted and show the ability of the kinetic model to be used beyond the conditions for which the model is developed and in practical conditions of MTH-system so in the simulation of the prototype in Chapter 6.

Table 4.8 Operating conditions and results of regression for Group-5159 based on single-site LHHW when loss of first hydrogen controls the rate

p (bar)	T_w (K)	$W/F_{A0}\times10^{-4}$ s·g-cat/mol	N	SSE	Adj(R^2)	F
1.013, 5, 9	653.2, 673.2, 693.2, 713.2, 733.2	1.55, 2.22, 3.11	29	0.00397	0.992	633.48
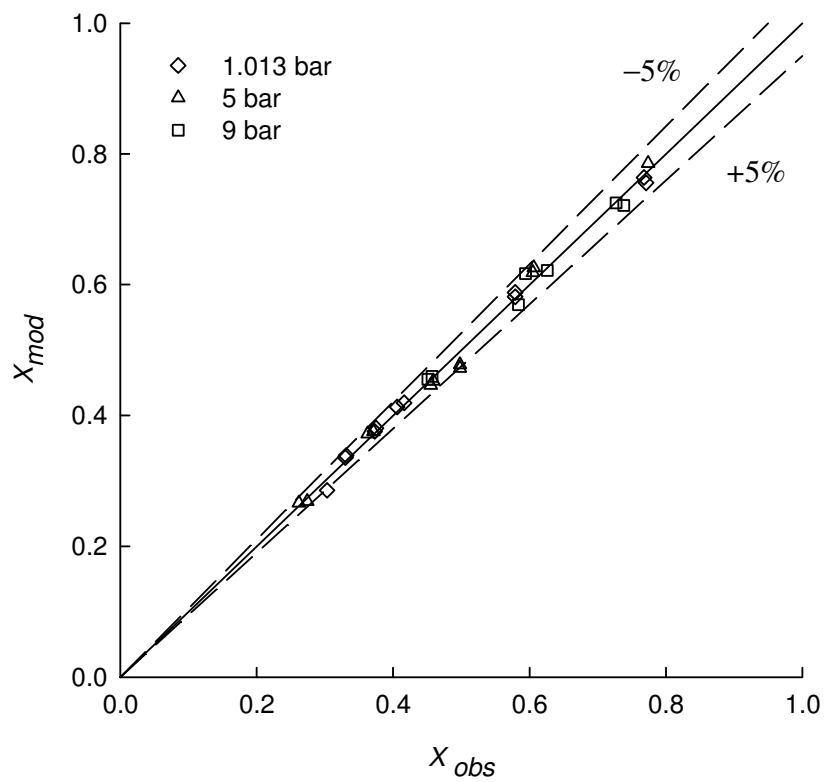
Fig. 4.13 Scatter diagram for Group-5159 based on the best fitting single-site LHHW kinetics when loss of first H_2 controls the rate.

4.6 Horiuti-Polanyi kinetics

The Horiuti-Polanyi (HP) mechanism, originated by Horiuti and Polanyi [1934], is an old but still notable mechanism for double bond hydrogenation. In its present form, which is slightly different from the original, it may be written for a simple olefin such as ethylene in Fig. 4.14 [Clarke and Rooney, 1977]

$$H_2 + 2\,s \rightleftharpoons 2\,H\cdot s \qquad\qquad\qquad (I)$$

$$
H_2C = CH_2 + 2\,s \rightleftharpoons
\begin{array}{c}
H_2C - CH_2 \\
|\quad\ | \\
s\quad\ s
\end{array}
\qquad\qquad (II)
$$

$$
\begin{array}{c}
H_2C - CH_2 \\
|\quad\ | \\
s\quad\ s
\end{array}
+ H\cdot s \rightleftharpoons
\begin{array}{c}
H_2C - CH_3 + 2\,s \\
| \\
s
\end{array}
\qquad (III)
$$

$$
\begin{array}{c}
CH_3 - CH_2 \\
| \\
s
\end{array}
+ H\cdot s \rightleftharpoons H_3C - CH_3 + 2\,s \qquad\qquad (IV)
$$
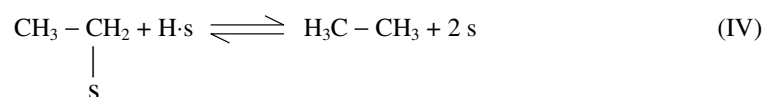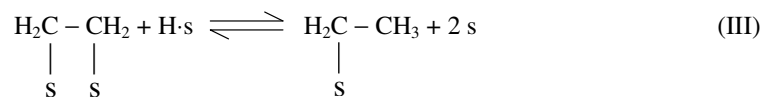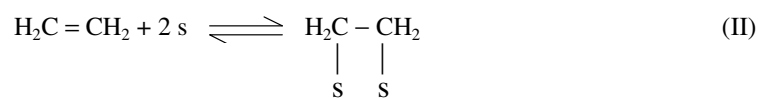
Fig 4.14 Present day Horiuti-Polanyi hydrogenation mechanism for a
simple olefin.

The mechanism involves the dissociative adsorption of hydrogen on the active sites and non-dissociative molecular adsorption of ethene. The adsorbed ethylene reacts with the adsorbed atomic hydrogen to form a half-hydrogenated ethylene species. Further atomic- or half-hydrogenation leads to the formation of the saturated ethane.

4.6.1 Kinetic schemes based on Horiuti-Polanyi mechanism

Considering competitive and non-competitive hydrogen adsorption, three separate mechanisms based on the HP kinetics can be defined: a competitive HP mechanism, a non-competitive HP mechanism and a combined competitive and non-competitive HP mechanism [Dumesic et al., 1993]. In the competitive HP mechanism, both hydrogen and hydrocarbon compete for the same type of active sites [Dumesic et al., 1993], while in the non-competitive HP mechanism, there are

separate classes of sites for both hydrogen and hydrocarbons. When hydrogen, alone, has an access to both kinds of sites and not the hydrocarbon, the combination of competitive and non-competitive mechanism prevails.

Van Trimpont et al. [1986] outlined the elementary steps for the dehydrogenation of MCH based on the competitive Horiuti-Polanyi concept as shown in Section 2.1 in Chapter 2. The kinetic equations developed for competitive HP will be more or less the same as those obtained from Scheme-I (LHHW dual-site surface reaction). On a similar basis to Van Trimpont et al. [1986], Alhumaidan [2008] outlined the following elementary steps for the non-competitive Horiuti-Polanyi mechanism, Scheme-III, as shown in Fig 4.15, different only in the hydrogen adsorption-desorption step which is taken here to be elementary as well.

$$MCH + s \rightleftharpoons MCH \cdot s \qquad (I)$$

$$MCH \cdot s + s^* \rightleftharpoons MCH1 \cdot s + H \cdot s^* \qquad (II)$$

$$MCH1 \cdot s + s^* \rightleftharpoons MCHe \cdot s + H \cdot s^* \qquad (III)$$

$$MCHe \cdot s + s^* \rightleftharpoons MCH2 \cdot s + H \cdot s^* \qquad (IV)$$

$$MCH2 \cdot s + s^* \rightleftharpoons MCHde \cdot s + H \cdot s^* \qquad (V)$$

$$MCHde \cdot s + s^* \rightleftharpoons MCH3 \cdot s + H \cdot s^* \qquad (VI)$$

$$MCH3 \cdot s + s^* \rightleftharpoons Tol \cdot s + H \cdot s^* \qquad (VII)$$

$$Tol \cdot s \rightleftharpoons Tol + s \qquad (VIII)$$

$$2 H \cdot s^* \rightleftharpoons H_2 + 2 s^* \qquad (IX)$$
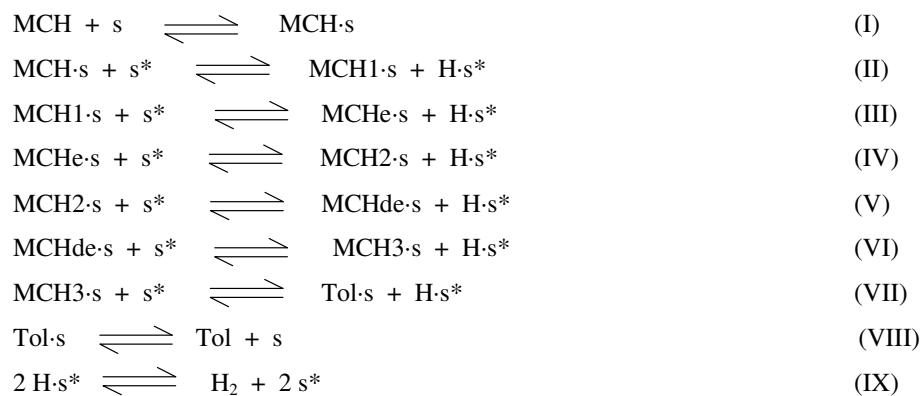
Fig 4.15 Scheme-III, non-competitive Horiuti-Polanyi mechanism.

The kinetic Scheme-III starts with the usual molecular adsorption of MCH and undergoes dehydrogenation to produce an adsorbed half-hydrogenated MCHe intermediate and adsorbed atomic hydrogen. Two separate kinds of sites are involved for hydrocarbons and hydrogen adsorption. Site "s" is a hydrocarbon site while site "s*" is a hydrogen site. Owing to the different categories of the two sites, the mechanism is non-Langmurian in nature. The half-hydrogenated MCHe further dehydrogenates to produce a MCHe intermediate. Similar abstractions of hydrogen finally lead to adsorbed toluene. The adsorbed toluene is then desorbed from the hydrocarbon sites and the adsorbed hydrogen is desorbed molecularly from the adjacent hydrogen sites in the final step.

126

Scheme-IV is shown in Fig. 4.16 and it is based on the combined-competitive-non-competitive HP mechanism. Unlike Scheme-III, Scheme-IV allows for hydrogen adsorption/desorption on both s and s* sites.

MCH + s $\rightleftharpoons$ MCH·s	(I)
MCH·s + s $\rightleftharpoons$ MCH1·s + H·s	(II)
MCH·s + s* $\rightleftharpoons$ MCH1·s + H·s*	(III)
MCH1·s + s $\rightleftharpoons$ MCHe·s + H·s	(IV)
MCH1·s + s* $\rightleftharpoons$ MCHe·s + H·s*	(V)
MCHe·s + s $\rightleftharpoons$ MCH2·s + H·s	(VI)
MCHe·s + s* $\rightleftharpoons$ MCH2·s + H·s*	(VII)
MCH2·s + s $\rightleftharpoons$ MCHde·s + H·s	(VIII)
MCH2·s + s* $\rightleftharpoons$ MCHde·s + H·s*	(IX)
MCHde·s + s $\rightleftharpoons$ MCH3·s + H·s	(X)
MCHde·s + s* $\rightleftharpoons$ MCH3·s + H·s*	(XI)
MCH3·s + s $\rightleftharpoons$ Tol·s + H·s	(XII)
MCH3·s + s* $\rightleftharpoons$ Tol·s + H·s*	(XIII)
Tol·s $\rightleftharpoons$ Tol + s	(XIV)
2 H·s $\rightleftharpoons$ H_2 + 2 s	(XV)
2 H·s* $\rightleftharpoons$ H_2 + 2 s*	(XVI)
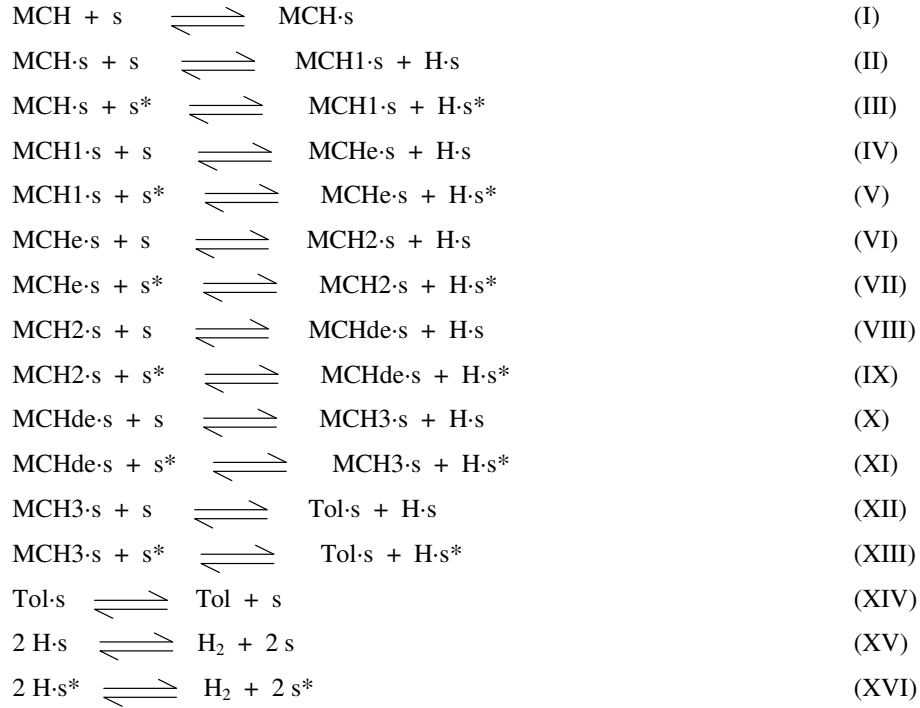
Fig 4.16 Scheme-IV, combined-competitive-non-competitive Horiuti-Polanyi mechanism.

4.6.2 Development of kinetic expressions

Following similar mathematical steps to those performed for Scheme-I and Scheme-II (Appendix E), two kinetic equations were developed based on the non-competitive HP mechanism (Scheme-III) and the combined-competitive-non-competitive HP mechanism (Scheme-IV). In the derivation of the model equations, the surface coverage of all intermediate species was assumed negligible and loss of the first hydrogen atom was considered as the rate-controlling step. The two model equations obtained are shown in Table 4.9.

Table 4.9 Kinetic equations developed based on HP mechanism

Model type	Kinetic equation
HP-I (Non-competitive)	$$(-r) = \frac{k \cdot K_A \cdot p_A \cdot \left(1 - \dfrac{p_B \cdot p_C^{\,3}}{K \cdot p_A}\right)}{(1 + K_A \cdot p_A + K_B \cdot p_B) \cdot (1 + \sqrt{K_{Cr}^* \cdot p_C})}$$
HP-II (Combined competitive-non-competitive)	$$(-r) = \frac{k \cdot K_A \cdot p_A \cdot \left(1 - \dfrac{p_B \cdot p_C^{\,3}}{p_A \cdot K}\right)}{(1 + K_A \cdot p_A + K_B \cdot p_B + \sqrt{K_C \cdot p_C}) \cdot (1 + \sqrt{K_{Cr}^* \cdot p_C})}$$

4.6.3 Kinetic treatment of the rate equations

Both competitive-non-competitive and non-competitive Horiuti-Polanyi models were fitted to the experimental data. Similar to the LHHW models, the discrimination was performed on the basis of the F-value. The regression of both competitive-non-competitive and non-competitive HP models resulted in extremely large values of adsorption coefficients for both MCH and toluene with similar F-values. Thus suggested a high surface coverage (HSC) assumption must be incorporated into the model equations. The original equations were then modified by the introduction of a new constant which is the ratio of the two adsorption equilibrium constants K_B and K_A. The modified equations resulted in one fewer parameter and led to correspondingly high F-values, as well as more realistic values of the kinetic coefficients.

$$(-r) = \frac{k \cdot \left(p_A - \dfrac{p_B \cdot p_C^{\,3}}{K}\right)}{(p_A + K_B' \cdot p_B) \cdot (1 + \sqrt{K_C^* \cdot p_C})} \tag{4.22}$$

since $\quad K_A \cdot p_A + K_B \cdot p_B \gg 1$ (4.23)

and $\quad K_B' = \dfrac{K_B}{K_A}$ (4.24)

In the modified form as shown in Eq. 4.22 to Eq. 4.24, the non-competitive HP model resulted in a higher F-value and was preferred to the combined-competitive-non-competitive HP model. For the non-competitive HP model the model F-value was increased from 620.2 to 778.7 when the HSC inequality (Eq. 4.23) was applied. Based on the previous power law results (Section 4.4.1), an Arrhenius temperature dependency term was introduced into K_{Cr}^{*} which led to the addition of a new parameter. The model F-value decreased from 778.7 to near the original value i.e. 621.6. Moreover, the 95% confidence limits for the heat of adsorption term included zero. In the next step, the previous temperature dependence term was dropped and instead a non-linear total pressure dependence was introduced as shown in Eq. 4.25. The total pressure dependence term was introduced in accordance with the power law results. It was found previously (Section 4.4.1) that the parameters and the initial rates vary non-linearly with the total pressure. Moreover, it was clearly shown during the discussion of the results of the power law model that the role of hydrogen on the catalyst performance depended on the total pressure. A non-linear pressure dependency was tried and K_C was taken as a function of pressure raised to the power c. The new model F-value was increased from 778.7 to 802.6, although not a large increase in F, with the exponent c approximately 2.0. In subsequent analysis, the value of the pressure exponent c was fixed as 2.0. This was done to increase the overall effect of the hydrogen partial pressure in the denominator. The equation then resembled to the forms of the best kinetic equations based on LHHW. The new model produced the highest F-value of 1008.2 and all the parameters were well defined. No 95% confidence limits included zero and all the t-values were well above 3.0. The results of the best kinetic treatment are shown in Table 4.10 and a scatter diagram to provide a comparison between the observed and model conversion values is provided in Fig. 4.17

$$K_C^{*} = K_{Cr}^{*} \cdot p^{c} \tag{4.25}$$

Table 4.10 Results of regression for the model based on the non-competitive HP when loss of first H-atom controls the rate

Kinetic model

$$(-r) = \frac{k \cdot \left(p_A - \dfrac{p_B \cdot p_C{}^3}{K} \right)}{(p_A + K'_B \cdot p_B) \cdot (1 + \sqrt{K_C^* \cdot p_C})} \cdot (1 - k_d \cdot t_d) \qquad (4.22)$$

$$K_A \cdot p_A + K_B \cdot p_B \gg 1 \qquad (4.23)$$

$$K'_B = \frac{K_B}{K_A} \qquad (4.24)$$

$$K_C^* = K_{Cr}^* \cdot p^2 \qquad (4.26)$$

$$k = k_r \cdot \exp\left(B \cdot \left(1 - \frac{T_r}{T} \right) \right) \qquad (4.8)$$

$$B = \frac{E}{R \cdot T_r} \qquad (4.9)$$

Kinetic parameters with parameters statistics

Parameter	Values	Units	t-values	95% confidence intervals	
				Lower	Upper
$k_r \times 10^5$	4.634±0.57	mol·g-cat^{-1}·s^{-1}	8.11	3.514	5.754
B	9.917±0.91	—	10.90	8.134	11.70
(E)	(50.91)	kJ/mol	—	—	—
K'_B	1.016±0.17	—	5.96	0.682	1.350
K_{Cr}^*	0.089±0.01	bar^{-3}	9.07	0.070	0.109
k_d	1.274±0.19	day^{-1}	6.57	0.894	1.655

Overall statistics

N	m	Adj(R^2)	SSE	F
210	5	0.950	0.56899	1008.19

Correlation matrix
of parameters

1				
0.713	1			
0.911	0.533	1		
0.780	0.749	0.601	1	
0.721	0.319	0.559	0.377	1

Fig. 4.17 Scatter diagram for the model based on non-competitive HP kinetics
when loss of first H-atom controls the rate.

4.6.4 The confirmation and validity check of the model using high temperatures and high flow conditions i.e. Group-5159

Similar to the preferred LHHW kinetic model the preferred HP kinetic model was also applied to the data in Group-5159. The main objective was to check that the model could be extrapolated to work in the more extreme conditions under which the real MTH-system might operate. It was recognised, though, that changes to some or all of the kinetic parameters might be necessary. Table 4.11 and Fig. 4.18 show the results obtained when the kinetic model was fitted to Group-5159 data. Table I.3 in Appendix I shows the parameter values. Although a low value of SSE of 0.00830 and a high value of Adj(R^2) i.e. 0.985 were obtained and the scatter diagram in Fig. 4.18

shows a good fit to the experimental data, the extrapolation was not as successful as with the best model obtained with LHHW.

Table 4.11 Operating conditions and results of regression for Group-5159 based on the non-competitive HP model when loss of first H-atom controls the rate

p (bar)	T_w (K)	$W/F_{A0}\times10^{-4}$ s·g-cat/mol	N	SSE	Adj(R^2)	F
1.013, 5, 9	653.2, 673.2, 693.2, 713.2, 733.2	1.55, 2.22, 3.11	29	0.00830	0.985	492.69
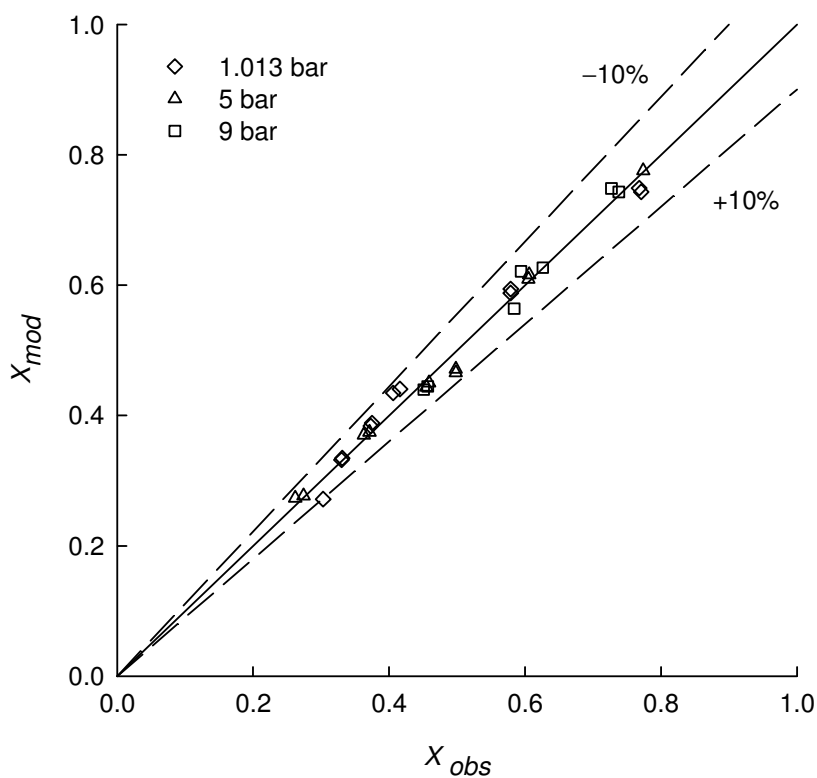
Fig. 4.18 Scatter diagram for Group-5159 based on the non-competitive HP kinetics when loss of first H-atom controls the rate.

4.7 Conclusions

The power law model, though, not suitable when subjected to regression for the overall experimental data, provided certain useful clues in paving the way for the mechanistic kinetic models. When subjected to LHHW single-site and dual-site mechanisms, the experimental data were best fitted by the single-site LHHW kinetics with loss of the first hydrogen molecule as rate-controlling and considering surface coverage by methylcyclohexadiene as negligible. The same kinetic model was then used with the separate data at high temperatures and high MCH flowrates and found excellent in fitting the data. The non-competitive HP mechanism also provided a good fit to the overall data but with an empirical insertion of a total pressure dependence to the hydrogen equilibrium constant. Containing two fewer parameters, the non-competitive HP model led to a higher SSE, and is less efficient in fitting the overall data and the data at high temperatures and high flowrates.

Chapter 5
By-Products Formation in Methylcyclohexane Dehydrogenation

A successful catalytic system, in general, depends on an active, selective and a stable catalyst. A highly active catalyst with low selectivity towards the desired product may be quite unacceptable in the final process flowsheet. Undesirable by-products not only increase the difficulty and cost associated with the purification of the target product, but they may also be harmful for the life of the catalytic system and may not be environmentally friendly. In the MTH-technology, a catalyst highly selective towards toluene is desired and as the product toluene has to be hydrogenated back to methylcyclohexane, any by-product, other than cyclohexane in some sense, causes a potential leak in the MCH-toluene cycle as well as the economy. Moreover, some of the by-products may be harmful towards the life of the catalyst itself. This chapter describes the brief chemistry behind the by-products formation and discusses the effect of operating parameters on the yields of the miscellaneous by-products. Throughout the following discussion the term yield is a % molar yield as defined by Eq. 5.1

$$Yield = \frac{moles\ of\ the\ arbitrary\ by\text{-}product}{moles\ of\ the\ MCH\ fed} \times 100 \qquad (5.1)$$

5.1 Potpourri of by-products

The products obtained in studying the dehydrogenation of MCH, as mentioned in Chapter 3, were analyzed using GC-MS and GC-FID. The details of the methods and the columns used with GC-MS and GC-FID are provided in Section 3.2.3 of Chapter 3.

The analysis of the products shows that the dehydrogenation of MCH is very selective towards toluene with % selectivity, defined as the moles of toluene formed

per mole of MCH consumed, generally greater than 98.2%. However, the selectivity towards toluene decreases with pressure and the lowest selectivity is observed at 9 bar pressure at the highest hydrogen concentration in the feed (8.4:1 H_2/MCH molar ratio) where it falls to 92.0%. It is important to mention here from a practical point of view that with nitrogen in the feed i.e. no hydrogen, even at 9 bar pressure, the selectivity is generally greater than 98.0%.

Besides the main product toluene, a number of condensable by-products are also identified. A typical GC-MS chromatogram is shown in Fig. 5.1 which shows most of the identified products. The potpourri of these by-products confirms the existence of several other chemical reactions along with the principal reaction of dehydrogenation of MCH. Table 5.1 shows a list of the products species identified and the possible reactions under which the by-products might be formed. Fig. 5.2 shows schematics of the by-products formation and the possible reactions taking place. The products were detected by GC-MS together with GC-FID with injection of their standard samples.
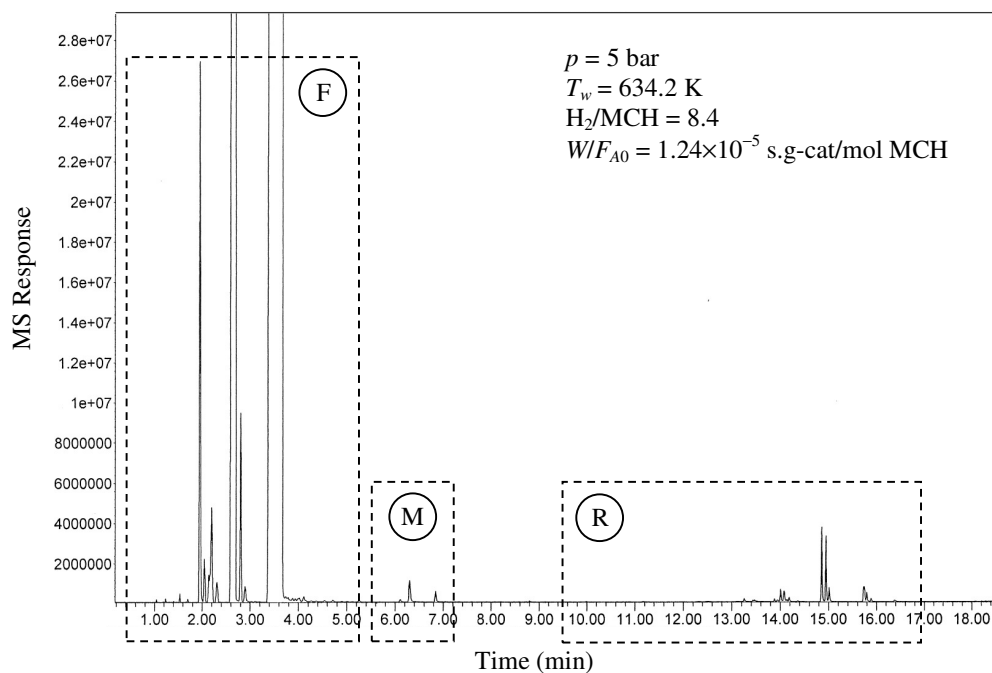
Fig. 5.1a A typical GC-MS chromatogram.

In the upper figure, the following parameters are shown:

p = 5 bar
T_w = 634.2 K
H_2/MCH = 8.4
W/F_{A0} = 1.24×10^{-5} s.g-cat/mol MCH
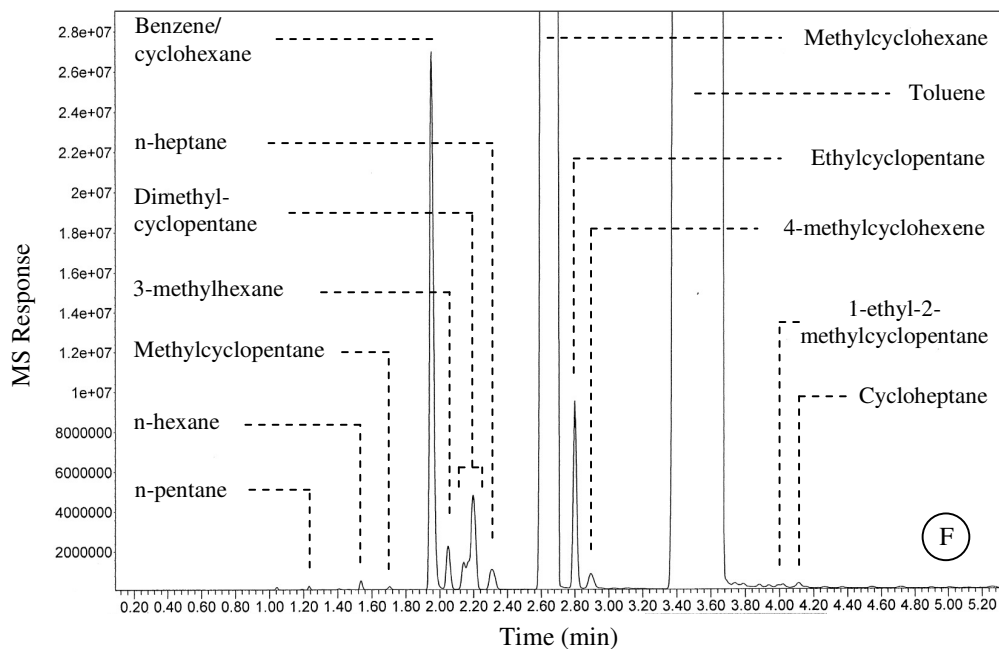
Fig. 5.1b The front end of the chromatogram shown in Fig. 5.1a with identified products.
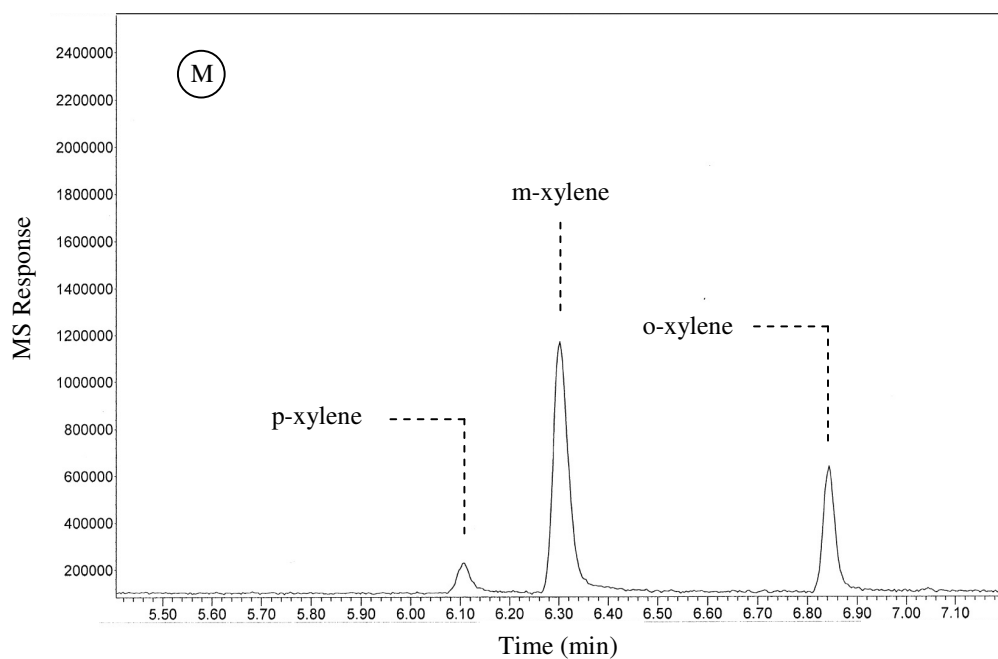
Fig. 5.1c The intermediate part of the chromatogram shown in Fig. 5.1a with identified products.
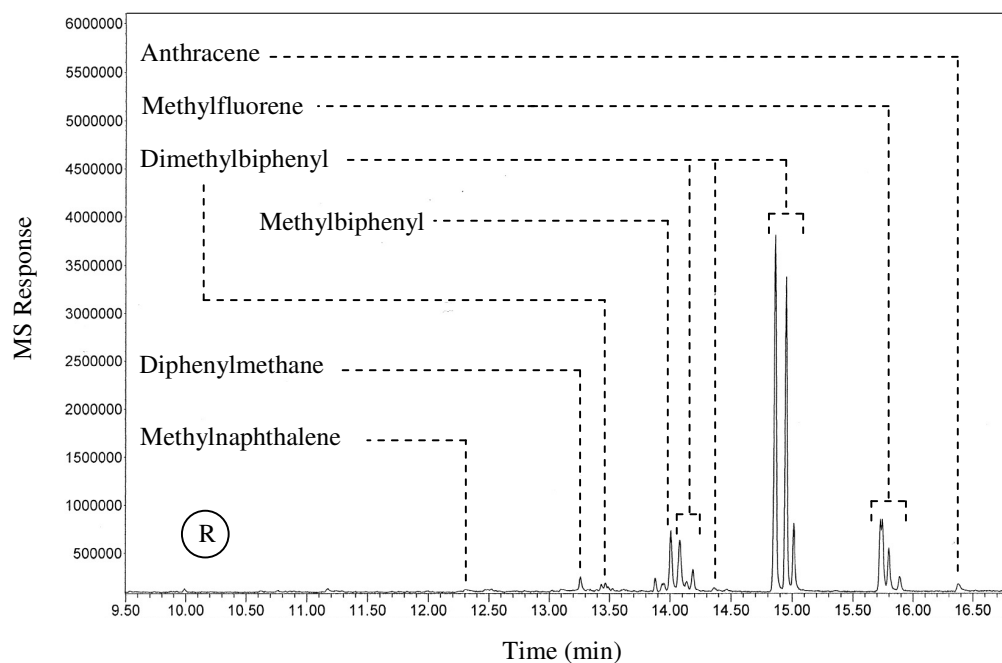
Fig. 5.1d The rear end of the chromatogram shown in Fig. 5.1a with identified products.

Table 5.1 List of condensable by-products formed during the dehydrogenation of MCH

By-product (condensable)	Chemical formula	Qualitative amount	Most likely reaction
Benzene	C_6H_6	Major	Dehydrogenation of cyclohexane
			Hydrodemethylation of toluene
			Disproportionation of toluene
Cyclohexane	C_6H_{12}	Major	Hydrodemethylation of MCH
			Hydrogenation of benzene
Ethylcyclopentane	C_7H_{14}	Major	Isomerisation of MCH
			Hydrogenation of ECPe
Dimethylcyclopentanes	C_7H_{14}	Major	Isomerisation of MCH
			Hydrogenation of DMCPes
Methylcyclohexenes	C_7H_{12}	Minor	Dehydrogenation of MCH
3-methylhexane	C_7H_{16}	Minor	Hydroisomerisation of MCH
n-heptane	C_7H_{16}	Minor	Hydroisomerisation of MCH
Xylene isomers	C_8H_{10}	Minor	Disproportionation of toluene
Dimethylbiphenyls	$C_{14}H_{14}$	Minor	Condensation of toluene
n-pentane	C_5H_{12}	Trace	Ring opening and cracking of MCH
n-hexane	C_6H_{14}	Trace	Ring opening and cracking of MCH
Methylcyclopentane	C_6H_{12}	Trace	Isomerisation of cyclohexane
Cycloheptane	C_7H_{14}	Trace	Isomerisation of MCH
1-ethyl-2-methylcyclopentane	C_8H_{16}	Trace	Ring enlargement
Methylnaphthalene	$C_{11}H_{10}$	Trace	Aromatisation of PDNC*
Diphenylmethane	$C_{13}H_{12}$	Trace	Condensation of toluene
Methylbiphenyl	$C_{13}H_{12}$	Trace	Condensation of benzene/toluene
Anthrancene	$C_{14}H_{10}$	Trace	Polyaromatisation of PDNC*
Methylfluorenes	$C_{14}H_{12}$	Trace	Condensation of toluene
Coke	—	—	Catalytic cracking
			Polycondensation of aromatics
			Polyaromatisation of PDNC*

*partially dehydrogenated naphthenic compounds

In the list above in Table 5.1, benzene (BZN), cyclohexane (CHN) and the ring closed products (RCPs) i.e. the sum of the dimethylcyclopentanes (DMCPs) and ethylcyclopenatne (ECP) are found generally with higher yields in the products as compared to all the other by-products. Under certain operating conditions, the yield of each of the benzene and ring closed products exceeds 1.5 %., while the yield of cyclohexane reaches approximately half a percent. Benzene, cyclohexane and ring closed products are therefore considered as the major by-products in the dehydrogenation of MCH. Isomers of xylene (XLN), methylcyclohexenes (MCHes), dimethylbiphenyls (DMBPhs), n-heptane (HTN) and 3-methylcyclohexane (3MHN) are found in smaller amounts and their individual yields seldom reach 0.1 %. These are, therefore, termed minor by-products. The remaining by-products in Table 5.1, appear as traces.
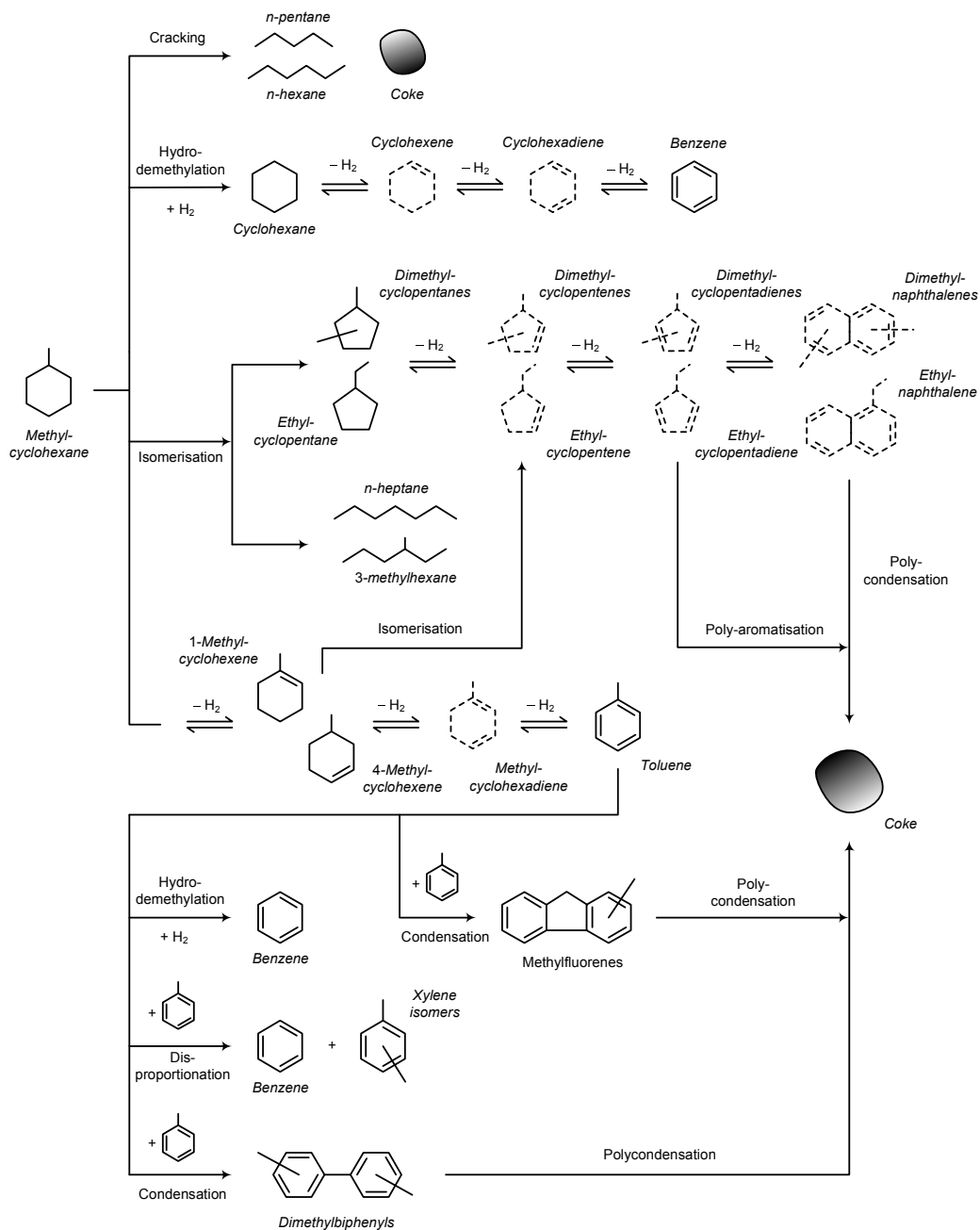
Fig. 5.2 Schematics of the by-products formations. The structures shown in broken lines are not found in the products.

In the following paragraphs the formation of major by-products will be discussed along with xylenes, since the formation of xylenes is associated with that of benzene. Moreover, MCHes will also be discussed as they are considered as intermediate species in the reaction mechanism suggested in Chapter 4.

5.2   Experimental groups

The experimental results are grouped in the same way as for the kinetic analysis of the overall MCH conversion, carried out in Chapter 4. A part of Table 4.1 is therefore reproduced here as Table 5.2 to help the reader in analysing the by-products results.

Table 5.2 Groups formation for the experimental rate data obtained for the dehydrogenation of MCH over 1.0 wt% Pt/γ-Al$_2$O$_3$

Group	Feed composition			T_w (K)	p (bar)	$W/F_{A0} \times 10^{-4}$ s.g-cat-/mol
	y_{A0}	y_{C0}	y_{I0}			
11	0.106	0.893	0.001	614.2, 634.2, 653.2	1.013	3.11, 6.22, 12.44
21	0.485	0.511	0.005	614.2, 634.2, 653.2	1.013	3.11, 6.22, 12.44
31	0.990	0	0.010	614.2, 634.2, 653.2	1.013	3.11, 6.22, 12.44
41	0.485	0	0.515	614.2, 634.2, 653.2	1.013	3.11, 6.22, 12.44
15	0.106	0.893	0.001	614.2, 634.2, 653.2	5.0	3.11, 6.22, 12.44
25	0.485	0.511	0.005	614.2, 634.2, 653.2	5.0	3.11, 6.22, 12.44
45	0.485	0	0.515	614.2, 634.2, 653.2	5.0	3.11, 6.22, 12.44
19	0.106	0.893	0.001	614.2, 634.2, 653.2	9.0	3.11, 6.22, 12.44
29	0.485	0.511	0.005	614.2, 634.2, 653.2	9.0	3.11, 6.22, 12.44
49	0.485	0	0.515	614.2, 634.2, 653.2	9.0	3.11, 6.22, 12.44

5.3   Results and discussion

Figs. 5.3 a–d show the yields of benzene (BZN), cyclohexane (CHN), xylenes (XLNs), ring closed products (RCPs) and methylcyclohexenes (MCHes) at 1.013 bar pressure under varying conditions of temperature and feed composition. The results for the higher pressures may be found in Appendix J.
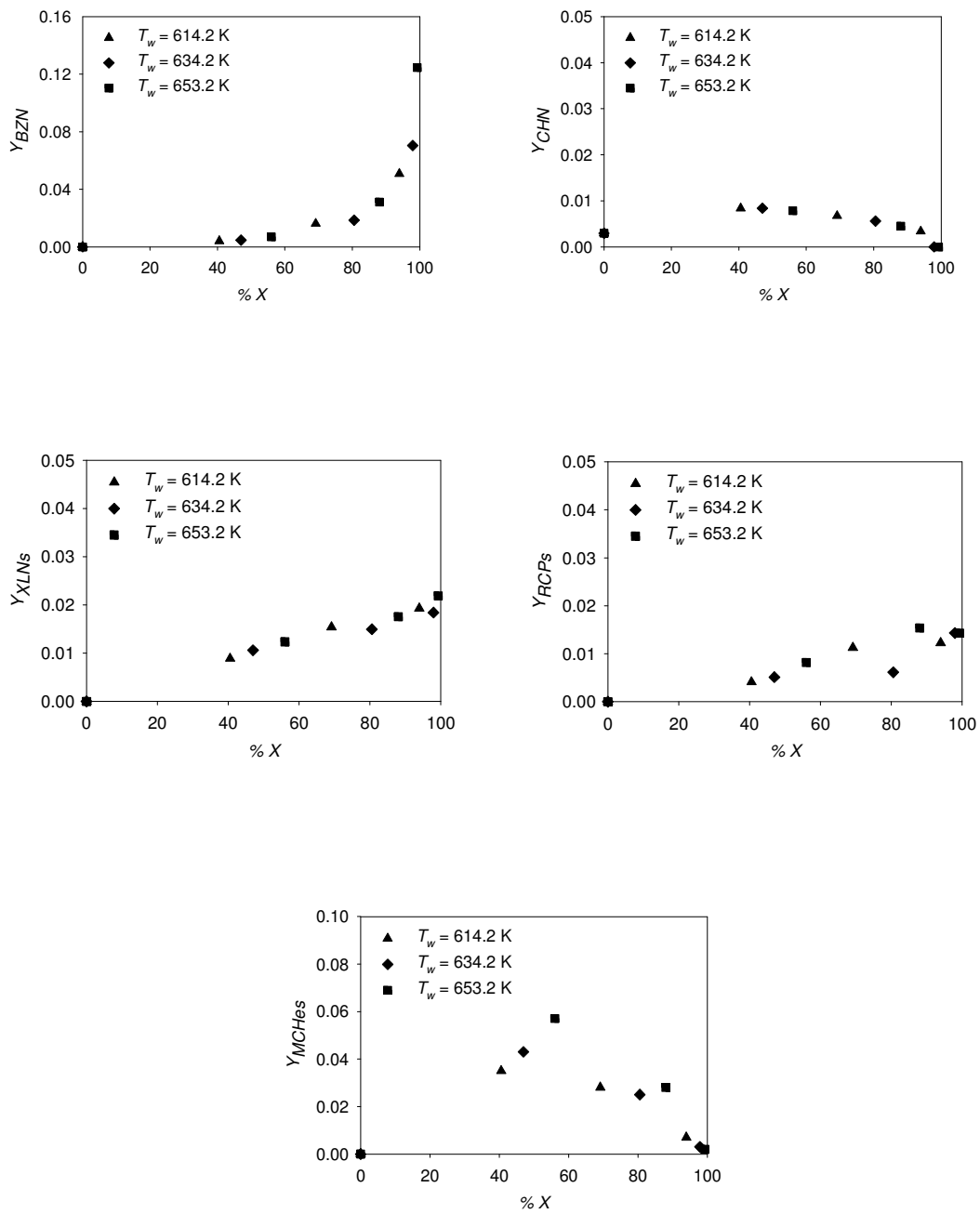
Fig. 5.3a Yields of the products obtained for Group-11.

Fig. 5.3b Yields of the products obtained for Group-21.
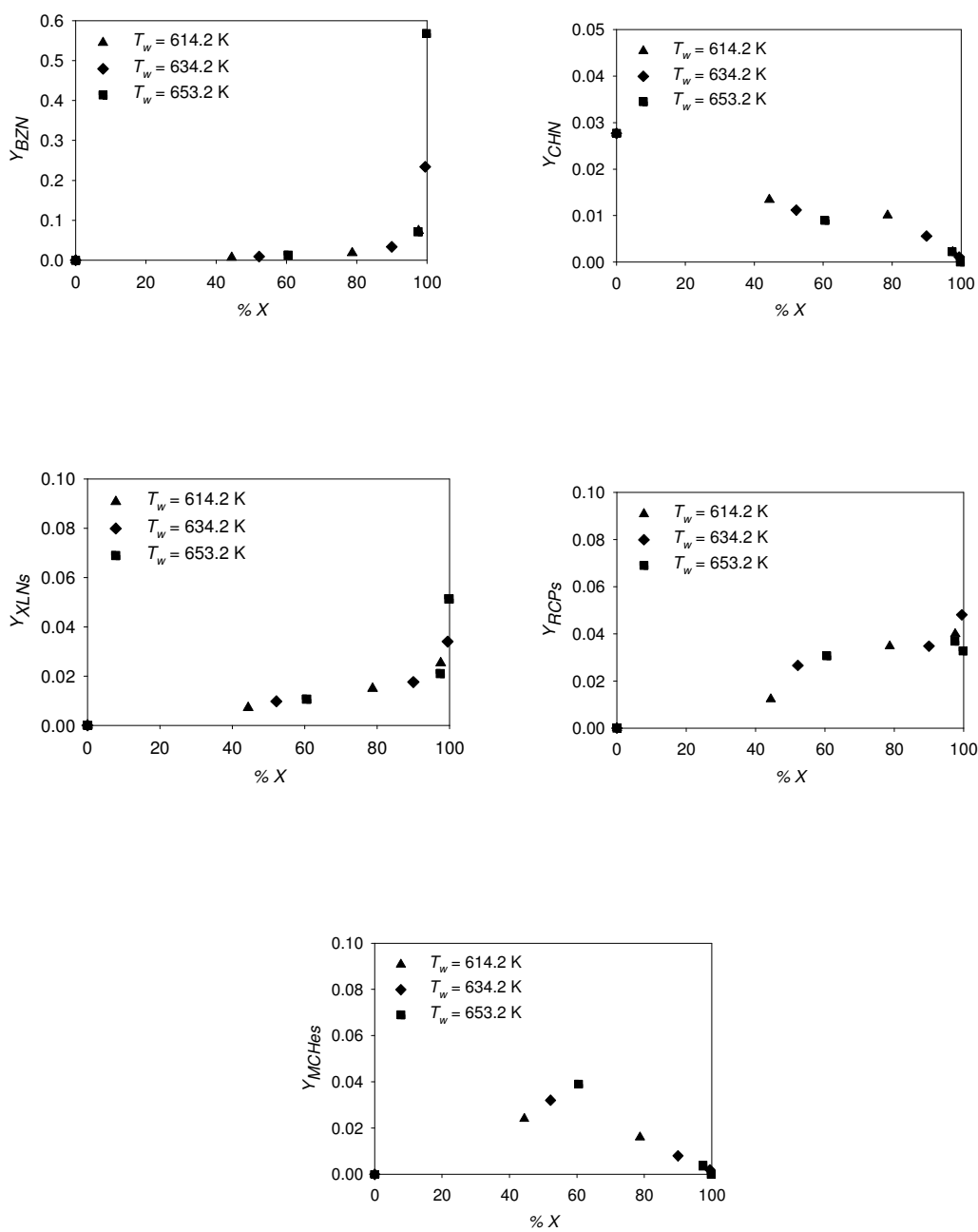
Fig. 5.3c Yields of the products obtained for Group-31.
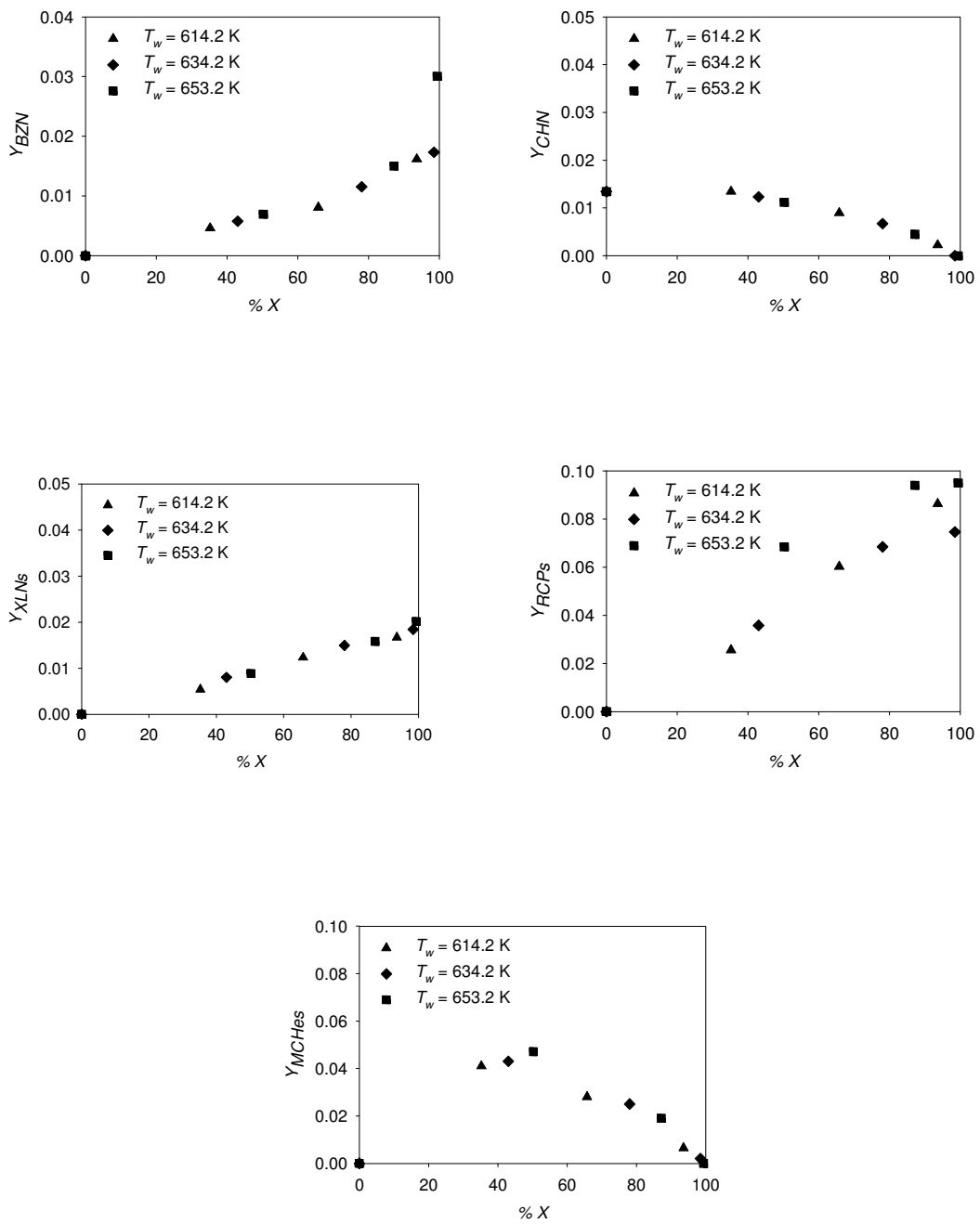
Fig. 5.3d Yields of the products obtained for Group-41.

5.3.1 Benzene, cyclohexane and xylenes

Benzene and cyclohexane have similar boiling points (80.1 °C and 80.7 °C respectively at 1 bar [Lide, 2007]) and co-elute on a boiling point GC column (HP-5 MS). To reconcile these two components it was necessary to employ a PONA column as mentioned in Chapter 3. Fig. 5.4 shows parts of the two GC-FID chromatograms produced over the above mentioned columns for a product sample taken under the same operating conditions. The single peak for the HP-5 MS column is observed to be separated into benzene and cyclohexane peaks over the CP-Sil PONA CB column.

Table 5.1 and Fig. 5.2 show that the following reactions may be responsible for the benzene, cyclohexane and xylenes formation:

- Dehydrogenation of MCH

$$C_7H_{14} \rightleftharpoons C_7H_8 + 3\ H_2 \qquad\qquad (5.2)$$
$$\text{MCH} \qquad\qquad \text{Toluene}$$

- Hydrodemethylation of MCH to cyclohexane

$$C_7H_{14} + H_2 \longrightarrow C_6H_{12} + CH_4 \qquad\qquad (5.3)$$
$$\text{MCH} \qquad\qquad \text{Cyclohexane}$$

- Dehydrogenation of cyclohexane

$$C_6H_{12} \rightleftharpoons C_6H_6 + 3\ H_2 \qquad\qquad (5.4)$$
$$\text{Cyclohexane} \qquad \text{Benzene}$$

- Disproportionation of toluene

$$2\ C_7H_8 \longrightarrow C_8H_{10} + C_6H_6 \qquad\qquad (5.5)$$
$$\text{Toluene} \qquad\qquad \text{Xylene} \quad \text{Benzene}$$

- Hydrodemethylation of toluene

$$C_7H_8 + H_2 \longrightarrow C_6H_6 + CH_4 \qquad\qquad (5.6)$$
$$\text{Toluene} \qquad\qquad \text{Benzene}$$
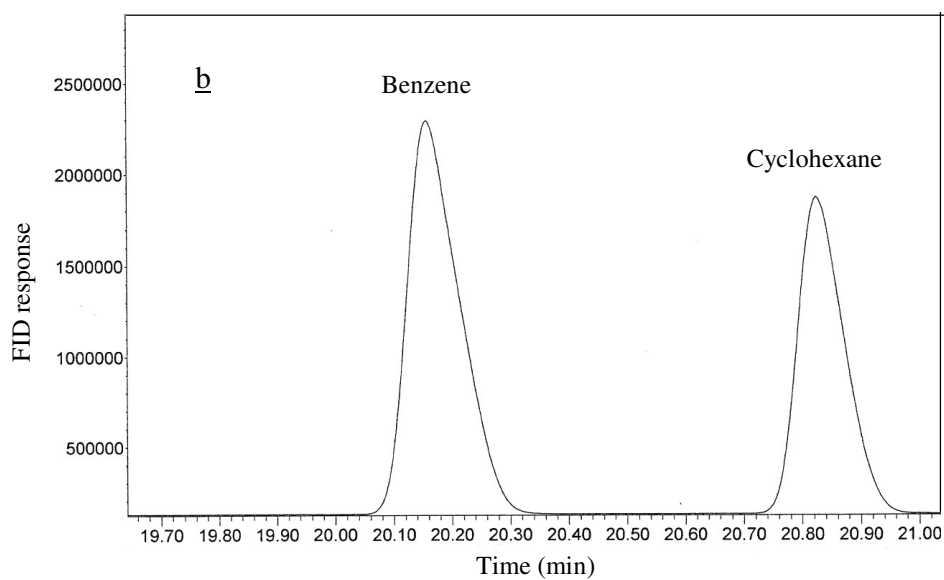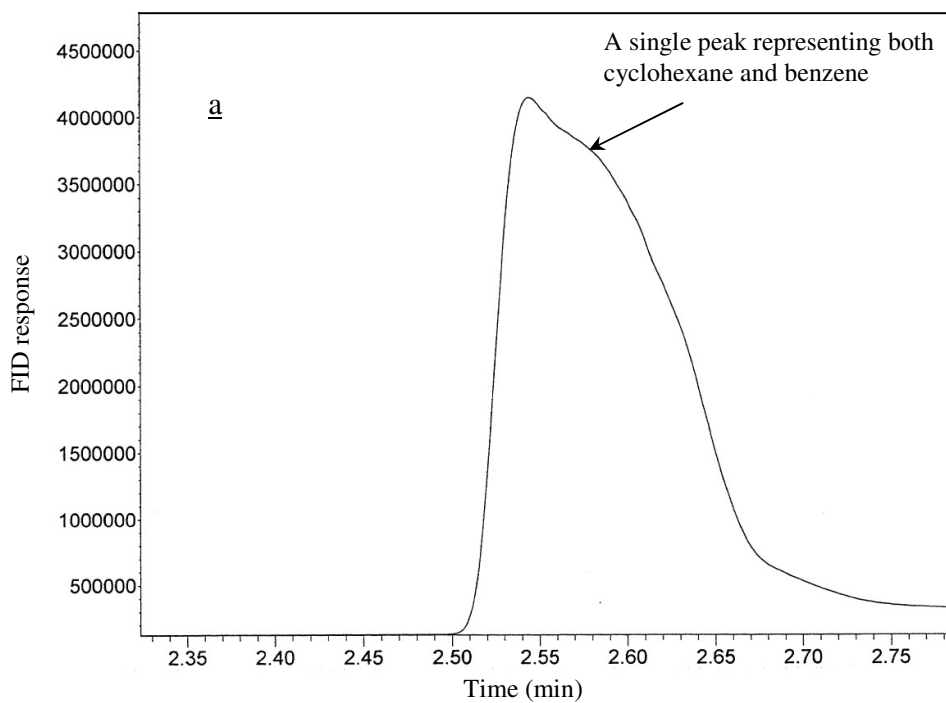
Fig. 5.4 GC-FID Chromatograms for benzene and cyclohexane a) Over HP-5 MS column and b) Over CP-Sil PONA CB column; p = 5 bar, T_w = 634.2 K, H_2/MCH = 8.4 and W/F_{A0} = 1.24×10^{-5} s.g-cat/mol MCH.

5.3.1.1　Cyclohexane — a reaction intermediate

At 1 bar pressure, the cyclohexane yield generally increases with an increase in the MCH conversion before passing through a maximum at some intermediate conversion and then monotonically decreases towards zero. With Group-45, when nitrogen is in the feed, the behaviour is similar to that at 1 bar pressure. This may be because nitrogen acts as an inert and decreases the overall pressure. These experimental observations at low pressures indicate that cyclohexane may be regarded as a reaction intermediate. It is likely an explanation that cyclohexane is formed directly from methylcyclohexane by hydrodemethylation, Reaction 5.3 in the above sequence of reactions. Direct evidence for the hydrodemethylation of MCH to cyclohexane is provided by Johnson and Hepp [Johnson and Hepp, 1970]. Over a Pt catalyst as used in the present study, the MCH demethylation reaction is much slower than the parallel dehydrogenation reaction [Johnson and Hepp, 1970]. However, this situation may be reversed for a supported Ni catalyst. Under favourable thermodynamic conditions, cyclohexane formed by demethylation may disappear to benzene by Reaction 5.4, the dehydrogenation of cyclohexane to benzene.

5.3.1.2　Benzene — a reaction end-product

Again at low pressures, unlike cyclohexane, benzene may be identified as an end product. The yield of benzene increases slowly at first with MCH conversion then increases sharply at high value of MCH conversion. Benzene is therefore not a primary by-product, rather a secondary by-product. Fig. 5.3 shows that the yield of benzene may be much larger than the maximum yield of cyclohexane. This fact, together with the monotonically increasing yield, suggests some other pathways for benzene formation. Clearly, the presence of xylenes shows the occurrence of the toluene disproportionation reaction, Reaction 5.5. Owing to the low yields of xylenes, their yields alone cannot explain the above fact. Thus another reaction pathway, Reaction 5.6, hydrodemethylation of toluene must be responsible for then majority of the benzene formation. The relative activities of Group VIIB and Group VIII metals

and their reaction kinetics for toluene dealkylation were discussed by Grenoble [1979a, 1979b].

5.3.1.3   Effect of temperature on the formation of cyclohexane and benzene

The effect of temperature on the yield/conversion patterns of cyclohexane and benzene is illustrated at one particular pressure and feed composition (Group-11). It should be borne in mind that the laboratory reactor is non-isothermal. As the space-time W/F_{A0} is varied to alter the MCH conversion (X), this causes a simultaneous change in the average bed temperature (T). Thus, a particular yield/conversion curve has associated with it a range of T values within which the data were gathered. This is indicated for the patterns in Fig. 5.5. The maximum yield of cyclohexane increases with temperature and occurs at progressively lower conversion. The data in Fig. 5.5 suggest a doubling of the maximum yield for an increase of 30−40 K in the average bed temperature. This suggests that the activation energy of Reactions 5.2 and 5.3 above are such that

$$E_{5.3} > E_{5.2} \qquad\qquad\qquad (5.7)$$

Further, the complete disappearance of cyclohexane is observed at high conversions and bed temperatures. This suggests further that Reaction 5.4 may be considered irreversible under the chosen reaction conditions. There is little, if any, effect of temperature upon the yield of benzene at low to intermediate conversions. Since benzene is being formed principally by Reaction 5.4 in this region, the suggestion is that

$$E_{5.4} = E_{5.2} \qquad\qquad\qquad (5.8)$$

At high conversion of MCH, benzene is being produced by Reaction 5.6. It is clear that temperature has a strong positive effect as X approaches unity, indicating

$$E_{5.6} \gg E_{5.2} \tag{5.9}$$
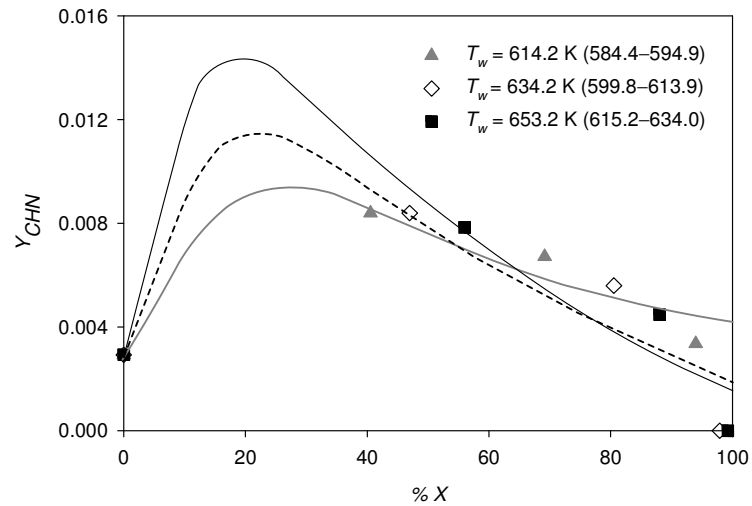
Fig 5.5a Effect of temperature on the yields of cyclohexane. The values in parentheses in the legend of the figure are the average temperatures in K.
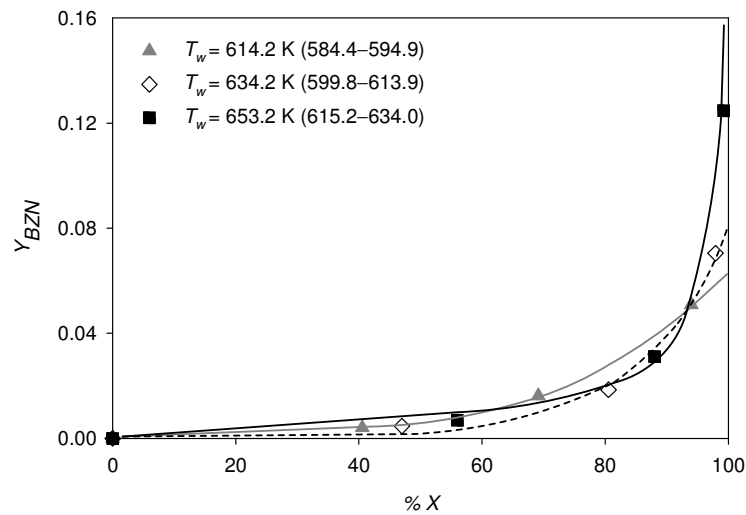
Fig 5.5b Effect of temperature on the yields of benzene. The values in parentheses in the legend of the figure are the average temperatures in K.

5.3.1.4 Effect of pressure upon the yield of benzene, cyclohexane and xylenes

The effect of pressure upon the yields of benzene, cyclohexane and xylenes is shown in Fig. 5.6. It is observed that at high pressures, the cyclohexane yield increases continuously with MCH conversion and cyclohexane reverts from being a reaction intermediate to become a reaction end product. The most likely explanation of this change may be ascribed to the reversibility of Reaction 5.4. However, an improved hydrogen adsorption may increase the rate of demethylation reaction to form cyclohexane. At low pressures, the dehydrogenation of cyclohexane to benzene is strongly favoured thermodynamically. Thus, Reaction 5.4 tends to run forward irreversibly, as does the main reaction (dehydrogenation of MCH to toluene, Reaction 5.1) and at high MCH conversion, cyclohexane may be totally consumed to benzene. At high pressures, the dehydrogenation of cyclohexane to benzene is prevented by thermodynamics. Reaction 5.4 is now reversed and cyclohexane becomes an end-product. For $X < 0.7$, the yield of cyclohexane is observed to exceed that of benzene.

The benzene yield increases dramatically with pressure, taking off exponentially as X tends to 1.0. A molar yield of almost 2.0% is observed at 5 bar pressure for $X > 9.0$ (Fig. 5.7). Though benzene becomes a reaction intermediate in the scheme above, the rate of reaction for Reaction 5.6 must greatly exceed that of Reaction 5.4. Above X equal to 0.7, the yield of benzene exceeds that of cyclohexane and far outstrips it at higher conversions.

The effect of pressure on the xylenes yields is observed to be negligible and the contribution of the disproportionation reaction of toluene is found unimportant in contributing to the increased yields of cyclohexane and benzene.
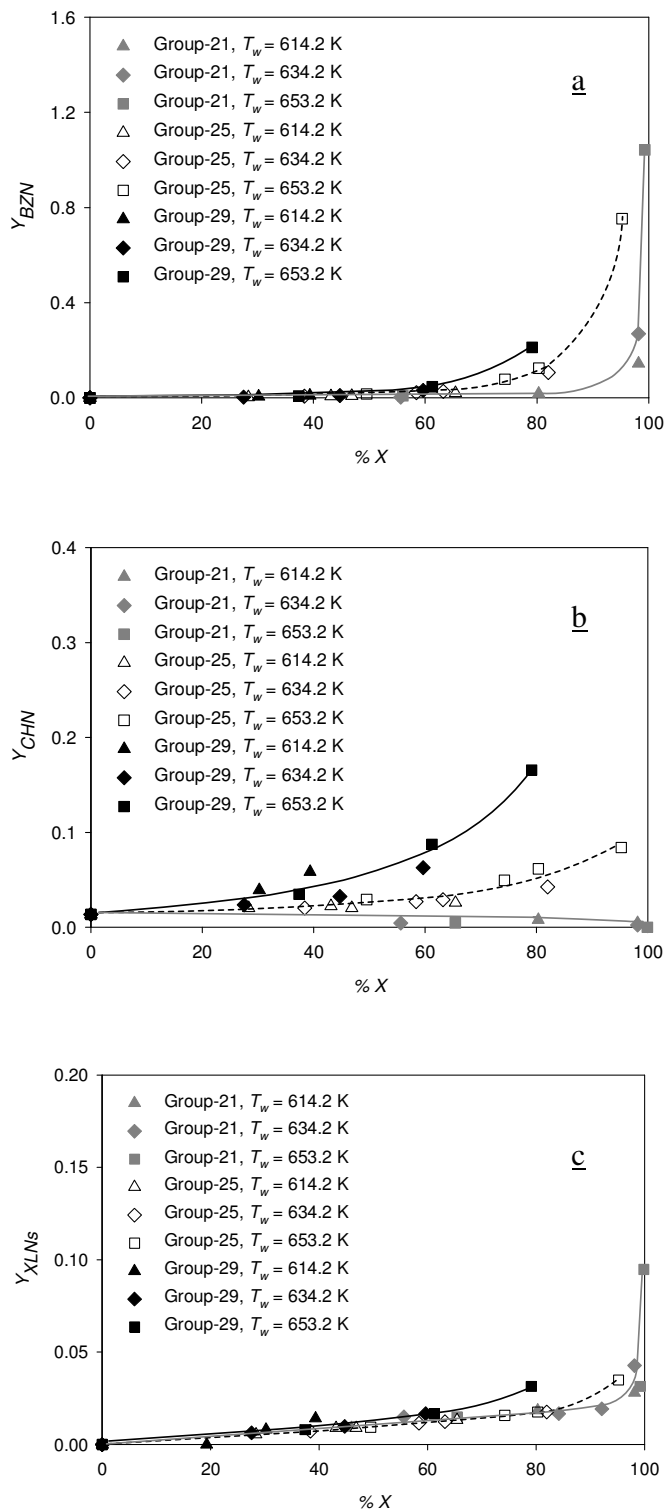
Fig. 5.6 (a-c) Effect of pressure on the yields of benzene,
cyclohexane and xylenes for Group-21.
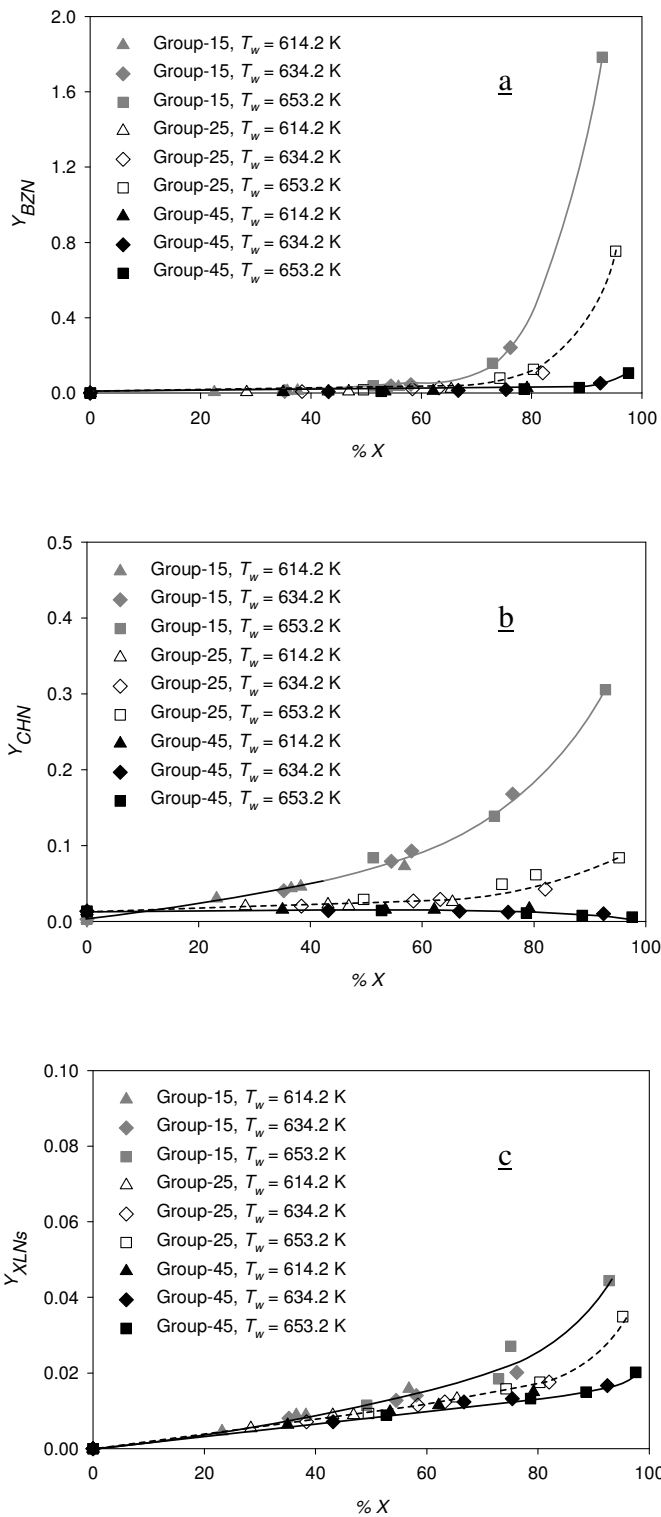
Fig. 5.7 (a-c) Effect of composition on the yields of benzene,
cyclohexane and xylenes at 5 bar.

5.3.1.5 Effect of feed composition upon the yield of benzene, cyclohexane and xylenes

At 1 bar pressure, cyclohexane appears as an intermediate product, irrespective of feed composition. The thermodynamics of cyclohexane dehydrogenation to benzene are favoured and benzene appears as an end-product, irrespective of feed composition. Feed compositional effects are most pronounced at high MCH conversions. In Fig. 5.3, comparing Group-11 and Group-21, high ultimate benzene yield is the result with Group-21 having less hydrogen in the feed. Moreover, comparing Group-21 and Group-41, shows that the presence of H_2 as a feed diluent, instead of nitrogen, also raises the benzene yield. These observations impart the significance of hydrogen concentration in carrying out the relative rates of Reactions 5.3 and 5.4. At high pressures, the ultimate benzene yield increases with the increase in the hydrogen concentration in the feed. The cyclohexane yield also increases with increase in the hydrogen concentration in the feed. A comparative effect of composition of the reactant feed on the yields of benzene, cyclohexane and xylenes at 5 bar pressure is shown in Fig. 5.7. However, at 9 bar, the relative importance of reactor temperature is also observed. As an example, for Group-19 shown in Fig. 5.3, the cyclohexane yield at the wall temperature of 614.2 K is higher than at 653.2 K. Again, the relative rates of the reactions in the reactions sequence outlined above, seem to be responsible. A slight effect of feed composition is observed on the xylenes formation.

5.3.2 Ring closed products (RCPs)

Ethylcyclopentane (ECP) and Dimethylcyclopentanes (DMCPs) are the two ring closed by-products observed in the dehydrogenated products. The development catalyst, 1.0 wt% Pt/Al_2O_3, is a bifunctional catalyst where the Pt metal takes on the function of hydrogenation-dehydrogenation while the alumina support provides with the acidic function. The presence of the acidity in the support used in the present study was confirmed by Alhumaidan [2008] using NH_3-TPD (temperature

programmed desorption). The measured acidity of γ-Al$_2$O$_3$ was $1.61{\times}10^{19}$ acid sites/g [Alhumaidan, 2008]. As chloroplatinic acid is used as a Pt precursor and HCl is employed to provide the right pH environment in the preparation of the catalyst, a little more acidity is expected due to chloride ions.

The formation of ECP and DMCPs is the result of isomerisation reactions and requires the acidic function of the catalyst. The following two reaction mechanisms may be proposed for the formation of these by-products.

- In the first mechanism, shown in Fig. 5.8, MCH may first dehydrogenate to methylcyclohexene on the Pt sites and the partially dehydrogenated methylcyclohexane then isomerises on acid sites to dimethylcyclopentenes (DMCPes) and ethylcyclopentene (ECPe). The DMCPes and ECPe exploit the metallic function of the bi-functional catalyst and hydrogenate to DMCPs and ECP respectively or dehydrogenate further to produce cyclopentadienes [Tsakiris, 2007]. For a bifunctional Pt/Al$_2$O$_3$ catalyst, this mechanism for MCH dehydrogenation is reported by Tsakiris [2007] and it is based on the suggestions of Sinfelt and Rohrer [1961] and the mechanism proposed by Haensel et al. [1965] for the formation of methylcyclopentene from cyclohexene.
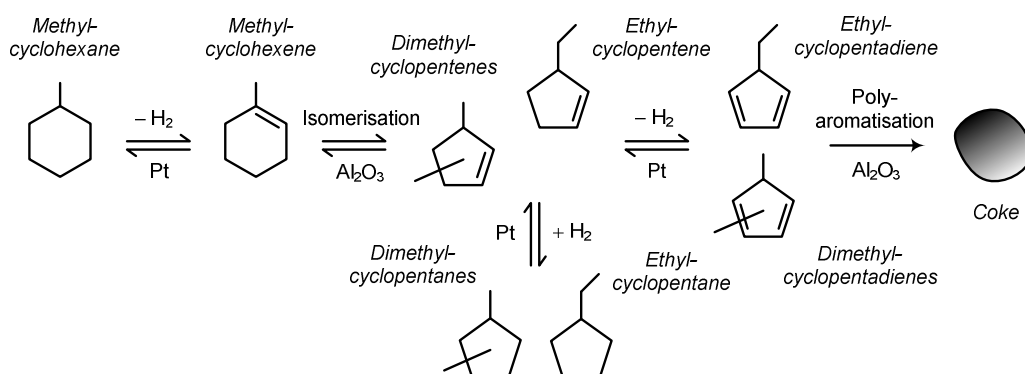
Fig. 5.8 Mechanism-I: Dehydrogenation of MCH to MCHe which isomerises to partially dehydrogenated ring closed products.

- In an alternate mechanism, as shown in Fig. 5.9, MCH isomerises on the acid support to form ECP and DMCPs. Under favourable thermodynamic conditions, ECP and DMCPs successively dehydrogenate to form DECPe and DMCPes respectively.

The cyclopentadienes formed in both Mechanism-I and Mechanism-II are very unstable and readily polymerise to polycyclics (coke), as proposed by Myers et al. [1961]. It is worthwhile to mention here that aromatic compounds and especially partially dehydrogenated naphthenic compounds formed during the dehydrogenation of MCH are potential precursors to coke formation and undergo polyaromatic and polycondensation reactions to form coke on the catalyst surface. For the present study, the presence of biphenyls, naphthalenes, diphenylmethane, fluorenes and anthracene in the dehydrogenation products supports the above argument.
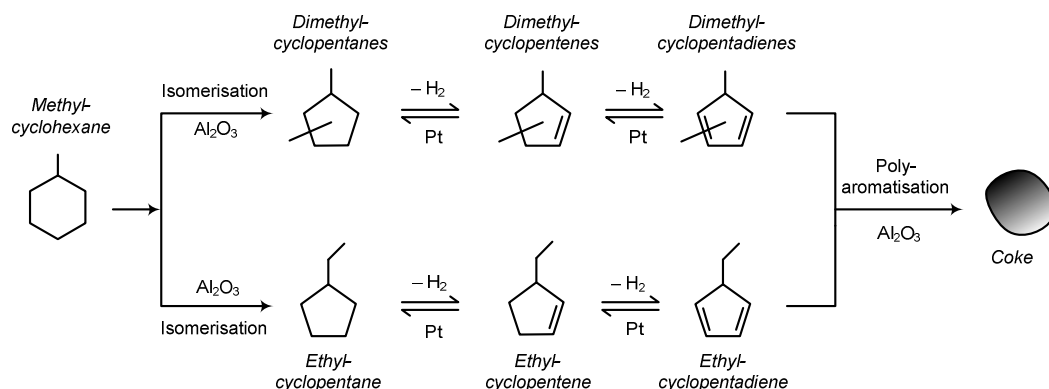
Fig. 5.9 Mechanism-II: Isomerisation of MCH to cyclopentanes which dehydrogenate to form partially dehydrogenated ring closed products.

5.3.2.1   Yield patterns of RCPs

Generally, the yield of RCPs increases with an increase in the MCH conversion, X. At 1 bar pressure, as shown in Figs. 5.3 a–d, the yield of RCPs first increases strongly with MCH conversion and then almost levelled off with the horizontal especially with high temperatures. The similar behaviour was observed by Al-Sabawi and de Lasa [2009] for the combined yields of ECP and DMCPs for

cracking of MCH over FCC zeolite catalyst (acidic catalyst) at low pressures. Owing to the favourable dehydrogenation conditions at 1 bar and comparison of the results with FCC catalyst, it is proposed that Mechanism-II is dominant at least at low pressures. At low conversion region, isomerisation activity was dominant, however as the reaction proceeds to completion, the naphthenes formed during the reaction started disappearing by dehydrogenating to cyclopentenes. Although cyclopentenes are not observed in the products but their ultimate product coke is observed on the catalyst surface. Fig. 5.10 shows the strong positive effect of pressure on the RCPs yields especially in the relatively high pressure region. At high pressures, unlike at 1 bar, the RCPs yield increases continuously with an increase in the pressure. At 9 bar pressure, the yield patterns are also found to be a function of temperature. The effect of composition on the yield of the RCPs is provided in Fig. 5.11. An increase in the yield with increase in the H_2/MCH feed ratio is observed.
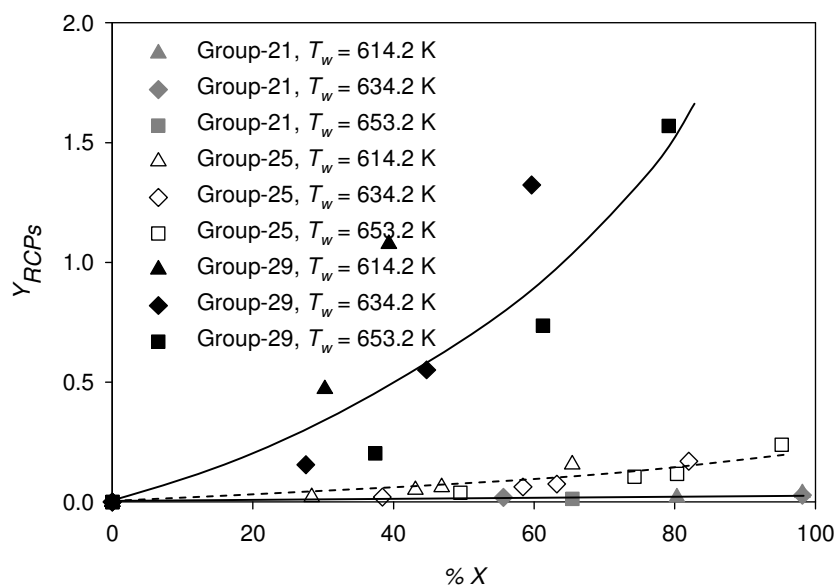
Fig. 5.10 Effect of pressure on the yields of ring closed products.

156
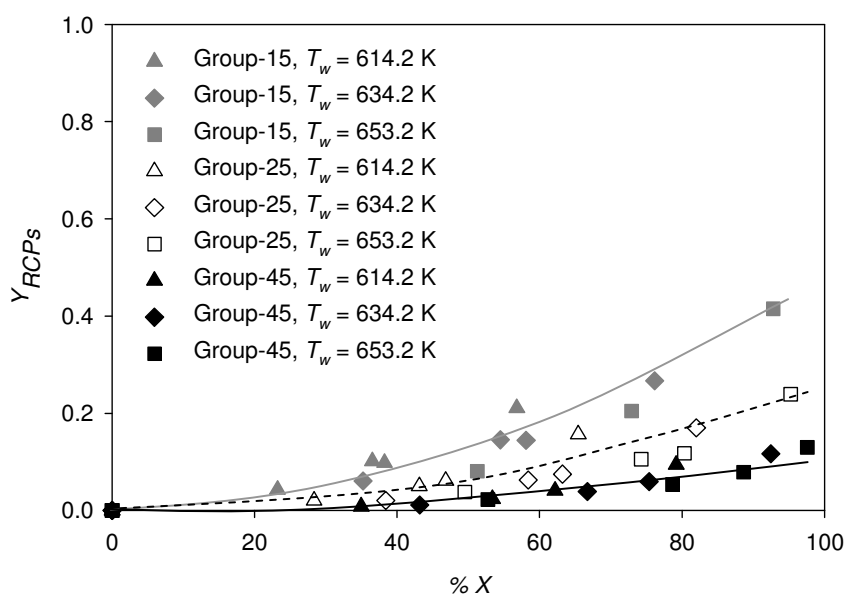
Fig. 5.11 Effect of composition on the yields of ring closed products.

5.3.3 Methylcyclohexenes

In Chapter 2 and Chapter 4, it is suggested that the overall dehydrogenation reaction of MCH to toluene may be comprised of successive dehydrogenation steps, as shown below:

$$\text{MCH} \underset{}{\overset{-H_2}{\rightleftharpoons}} \text{MCHe} \underset{}{\overset{-H_2}{\rightleftharpoons}} \text{MCHde} \underset{}{\overset{-H_2}{\rightleftharpoons}} \text{Tol} \qquad (5.10)$$

In the reactions sequence, Eq. 5.10, MCHe (methylcyclohexene) and MCHde (methylcyclohexadiene) are the reaction intermediates. The presence of MCHe in the products, therefore, confirms that the reaction follows the route given in the above sequence. Although, MCHde has never been found present in the dehydrogenated products, it can not be ruled out that it is formed once the reaction has started following the sequence given in Eq. 5.10.

Fig. 5.3 shows the yields of MCHe formed under various groups of operating conditions. The yields for the remaining groups may be found in Appendix J. The yield of methylcyclohexenes is a combination of 1-MCHe and 4-MCHe. 3-MCHe has

not been found and identified in the reaction products. Generally, the yield of MCHes first increases at low conversions, reaches a maximum and then decreases at high conversions of MCH to toluene. This maximum in MCHes yield generally occurs around 50% MCH conversion. This behaviour shows that the ratio of the rate of the formation of MCHe in first step of the reaction sequence, Eq. 5.10, to the rate of disappearance of MCHe in the following step is a function of the progress of the reaction. The yields of MCHe tend to approach zero at the complete conversion of MCH.

Fig. 5.12 shows the effect of pressure upon the MCHe formation. It can be clearly seen that an enhanced yield of MCHes is the result at high pressures. This may be attributed to the reversible nature of the dehydrogenation reaction. The relative increase in the yields with pressure is observed to be higher at high pressures than at the lower pressures.
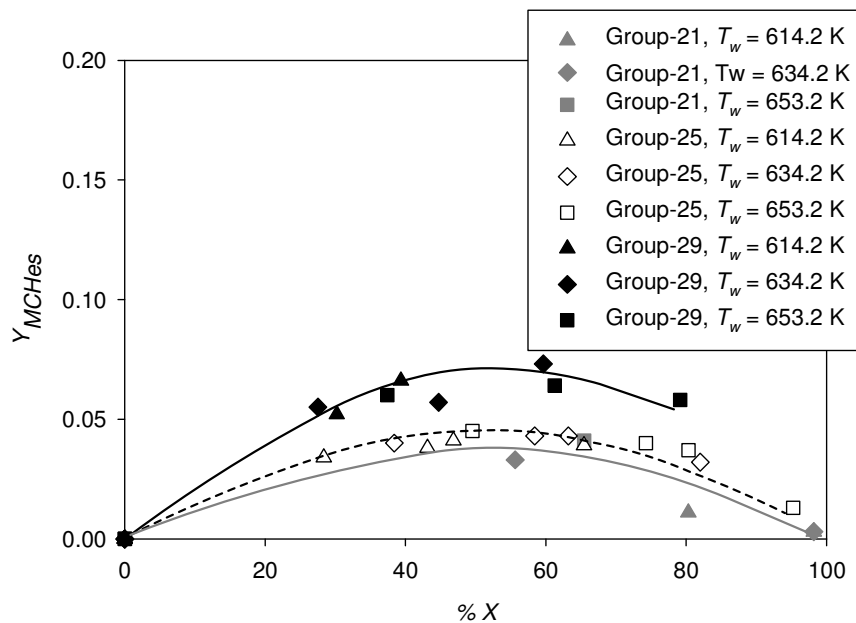
Fig. 5.12 Effect of pressure on the yields of methylcyclohexenes by-products.

Fig. 5.13 shows the effect of feed composition on the MCHe formation and indicates that the concentration of hydrogen has a direct effect on the formation of MCHes. However, the effect is appeared to vanish at high conversions of MCH. An

increased conversion of MCHes with increase in the hydrogen concentration shows the increased rates of reversible reactions.
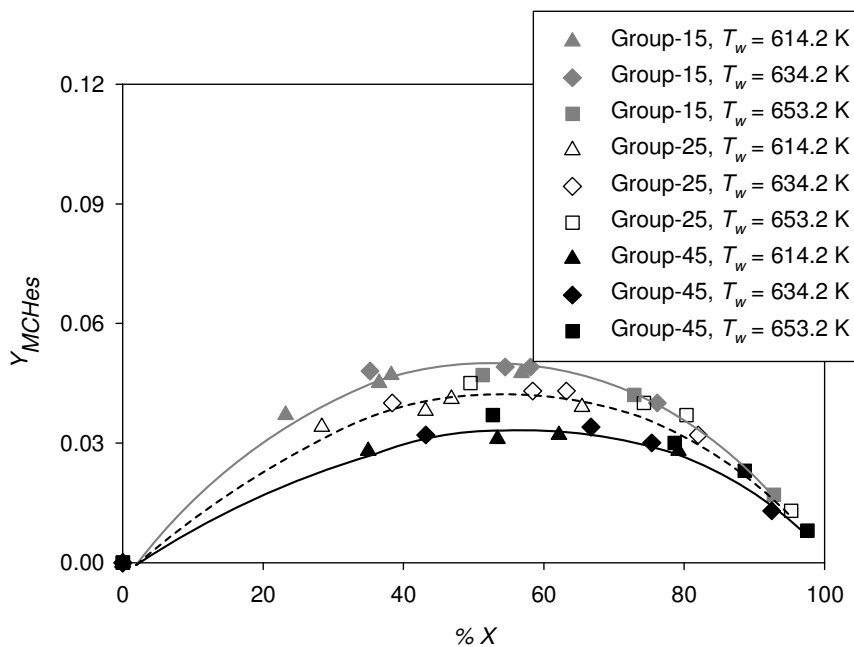
Fig. 5.13 Effect of composition on the yield of methylcyclohexenes by-products.

Chapter 6

Simulation of Laboratory Fixed Bed Reactor and Estimation of the Radial Thermal Conductivities and Wall Heat Transfer Coefficients

The dehydrogenation of methylcyclohexane is a highly endothermic reaction for which large temperature gradients exist in the fixed bed dehydrogenation reactor [Hawthorn et al., 1968]. The gradients of temperature and concentration result from the interaction between reaction kinetics and the transport phenomena associated with the reactor system [Hawthorn et al., 1968]. Evidently in such a case the radial heat transfer parameters will affect the activity, selectivity and deactivation characteristics of the catalyst [Specchia et al., 1980]. The radial thermal conductivity and wall heat transfer coefficients thus become key parameters in the design and understanding of the behaviour of the fixed bed catalytic reactor. The purpose of this chapter is to develop a non-isothermal fixed bed reactor model which can satisfactorily predict the observed axial temperature profiles. If successful, the model will be developed further to design a prototype reactor system for "on-board" use (Chapter 7).

6.1   Mathematical modelling of the laboratory fixed bed reactor

A two-dimensional pseudo-homogeneous model was used as a basis for the mathematical modelling of the laboratory fixed bed reactor. A pseudo-homogeneous model, in contrast to a heterogeneous model, assumes negligible gradients of temperature and concentration between the catalyst and the fluid surrounding the catalyst particles and, therefore, the catalytic bed behaves like a single phase [De Wasch and Froment, 1972; Missen et al., 1999]. The pseudo-homogeneous model requires a lower computing effort than the heterogeneous model [Pereira Daurte et al., 1984]. This type of model has been used extensively in the literature [Pereira Duarte et al., 1984; Ahmed and Fahien, 1980] and the two-dimensional form is recommended for reactors undergoing large heat effects [Froment and Bischoff,

1979]. In the development of the model equations, a steady-state plug flow process is assumed. Mass and energy balances around a thin cylindrical shell of the catalyst bed lead to two parabolic partial differential equations (PDEs). A complete derivation procedure for the following PDEs may be found in Appendix K.

6.1.1 Mass balance equation

$$\frac{\partial X}{\partial z} = \frac{d_p}{Pe_{r,m}}\left[\frac{\partial^2 X}{\partial r^2} + \frac{1}{r}\cdot\frac{\partial X}{\partial r}\right] + \frac{\rho_b\cdot(-r)\cdot M_F}{G\cdot y_{A0}}$$ (6.1)

where, $Pe_{r,m}$ is the radial Peclet number for mass transfer and is given by

$$Pe_{r,m} = \frac{G\cdot d_p}{\rho\cdot D_r}$$ (6.2)

6.1.2 Energy balance equation

$$\frac{\partial T}{\partial z} = \frac{d_p}{Pe_{r,h}}\left(\frac{\partial^2 T}{\partial r^2} + \frac{1}{r}\cdot\frac{\partial T}{\partial r}\right) + \frac{\rho_b\cdot(-r)\cdot(-\Delta h_{rxn})}{G\cdot c_p}$$ (6.3)

where, $Pe_{r,h}$ is the radial Peclet number for heat transfer and is given by

$$Pe_{r,h} = \frac{G\cdot c_p\cdot d_p}{k_r}$$ (6.4)

6.1.3 Boundary conditions

$$X = 0 \text{ and } T = T_0 \qquad\qquad\qquad \text{at } z = 0 \qquad\qquad (6.5)$$

$$\frac{\partial X}{\partial r} = \frac{\partial T}{\partial r} = 0 \qquad\qquad\qquad \text{at } r = 0 \qquad\qquad (6.6)$$

$$\frac{\partial X}{\partial r} = 0 \qquad\qquad\qquad\qquad \text{at } r = R_i \qquad\qquad (6.7)$$

$$\frac{\partial T}{\partial r} = Bi_h \cdot (T_w - T) \qquad\qquad \text{at } r = R_i \qquad\qquad (6.8)$$

where, Bi_h is the Biot number for heat transfer, and is given by

$$Bi_h = \frac{h_w \cdot R_i}{k_r} \qquad\qquad\qquad\qquad\qquad\qquad (6.9)$$

The parabolic differential equations along with the boundary conditions were numerically solved using an explicit finite-difference approach [Beek, 1962; Walas, 1991; Smith, 1981]. The details of the solution method and the methods applied for the estimation of the thermophysical properties are given in Appendix K and Appendix L, respectively.

6.2 Kinetic equation

The kinetic equation developed in Chapter 4 was used in the simulation of the laboratory reactor and is shown here for the convenience of the reader.

$$(-r) = \frac{40.907 \cdot k \cdot p_A \cdot \left(1 - \dfrac{p_B \cdot p_C^3}{K \cdot p_A}\right)}{1 + 40.907 \cdot p_A + 22.194 \cdot p_B + K' \cdot p_B \cdot p_C^2} \cdot (1 - 1.471 \cdot t_d),$$

$$\text{mol·s}^{-1}\text{·g-cat}^{-1} \qquad\qquad (6.10)$$

$$K = 3600 \cdot \exp\left(\frac{-217650}{R}\left(\frac{1}{T} - \frac{1}{650}\right)\right), \text{ bar}^3 \qquad (6.11)$$

$$k = 4.064 \times 10^{-5} \cdot \exp\left(7.652 \cdot \left(1 - \frac{617.2}{T}\right)\right), \text{ mol} \cdot \text{s}^{-1} \cdot \text{g-cat}^{-1} \qquad (6.12)$$

$$K' = 6.688 \cdot \exp\left(-24.038 \cdot \left(1 - \frac{617.2}{T}\right)\right), \text{ bar}^{-3} \qquad (6.13)$$

The values of p_A, p_B and p_C were calculated using the mole balance equations developed in Section 4.2.2 of Chapter 4.

6.3   Reactor bed properties

The laboratory reactor was a simple fixed bed micro-continuous reactor equipped with a high capacity electrical furnace to maintain a uniform reactor wall temperature. Fig. 6.1 shows a simple sketch of the reactor geometry and Table 6.1 provides the reactor bed dimensions and properties. A detailed description of the dehydrogenation reactor is provided in Section 3.1 of Chapter 3.

6.3.1   Bulk density and bed voidage

The bulk density of the bed was determined in-situ. A known mass (2.01 g) of the catalyst particles was loaded in the reactor tube and the volume occupied by the catalyst was measured. Taking skeletal density of the alumina as 3970 kg/m^3 (Supplier Alfa-Aesar), the particle density was calculated using the following relation

$$\rho_p = \frac{\rho_s}{(\rho_s \times v_P) + 1} \qquad (6.14)$$
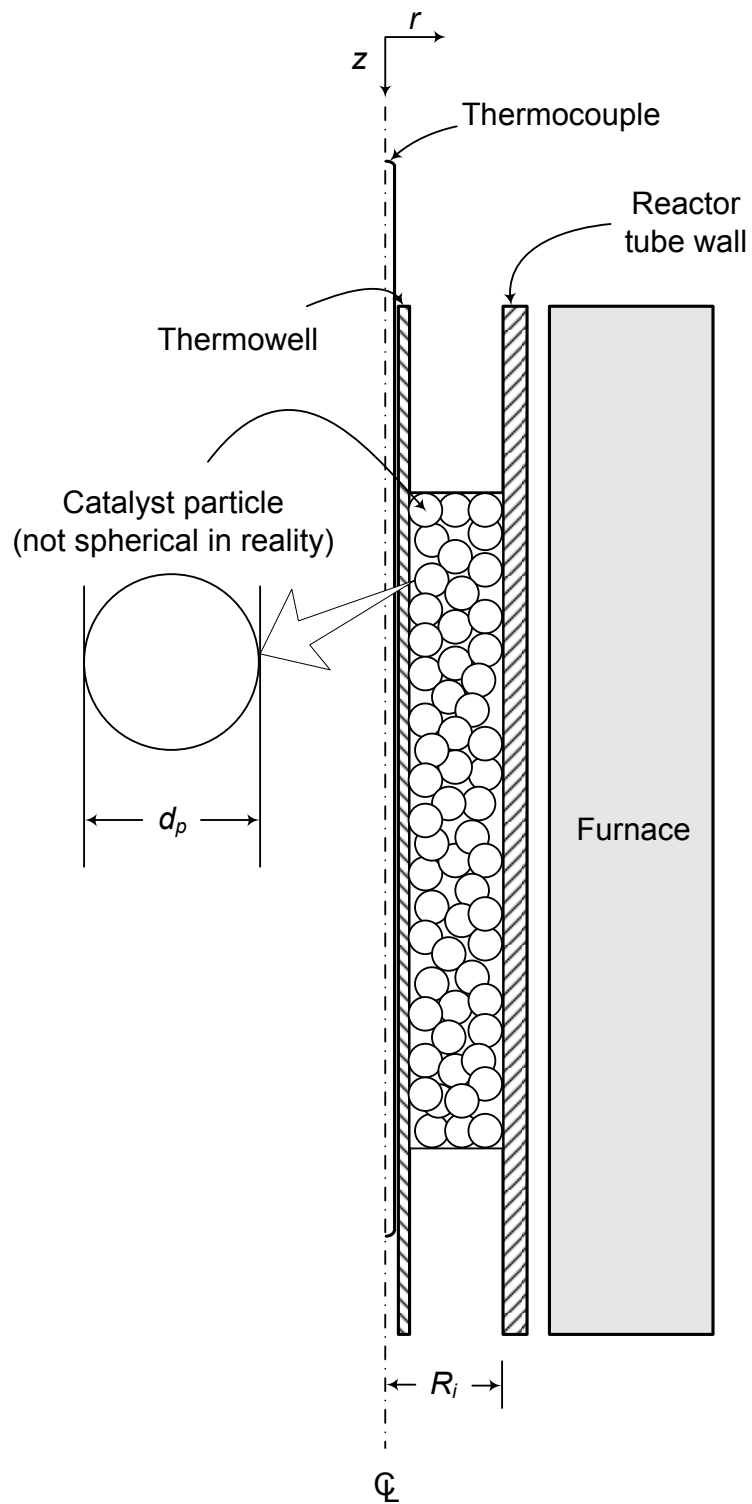
Fig. 6.1 Axi-symmetrical geometry of the laboratory MCH
dehydrogenation reactor (not to scale)

The bed voidage was then calculated using the equation

$$\varepsilon_b = 1 - \frac{\rho_b}{\rho_p} \qquad (6.15)$$

The results obtained from Eq. 6.14 and Eq. 6.15 are shown in Table 6.1.

Table 6.1 Reactor bed dimensions and properties

D_i (m)	$D_{tw} \times 10^3$ (m)	$d_p \times 10^4$ (m)	L_b (m)	$v_P \times 10^{-3}$ (m^3/kg)	ρ_b (kg/m^3)	ρ_p (kg/m^3)	ε_b
0.0102	3.175	5.68	0.040	0.58	680.94	1202.1	0.43
0.0102	2.880	5.68	0.032	0.58	835.29	1202.1	0.31

6.4 Radial transport properties and wall heat transfer coefficient

The particle Reynolds number (Re_p), as defined by Eq. 6.16, was calculated for the various operating conditions. Low values of the Reynolds number close to unity ($Re_p \sim 1.0$) suggested a close approach to stagnant flow conditions ($Re_p = 0$).

$$Re_p = \frac{d_p \cdot G}{\mu} \qquad (6.16)$$

6.4.1 Radial thermal conductivity (k_r)

Preliminary runs of the model showed the effective radial thermal conductivity (k_r) was a strong function of the properties of the reaction mixture. Thus the model equations were modified to account for the changes in physical properties with both composition and temperature. The effective radial thermal conductivity was updated step by step in accordance with the physical property changes.

A number of investigators have proposed correlations for the prediction of the stagnant radial thermal conductivity, k_r^o in a fixed bed reactor. Melanson and Dixon

[1985] reviewed the literature correlations and based on experimental support recommended the use of the Kunii-Smith formula [Kunii and Smith, 1960] for the estimation of stagnant radial thermal conductivity. Moreover, the formula includes the effect of gas thermal conductivity and is well suited to be used for the present study. The Kunii-Smith formula with negligible contribution of radiation heat transfer is provided in Table 6.2 (Eq. 6.17–6.25).

Table 6.2 Kunii-Smith formula for the estimation of stagnant radial thermal conductivity of the bed

$$\frac{k_r^o}{k_g} = \varepsilon_b + \frac{\beta \cdot (1 - \varepsilon_b)}{\phi + \gamma \cdot \left(\dfrac{k_g}{k_s}\right)} \tag{6.17}$$

$$\phi = \phi_2 + (\phi_1 - \phi_2) \cdot \frac{\varepsilon_b - 0.260}{0.216} \tag{6.18}$$

$$\beta = 0.95 \tag{6.19}$$

$$\gamma = \frac{2}{3} \tag{6.20}$$

$$\phi_1 = \frac{1}{2} \cdot \frac{\left(\dfrac{\kappa-1}{\kappa}\right)^2 \cdot \sin^2 \theta_{o,1}}{\ln\left(\kappa - (\kappa-1) \cdot \cos \theta_{o,1}\right) - \dfrac{\kappa-1}{\kappa} \cdot (1 - \cos \theta_{o,1})} - \frac{2}{3} \cdot \frac{1}{\kappa} \tag{6.21}$$

$$\phi_2 = \frac{1}{2} \cdot \frac{\left(\dfrac{\kappa-1}{\kappa}\right)^2 \cdot \sin^2 \theta_{o,2}}{\ln\left(\kappa - (\kappa-1) \cdot \cos \theta_{o,2}\right) - \dfrac{\kappa-1}{\kappa} \cdot (1 - \cos \theta_{o,2})} - \frac{2}{3} \cdot \frac{1}{\kappa} \tag{6.22}$$

$$\kappa = \frac{k_s}{k_g} \tag{6.23}$$

$$\theta_{o,1} = \sin^{-1}\left(\frac{1}{1.5}\right)^{0.5} \tag{6.24}$$

$$\theta_{o,2} = \sin^{-1}\left(\frac{\sqrt{3}}{12}\right)^{0.5} \tag{6.25}$$

The value of the thermal conductivity of the porous catalyst, k_s, for the Kunii-Smith formula was estimated using the correlation [Chiew and Glandt, 1983; Gonzo, 2002] provided in Eq. 6.26 and Eq. 6.27.

$$\frac{k_s}{k_g} = \frac{1 + 2 \cdot \beta' \cdot \phi' + (2 \cdot \beta'^3 - 0.1 \cdot \beta') \cdot \phi'^2 + 0.05 \cdot \exp(4.5 \cdot \beta') \cdot \phi'^3}{(1 - \beta' \cdot \phi')} \tag{6.26}$$

$$\beta' = \frac{k_s' - k_g}{k_s' + 2 \cdot k_g} \tag{6.27}$$

The correlation is a useful means for estimating the thermal conductivity of a porous catalyst, k_s, when the value of ϕ' (the volume fraction of the dispersed microspheres in the catalyst particles) lies between 0.15 and 0.85 [Gonzo, 2002]. The dispersed microspheres are the solid alumina plus micro-mesopores having combined thermal conductivity as k_s' and the continuous catalyst phase is the space occupied by the pores larger than the size of the micro-mesopores in the microspheres and has thermal conductivity as k_g (see Fig. 6.2 for the explanation of the terms "dispersed microspheres" and the "continuous phase"). Using the value of $k_s = 0.222$ W·m^{-1}·K^{-1}, experimentally measured by Sehr [1958], for the Pt/Al$_2$O$_3$-Air system, the value of thermal conductivity of the microspheres (k_s') for the Pt/Al$_2$O$_3$ catalyst was back calculated from Eq. 6.26. The value of k_s' obtained for the catalyst was 0.18 W·m^{-1}·K^{-1}. The value of ϕ' used in these calculations was 0.71 and was calculated

from the Hg-micromeritics information on a representative bimodal alumina support [Cresswell, 2010] having virtually the same surface area as that of the catalyst. Eq. 6.28 was used for this purpose. It is important to mention that the value of the ϕ' employed in Sehr's [1958] work was 0.70, nearly the same as that used in the present work.

$$\phi' = \frac{\dfrac{1}{\rho_s} + \text{volume of the pores with size} \leq 150\,\text{Å}}{\dfrac{1}{\rho_s} + \text{totol volume of the pores}} \qquad (6.28)$$

Dispersed microspheres
(solid alumina + pores with
pore size ≤ 150 Å)

Continuous matrix
(pore size > 150 Å)

Single catalyst particle
(size 0.57 mm i.e. 5.68×10^7 Å)
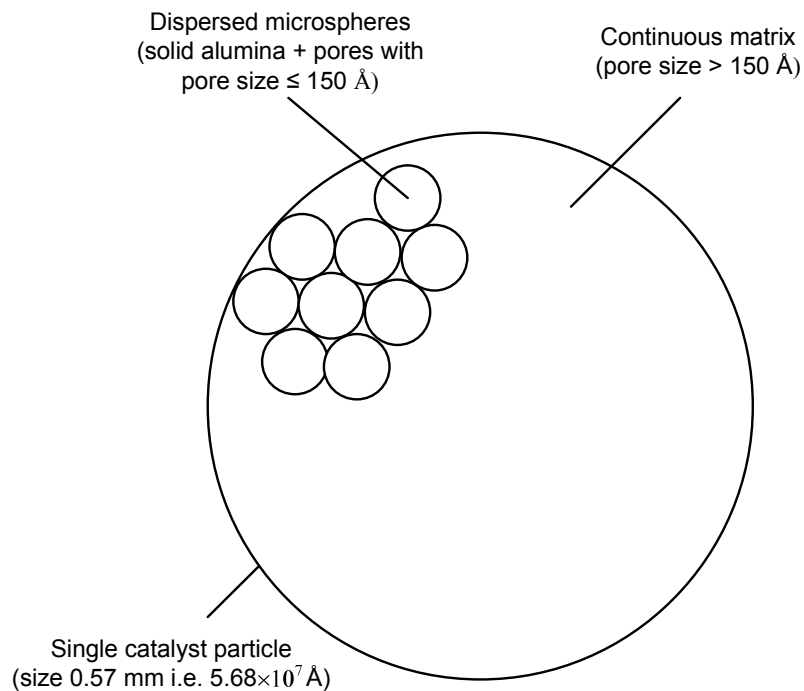
Fig 6.2 Single catalyst particle and the terminology used with Eq. 6.26 and Eq. 6.27 (not to scale).

6.4.2   Radial diffusivity (D_r)

The effective radial diffusivity was approximated as the binary molecular diffusivity of MCH in H_2, owing to the close approach to stagnant flow. The

molecular diffusivity was calculated using the Chapman-Enskog equation [Bird et al., 2002] as shown in Eq. 6.29. The diffusion coefficient was calculated at the temperatures of the reaction mixture at each node of the finite difference grid.

$$D_r = 1.8824579 \times 10^{-7} \cdot \sqrt{T^3 \cdot \left(\frac{1}{M_A} + \frac{1}{M_C}\right)} \cdot \frac{1}{p \cdot \sigma_{AC}^2 \cdot \Omega_{AC}} \qquad (6.29)$$

where,

$$\sigma_{AC} = \frac{1}{2} \cdot (\sigma_A + \sigma_C) = \text{Collision diameter of MCH-H}_2 \text{ system, Å} \quad (6.30)$$

$$\Omega_{D,AC} = \text{Collision integral for diffusivity of MCH in H}_2$$

The collision integral was estimated from Neufeld's equation, employing the dimensionless temperature T^* [Neufeld et al., 1972]

$$\Omega_{D,AC} = \frac{1.06036}{T^{*0.15610}} + \frac{0.19300}{\exp(0.47635 \cdot T^*)} + \frac{1.03587}{\exp(1.52996 \cdot T^*)} + \frac{1.76474}{\exp(3.89411 \cdot T^*)}$$

$$(6.31)$$

$$T^* = \frac{\mathrm{K}T}{\varepsilon_{AC}} \qquad (6.32)$$

$$\varepsilon_{AC} = \sqrt{\varepsilon_A \cdot \varepsilon_C} \qquad (6.33)$$

σ_{AC} and $\mathrm{K}/\varepsilon_{AC}$ are the combined Lennard-Jones parameters. The Lennard-Jones parameters for the individual components are given in Table 6.3.

Table 6.3 Lennard-Jones parameters for the individual components

Components	σ (Å)	ε/K (K)	Reference
Hydrogen (C)	2.915	38.0	Flynn and Thodos [1964]
MCH (A)	6.143*	313.0*	Hirschfelder et al. [1964] in Bird et al. [2002]

*The parameter values used for MCH are those of cyclohexane

Preliminary simulation results showed that the coefficient of radial diffusion had only a relatively small effect on the temperature and conversion profiles.

6.4.3 Wall heat transfer coefficient (h_w)

For stagnant flow conditions, the correlations for the estimation of apparent wall heat transfer coefficient diverged more widely than those for the effective radial thermal conductivity. Ofuchi and Kunii [1965] have reviewed a number of correlations and suggested that several of them are not suitable for stagnant flow conditions. However, they recommended the use of the Yagi-Kunii correlation [1962] and applied this to a wide body of experimental data. Quite large deviations between the experimental and model values were reported in their work, especially in the range $\dfrac{k_s}{k_g} \sim< 1.5$. The use of this correlation for the present study, where the value of $\dfrac{k_s}{k_g} \sim< 1.0$, is thus discouraged.

The apparent wall heat transfer coefficient was therefore defined in the form of the apparent Biot number [Melanson and Dixon, 1985] based on the inner wall of the reactor tube (Bi_b) and is incorporated into the simulation by Eq. 6.34

$$Bi_b = \frac{h_w \cdot D_i}{2 \cdot k_r} \propto \frac{Conduction\ heat\ transfer\ resistance\ in\ the\ bed}{Convective\ heat\ transfer\ resistance\ at\ the\ wall} \qquad (6.34)$$

This information was used with Eq. 6.9.

6.5   Simulation of the laboratory reactor

6.5.1   Simulation procedure and parameter estimation

The following steps were undertaken to carryout the simulation of the laboratory reactor:

- Explicit finite-differences for the PDEs were set-up in the Microsoft$^®$ Excel work sheet. Reaction kinetics and the other ancillary equations were incorporated. All the necessary information such as reactor dimensions, catalyst size and properties, reaction conditions and the physical properties of the components were put together in the simulation worksheet.
- The inlet radial temperature distribution for the reactor was inserted by the following equation

$$T_{m,0} = T_{0,0} + (Bi_b /(2 + Bi_b) \times (T_w + T_{0,0}) \times \left(\frac{m}{5}\right)^2 , \text{K} \qquad (6.35)$$

Eq. 6.35 was derived assuming a parabolic temperature distribution at the inlet of the reactor tube. See Appendix K.

- An initial value of Bi_b was assumed and used to calculate the wall heat transfer coefficient. The initial estimate was taken from the work of Melanson and Dixon [1985].
- The value of Bi_b was varied and adjusted so as to obtain a close fit of the model predicted centreline temperatures to the measured centreline temperatures (minimum SSE values), while maintaining a difference between the measured and model overall conversions in the range $< \pm 10\%$.

6.5.2 Results and discussion

Laboratory experimental data for a number of different experimental runs made under varying conditions of pressure, W/F_{A0} and feed composition were simulated for the temperatures and fractional conversions at various points of the dehydrogenation reactor. Table 6.4 provides the operating conditions for each experimental run subjected to the simulation and the specified results of these simulations.

6.5.2.1 Simulation results for centre-line temperature distributions

Fig. 6.3 shows the experimentally observed and the calculated reactor centreline temperatures for twelve different experimental runs. It is observed in Fig. 6.3 that in most of the cases, good agreement between predicted and observed centreline temperatures is found. These results support the validity of the two-dimensional pseudo-homogeneous reactor model. However, at low Reynolds numbers, as the case of the laboratory reactor, mass and heat diffusion in the axial direction may well be a contributing factor. However, inclusion of axial diffusivities gives rise to a set of two-point boundary value elliptical PDEs instead of initial value parabolic PDEs [Ahmed and Fahien, 1980]. The more complicated solution of these elliptical PDEs, coupled with the need for additional parameters, seems scarcely justified in the present work.

Table 6.4 Results of the simulation for the various runs of operating conditions

Run	p (bar)	T_w (K)	H$_2$/MCH ratio	N$_2$/MCH ratio	$W/F_{A0} \times 10^{-4}$ (s.g-cat/mol)	Bi_b	Measured $T^\ddagger$ (K)	Calculated T (K)	k_g (W·m^{-1}·K^{-1})	k_r (W·m^{-1}·K^{-1})	h_w (W·m^{-2}·K^{-1})
1	1.013	653.2	0	0	6.22	8.03	609.8	606.9	0.047–0.145	0.096–0.157	151.0–246.7
2	1.013	653.2	0	1.1	6.22	4.51	615.1	596.3	0.045–0.115	0.094–0.140	83.4–123.8
3	1.013	653.2	8.4	0	6.22	1.80	619.8	603.1	0.218–0.235	0.200–0.211	70.9–74.6
4	5	653.2	0	1.1	6.22	9.50	622.0	614.1	0.045–0.121	0.076–0.137	142.2–254.6
5	5	653.2	1.1	0	6.22	5.84	625.3	618.7	0.095–0.162	0.117–0.165	134.4–188.5
6	5	653.2	8.4	0	6.22	3.70	627.6	621.3	0.218–0.240	0.200–0.213	145.0–154.6
7	9	653.2	0	1.1	6.22	10.47	625.3	617.4	0.045–0.114	0.095–0.139	194.2–285.1
8	9	653.2	0	1.1	3.11	9.19	616.3	609.2	0.045–0.089	0.094–0.124	170.1–223.7
9	9	653.2	1.1	0	6.22	6.06	630.9	624.0	0.097–0.152	0.129–0.160	153.6–190.5
10	9	653.2	1.1	0	3.11	6.72	623.9	619.4	0.097–0.132	0.129–0.150	169.8–197.0
11	9	653.2	8.4	0	6.22	2.54	634.4	626.8	0.226–0.236	0.200–0.205	99.4–102.1
12	9	653.2	8.4	0	3.11	3.11	629.3	622.2	0.223–0.230	0.198–0.202	120.7–123.1

‡Calculated by Eq. 4.12 for the experimentally measured centreline and reactor wall temperatures
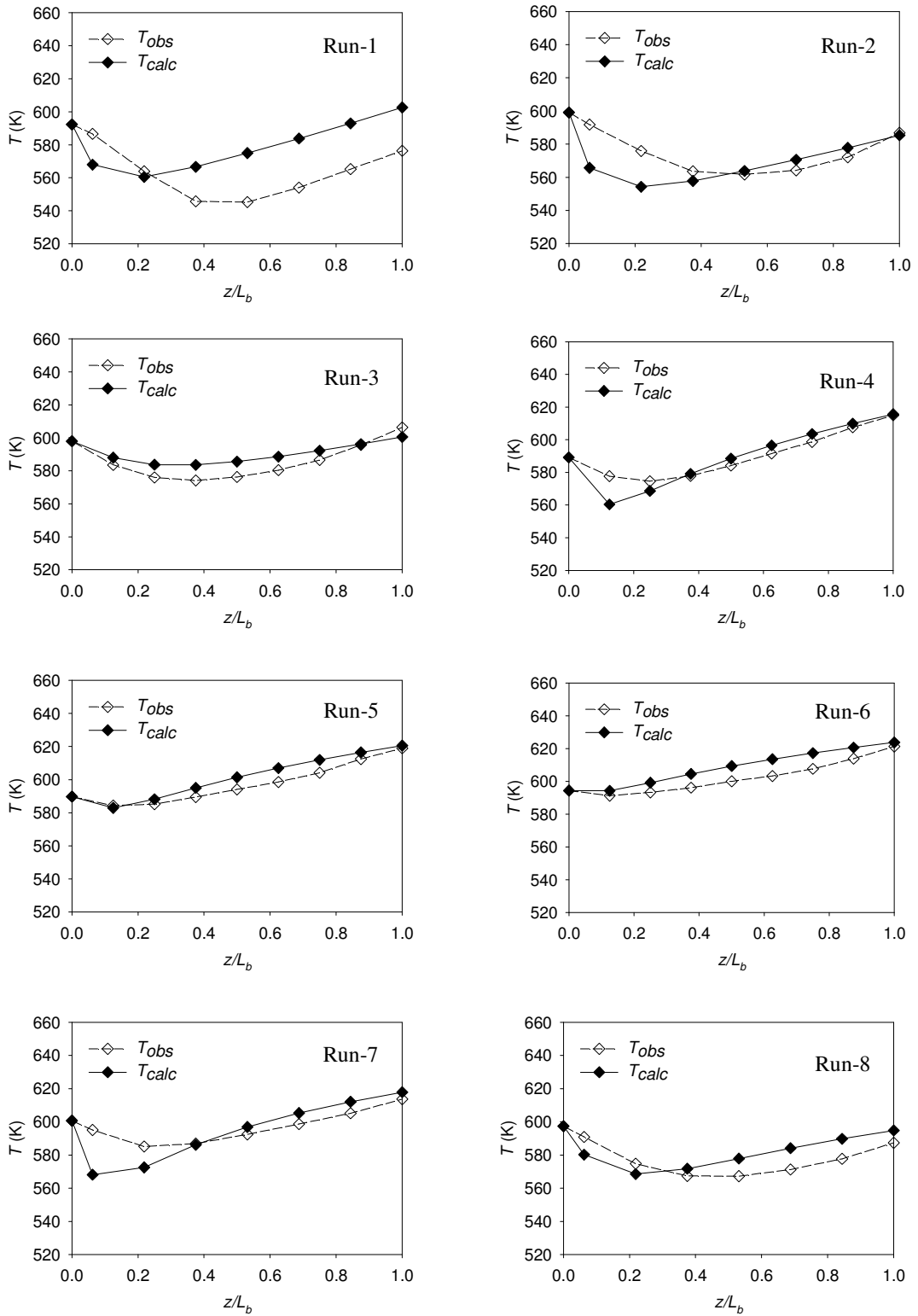
Fig. 6.3 Relations between experimental and predicted axial temperature distribution.
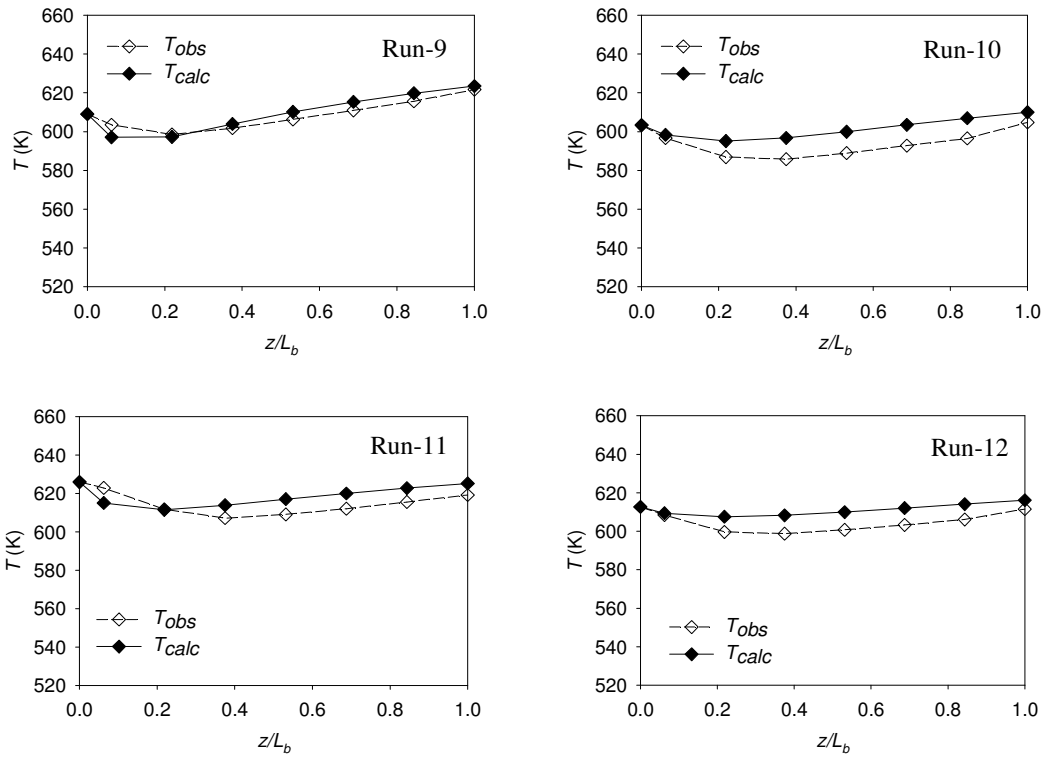
Fig. 6.3 Continued.

6.5.2.2 Radial conversions and temperature distributions

A knowledge of the radial conversion and temperature distributions at various axial positions of the reactor gives further useful insight of the behaviour of the dehydrogenation reactor. For illustration, the experimental results at the highest pressure of 9 bar without hydrogen in the feed i.e. Run-8 in Table 6.4 are chosen to show the typical radial variations of T and X.
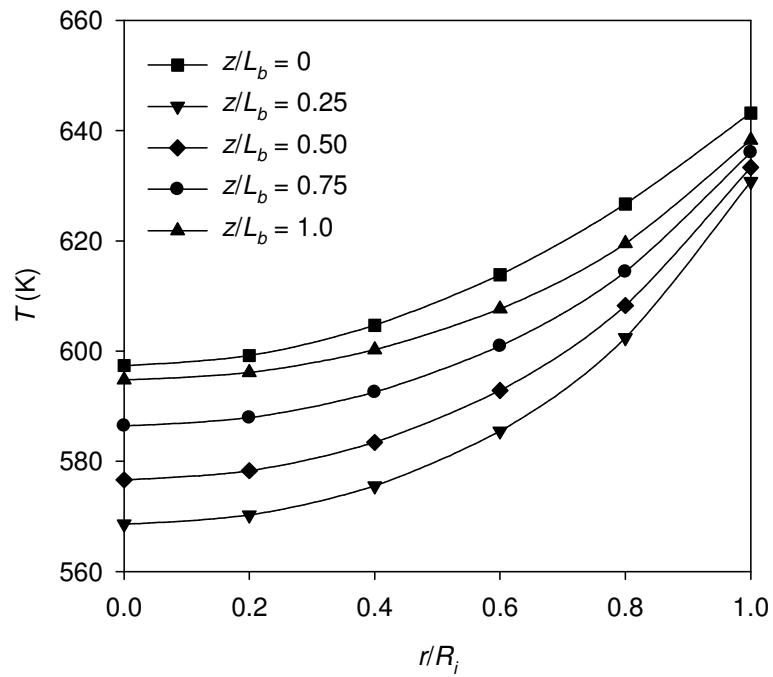
Fig. 6.4 Radial temperature variations at various lengths of the reactor bed for Run-8 in Table 6.4.
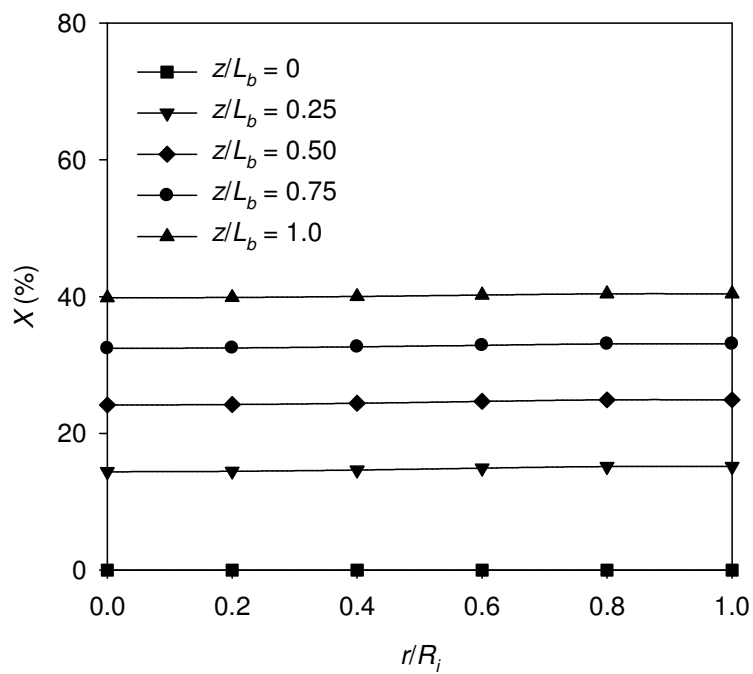
Fig. 6.5 Radial conversions at various lengths of the reactor bed for Run-8 in Table 6.4.

Fig. 6.4 and Fig. 6.5, respectively, show the variations of T and X with the dimensionless radius (radial position at any chosen point of the reactor divided by total radius of the reactor). Parabolic temperature distributions with radial direction are observed with low values at the centreline of the reactor. The parabolic nature of the temperature distributions clearly indicates the endothermic nature of the reaction and emphasises that the major radial resistance to heat transfer lies in the bed of catalyst particles rather than at the wall. No appreciable spatial variation is observed for the fractional conversion.

6.5.2.3 Effective radial thermal conductivities and apparent wall heat transfer coefficients

The effect of spatial position on the radial thermal conductivities at varying lengths of the bed is provided in Fig. 6.6.
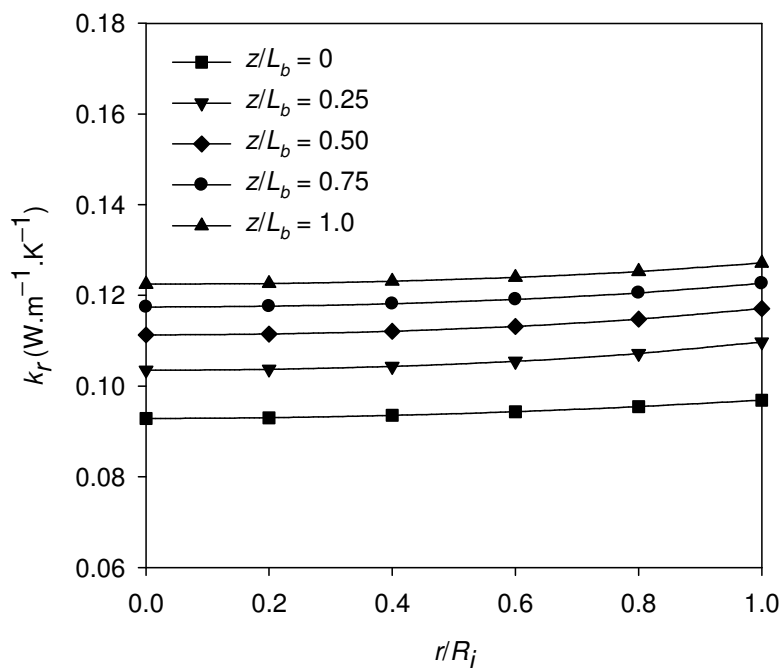
Fig. 6.6 Effective radial thermal conductivities at various radial
positions and lengths of the reactor bed for Run-8 in Table 6.4.
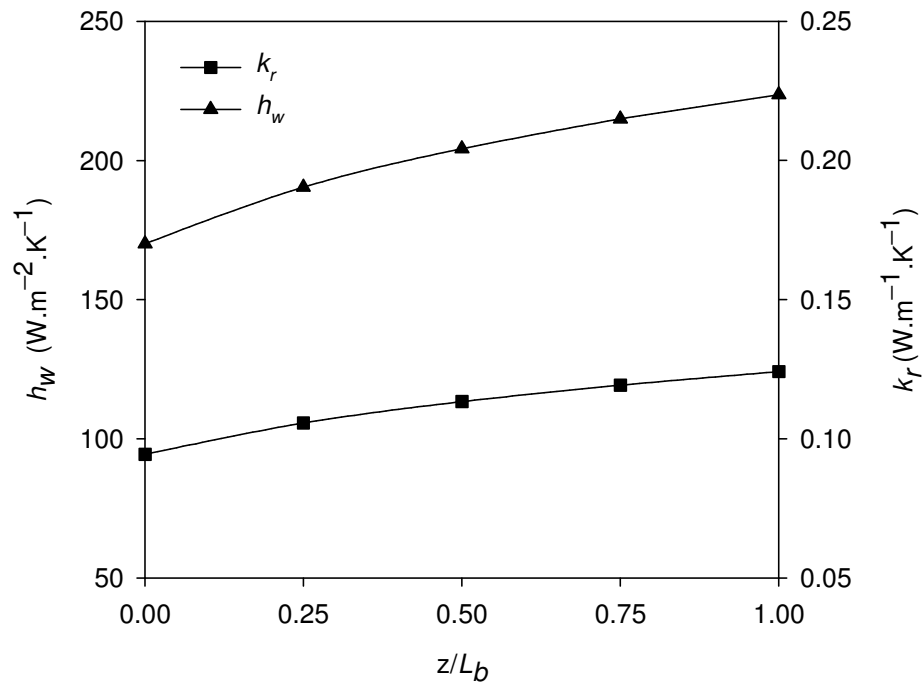
Fig. 6.7 Effective radial thermal conductivities and apparent wall heat transfer coefficients at various lengths of the reactor bed for Run-8 in Table 6.4.

It is evident from Fig. 6.6 that the effective radial thermal conductivity is more or less independent of radial position. This observation shows that the effective radial thermal conductivity is more a function of composition of the reaction fluid mixture than the temperature in the reactor. Fig. 6.7 is plotted to show the variations in mean effective radial thermal conductivity and the apparent wall heat transfer coefficient with the length of the reactor. An increase in both parameters is observed along the length of the reactor largely as a result of the increased H_2 concentration. For the case discussed here, Bi_b, which is proportional to the ratio of the wall heat transfer coefficient to the radial thermal conductivity, is relatively high, 9.9, as shown in Table 6.4. This indicates the resistance in the radial heat transfer mainly lies in the bed of the reactor rather than at the wall. It is observed in Table 6.4 that for each run, the Bi_b value appears to depend upon the value of k_g and increases with a decrease in k_g. As an example, for Run-7 and Run-11, an overall average decrease in the k_g value of three folds, increases Bi_b by a factor of more than four. A low value of Bi_b means

more convective thermal resistance at the wall relative to radial thermal conduction. This occurs for high k_g values (e.g. H_2 rich gas). A high Bi_b means more conductive thermal resistance within the bed relative to wall convective heat transfer (e.g. low conductive gas as MCH or N_2). The apparent trend in Bi_b with k_g (or H_2 to MCH ratio in the feed) is shown in Fig. 6.8, where Bi_b appears to decrease continuously with increasing hydrogen concentration in the feed. This suggests that the gas conductivity k_g exerts a greater positive influence on the wall heat transfer coefficient h_w than on the effective radial thermal conductivity k_r.
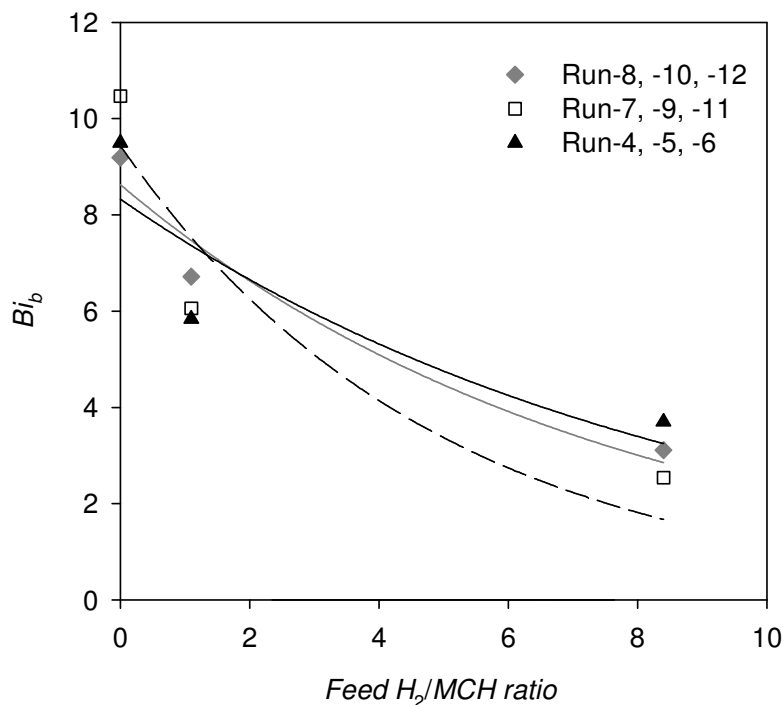
Fig. 6.8 The effect of H_2 addition in the feed on the value of Bi_b.

6.6   Discussion on the validity of the developed model

The two-parameter (k_r and h_w) two-dimensional pseudo-homogeneous model appears to be supported by the experimental laboratory results. This model may therefore easily be applied for the scale up of the laboratory reactor to a prototype commercial MTH dehydrogenation reactor. Moreover, as shown in Table 6.4, the

average reaction temperatures used in the development of the kinetic model in Chapter 4 using Eq. 4.10 was fairly close to the average temperatures found in the simulation results. These results validate the assumption of a parabolic radial temperature distribution within the reactor bed.

Chapter 7

Options for "On-board" Use of Hydrogen Based on the MTH-System — Prototype Reactor Design

The dehydrogenation of MCH is a highly endothermic reaction that requires a considerable amount of thermal energy input for the reaction to take place. Also the optimum temperature required for releasing hydrogen from the organic hydride is not less than 380 °C. For "on-board" applications, the energy available in the exhaust gases, from an IC engine or a solid oxide fuel cell (SOFC) stack, at high temperatures may be utilised to heat the incoming MCH feed and to maintain the reaction temperature. The questions here arise as to whether the exhaust gas has enough energy to support the dehydrogenation reaction, what would be the size of the dehydrogenation reactor and associated heat exchangers and storage tanks required for the MCH feed and the product toluene. Failure to meet such set targets would suggest an alternative option — a hybrid of H_2 and gasoline (hybrid MTH-gasoline-system). Moreover, the low heat transfer coefficient associated with the exhaust gases has to be considered in any of the above options and is extremely crucial in the design of the dehydrogenation reactor-heat exchanger system. In this chapter, a base case process flow diagram for the "on-board" MTH-system capable of producing 66.2 kW for a 1200 cc vehicle is developed and while maximising the heat economy, the feasibility of the various options based on the MTH-system under practical conditions is reviewed. A viable dehydrogenation reactor-heat exchanger system is proposed and simulated for practical "on-board" applications. Finally, a simplified dynamic model is employed to estimate the "start up" time required.

7.1   Design Basis

A 1.2×10^{-3} m^3 (1200 cc) vehicle, equivalent to Honda Jazz 1.2 *i-VTEC*, has been taken as a basis for the calculations. Table 7.1 shows the specifications of the vehicle.

Table 7.1 Relevant specifications of the Honda
Jazz 1.2 *i-VTEC* [Honda, 2010]

Cylinder volume (cc)	1198
Bore (mm)	73
Stroke (mm)	71.58
Maximum load (kg)	1520
No. of cylinders	4
No. of valves	16
Compression ratio	10.8
Maximum speed (mph)	110
Maximum power (bhp)	89 (66.2 kW)
Max. torque (N·m)	114
Number of gears	5
Fuel type	Gasoline
Fuel tank size (L)	42
CO_2 emissions (g/km)	125

7.2   Various options for the "on-board" use of the MTH-system

The MTH-system may be used in a variety of ways and the following different options may be adopted for "on-board" use

- Total replacement of gasoline in an IC engine with H_2 from the MTH-system
- Total replacement of gasoline in a SOFC stack with H_2 from the MTH-system
- Hybrid use of gasoline and hydrogen from the MTH-system in an IC engine

7.2.1   Total replacement of gasoline in an IC engine with H_2 from the MTH-system

7.2.1.1   Basis of the calculations

The maximum brake power output of 66.2 kW for the vehicle as provided in Table 7.1 is taken as the basis for the calculations for the MTH-system discussed below. Assuming 90 % conversion of MCH in the dehydrogenation reactor at 9 bar and 380 °C, 0.1892 mol/s of pure MCH is required to generate the above mentioned

power output. The quantity 0.1892 mol MCH/s is calculated based upon an ideal Otto cycle corrected for a real IC engine [Pulkrabek, 1997]. For real Otto cycle, 85% of indicated efficicncy was taken as that of air-standard cycle and a mechanical efficiency of 86% was applied [Pulkrabek, 1997].

7.2.1.2   Process flow diagram (PFD)

Fig. 7.1 is the process flow diagram (PFD) for the hydrogen internal combustion (H_2-IC) engine operated on the MTH-technology. The PFD starts with the pure MCH intake from the feed tank at ambient pressure and ambient temperature. The MCH feed passes through a pre-heater and a vaporiser while exchanging heat with the reactor outlet stream. The vaporised MCH is superheated in a superheater by taking heat from the exhaust gases of the hydrogen engine. The superheated feed then enters into the dehydrogenation reactor packed with 1.0 wt% Pt/γ-Al$_2$O$_3$ catalyst particles. Dehydrogenation is an endothermic reaction and the heat required for the reaction is provided by the exhaust gases coming from the hydrogen engine. It requires the dehydrogenation reactor to act as a reactor-heat exchanger assembly. The products leaving the reactor are at high temperature and need to be cooled down to separate out the condensables (toluene and the unreacted MCH) from the hydrogen rich gas. The product gas exchanges heat with the feed MCH, as mentioned previously, and passes into an air-cooled condenser, followed by a phase separator. The separator vessel separates out toluene and the un-reacted MCH from the hydrogen gas. The hydrocarbons are sent to a toluene storage tank while the hydrogen gas containing a small concentration of hydrocarbons is admitted to the hydrogen engine. A hydrogen storage tank is incorporated to ensure a steady flow of hydrogen and its supply in the start-up period. The hydrogen under pressure may be directly injected into the cylinder head or mixed with air upstream. The exhaust gases, after exchanging heat in the reactor and the superheater, as mentioned previously, leave through the exhaust pipe to the surroundings.

7.2.1.3   Aspen HYSYS® Simulation

The PFD shown in Fig. 7.1 was simulated in Aspen HYSYS® 2006, a highly recommended and powerful simulation software. The simulation flowsheet is shown in Fig. 7.2 and the corresponding results of material balance are provided in Table 7.2. In carrying out the simulation of the MTH-system, the following assumptions were made:

- The calculations were performed for the maximum power of 66.2 kW and a steady-state operation was assumed.
- The H_2-IC engine was considered 30 % more efficient than the ordinary real Otto cycle under these conditions.
- The dehydrogenation reaction was assumed to achieve 90 % conversion and to operate isothermally at 380 °C and 9 bar absolute.
- The Peng-Robinson (PR) equation of state was applied for the calculation of thermodynamic properties [Tsuji et al., 2005].
- The pressure drop within each piece of equipment was assumed zero. This assumption is not invalid as very low pressure drops were expected.
- Heat loss to the surroundings was considered negligible.
- For hydrogen combustion in the IC engine, an equivalence ratio of 0.5 was used [Yi et al., 2000; Das, 2005]. The equivalence ratio is the ratio of actual air to fuel ratio to the theoretical air to fuel ratio, both in terms of mass. For the combustion of trace quantities of MCH and toluene, theoretical amounts of air based on moles were employed (as these gases were highly dispersed in the hydrogen phase).

P-101	E-101	E-102	E-103	R-101	E-104	V-101	C-101	T-101	ICE-101
Feed	Feed	Feed	Feed	Dehydrogenation	Product	Phase	Air	Hydrogen	Hydrogen-IC
Pump	Pre-heater	Vaporiser	Superheater	Reactor-Heat	Condenser	Separator	Compressor	Accumulator	Engine
				Exchanger					

Fig. 7.1 Process plow diagram for the "on-board" MTH-system.

185
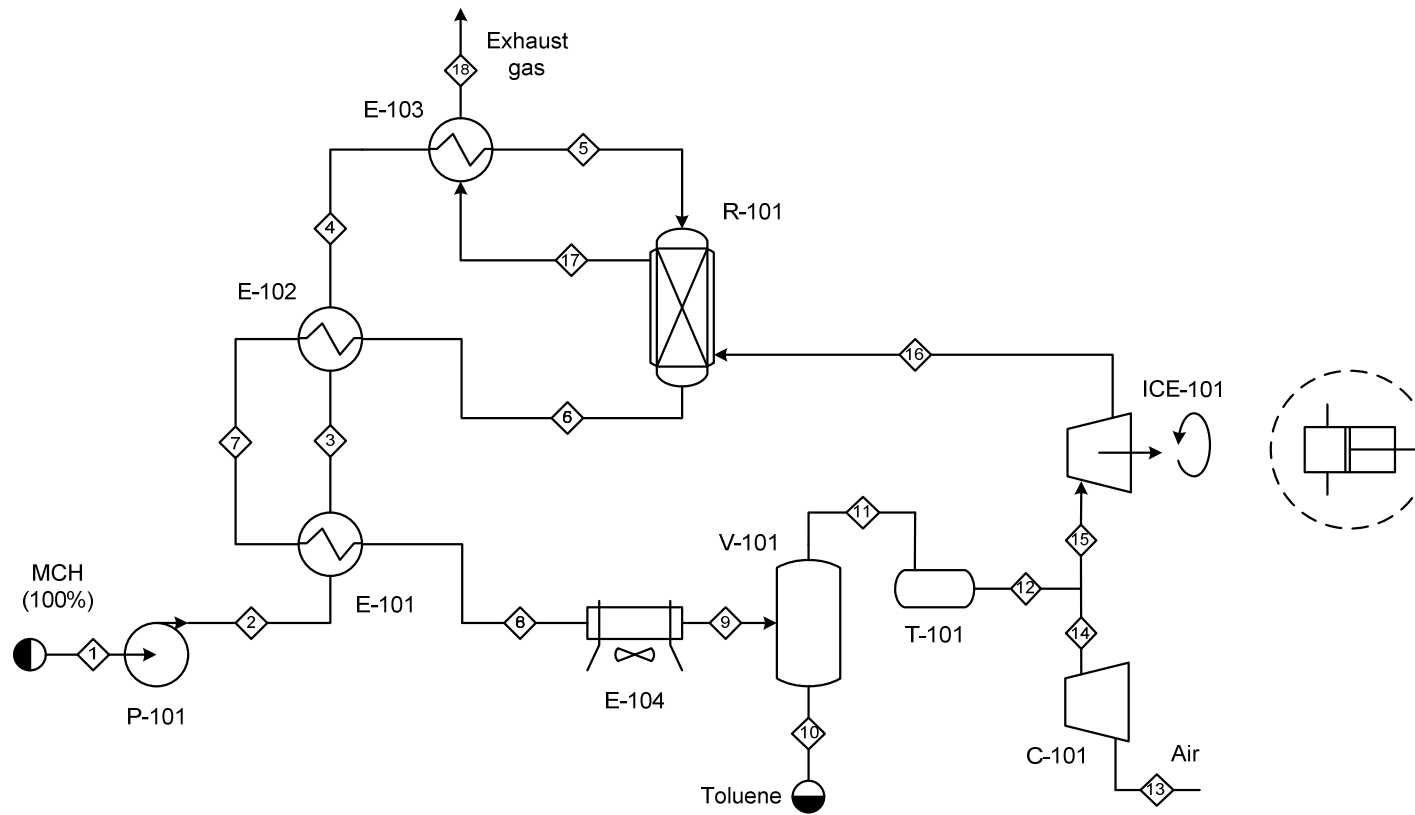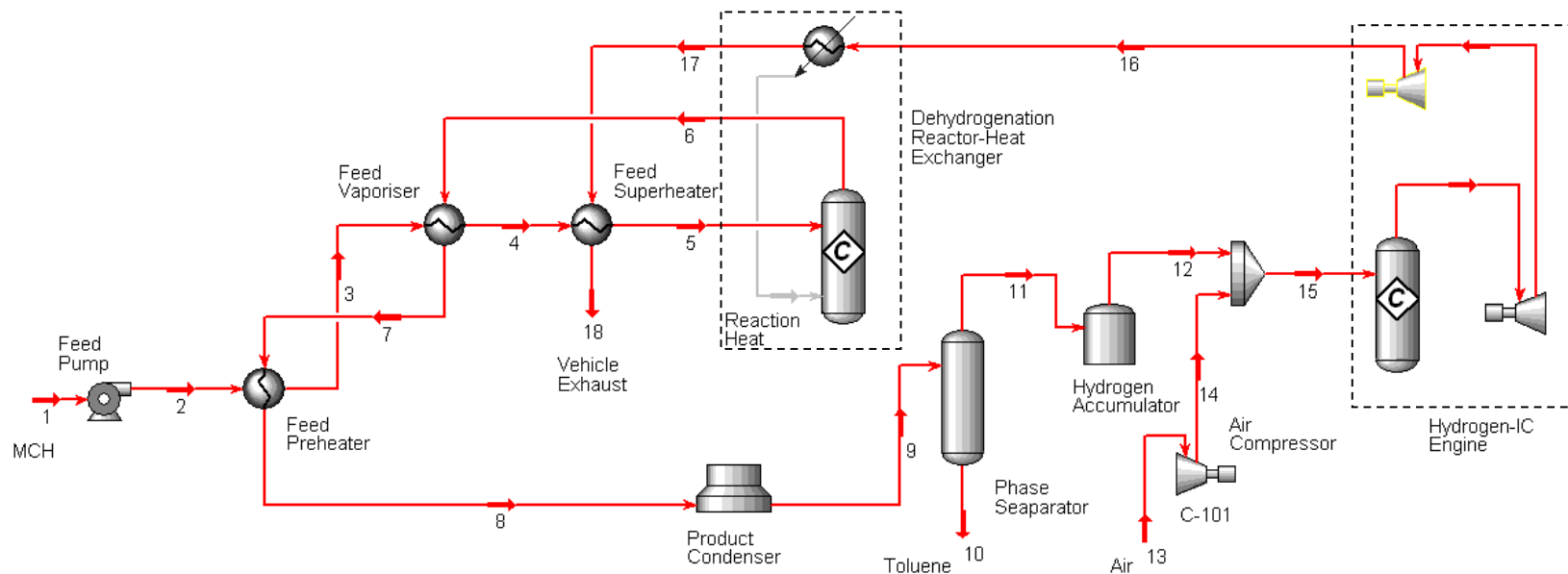
Fig. 7.2 Aspen HYSYS® simulation flowsheet for the "on-board" MTH-system based on total replacement of gasoline by H_2 from MTH-system.

Table 7.2 Material balance sheet for 66.2 kW H_2-IC engine based on total replacement of gasoline by H_2 from MTH-system with engine exhaust gas at 850 °C

Stream no.	Stream name	T (°C)	p (bar)	Phase*	Molar flowrate (mol/s)							
					MCH	H_2	Toluene	O_2	N_2	H_2O	CO_2	Total
1	MCH feed	15.0	1.013	l	0.1892	-	-	-	-	-	-	0.1892
2	Feed to pre-heater	15.37	9.0	l	0.1892	-	-	-	-	-	-	0.1892
3	Feed to vaporiser	202.2	9.0	sl	0.1892	-	-	-	-	-	-	0.1892
4	Feed to feed superheater	202.2	9.0	sv	0.1892	-	-	-	-	-	-	0.1892
5	Reactor feed	380	9.0	g	0.1892	-	-	-	-	-	-	0.1892
6	Reactor exit	380	9.0	g	0.0189	0.5109	0.1703	-	-	-	-	0.7001
7	Reactor exit to the pre-heater	295.8	9.0	g	0.0189	0.5109	0.1703	-	-	-	-	0.7001
8	Air cooler inlet	139.0	9.0	g	0.0189	0.5109	0.1703	-	-	-	-	0.7001
9	Separator inlet	27.0	9.0	g/l	0.0189	0.5109	0.1703	-	-	-	-	0.7001
10	Separator bottom product	27.0	9.0	sl	0.0185	0.0006	0.1678	-	-	-	-	0.1869
11	Separator top product	27.0	9.0	sv	0.0005	0.5103	0.0024	-	-	-	-	0.5132
12	Hydrogen off accumulator	27.0	9.0	g	0.0005	0.5103	0.0024	-	-	-	-	0.5132
13	Inlet air	15.0	1.013	g	-	-	-	0.5378	2.023	-	-	2.561
14	Compressed air	335.8	9	g	-	-	-	0.5378	2.023	-	-	2.561
15	Feed to hydrogen engine	286.2	9.0	g	0.0005	0.5103	0.0024	0.5378	2.023	-	-	3.074
16	Engine exhaust gas	850.0	5.0	g	-	-	-	0.2558	2.023	0.5234	0.0204	2.823
17	Exhaust inlet to feed superheater	467.8	5.0	g	-	-	-	0.2558	2.023	0.5234	0.0204	2.823
18	Vehicle exhaust	372.5	5.0	g	-	-	-	0.2558	2.023	0.5234	0.0204	2.823

* l: liquid; sl: saturated liquid; sv: saturated vapour; g: gas

- Exhaust gases leaving the H_2 engine are assumed to be at 5 bar and 850 °C [Pulkrabek, 1997].

7.2.1.4   Pinch analysis for the heat recovery

Examination of Fig. 7.1 reveals that the system flowsheet has 4 cold streams (cold stream is one that needs to be heated to reach the required heat content and temperature) and 5 hot streams (hot stream is one that needs heat removal). Table 7.3 below enlists the two kinds of streams.

Table 7.3 List of hot and cold streams for Fig. 7.3

Cold streams	Hot streams
2–3	6–7
3–4	7–8
4–5	8–9 ×
5–6	16–17
	17–18

A small cross (×) immediate to the hot stream 8−9 shows the insignificance of this stream in the pinch analysis, because this stream requires outside cooling air and hence it is excluded from the set of streams that are to be manipulated to reach the pinch. Now 4 hot and 4 cold streams are left. Stream 16−17 is providing heat to the reactor (for endothermic heat content) and the heat content of this stream is important to the feasibility of the MTH-system.

Fig. 7.3 is a plot of the hot and cold streams on a *T-H* diagram. As mentioned earlier, an exhaust temperature of 850 °C was assumed for the flowsheeting and pinch analysis. Aspen HYSYS® produced an exhaust gas temperature of 767.9 °C as the minimum temperature at which the pinch occurred. The pinch calculations suggest the temperature of the exhaust gases should not be less than 767.9 °C. Including design constraints, such as the unavoidable temperature differences in heat exchangers, catalyst deactivation and the heat losses associated in the real design, this temperature may or may not be sufficient to realise the stated objectives.
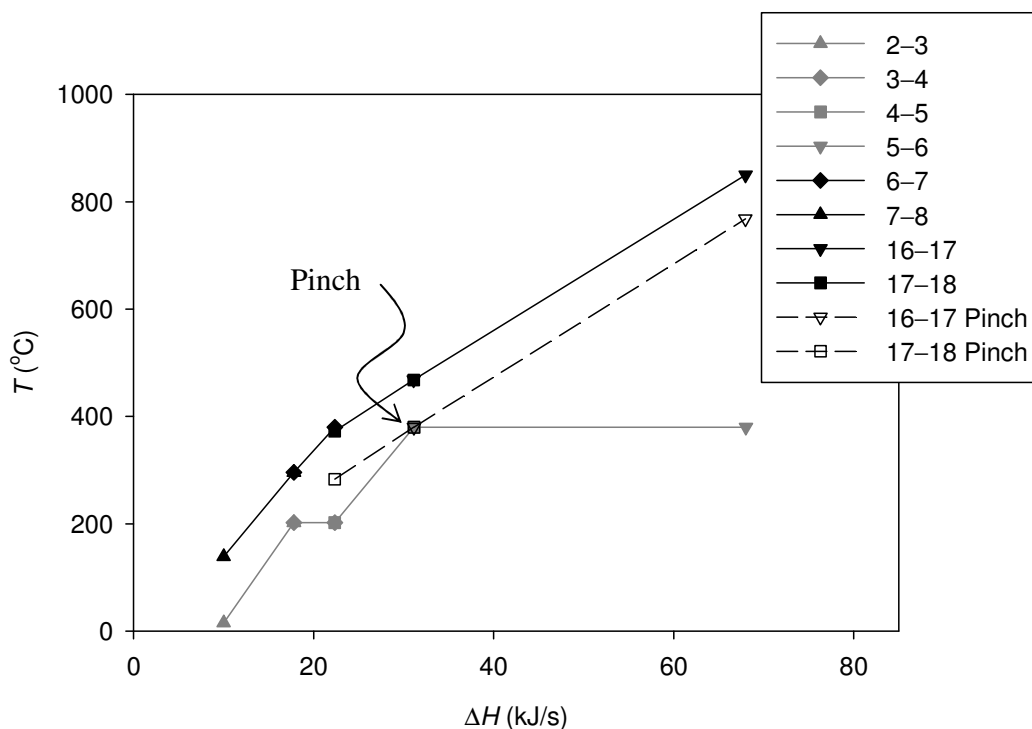
Fig. 7.3 *T-H* diagram for the pinch analysis.

7.2.1.5 Size of the storage tanks required

It is important to know the volumes and weights occupied by the dehydrogenation reactor and the storage tanks for fuel (MCH) and toluene (product of the dehydrogenation) for "on-board" applications. The size and weight of these pieces of equipment alone can easily rule out the idea of using the MTH-system for "on-board" applications. Taking 90 % conversion at 9 bar and 380 °C and assuming an 8 h period of vehicle drive at medium speed at 30 kW, the size of the MCH tank calculated is 315.2 L (11.13 ft^3) having a linear dimension of 2.23 ft of a cubical tank. Another similar volume tank for product toluene is required and a total of 630.4 L volume tank is required unless a unique tank design is applied, as mentioned in Section 7.2.3.2. The Honda Jazz, the model car selected for the calculations, has only

a 42 L gasoline tank in its body. It is important to note that these sizes are for an engine brake power less than half the maximum power.

7.2.1.6 Discussion and conclusion

The thermal pinch analysis (Fig. 7.3) shows theoretical feasibility on the basis of an exhaust gas available at 850 °C for the option "total replacement of gasoline by H_2 from MTH-technology". However, the size of storage tanks required completely rules out the idea of using the MTH-system as a total replacement for gasoline for the provided vehicle. Moreover, the mass and volume required for heat exchangers, dehydrogenation reactor, separator and hydrogen accumulator suggest the option to be practically impossible for a vehicle of this size and most others.

7.2.2 Total replacement of gasoline in a SOFC stack with H_2 from the MTH-system

Fuel cells are considered twice as efficient as an ordinary gasoline engine [Schlapbach and Züttel, 2001]. Replacing a gasoline system with a fuel cell stack should therefore be a more practical solution. Applying the assumption that a fuel cell vehicle is twice as efficient as an ordinary gasoline one, the size of tank is reduced to 204.9 L for MCH for a power of 30 kW. Again, this is much too large and discourages the use of even a SOFC stack for the MTH-system. Moreover, as already described in Chapter 1, the fuel cell technology is far from being commercialised at low cost and with a durable life span in the near future. The second option therefore also does not seem practically viable.

7.2.3 Hybrid use of gasoline and hydrogen from the MTH-system in an IC engine

A more practical solution based on the MTH-system can be seen in a hybrid MTH-gasoline-system, as proposed by Hrein Energy Corporation [Hrein, 2008] which has already been discussed in Chapter 1.

The conventional gasoline-fuelled spark ignition (SI) engine has associated with it effects detrimental to the environment and to human health. Toxic hydrocarbon emissions, C (soot), CO, CO_2, NOx and some sulphurous compounds (SOx) and even metal particles are among the typical pollutants. A hybrid hydrogen-gasoline engine may well be an improvement over the conventional gasoline one and thereby helpful in reducing the harmful pollutant levels in the exhaust. In a hybrid MTH-gasoline-system, the hydrogen generated in-situ by the dehydrogenation of MCH is allowed to mix with the gasoline fuel. The gasoline-hydrogen mixture provides an opportunity to work in the lean burn regime. It is observed that adding 3.0 to 5.0 mol % hydrogen to the intake air improves the engine efficiency by 30% [Hrein, 2008] and provides a 30% reduction in the CO_2 emissions [Hrein, 2008]. Moreover, owing to the possibility of the low adiabatic flame temperatures, reduced concentrations of NOx are expected. This system requires a far smaller tank size and reactor volume and provides a much more practical alternative.

7.2.3.1 Process flow diagram (PFD) and Aspen HYSYS® simulation for the hybrid MTH-gasoline-system

The base case PFD in Fig. 7.1 is modified to accommodate an extra fluid stream (stream 12a) of isooctane (2,2,4-trimethylpentane, C_8H_{18}), the representative of gasoline. The isooctane is selected because it has burning characteristics similar to gasoline. It has a similar air-fuel ratio and a high octane number of 100 (gasoline has an octane number of 88−98, as shown in Table 1.1 of Chapter 1). The modified PFD is shown in Fig. 7.4 and the simulation PFD is shown in Fig. 7.5. The pure isooctane is mixed with the hydrogen stream and enters the H_2-IC engine with an overall 4.0

mol % hydrogen in the fuel-air mixture. Similar assumptions to those outlined in Section 7.2.13 are used except the reactor outlet temperature is set at 450 °C and the exhaust gas temperature is set at 625 °C. These assumptions are made so as to remain close to the base case operating conditions for the prototype assembly as shown in Table 7.5 in Section 7.8.1. The system is simulated in Aspen HYSYS$^{®}$ and the material balance results are shown in Table 7.4. It is important to mention here that in HYSYS's components library, isooctane is available with its name "224-Mpentane" and not as isooctane.

Fig. 7.4 Process plow diagram for the "on-board" hybrid MTH-isooctane-system.
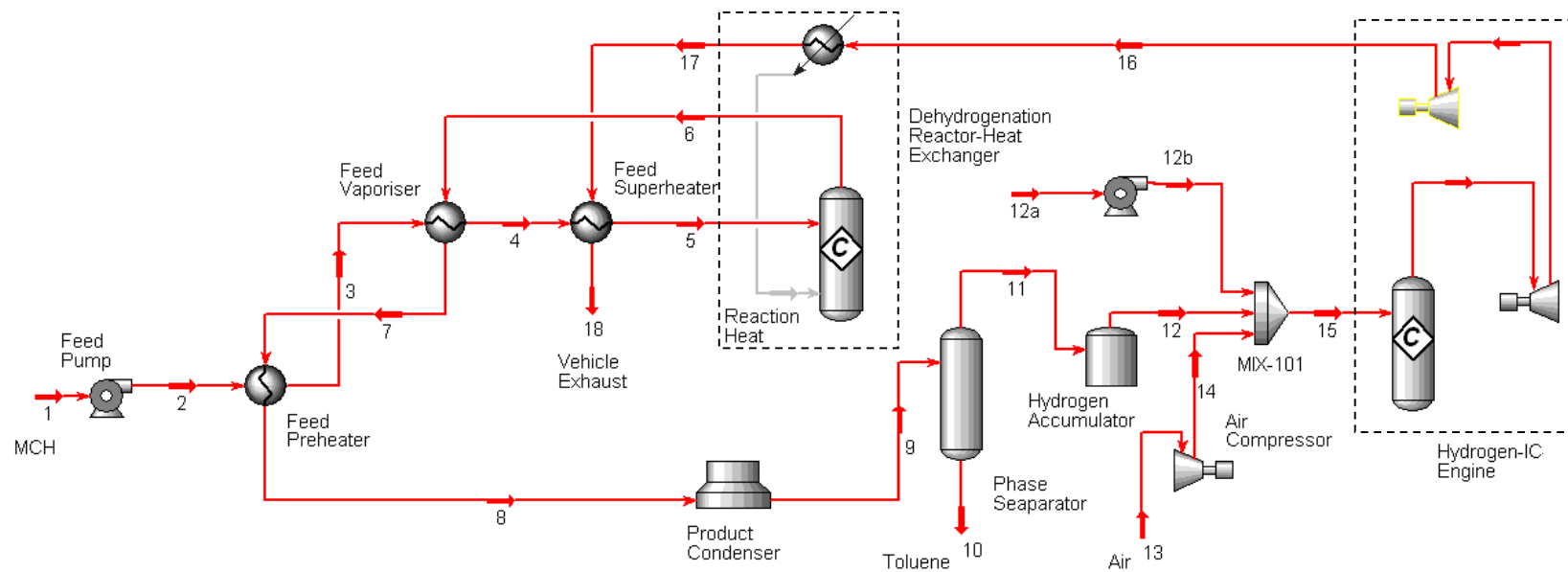
Fig. 7.5 Aspen HYSYS® simulation for the "on-board" hybrid hydrogen-isooctane-system.

Table 7.4 Material balance sheet for 66.2 kW hybrid MTH-gasoline-system with engine exhaust gas at 625 °C

Stream no.	Stream name	T (°C)	p (bar)	Phase*	Molar flowrate (mol/s)								
					MCH	H_2	Toluene	C_8H_{18}	O_2	N_2	H_2O	CO_2	Total
1	MCH feed	15.0	1.013	l	0.0245	-	-	-	-	-	-	-	0.0245
2	Feed to pre-heater	15.37	9	l	0.0245	-	-	-	-	-	-	-	0.0245
3	Feed to vaporiser	202.2	9	sl	0.0245	-	-	-	-	-	-	-	0.0245
4	Feed to superheater	202.2	9	sv	0.0245	-	-	-	-	-	-	-	0.0245
5	Reactor feed	380	9	g	0.0245	-	-	-	-	-	-	-	0.0245
6	Reactor exit	450	9	g	0.0024	0.0663	0.0221	-	-	-	-	-	0.0908
7	Reactor exit to the pre-heater	370.4	9	g	0.0024	0.0663	0.0221	-	-	-	-	-	0.0908
8	Air cooler inlet	219.7	9	g	0.0024	0.0663	0.0221	-	-	-	-	-	0.0908
9	Separator inlet	27.0	9	g/l	0.0024	0.0663	0.0221	-	-	-	-	-	0.0908
10	Separator bottom product	27.0	9	l	0.0024	0.0001	0.0218	-	-	-	-	-	0.0243
11	Separator top product	27.0	9	v	0.0001	0.0662	0.0003	-	-	-	-	-	0.0666
12	Hydrogen off accumulator	27.0	9	g	0.0001	0.0662	0.0003	-	-	-	-	-	0.0666
12a	Isooctane inlet	15.0	1.013	l	-	-	-	0.0211	-	-	-	-	0.0211
12b	Isooctane to engine	15.36	9	l	-	-	-	0.0211	-	-	-	-	0.0211
13	Inlet air	15.0	1.013	g	-	-	-	-	0.3335	1.254	-	-	1.588
14	Compressed air	335.8	9	g	-	-	-	-	0.3335	1.254	-	-	1.588
15	Feed to hydrogen engine	281.6	9	g	0.0001	0.0662	0.0003	0.0211	0.3335	1.254	-	-	1.675
16	Engine exhaust gas	625	5	g	-	-	-	-	0.0333	1.254	0.2577	0.1713	1.717
17	Exhaust inlet to feed superheater	450.4	5	g	-	-	-	-	0.0333	1.254	0.2577	0.1713	1.717
18	Vehicle exhaust	354.5	5	g	-	-	-	-	0.0333	1.254	0.2577	0.1713	1.717

* l: liquid; sl: saturated liquid; sv: saturated vapour; g: gas

7.2.3.2 Size of the storage tanks required

For the hybrid MTH-gasoline-system, the tank size for MCH is only 40.9 L (1.44 ft^3) with a linear dimension 1.23 ft of a cubical tank. Another similar tank for the product toluene may be required. In addition to these tanks a gasoline tank is also required. However, combining MCH and toluene volumes in a floating-partition tank similar to the floating-head tanks used for the storage of these volatiles can save even more space and load on the vehicle. A floating-partition tank proposed by the author is shown in Fig. 7.5.
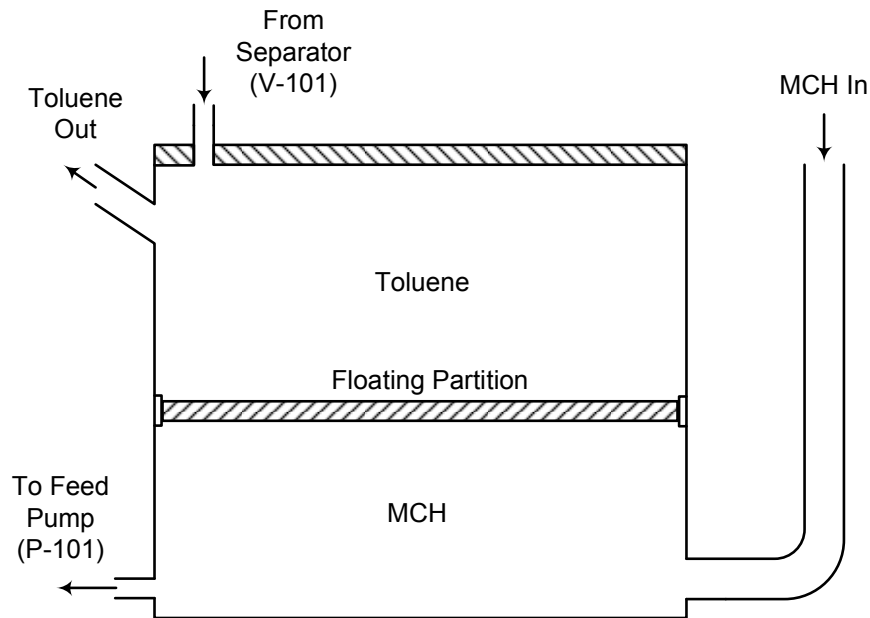
Fig. 7.6 Floating partition tank for MCH and toluene storage.

7.2.3.3 Discussion and conclusion

The tank size for the hybrid MTH-gasoline-system is far smaller and far more practical than that required for the simple MTH-system. For a medium speed at 30 kW, and for an operation of 8 h, requires a tank 8 times smaller for the hybrid MTH-gasoline-system option compared to the simple MTH-system option. For the hybrid option, not only are the size and the weight of the storage tanks minimised but also

196

the volume and weight of the dehydrogenation reactor-heat exchanger and other process equipment are drastically reduced.

The following study therefore focuses on the hybrid MTH-gasoline-system.

7.3   Proposed reactor design for the prototype hybrid MTH-gasoline-system

A novel heat exchanger-reactor system for the MTH-technology is proposed. The system consists of a multiple double-tube heat exchanger. In each double-tube of the heat exchanger, the inner tube is packed with the dehydrogenation catalyst and it is surrounded by a shroud tube incorporated into the design to increase the fluid velocity over the inner tube outer surface. Also the inner tube is fitted with longitudinal fins on its outer surface to enhance heat transfer at the outside surface of the inner tube. These two design features are used to accommodate the inherent nature of the low heat transfer coefficients associated with non-condensable gases. The hot exhaust gases pass through the annulus formed between the inner tube and the shroud tube. A bundle of such double-tubes forms a multiple shrouded-finned-tube heat exchanger. A single packed shrouded-tube is shown in Fig. 7.7.
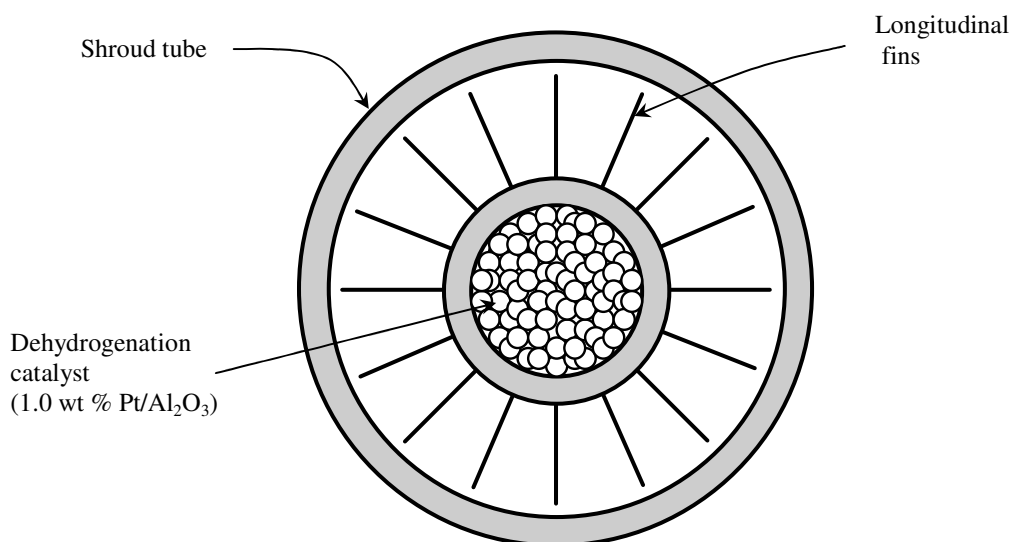
Fig. 7.7 Cross-sectional view of a single packed shrouded-tube.

7.3.1 Mathematical modelling of the shrouded-finned-tube heat exchanger

The two-dimensional pseudo-homogeneous model developed and tested for the laboratory reactor data (Chapter 6) was applied for the simulation of the prototype reactor. Again, an explicit finite-difference approach was used to solve the mathematical model. Owing to the relatively large values of the Reynolds numbers compared to the laboratory reactor, different methods for predicting the effective radial transfer coefficient and the reactor wall heat transfer coefficient to that of laboratory reactor (Chapter 6) were applied. Moreover, the prototype is different to the laboratory reactor in that the external surface of the reactor tubes is finned and the exhaust gases are used to provide the necessary amount of heat to carry out the dehydrogenation reaction. These two factors have to be accounted for in defining the external heat transfer. The apparent wall heat transfer coefficient in Eq. 6.9 in Chapter 6 has to be replaced with an overall heat transfer coefficient that takes into account the internal and external fluid resistances as well as the tube wall resistance. Eq. 6.9 is therefore re-written as Eq. 7.1

$$Bi_h = \frac{U_i \cdot R_i}{k_r} \tag{7.1}$$

7.3.2 External heat transfer

As mentioned above, the mathematical description can not be completed without defining the shell side (outside) temperature distribution $T_{eg} = f(z)$. Realistically, it cannot be specified explicitly but emerges by simultaneous solution of an additional energy balance. As there are longitudinal fins on the outside surface of the packed reactor tubes, the immediate question then is how to specify an appropriate boundary condition at the shroud tube internal surface $(r = R_{si})$. One possibility would be to assume the external surface of the shroud was sufficiently well insulated that negligible heat loss from the shroud tube occurred, making the

shroud tube adiabatic. If radial heat transfer with in the finned annulus is sufficiently rapid then heat transfer within the annulus becomes one-dimensional.

7.3.3 Equivalent diameter

For several pairs of longitudinal fins, single pair of which is shown in Fig. 7.8, attached to the outside surface of a circular tube, the mean hydraulic diameter of the annular region can be defined by the following expression
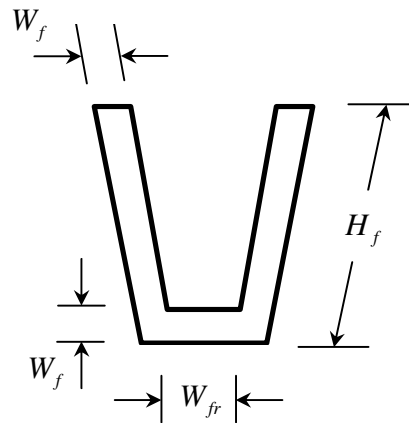
Fig. 7.8 Single pair of longitudinal fins.

$$D_e = \frac{\pi \cdot (D_{is}^2 - D_o^2) - 4 \cdot N_f \cdot W_f \cdot \left(H_f + \frac{W_{fr}}{2} \right)}{\pi \cdot (D_{is} + D_o) + N_f \cdot (2H_f - W_f)} \qquad (7.2)$$

The usual equations for friction factor and Nusselt number derived for pipe flow may be used when the pipe diameter is replaced by the above mentioned D_e. The details of the derivation for D_e are provided in Appendix M. It is worthwhile mentioning here that the critical Reynolds number (Reynolds number at which transition from laminar to turbulent flow occurs) is ~400 for the finned annulus. If, therefore, the annular region is considered as an equivalent pipe the critical Reynolds number of 2100 may well underestimate the outside heat transfer surface [Serth, 2007].

7.3.4 Overall heat transfer coefficient

The overall heat transfer coefficient to be used may be written for an un-finned surface as below

$$\frac{1}{U_i} = \frac{1}{h_i} + \frac{1}{k_w} \cdot R_i \cdot \ln\left(\frac{R_o}{R_i}\right) + \frac{1}{h_o} \cdot \frac{R_i}{R_o} \qquad (7.3)$$

The expression to be used for the outer surface finned is modified to

$$\frac{1}{U_i} = \frac{1}{h_i} + \frac{1}{k_w} \cdot R_i \cdot \ln\left(\frac{R_o}{R_i}\right) + \frac{1}{h_o} \cdot \frac{R_i}{R_o} \cdot \frac{1}{\left(1 - \dfrac{N_f \cdot W_f}{2 \cdot \pi \cdot R_o} + \dfrac{N_f \cdot H_f \cdot \eta_f}{\pi \cdot R_o}\right)}$$

$$(7.4)$$

where, η_f is the fin efficiency and is equal to

$$\eta_f = \frac{Q}{Q_{max}} = \frac{\tanh(M)}{M} \qquad (7.5)$$

M is a dimensionless quantity, which is defined by the following expression

$$M = H_f \cdot \sqrt{\frac{2 \cdot h_o}{k_f \cdot W_f}} \qquad (7.6)$$

The fin efficiency, η_f, approaches unity as *M* approaches zero. This would be most easily approached by maximising the thermal conductivity of the fin. Copper, if possible, rather than stainless steel, would be the preferred material of choice in this regard.

The detailed derivations of Eq. 7.4, Eq. 7.5 and Eq. 7.6 are provided in Appendix M.

7.4 Catalyst details

The catalyst used in the simulation of the prototype reactor is 1.0 wt% Pt/Al_2O_3 over which the kinetic experiments were performed. However, it is assumed that the same catalyst is commercialised and the commercial catalyst with spherical shape of 1.2 mm diameter is available. The problem of diffusion can easily be avoided by making an egg-shell type catalyst. The size of the catalyst is so chosen that the ratio of the inside diameter of tube to the catalyst particle always remain greater than 10 ($D_i/d_p > 10$) [Froment and Bischoff, 1979; Richardson, 1989], so as to minimise flow channelling along the wall.

7.5 Reactor bed properties

The fractional bed voidage of the catalyst bed is computed using the following empirical correlation proposed for spheres by Dixon [1988]

$$\varepsilon_b = 0.4 + 0.05 \cdot \left(\frac{d_p}{D_i}\right) + 0.412 \cdot \left(\frac{d_p}{D_i}\right)^2 \qquad \text{for } \frac{d_p}{D_i} \le 0.5 \qquad (7.7)$$

The bulk density of the catalyst is calculated using the following formula

$$\rho_b = \rho_p \cdot (1 - \varepsilon_b) \qquad (7.8)$$

where, ρ_p is the catalyst particle density, given in terms of skeletal density ρ_s and pore volume v_P by

$$\rho_p = \frac{\rho_s}{(\rho_s \times v_P) + 1} \tag{6.14}$$

The corresponding values of the ρ_s and v_P are 3970 kg/m^3 and 0.58×10^{-3} m^3/kg, respectively as mentioned in Chapter 6.

7.6 Effective transport properties and inside wall heat transfer coefficient

A number of correlations have been developed in the literature for the effective transfer properties and heat transfer coefficient of the catalyst bed side (inside). Preliminary calculations suggested the Reynolds numbers were generally less than 300 on the catalyst side. For the said range, the following correlations were applied.

7.6.1 Effective radial thermal conductivity (k_r)

The correlation suggested by Rase [1990], due to Kulkarni and Doraiswamy [1980], was not applicable in this range. Therefore, that proposed by Dixon et al. [1978] was used instead.

$$\frac{h_w \cdot D_i}{2 \cdot k_r} \cdot \left(\frac{d_p}{D_i}\right)^{0.5} = 5.3 \cdot Re_p^{-0.262} \tag{7.9}$$

This correlation needs a value of h_w to calculate k_r or vice-versa, see Section 7.6.3.

7.6.2 Effective radial mass diffusivity (D_r)

The following correlation [Kulkarni and Doraiswamy, 1980] was recommended by Rase [1990] to calculate the effective radial mass diffusivity

$$\frac{\varepsilon_b \cdot D_r}{u' \cdot d_p} = \frac{1}{m} + \frac{0.38}{Re_p} \tag{7.10}$$

For, $d_p / D_i > 0.1$ $m = 11$ for $Re_p > 400$ and

$m = 57.85 - 35.36 \cdot \log Re + 6.68 \cdot (\log Re_p)^2$ for $20 < Re < 400$.

For $\frac{d_p}{D_i} < 0.1$ divide, D_r calculated from above by $\left[1 + 19.4 \cdot \left(\frac{d_p}{D_i} \right)^2 \right]$.

7.6.3 Inside wall heat transfer coefficient

The following correlation proposed by Li and Finlayson [1977] was recommended by Rase [1990] and Wen and Ding [2006] for estimating the wall heat transfer coefficient on the catalyst bed side.

$$\frac{h_i \cdot d_p}{k_g} = 0.19 \cdot Re_p^{0.79} \cdot Pr^{0.33} \tag{7.11}$$

For $20 \le Re_p \le 7600$ and $0.05 \le \frac{d_p}{D_i} \le 0.3$

7.7 Outside heat transfer coefficient

7.7.1 Finned-tube

DeLorenzo and Anderson [1945] measured heat transfer coefficients for finned-tube heat exchangers, the results of whom are curve-fitted in terms of the heat transfer j-factor (j_H), as shown in Eq. 7.12 [Serth, 2007]

$$j_H = (0.0263 \cdot Re^{0.91} + 4.9 \times 10^{-7} \cdot Re^{2.62})^{1/3} \cdot \left(\frac{574}{(L/D_e)} \right)^{\frac{1}{3}} \qquad (7.12)$$

where,

$$j_H = \frac{h_o \cdot D_e}{k_{eg}} \cdot \left(\frac{c_p \cdot \mu}{k_{eg}} \right)^{-\frac{1}{3}} \cdot \left(\frac{\mu}{\mu_w} \right)^{-0.14} \qquad (7.13)$$

For low viscosity fluids, the viscosity correction factor $\left(\dfrac{\mu}{\mu_w} \right)^{-0.14}$ is ignored [Kern,

1950].

7.7.2 Un-finned tube

For an unfinned tube, the following equations are usually recommended.

7.7.2.1 Turbulent flow regime: Dittus-Boetler Equation [Bejan, 2003]

$$Nu = 0.023 \cdot Re^{0.8} \cdot Pr^{\frac{1}{3}} \cdot \left(\frac{\mu}{\mu_w} \right)^{0.14} \quad \text{for } Re > 10000 \qquad (7.14)$$

where, $Nu = \dfrac{h_o \cdot D_e}{k_{eg}}$ $\qquad (7.15)$

7.7.2.2 Transition flow regime: Hausen equation [Serth, 2007]

$$Nu = 0.116 \cdot \left(Re^{\frac{2}{3}} - 125 \right) \cdot Pr^{\frac{1}{3}} \cdot \left(\frac{\mu}{\mu_w} \right)^{0.14} \cdot \left(1 + \left(\frac{D_e}{L} \right)^{\frac{2}{3}} \right) \qquad (7.16)$$

for $2100 < Re < 10^4$

7.7.2.3 Laminar flow regime: Seider-Tate equation [Serth, 2007]

$$Nu = 1.86 \cdot \left(Re \cdot Pr \cdot \left(\frac{D_e}{L} \right) \right)^{\frac{1}{3}} \cdot \left(\frac{\mu}{\mu_w} \right)^{0.14} \quad \text{for } Re \leq 2100 \qquad (7.17)$$

7.8 Simulation of the prototype reactor-heat exchanger

In this section a base case design for the prototype dehydrogenation reactor-heat exchanger system is defined and simulated. The effect of the parameters, such as flow direction (co-current or counter-current), exhaust gas temperature, number of fins, catalyst activity and catalyst deactivation and an appropriate material of construction (MoC) are studied in order to optimise the design.

7.8.1 Shrouded-tube dehydrogenation reactor specifications — base case

The operating conditions, dimensions of the reactor and catalyst information for the base case design of the dehydrogenation reactor-heat exchanger are listed in Table 7.5. The high inlet temperature of 380 °C is used to have high initial rates of dehydrogenation. A pressure of 9 bar is selected to take advantage of supercharging or turbo operation of hydrogen engine. Moreover, the high pressure will reduce the size of the hydrogen accumulator and other pieces of equipment.

Table 7.5 Operating conditions, mechanical features and the catalyst information for the base case design and simulation of the prototype reactor-heat exchanger

Operating conditions	
Mole percent hydrogen in the gasoline, %	4.0
Operating pressure, bar	9.0
Reactor inlet temperature, K	653.2
Final conversion	0.90
Pure MCH (feed) flowrate, kmol/h	0.0884
MCH gas mass velocity per tube, $kg \cdot s^{-1} \cdot m^{-2}$	0.933
Air flowrate required*, kmol/h	5.653

Inlet exhaust gas temperature, K	898
Exhaust gas flowrate*, kmol/h	6.114
Exhaust gas mass velocity per tube, $kg \cdot s^{-1} \cdot m^{-2}$	6.818
Exhaust gas composition*	
$\quad CO_2$	0.10
$\quad H_2O$	0.15
$\quad O_2$	0.02
$\quad N_2$	0.73
Flow direction	Counter-current

Mechanical design	
Tube material	Stainless steel
Effective length of the reactor (mm)	500
O.D. of the outer tube, in (mm)	1.5 (38.1)
I.D. of the outer tube, in (mm)	1.37 (34.798)
O.D. of the inner tube, in (mm)	0.75 (19.05)
I.D. of the inner tube, in (mm)	0.652 (16.561)
Number of tubes	12
Fin material	Stainless steel
No. of fins	12
Fin height, in (mm)	0.21 (5.334)
Fin thickness, in (mm)	0.035 (0.889)

Catalyst	
Catalyst shape	Spherical
Catalyst size (mm)	1.20
Catalyst material	1.0 wt% Pt/Al_2O_3
Weight of the catalyst (kg)	0.9232

* Neglecting minute amounts of MCH and toluene

7.8.2 Simulation procedure and criteria

- The finite-differences for the model equations are set-up.
- As discussed above, the moles per second of MCH and isooctane required for a 4.0 mol% of hydrogen in air-fuel mixture were calculated based on the calculations with an ideal Otto cycle corrected for the real efficiencies. The maximum power output of 66.2 kW was used for the calculations. On the same basis, the moles of air required and the moles and the composition of the exhaust gas were calculated.

- An iterative solution was required with counter-current operation. A guessed value of the outlet temperature of the exhaust gas was input in the simulation worksheet and was varied until the inlet exhaust temperature equals the set value.

- The mass of the catalyst and the outlet exhaust gas temperature were varied to meet the desired MCH conversion.

- Knowing the mass of the catalyst and the bulk density of the catalyst enabled the number of tubes required to be calculated. This was rounded up and the mass of the catalyst was corrected accordingly.

- The inlet temperature of MCH vapour was kept constant at 380 °C.

7.8.3 Parameter sensitivities

Below are the results of the simulation of the prototype along with the discussion on the parameter sensitivities.

7.8.3.1 Base case design

Fig. 7.9 and 7.10 show the variations in the average temperatures and average conversions in the axial direction, while Fig. 7.11 and Fig. 7.12 show the radial variations in the temperatures and fractional conversions for the base case design. A rather steady increase in the conversion in the axial direction of the reactor tube indicates a compromise between the average concentration of MCH, which decreases along the length of the tube, and the average bed temperature which increases in the axial direction, except at the initial stage where the highly endothermic nature of the reaction causes a small decrease as shown in Fig. 7.9. A near constant difference of 180 °C, between the exhaust gas temperature and the average bed temperature places the base case system well away from a "pinch" and maintains the catalyst temperature within acceptable limits.
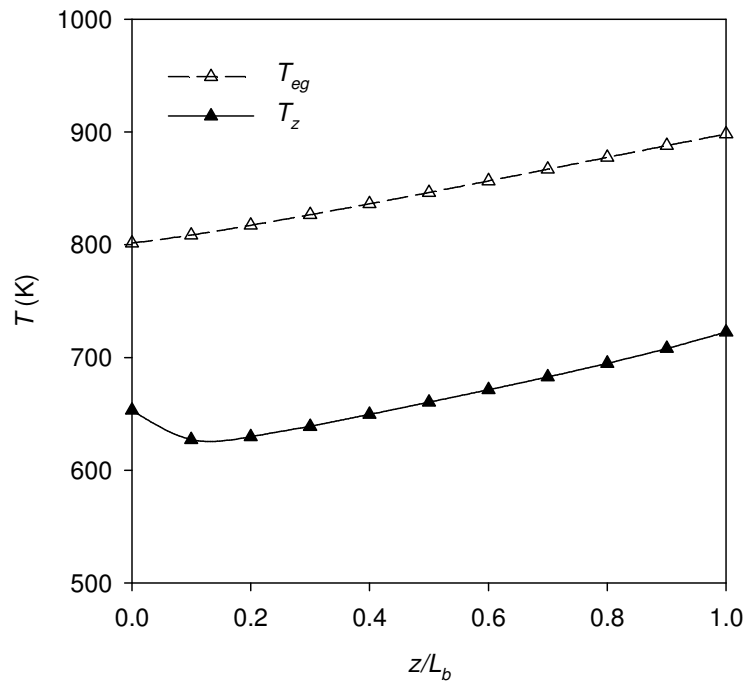
Fig. 7.9 Variation of the bed temperature and the exhaust gas
temperature in the axial direction for the base case design.
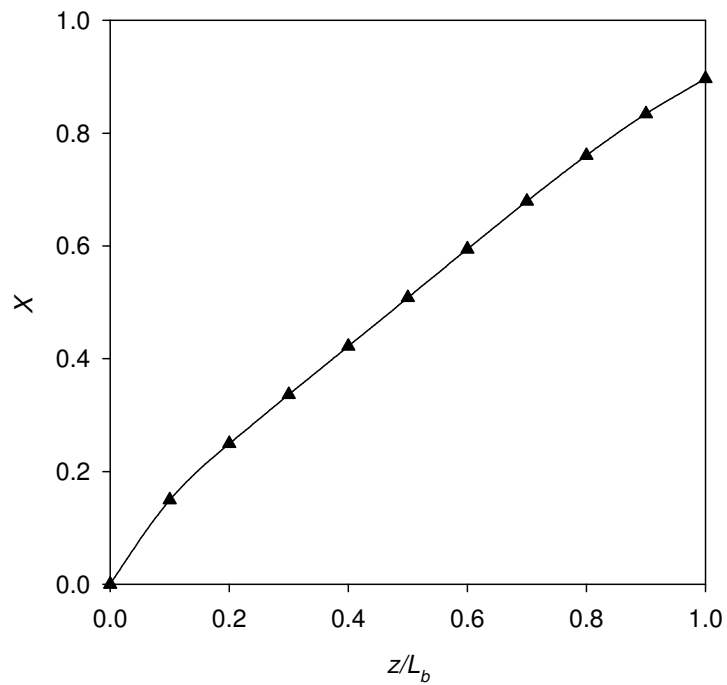
Fig. 7.10 Variation of the average conversion in the axial
direction for the base case design.

208
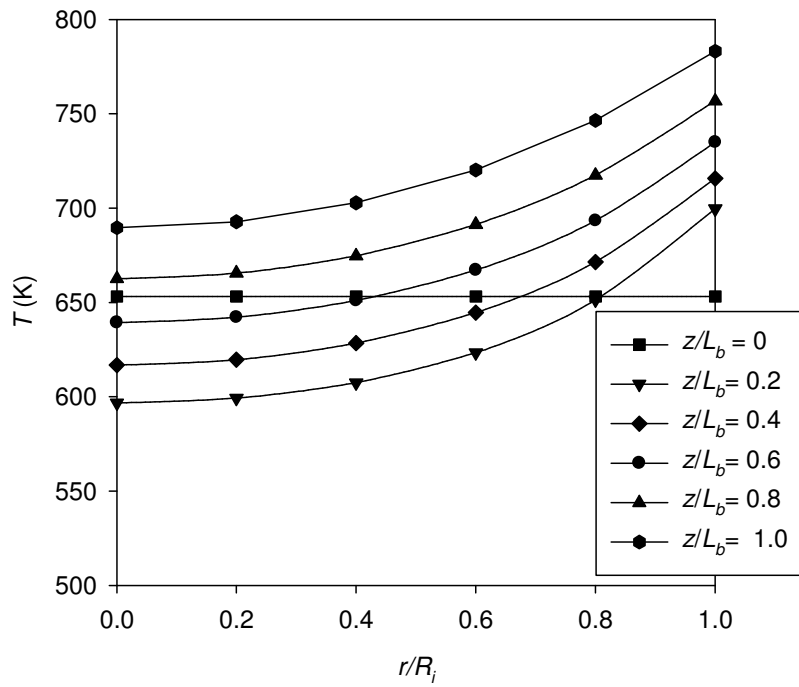
Fig. 7.11 Variation of the average bed temperature in the radial
direction for the base case design.
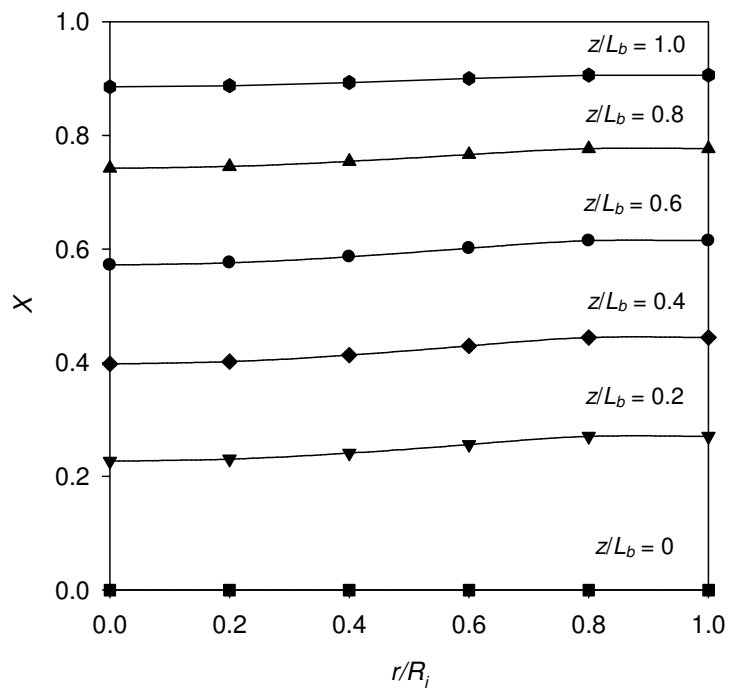
Fig. 7.12 Variation of the conversion in the radial direction for the
base case design.

7.8.3.2   Effect of flow direction

Fig. 7.13 and Fig. 7.14 show the axial temperature profiles and axial conversion profiles respectively, for both co-current and counter-current operations. The two operations were compared for the base case process conditions. It was observed that under the same conditions of exhaust gas inlet temperature of 625 °C and the same inlet reactor temperature of 380 °C, the maximum conversion in the case of the co-current process is slightly higher than in the counter-current operation. For the co-current operation, the exit conversion was 92.0 %, while for the counter-current operation, it was 90.0 %. Moreover, the exhaust gas temperature leaving the reactor-heat exchanger is also slightly higher and the outlet reactor bed temperature is slightly lower (less possible catalyst deactivation). A co-current operation at first instance seems slightly more beneficial than the counter-current. However, due to the large temperature gradients present in the reactor system, thermal expansion problems may arise and may make the design of a co-current reactor mechanically difficult. Thermal expansion of the metal tubes may lead to deformation and rupture. These thermal expansion problems are easier to accommodate in a counter-current process. One such solution is devised by Andrew et al. [1989], and is shown in Fig. 7.15.
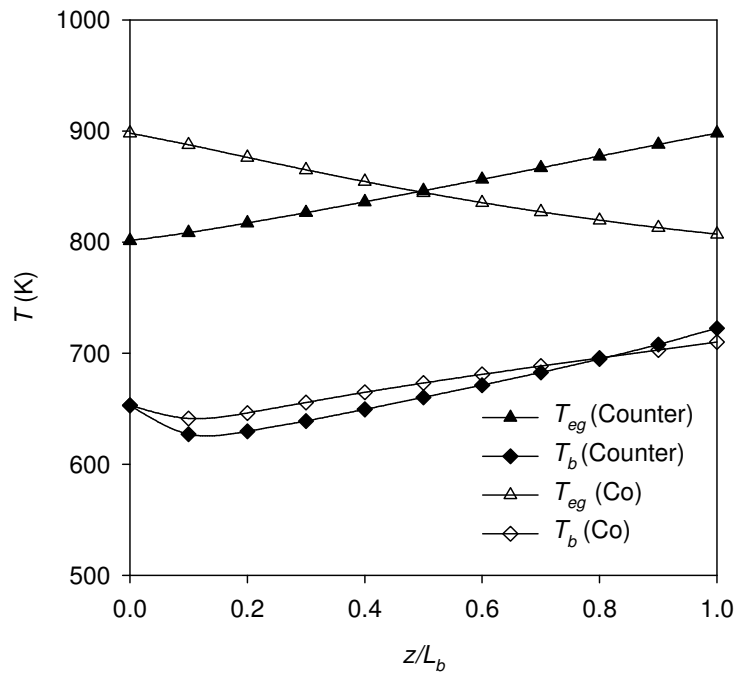
Fig. 7.13 Axial temperature profiles for the co-current and
counter-current operations for the base case conditions.
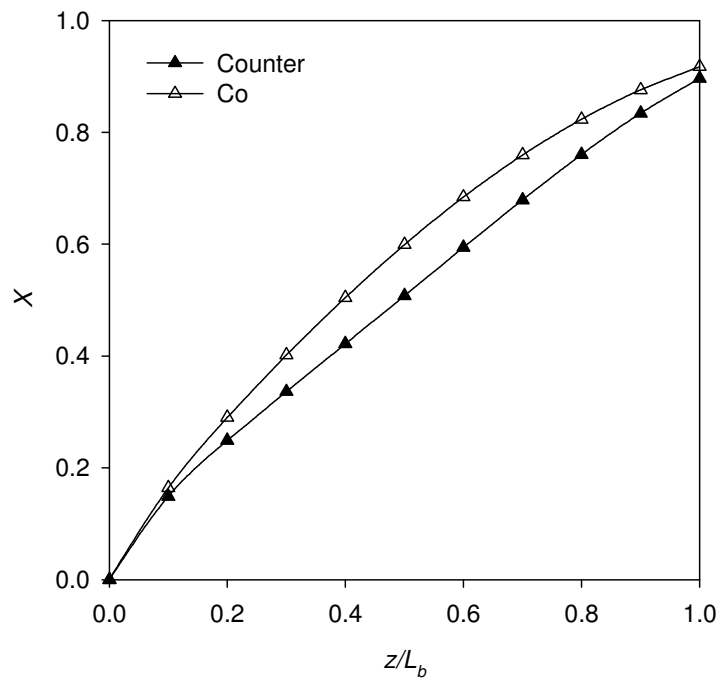
Fig. 7.14 Axial conversion profiles for the co-current and
counter-current operations for the base case conditions.

211

Reactants
in

Reactants
out

Reactants
outlet

Insulation

Shroud
tube

Fins

Reactor
tube

a

Exhaust gas
in

Reactants
out

Reactants
in

Reactants
in

Exhaust
gas out

Shroud
tube

Fin

Catalyst

b
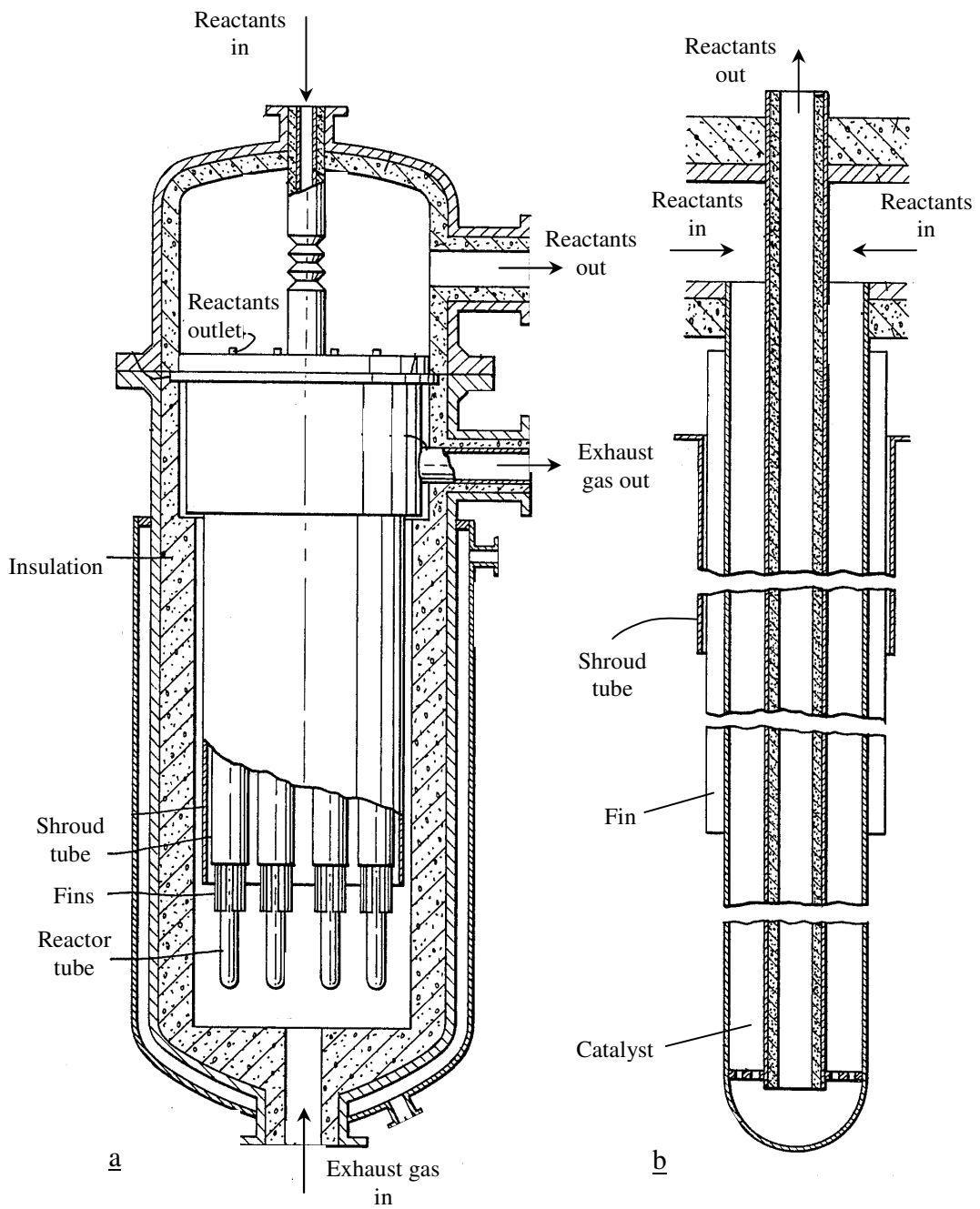
Fig. 7.15 An example design for the counter-current operation to accommodate the
thermal expansion problem a) bank of reactor tubes in parallel b) single reactor
tube geometry. *Source*: Andrew, et al. [1989].

7.8.3.3   Effect of exhaust gas temperature

A high exhaust gas temperature will improve the heat transfer rate and lead to a smaller number of tubes and a reduced catalyst volume. However, the tube wall thickness must be reduced as a result of the lower allowable working stress of the material. Excessively high temperatures may lead to unacceptable rates of catalyst deactivation due to "coking" or even sintering of the platinum crystallites or support may occur. A low exhaust temperature on the other hand, will lead to a more bulky reactor system with a larger number of tubes. However, the catalyst deactivation rates will be reduced and the tube wall thickness minimised. Fig. 7.16 shows the effects of the exhaust gas temperature for the base case design on the final conversion reached and on the number of reactor tubes required for a fractional conversion of 0.90.

The reactor conversion decreases almost linearly with the exhaust gas temperature below $X = 0.90$ while the number of tubes increases linearly. A base case design of $X = 0.90$ seems reasonable, therefore.

An exhaust gas temperature higher than 750 °C may have virtually no benefit in decreasing the number of tubes and hence the volume of the catalyst. The average catalyst bed temperature also increases and greater catalyst deactivation may be the result. As an example, for the case when the exhaust gas temperature is 700 °C, the catalyst bed temperature reaches nearly 500 °C for virtually the same conversion.
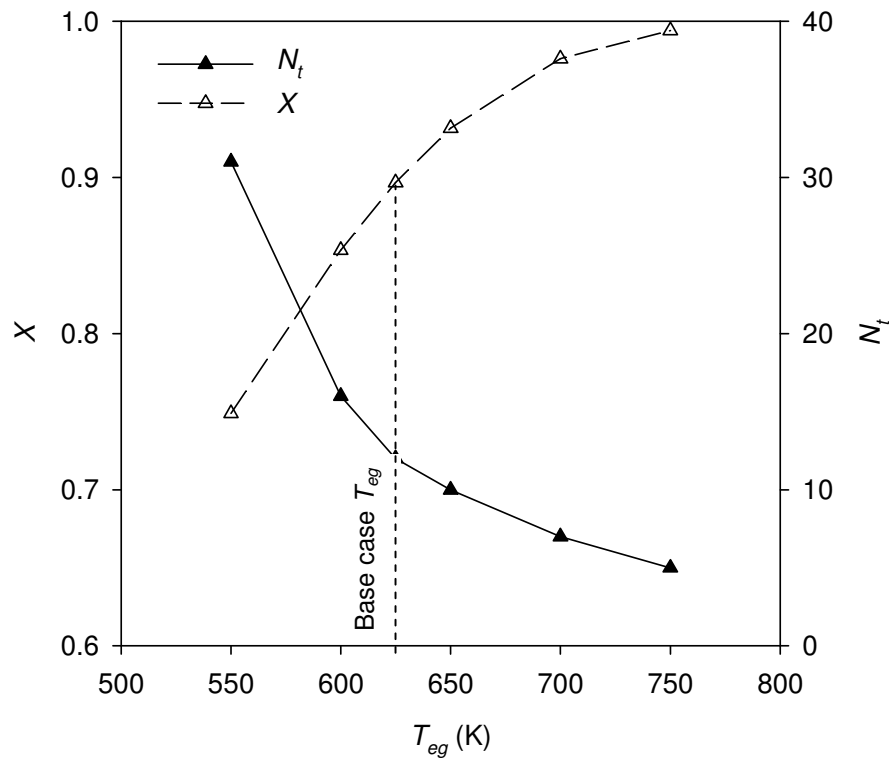
Fig. 7.16 Effect of exhaust gas temperature for the base case design on the final conversion and number of tubes.

7.8.3.4 Effect of number of fins

Increasing the number and height of fins should have a profound effect on the heat transfer characteristics of the dehydrogenation reactor-heat exchanger system. Fig. 7.17 shows the results obtained for the simulation with no fins to the maximum possible number of fins on the base case tube diameter. The maximum possible number of fins is suggested by the finned-tube manufacturer, Vulcan Finned Tubes [Vulcan, 2010]. Clearly, Fig. 7.17 shows the advantage of adding fins to the tube geometry. With no fin conditions, under the same design parameters, the final conversion is only 0.53 which is 64% less than the conversion (0.90) obtained with only 12 fins. Increasing number of fins beyond 12 leads to only marginal benefits.
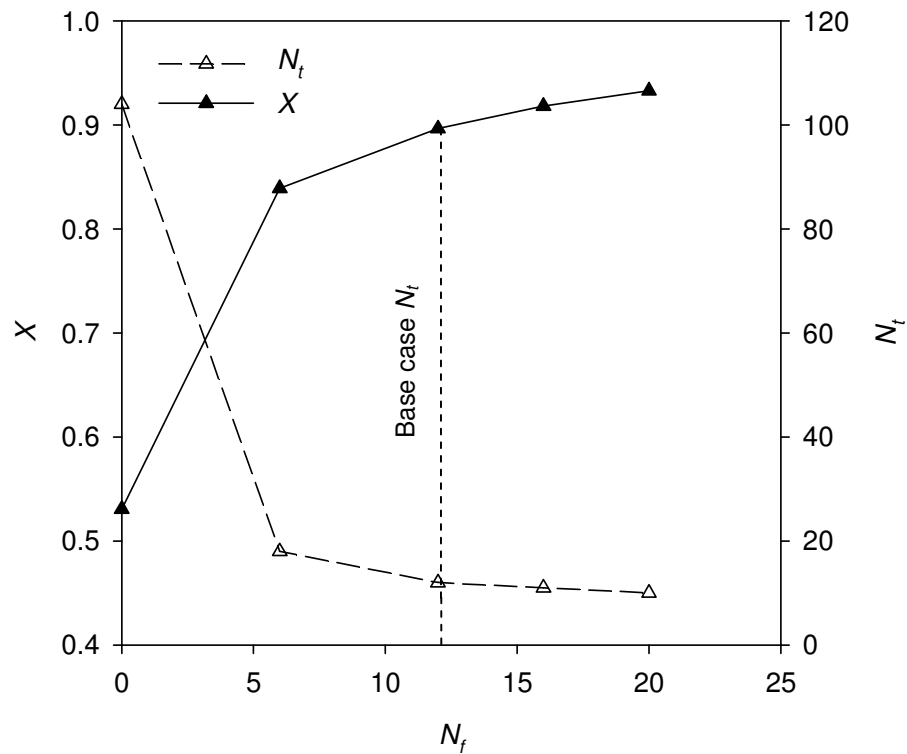
Fig. 7.17 Effect of number of fins for the base case design on final
conversion and number of tubes.

7.8.3.5 Effect of catalytic activity

The dehydrogenation catalyst is expected to lose its activity both by reversible
and irreversible deactivation. The effect of the initial activity of the catalyst is shown
in Fig. 7.18. For the base case design, assuming half the initial activity of the catalyst,
the final conversion obtained is only 11% lower than the base case. This is quite an
encouraging result and suggests that the reactor performance can tolerate a significant
loss of catalyst activity.
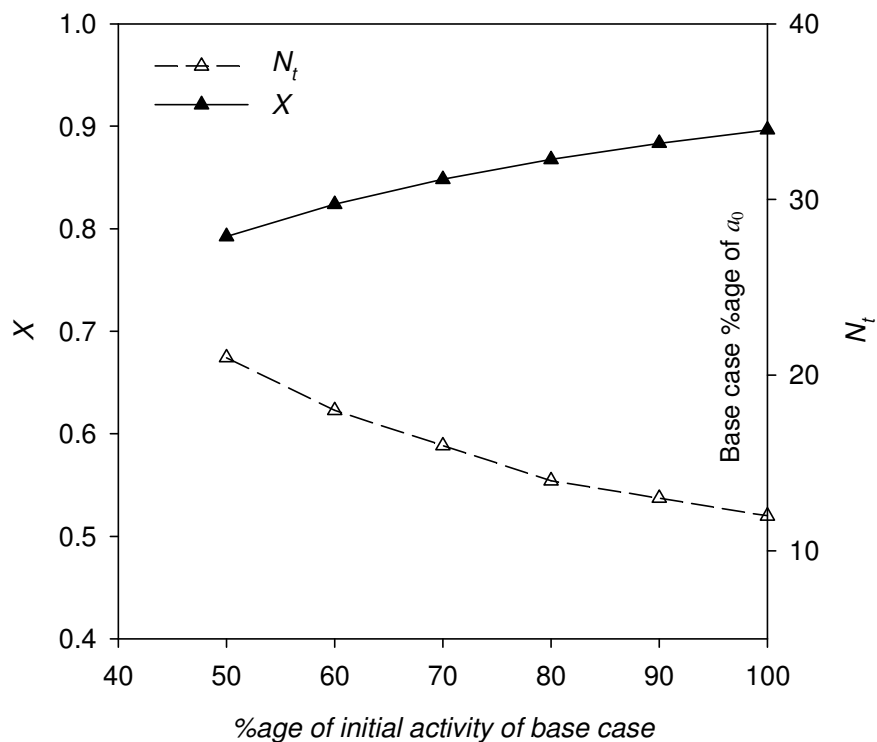
Fig. 7.18 Effect of %age of initial activity (a_0) for the base case design on
the final conversion and the number of reactor tubes.

Alhumaidan [2008] studied the long term deactivation of the development catalyst (1.0 wt % Pt/Al$_2$O$_3$) used here. The results of Alhumaidan [2008] together with the experimental conditions are shown in Fig. 7.19. Alhumaidan's results showed that less than 8% of the initial activity is lost in 600 h of continuous operation. Assuming the deactivation behaviour shown by the simple expression, $X = 1.0039 - 0.0001 \cdot t_d$, where t_d is in h, applies to the base case, the activity would fall to ~80% of the initial value after 3 months. The development catalyst may even be more stable for the base case because the operation is at a higher pressure of 9 bar. It has been shown in Chapter 4 that increased pressure reduces the rate of catalyst deactivation.
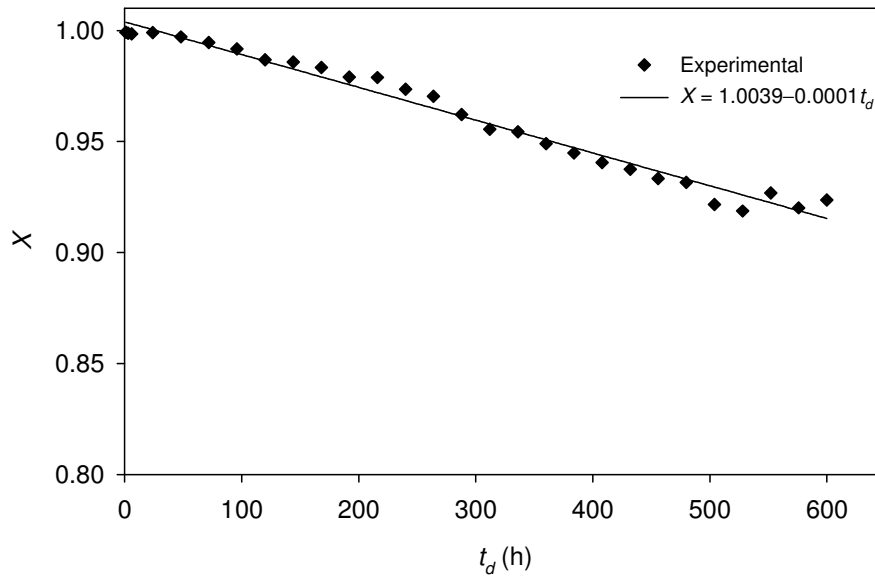
Fig. 7.19 Long-term deactivation test of development catalyst, 1.0 wt % Pt/Al$_2$O$_3$, as carried out by Alhumaidan [2008]; p = 1.013 bar, T_w = 380 °C, pure MCH (no hydrogen in the feed) and W/F_{A0} = 12.44×10^{-4} s.g-cat/mol MCH.

7.8.3.6 Effect of material of construction (MoC)

Stainless steel grade 316 (SS-316), an austenitic steel with 18%Cr-8%Ni, is used in the base case design of the heat exchanger-reactor system. SS-316 is selected because it has a high temperature oxidation resistance upto 900 °C [Hansen, 2009]. It is considered the most corrosion resistant stainless steel [Gardner, 2001]. It has good mechanical strength and excellent weldability characteristics [Materials, 2010]. In addition to SS-316, a relatively less costly SS-304 may also be used though this has inferior corrosion resistant properties. SS-321 is an alternative at higher temperatures. The above mentioned SS materials have moderate thermal conductivities and specific gravities. A material with high thermal conductivity, such as copper or silver, would be desirable since it will reduce the heat transfer area requirement and thus lead to a lower volume reactor system. Moreover, a material with low density would be helpful in reducing the overall weight of the reactor-system. In this case, aluminium or titanium may be selected. The high cost of silver and the low service temperatures of copper and aluminium alloys rule out these materials. Titanium and most of its alloys

217

have a service temperature not greater than 600 °C [Moiseyev, 2006]. However, titanium aluminides may be employed up to 900 °C [Kestler and Clemens, 2003]. Although, titanium has a density (4.51 g/cm^3), nearly half that of austenitic stainless steel (8.0 g/cm^3), it's relative cost is 7 to 1 compared to SS-316 [Towler and Sinnot, 2008]. Moreover, titanium alloys are also susceptible to hydrogen embrittlement, which however can be avoided if a small amount of water or oxygen is present in the hydrogen atmosphere [Schutz, 1992]. Considering the above mentioned properties of titanium alloys, it may be the only material which may offers a viable alternative to stainless steel.

7.9   Transient heat transfer

It is important to know the time required for the reactor mass and the incoming MCH feed to the reactor to reach the required temperature. This is important in the start-up and to know the size of the hydrogen accumulator which will be used for providing hydrogen gas to the engine for the interim period when there is no hydrogen generation.

The following assumptions were made in developing the dynamic model and calculating the time required to reach the required temperature.

- The reactor and the auxiliary heat exchangers (preheater, vaporiser and superheater) were lumped together in a single piece of equipment, here called "lumped reactor" as shown in Fig. 7.20. The mass of the preheater, vaporiser and superheater together is taken equal to the mass of the reactor-heat exchanger. The mass of the shell 1 mm thick and 0.5 m long with 0.129 m outer diameter which accommodates the tube bundle was also added to the above mass.
- Only the exhaust gas was assumed to heat the entire system and no feedback of the reactor outlet gas was considered.
- The MCH feed was assumed to behave under mixed flow conditions instead of plug flow conditions. This ensures that the temperature of the feed reactant

218

(MCH) inside the "lumped reactor" is same as the product gases. This was done to simply the dynamic model calculations.

- Pseudo-equilibrium conditions were considered for the dehydrogenation reaction and negligible mass accumulation within the reactor was assumed.

- Negligible heat capacity in the exhaust gases is assumed.

- Average heat capacity of the Al_2O_3 catalyst was considered as 900 $J \cdot kg^{-1} \cdot K^{-1}$, while that of reactor and exchangers' materials (stainless steel or titanium alloy) is 500 $J \cdot kg^{-1} \cdot K^{-1}$.

- The total heat transfer surface area of the "lumped reactor" is considered as twice the outside surface area of the reactor-heat exchanger. For the reactor-heat exchanger assembly the total area calculated was 1.038 m^2.

- The average overall heat transfer coefficient for the "lumped reactor" is 150 $W \cdot m^{-2} \cdot K^{-1}$

- The densities of stainless steel and titanium alloy (aluminide) are 7900 kg/m^3 and 4000 kg/m^3, respectively.
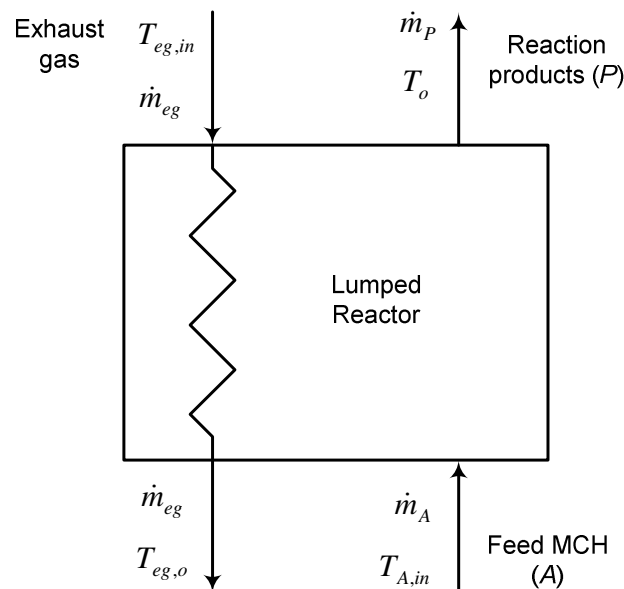
Fig. 7.20 "Lumped reactor" for the simplified calculations of the dynamic system.

Based on the above mentioned assumptions, the following three energy balances were developed and for the base case defined in Table. 7.5, Eq. 7.18 to Eq. 7.20 were solved simultaneously. The ordinary differential equation (Eq. 7.18) was solved using Euler's approximation between the limits $T_o = 15$ °C at $t = 0$ min and $T_o = 380$ °C at $t = t$ min.

$$m_{lr} \cdot c_{p,lr} \cdot \frac{dT_o}{dt} = \dot{m}_{eg} \cdot c_{p,eg} \cdot (T_{eg,in} - T_{eg,o}) - \dot{m}_A \cdot (c_{p,A})_L \cdot (T_{sl,A} - T_{A,in})$$

$$- \dot{m}_A \cdot \Delta h_{v,A} - \dot{m}_A \cdot c_{p,A} \cdot (T_o - T_{sv,A}) - W \cdot (-r) \cdot \Delta h_{rxn}^\circ$$

(7.18)

$$\dot{m}_{eg} \cdot c_{p,eg} \cdot (T_{eg,in} - T_{eg,o}) = U_{lr} \cdot A_{lr} \cdot (T_{eg,o} - T_o)$$ (7.19)

$$\frac{W \cdot M_A}{X \cdot \dot{m}_A} = \frac{X}{(-r)}$$ (7.20)
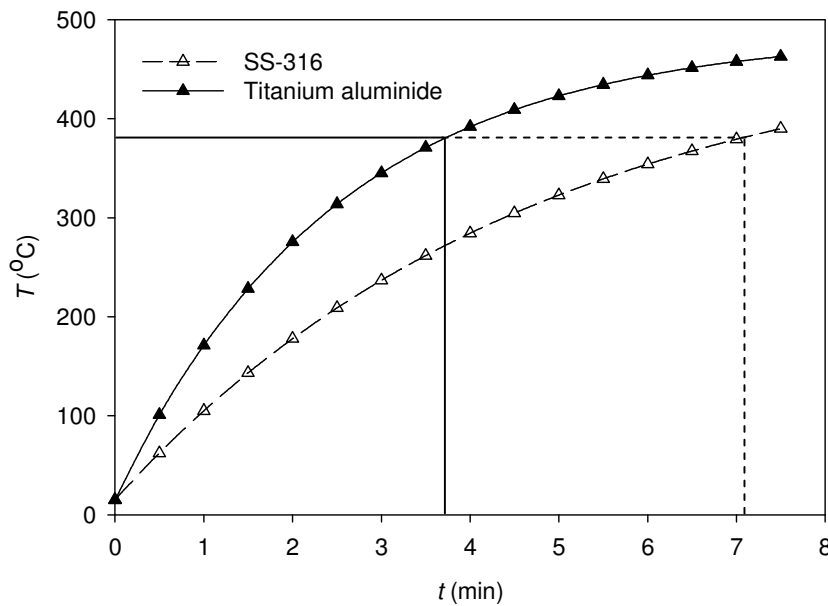
Fig. 7.21 Dynamic response for SS-316 and titanium aluminide for the startup period of the "lumped reactor".

Fig. 7.21 shows the dynamic modelling results for both SS-316 and titanium aluminide. The time required to heat up to 380 °C for stainless steel (base case material) is 7.1 min while the time required for titanium alloy, which had a lower mass capacity, was only 3.7 min. The size of the hydrogen accumulator, when titanium was the MoC for the "lumped reactor" at full power of the vehicle (66.2 kW), was calculated to be 40.8 L and for the stainless steel, 78.3 L.

Alternately, to avoid the above accumulator, the engine can be switched to the hybrid H_2-gasoline-system after running the vehicle on gasoline only fuel for the initial period.

Chapter 8
Conclusions and Future Directions

8.1 Conclusions

The review of the literature has shown that there is a huge disagreement in describing the kinetic mechanism of the dehydrogenation reaction of methylcyclohexane. There is no consensus on the rate-determining step and the inhibition offered by the products. Moreover, there is no detailed kinetic investigation over a wide range of operating conditions including experiments without hydrogen in the feed and under integral conditions. A kinetic model associated with a kinetic mechanism is therefore developed. The kinetic model is used to predict observed longitudinal temperature profiles (i.e. under non-isothermal, non-adiabatic conditions found in practice). Alternative configurations and schemes for "on-board" hydrogen generation are compared and a prototype reactor, suitable for "on-board" hydrogen generation, is designed in detail, incorporating the kinetic model.

8.1.1 Kinetic modelling of the main reaction

The catalytic dehydrogenation of methylcyclohexane (MCH) was investigated for "on-board" hydrogen storage and utilisation. The experiments were performed in a laboratory fixed bed tubular reactor under integral conditions. A 1.0 wt% Pt/Al_2O_3 catalyst (to date the best catalyst with respect to a combination of activity, selectivity and long life) was prepared to carry out the dehydrogenation work. A wide range of experimental conditions with regards to temperature, pressure, feed composition and space velocity was studied. The extensive experimental data was used to study the reaction mechanism and to develop the best kinetic rate expression. A number of kinetic models were applied based on the power law, Langmuir-Hinshelwood-Hougen-Watson (LHHW) and Horiuti-Polanyi (HP) mechanisms. Power law kinetics show a non-linear relationship between the initial rate and the partial pressure of

hydrogen. Generally, order of the reaction and activation energy increase with an increase in the total pressure of the system. A kinetic model based on LHHW kinetics with loss of the first hydrogen molecule in a single-site mechanism was found to best fit the data. Experiments with the intermediate (methylcyclohexene) confirm the rate-controlling step does not lie beyond loss of the first hydrogen molecule in the reaction scheme.

8.1.2 By-products selectivity

The analysis of the products shows that the dehydrogenation of MCH is very selective towards toluene with a % selectivity, defined as the moles of toluene formed per mole of MCH consumed, generally greater than 98.2%. Besides the main product toluene, a number of condensable by-products were also identified. Benzene, cyclohexane and ring closed products (ethylcyclopentane and dimethylcyclopentanes) are the major by-products. At low pressures, cyclohexane is found to be a reaction intermediate. It is formed by hydrodemethylation of MCH and disappears by the dehydrogenation of cyclohexane to benzene. At high pressures, however, cyclohexane reverts from being a reaction intermediate to become a reaction end-product. Benzene, on the other hand, is always an end-product and may be formed by the dehydrogenation of cyclohexane, disproportionation of toluene and hydrodealkylation of toluene.

8.1.3 Modelling and simulation of the laboratory reactor

A two-dimensional pseudo-homogeneous model was used as a basis for the mathematical modelling of the laboratory fixed bed reactor. Laboratory experimental data for the 12 experimental runs made under varying conditions of pressure, space velocity and feed composition were simulated for the temperatures and fractional conversions at various points of the dehydrogenation reactor. Good agreement between predicted and observed centreline temperatures was found. These results support the validity of the two-dimensional pseudo-homogeneous reactor model. It is

observed that the effective radial thermal conductivity is more a function of composition of the reaction fluid mixture than the temperature in the reactor and that the major radial resistance to heat transfer lies in the bed of catalyst particles rather than at the wall.

8.1.4   Modelling and simulation of the prototype reactor-heat exchanger system

8.1.4.1   Alternative configurations and schemes for "on-board" hydrogen generation

A base-case process flow diagram for the "on-board" MTH-system capable of producing 66.2 kW for a 1200 cc vehicle was developed. The thermal pinch analysis shows theoretical feasibility on the basis of an exhaust gas available at 850 °C for the option "total replacement of gasoline by H_2 from MTH-technology". However, the size of storage tanks and the associated equipment required completely rule out the idea of using the MTH-system as a total replacement for gasoline for the provided vehicle. Also, total replacement of gasoline in a SOFC stack with H_2 from the MTH-system is not found practical on the basis of the same reasoning. Moreover, the fuel cell technology is far from being commercialised at low cost and with a durable life span in the near future. For a medium speed at 30 kW, and for an operation of 8 h, requires a tank 8 times smaller for the hybrid MTH-gasoline-system option compared to the simple MTH-system option. This system requires a far smaller tank size and reactor volume and provides a much more practical alternative.

8.1.4.2   Design and simulation of the prototype reactor-heat exchanger system

A novel heat exchanger-reactor system for the MTH-technology is proposed. The system consists of a multiple-double-tube reactor-heat exchanger. The two-dimensional pseudo-homogeneous model developed and tested for the laboratory reactor data is applied for the simulation of the prototype reactor. The effect of the parameters, such as flow direction (co-current or counter-current), exhaust gas

temperature, number of fins, catalyst activity and catalyst deactivation and an appropriate material of construction (MoC) were studied in order to optimise the design.

- A near constant difference of 180 °C, between the exhaust gas temperature and the average bed temperature places the base case system well away from a "pinch" and maintains the catalyst temperature within acceptable limits.

- Due to the large temperature gradients present in the reactor system, thermal expansion problems may arise and may make the design of a co-current reactor mechanically difficult.

- A base-case exhaust gas temperature of 625 °C is found reasonable. Above this temperature, no appreciable benefit in reducing the number of tubes and hence the volume of the catalyst is found. Moreover, the catalyst deactivation rates are also acceptable.

- There is a significant advantage in adding fins to the tube geometry. With no fins, under the same design parameters, the final conversion is only 0.53 compared with 0.90 obtained with only 12 fins. Increasing the number of fins beyond 12 leads to only marginal benefits.

- For the base-case design, assuming half the initial activity of the catalyst, the final conversion obtained is only 11% lower than the base-case. This is quite an encouraging result and suggests that the reactor performance can tolerate a significant loss of catalyst activity.

- Titanium aluminides having low density, only half that of the stainless steel and high service temperatures, may offer a viable alternative to stainless steel.

8.1.4.3   Dynamic modelling of the prototype reactor-heat exchanger system

A simplified dynamic model for the prototype was developed and the time required to heat up the system to 380 °C was calculated.

- For stainless steel, the time is 7.1 min, while the time required for titanium alloy, which has a lower mass capacity, is only 3.7 min.

- The size of the hydrogen accumulator, when titanium is the MoC for the system at full power of the vehicle (66.2 kW), is calculated to be 40.8 L and for the stainless steel, 78.3 L. Alternately, to avoid the above accumulator, the engine can be switched to the hybrid H_2-gasoline-system after running the vehicle on gasoline-only fuel for the start up period.

8.2 Future directions

The present study suggests the following future directions

- Improvements to the catalyst by use of promoters to further improve the selectivity of the catalyst under high pressure and high temperature operations and reduce the deactivation under high temperature conditions.
- Adopting new "state of the art" technologies to better handle the heat transfer requirements. A compact heat exchanger, such as a finned-plate-type heat exchanger, may be used.
- The conventional dehydrogenation reactor used in the present study may be modified to a structured wall-coated reactor to improve the heat transfer rates.
- Building up a single shroud tube reactor-heat exchanger at the laboratory scale while exchanging heat with a model exhaust gas (heated N_2) stream. The system may be closer to the actual reactor-heat exchanger system and may be useful in measuring the real-time temperature profiles and to improve the mathematical model.
- The use of Comsol® Multiphysics (finite element method) may be employed to solve the set of PDEs, which may or may not be more convenient.

References

Aberuagba, F. and Susu, A.A., "The Role of Nitrogen in Facilitating Methylcyclohexane Aromatization on Pt/Al_2O_3 and $Pt-Re/Al_2O_3$ Catalysts", J. Pet. Sci. Technol. **22**, 565−587 (2004).

Ackerman, G.H., Faith, L.E., Heck, C.K., Henderson, H.T., Ritchie, A.W. and Ryland, L. B., "Hydrocarbon Fuels Got Advanced Systems" Shell Development Company, AFAPL-TR-70-71, Part I (1970).

Ahmed, M. and Fahien, R.W., "Tubular Reactor Design−I: Two Dimensional Model", Chem. Eng. Sci. **35**, 889−895 (1980).

Akyurtlu, J.F., and Stewart, W.E., "Competitive Hydrogenation of Benzene and Toluene and Dehydrogenation of the Corresponding Naphthenes over Platinum Wire", J. Catal. **51**, 101−107 (1978).

Alhumaidan, F.S., "Hydrogen Storage in Liquid Organic Hydrides: Producing Hydrogen Catalytically from Methylcyclohexane", Ph.D. Thesis, The University of Manchester, Manchester (2008).

Ali, J.K. and Baiker, A., "Dehydrogenation of Methylcyclohexane to Toluene in a Pilot-Scale Membrane Reactor", Appl. Catal. A: Gen. **155**, 41−57 (1997).

Al-Sabawi, M. and de Lasa, H., "Kinetic Modeling of Catalytic Conversion of Methylcyclohexane over USY Zeolites: Adsorption and Reaction Phenomena", AIChE J. **55**, 1538−1558 (2009).

Andrew, S.P., Doy, R.J. and Limbach, P.J., "Apparatus for Steam Reforming Hydrocarbons", US Patent No. 4,810,472, March 7, 1989.

Beek, J., "Design of Packed Catalytic Reactors", Adv. Chem. Eng. **3**, 203−271 (1962).

Bejan, A., "Heat Transfer", John Wiley & Sons, Inc., New York, 1993.

Bejan, A., "Forced Convection: Internal Flows", In: Bejan, A. and Kraus, A.D. (Eds.), "Heat Transfer Handbook", John Wiley & Sons, Inc., 2003.

Bird, R.B., Stewart, W.E. and Lightfoot, E.N., "Transport Phenomena", 2nd ed., John Wiley & Sons, Inc., New York, 2007.

Blakely, D.W. and Somorjai, G.A., "The Dehydrogenation and Hydrogenolysis of Cyclohexane and Cyclohexene on Stepped (High Miller Index) Platinum Surfaces", J. Catal. **42**, 181−196 (1976).

Brunelle, J.P., "Preparation of Ctalysts by Metallic Complex Adsorption on Mineral Oxides", Pure & Appl. Chem. **50**, 1211−1229 (1978).

Bustamante, G.V.S.C., Swesi, Y., Pitault, I., Meille, V. and Heurtaux, F., "A Hydrogen Storage and Transportation Mean", Proc. Int. Hydrogen Energy Cong. Exh. IHEC, Istanbul (2005).

Campbell, C.T., Campbell, J.M., Dalton, P.J., Henn, F.C., Rodriguez, J.A. and Seimanides, S.G., "Probing Ensemble Effects in Surface Reactions. 1. Site-Size Requirements for the Dehydrogenation of Cyclic Hydrocarbons on Pt(111) Revealed by Bismuth Site Blocking", J. Phys. Chem. **93**, 806−814 (1989a).

Campbell, J.M., Seimanides, S.G. and Campbell, C.T., "Probing Ensemble Effects in Surface Reactions. 2. Benzene Adsorption on Clean and Bismuth-Covered Pt(111)", J. Phys. Chem. **93**, 815−826 (1989b).

Carberry, J.J., "Chemical and Catalytic Reaction Engineering", Dover Publications, Inc., New York, 2001.

Carslaw, H.S. and Jaeger, J.C., "Conduction of Heat in Solids", 2nd ed., Oxford University Press, New York, 1959.

Chai, M-R. and Kawakami, K., "Kinetic Model and Simulation for Catalyst Deactivation During Dehydrogenation of Methylcyclohexane over Commercial Pt-, PtRe- and Presulfided PtRe-Al$_2$O$_3$ Catalysts", J. Chem. Tech. Biotechnol. **51**, 335−345 (1990).

Chaouki, J. and Klvana, D., "Influence of the Deactivation of an Industrial Pt-Sn/Al$_2$O$_3$ Catalyst on the Performance of the Dehydrogenation Reactor", Chem. Eng. Sci. **49**, 4639−4646 (1994).

Chaouki, J., Klvana, D., Pontier, T. and Belanger, G., "Modélisation de la Désactivation du Catalyseur Pt-Sn/Al$_2$O$_3$ lors de la Déshydrogénation du Méthylcyclohexane", Chem. Eng. J. **46**, 109−118 (1991).

Chaouki, J., Touzani, A., Klvana, D., Bournonville, J.P. and Bélanger, G., "Déshydrogénation du Méthylcyclohexane sur le Catalyseur Industriel Pt-Sn/A$_2$O$_3$", Rev. de L'Inst. Fran. Pét. **43**, 874−881 (1988).

Chiew, Y.C. and Glandt, E.D., "The Effect of Structure of the Conductivity of a Dispersion", J. Colloid and Interface Sci. **94**, 90−104 (1983).

Clarke, J.K.A. and Rooney, J.J. "Stereochemical Approaches to Mechanisms of Hydrocarbon Reactions on Metal Catalysts", Adv. Catal. **25**, (125−181) 1977.

Clot, E., Eisenstein, O. and Crabtree, H., "Computational Structure-Activity Relationships in H_2 Storage: How Placement of N Atoms Affects Release Temperatures in Organic Liquid Storage Materials", Chem. Commun., 2231−2233 (2007).

Corma, A., Cid, R. and Agudo, L., "Catalyst Decay in the Kinetics of Methylcyclohexane Dehydrogenation over Pt-NaY Zeolite", Can. J. Chem. Eng. **57**, 638−642 (1979).

Corma, A., Reyes, P. and Pajares, J.A., "Metal Dispersity and Activity for Methylcyclohexane Dehydrogenation on Pt/NaY Zeolite", Raect. Kinet. Catal. Lett. **18**, 79−84 (1981).

Coughlin, R.W., Hasan, A., and Kawakami, K., "Activity, Yield Patters, and Coking Behavior of Pt and PtRe Catalysts during Dehydrogenation of Methylcyclohexane: II. Influence of Sulfur", J. Catal. **88**, 163−176 (1984a).

Coughlin, R.W., Kawakami, K. and Hasan, A., "Activity, Yield Patters, and Coking Behavior of Pt and PtRe Catalysts during Dehydrogenation of Methylcyclohexane: I. In the Absence of Sulfur", J. Catal. **88**, 150−162 (1984b).

Crabtree, G.W., Dresselhaus, M.S. and Buchanan, M.V., "The Hydrogen Economy", Physics Today, December 2004, 39−44.

Cresswell, D.L., "Private Communication", 2010.

Cresswell, D.L., Metcalfe, I.S., "Energy Integration Strategies for Solid Oxide Fuel Cell Systems", Solid State Ionics **177**, 1905−1910 (2006).

Cresswell, D.L., Milisavljevic, B., Rippin, D.W.T. and Srivastava, D., "The Catalytic Production of Hydrogen for the Use of Road Vehicles: A Status Report", Proc. Int. Chem. React. Eng. Conf., Poona (1984).

Cusumano, J.A., Dembinski, G.W. and Sinfelt, J.H., "Chemisorption and Catalytic Properties of Supported Platinum", J. Catal. **5**, 471−475 (1966).

Dalai, A.K. and Bakhshi, N.N., "Carbon Monoxide Hydrogenation over Cobalt Catalyst in a Tube-Wall Reactor: Part 1 Experimental Studies", Can. J. Chem. Eng. **70**, 269−277 (1992).

Dancuart, L.P., de Haan R. and de Klerk, A., "Processing of Primary Fischer-Tropsch Products", Stud. Surf. Sci. Catal. **152**, 488 (2004).

Das, L.M., "Hydrogen Engine: Research and Development (R&D) Programmes in Indian Institute of Technology (IIT), Delhi", Int. J. Hydrogen Energy **27**, 953−965 (2000).

DeLorenzo, B. and Anderson, E.D., "Heat Transfer and Pressure Drop of Liquids in Double-Pipe Fin-Tube Exchangers, Trans. ASME **67**, 697−702 (1945).

De Wasch, A.P. and Froment, G.F., "Heat Transfer in Packed Beds", Chem. Eng. Sci. **27**, 567−576 (1972).

DIPPR$^®$ Project 801, Available from: http://www.knovel.com/web/portal/browse/display?_EXT_KNOVEL_DISPLAY_bookid=1187 [Accessed on March 01, 2010]

Dixon, A.G., "Correlations for Wall and Particle Shape Effects on Fixed Bed Bulk Voidage", Can. J. Chem. Eng. **66**, 705−708 (1988).

Dixon, A.G., Paterson, W.R. and Cresswell, D.L., "Heat Transfer in Packed Beds of Low Tube/Particle Diameter", ACS Symp. Ser. **65**, 238 (1978).

DOE (U.S. Department of Energy), "Properties of Fuels", Available form: http://www.afdc.energy.gov/afdc/pdfs/fueltable.pdf [Accessed on December 29, 2009].

Dumesic, J.A., Rudd, D.F., Aparicio, L.M., Rekoske, J.E. and Treviño, A.A., "The Microkinetics of Heterogeneous Catalysis", ACS Professional Reference Book, 1993.

El-Sawi, M., Infortuna, F.A., Lignola, P.G., Parmaliana, A., Frusteri, F. and Giordano, N., "Parameter Estimation in the Kinetic Model of Methylcyclohexane Dehydrogenation on a Pt-Al_2O_3 Catalyst by Sequential Experiment Design", Chem. Eng. J. **42**, 137−144 (1989).

Faith, L.E., Ackerman, G.H., Heck, C.K., Henderson, H.T., Ritchie, A.W. and Ryland, L.B., "Hydrocarbon Fuels for Advanced Systems", Shell Development Company, AFAPL-TR-70-71, Part II, 1971.

Faith, L.E., Ackerman, G.H., Heck, C.K., Henderson, H.T., Ritchie, A.W. and Ryland, L.B., "Hydrocarbon Fuels for Advanced Systems", Shell Development Company, AFAPL-TR-70-71, Part III, 1972.

Ferreira-Aparicio, P., Rodrígues-Ramos, I. and Guerrero-Ruiz, A., "Pure Hydrogen Production from Methylcyclohexane using a New High Performance Membrane Reactor", Chem. Commun., 2082−2083 (2002).

Flynn, L.W. and Thodos, G., "Lennard-Jones Force Constants from Viscosity Data: Their Relationship to Critical Properties", AIChE J. **8**, 362−365 (1962).

Froment, G.F. and Bischoff, K.B., "Chemical Reactor Analysis and Design", John Wiley & Sons, New York, 1979.

Fung, A.S., Kelley, M.J., Koningsberger, D.C. and Gates, B.C., "γ-Al$_2$O$_3$-Supported Re-Pt Cluster Catalyst Prepared from [Re$_2$Pt(CO)$_{12}$]: Characterization by Extended X-ray Absorption Fine Structure Spectroscopy and Catalysis of Methylcyclohexane Dehydrogenation", J. Am. Chem. Soc. **119**, 5877−5887 (1997).

García de la Banda, J.F., Corma, A. and Melo, F.V., "Dehydrogenation of Methylcyclohexane on a PtNaY Catalyst. Study of Kinetics and Deactivation", Appl. Catal. **26**, 103−121 (1986).

Gardner, J.D., "Ferrous Metals", In: Harper, C.A., "Handbook of Materials for Product Design", 3rd ed., McGraw-Hill, New York, 2001.

Garland, M., Baiker, A. and Wokaun, A., "Alumina-Supported Platinum-Rhenium Dehydrogenation Catalysts: Influence of Metal Ratio and Precursors on Catalytic Behavior", Ind. Eng. Chem. Res. **30**, 440−447 (1991).

Gland , J.L., Baron, K. and Somorjai, G.A., "Low-Energy Electron Diffraction, Work Function Charge and Mass Spectrometric Studies of Chemisorption and Dehydrogenation of Cyclohexane, Cyclohexene and 1,3-Cyclohexadiene on the Pt(111) Surface", J. Catal. **36**, 305−312 (1975).

Gonzo, E.E., "Estimating Correlations for the Effective Thermal Conductivity of Granular Materials", Chem. Eng. J. **90**, 299−302 (2002).

Gora, A., Tanaka, D.A.P., Mizukami, F. and Suzuki, T.M., "Lower Temperature Dehydrogenation of Methylcyclohexane by Membrane-Assisted Equilibrium Shift", Chem. Lett. **35**, 1372−1373 (2006).

GPSA (Gas Processors Suppliers Association), "Engineering Data Book", FPS Version, Vol. I & II, 11th ed. (electronic), Gas Processors Associations, 1998.

Green Car Congress, "Researchers Test On-Board System for Hydrogen Storage in Organic Hydride Liquids", Available form: http://www.greencarcongress.com/20-07/08/researchers-tes.html [Accessed on April 18, 2008]

Grenoble, D.C., "The Chemistry and Catalysis of the Toluene Hydrodealkylation Reaction, I. The Specific Activities and Selectvities of Group VIIB and Group VIII Metals Supported on Alumina", J. Catal. **56**, 32−39 (1979a).

Grenoble, D.C., "The Chemistry and Catalysis of the Toluene Hydrodealkylation Reaction: Kinetic Analysis", J. Catal. **56**, 40−46 (1979b).

Grünenfelder, N. and Schucan, T.H., "Seasonal Storage of Hydrogen in Liquid Organic Hydrides: Description of the Second Prototype Vehicle", Int. J. Hydrogen Energy **14**, 579−586 (1989).

Haensel, V. and Donaldson, G.R., "Platforming of Pure Hydrocarbons", Ind. Eng. Chem. **43**, 2102−2104 (1951).

Haensel, V., Donaldson, G.R. and Riedl, F.J., "Mechanisms of Cyclohexane Conversion over Platinum-Alumina Catalysts", Proc. 3rd. Int. Congr. Catal. **1**, 294−307 (1965).

Hansen, D.A., "Selecting Material of Construction (Steels and Other Metals)" In: Albright, L.F., "Albright's Chemical Engineering Handbook", CRC Press, 2009.

Hawthorn, R.D., Ackerman, G.H. and Nixon, A.C., "A Mathematical Model of a Packed-Bed Heat-Exchanger Reactor for Dehydrogenation of Methylcyclohexane: Comparison of Predictions with Experimental Results", AIChE J. **14**, 69−76 (1968).

Heise, M.S. and Schwarz, J.A., "Preparation of Metal Distribution within Catalyst Supports — 1. Effect of pH on Catalytic Metal Profiles", J. Colloid Interface Sci. **107**, 237−243 (1985).

Henn, F.C., Dalton, P.J. and Campbell, C.T., "Probing Ensemble Effects in Surface Reactions. 4. Cyclopentene Adsorption on Clean and Bismuth-Covered Pt(111)", J. Phys. Chem. **93**, 836−846 (1989).

Herz, R.K., Gillispie, W.D., Petersen, E.E. and Somorjai, G.A., "The Structure Sensitivity of Cyclohexane Dehydrogenation and Hydrogenolysis Catalyzed by Platinum Single Crystals at Atmospheric Pressure", J. Catal. **67**, 371−386 (1981).

Hettinger, W.P., Keith, C.D., Gring, J.L. and Teter, J.W., "Hydroforming Reactions–Effect of Certain Catalyst Properties and Poisons", Ind. Eng. Chem. **47**, 719–730 (1955).

Hill, Jr., C.J., "An Introduction to Chemical Engineering Kinetics & Reactor Design", John Wiley & Sons, New York, 1977.

Hirschfelder, J.O., Curtiss, C.F. and Bird, R.B., "Molecular Theory of Gases and Liquids, corrected printing with notes added, Wiley, New York, 1964.

Hoffmann, P., "Tomorrow's Energy: Hydrogen, Fuel Cells, and the Prospects for a Cleaner Planet", The MIT Press, Cambridge, 2001.

Honda, Available from: http://www.honda.co.uk/cars/jazz/#fullspecification [Accessed on July 10, 2010].

Horiuti, I. and Polanyi, M., "Exchange Reactions of Hydrogen on Metallic Catalysts", Trans. Faraday Soc. **30**, 1164–1172 (1934).

Hougen, O.A. and Watson, K.M., "Chemical Process Principles: Kinetics and Catalysis", John Wiley & Sons, Inc., 1943.

Hrein Energy, "Success of the World First Test Drive on a Bifuel Car That Runs on Bifuel Made of Gasoline and Hydrogen Based on Organic Hydrides", Available from: http://www.hrein.jp/english/pressrelease/release.070830.htm [Accessed on April 18, 2008].

Hsiung, S. "Hydrogen Fuel Cell Engines and Related Technologies", Federal Transit Administration, U.S. Department of Transportation, FTA-CA-26-7022-01.1, College of the Desert, Palm Desert, 2001.

Itoh, N., Shindo, Y., Haraya, K. and Hakuta, T., "A Membrane Reactor using Microporous Glass for Shifting Equilibrium of Cyclohexane Dehydrogenation", J. Chem. Eng. Japan **21**, 399–404 (1988).

Johnson, M.M. and Hepp, H.J., "Kinetics of the Demethylation of Methylcyclohexane", Adv. Chem. **97**, 179–192 (1970).

Jossens, L.W. and Petersen, E.E., "A Novel Reactor System That Permits the Direct Determination of Deactivation Kinetics for a Heterogeneous Catalyst", J. Catal. **73**, 366–376 (1982a).

Jossens, L.W. and Petersen, E.E., "Fouling of a Platinum Reforming Catalyst Accompanying the Dehydrogenation of Methyl Cyclohexane", J. Catal. **73**, 377−386 (1982b).

Jossens, L.W. and Petersen, E.E., "Fouling of a Platinum-Rhenium Reforming Catalyst Using Model Reforming Reactions", J. Catal. **76**, 265−273 (1982c).

Jothimurugesan, K., Bhatia, S. and Srivastava, R.D., "Kinetics of Dehydrogenation of Methylcyclohexane over a Platinum-Rhenium-Aluminium Catalyst in the Presence of Added Hydrogen", Ind. Eng. Chem. Fundam. **24**, 433−438 (1985a).

Jothimurugesan, K., Nayak, A.K., Mehta, G.K., Rai, K.N., Bhatia, S. and Srivastava, R.D., "Role of Rhenium in Pt-Re-Al$_2$O$_3$ Reforming Catalysis: An Integrated Study" AIChE J. **13**, 1997−2007 (1985b).

Keith, D.W. and Farrell, A.E., "Rethinking Hydrogen Cars", Science **301**, 315−316 (2003).

Kern, D.Q., "Process Heat Transfer", McGraw-Hill Book Co., Hamburg, 1950.

Kestler, H. and Clemens, H., "Production, Processing and Applications of γ(TiAl)-Based Alloys", In: Leyens, C. and Peters, M., "Titanium and Titanium Alloys: Fundamentals and Applications", Wiley-VCH, 2003.

Keulemans, A.I.M. and Voge, H.H., "Reactivities of Naphthenes over a Platinum Reforming Catalyst by a Gas Chromatographic Technique", J. Phys. Chem. **63**, 476−480 (1959).

Kittrell, J.R., "Mathematical Modeling of Chemical Reactions", Adv. Chem. Eng. **8**, 97−183 (1970).

Klaus, R., "A Computer-Based Methodology for Regression and Experimental Design with Nonlinear Algebraic and Ordinary Differential Equation Multi-Response Models", Ph.D. Thesis, No. 6866, ETH Zürich, 1981a.

Klaus, R., "User Manual for the Multipurpose Regression Program: RKPES", Technisch-Chemisches Laboratorium, ETH-Zentrum, 1981b.

Kluksdahl, H.E., "Reforming a Sulfur-Free Naphtha with a Platinum-Rhenium Catalyst", US Patent 3415737, 1968.

Klvana, D., Touzani, A., Chaouki, J. and Bélanger, G., "Dehydrogenation of Methylcyclohexane in a Reactor Coupled to a Hydrogen Engine, Int. J. Hydrogen Energy **16**, 55−60 (1991).

Kraft, M. and Spindler, H., Proc., 4th Int. Congr. Catal., Moscow (1968).

Kulkarni, B.D. and Doraisway, L.K., "Estimation of Effective Transport Properties in Packed Bed Reactors", Catal. Rev. Sci. Eng. **22**, 431−483 (1980).

Kunii, D. and Smith, J.M., "Heat Transfer Characteristics of Porous Rocks", AIChE J. **6**, 71−78 (1960).

Lander, H.R. Jr., "A Kinetic Study of the Catalytic Dehydrogenation of Methylcyclohexane at 600, 650, and 700 °F and a Pressure of 5 Atmospheres", Air Force Aero Propulsion Lab Wright-Patterson AFB Ohio, AD0715926, 1970.

Levenspiel, O., "Chemical Reaction Engineering", 3rd ed., John Wiley & Sons, New York, 1999.

Li, C-H. and Finlayson, B.A., "Heat Transfer in Packed Beds: A Reevaluation", Chem. Eng. Sci. **32**, 1055−1066 (1977).

Lide, D.R., "CRC Handbook of Chemistry and Physics", 87th ed., CRC Press, Boca Raton, 2007.

Maatman, R.W. and Prater, C.D., "Adsorption and Exclusion in Impregnation of Porous Catalytic Supports", Ind. Eng. Chem. **49**, 253−257 (1957).

Maatman, R.W., "How to Make a More Effective Platinum-Alumina Catalyst", Ind. Eng. Chem. **51**, 913−914 (1959).

Maatman, R.W., Mahaffy, P., Hoekstra, P. and Addink, C., "The Preparation of Pt-Alumnina Catalyst and Its Role in Cyclohexane Dehydrogenation", J. Catal. **23**, 105−117 (1971).

Mang, T., Breitscheidel, B. Polanek, P. and Knözinger, H., "Adsorption of Platinum Complexes on Silica and Alumina: Preparation of Non-Uniform Metal Distributions within Support Pellets", Appl. Catal. A: Gen. **106**, 239−258 (1993).

Manser Sonderer, R.H., "Methylcyclohexane Dehydrogenation Kinetics, Reactor Design and Simulation for a Hydrogen Powered Vehicle", Ph.D. Thesis, ETH No. 9996, Swiss Federal Institute of Technology, Zürich, 1992.

Maria, G., Marin, A., Wyss, C., Müller, S. and Newson, E., "Modelling and Scalup of the Kinetics with Deactivation of Methylcyclohexane Dehydrogenation for Hydrogen Energy Storage", Chem. Eng. Sci. **51**, 2891−2896 (1996).

Materials: The A to Z of Materials, "Stainless Steel — Grade 316 — Properties, Fabrication and Applications", Available form: http://www.azom.com/details.asp?ArticleID=863 [Accessed on August 08, 2010]

Melanson, M.M. and Dixon, A.G., "Solid Conduction in Low d_t/d_p Beds of Spheres, Pellets and Rings", Int. J. Heat Mass Transfer **28**, 383−394 (1985).

Menon, P.G. and Prasad, J., Proc. 6th Int. Congr. Catal. **2**, 1061 (1977).

Missen, R.W., Mims, C.A. and Saville, B.A., "Introduction to Chemical Reaction Engineering and Kinetics, John Wiley & Sons, Inc., New York, 1999.

Mitrofanova, A.M., Boronin, V.S. and Poltorak, O.M., Vestn. Mosk. Univ. **5**, 14 (1966).

Moiseyev, V.N., "Titanium Alloys: Russian Aircraft and Aerospace Applications", Taylor & Francis, New York, 2006.

Müller, S., "Heterogenisierte platin-(0)-cluster als dehydrierungskatalysatoren" Ph.D. Thesis, ETH No. 11160, Eidgenössischen Technischen Hochschule, Zürich, 1995.

Myers, C.G., Lang, W.H. and Weisz, P.B., "Aging of Platinum Reforming Catalysts", Ind. Eng. Chem. **53**, 299−302 (1961).

Neufeld, P.D., Janzen, A.R. and Aziz, R.A., "Empirical Equations to Calculate 16 of the Transport Collision Integrals $\Omega^{(l,\,s)*}$ for the Lennard-Jones (12-6) Potentials", J. Chem. Phys. **57**, 1100−1102 (1972).

Newson, E., Haueter, TH., Von Roth, P.H.F., Scherer, G.W.H. and Schucan, TH.H., "Seasonal Storage of Hydrogen in Stationary Systems with Liquid Organic Hydrides", Int. J. Hydrogen Energy **23**, 905−909 (1998).

NIOSH (National Institute of Occupational Safety and Health), NIOSH "Pocket Guide to Chemical Hazards", Available from: http://www.cdc.gov/niosh/npg/default.html, [Accessed on December 30, 2009].

Nixon, A.C., Ackerman, G.H., Faith, L.E., Hawthorn, H.W., Henderson, H.T., Ritchie, A.W. and Ryland, L.B., "Vaporizing and Endothermic Fuels for Advanced Engine Application", Shell Development Company, AFAPL-TR-67-114, Part I, 1967.

Nixon, A.C., Ackerman, G.H., Faith, L.E., Henderson, H.T., Ritchie, A.W., Ryland, L.B. and Shryn, T.M., "Vaporizing and Endothermic Fuels for Advanced Engine Application", Shell Development Company, AFAPL-TR-67-114, Part III, 1970.

Nixon, A.C., Ackerman, G.H., Faith, L.E., Henderson, H.T., Ritchie, A.W. and Ryland, L.B., "Vaporizing and Endothermic Fuels for Advanced Engine Application", Shell Development Company, AFAPL-TR-67-114, Part II, 1968.

Ofuchi, K. and Kunii, D., "Heat-Transfer Characteristics of Packed Beds with Stagnant Fluids", Int. J. Heat Mass Transfer **8**, 749–757 (1965).

Okada, Y., Sasaki, E., Watanabe, E., Hyodo, S. and Nishijima, H., "Development of Dehydrogenation Catalyst for Hydrogen Generation in Organic Chemical Hydride Method", Int. J. Hydrogen Energy **31**, 1348–1356 (2006).

Olsbye, U., Wendelbo, R. and Akporiaye, D., "Study of Pt/Alumina Catalysts Preparation", Appl. Catal. A: Gen. **152**, 127–141 (1997).

Pacheco, M.A. and Petersen, E.E., "On a General Correlation for Catalyst Fouling", J. Catal. **86**, 75–83 (1984).

Pacheco, M.A. and Petersen, E.E., "Reaction Kinetics of Methylcyclohexane Dehydrogenation over a Sulfided Pt + Re/Al$_2$O$_3$ Reforming Catalyst," J. Catal. **96**, 507–516 (1985).

Pal, A.K., Bhowmick, M. and Srivastava, R.D., "Deactivation Kinetics of Platinum-Rhenium Re-forming Catalyst Accompanying the Dehydrogenation of Methylcyclohexane", Ind. Eng. Chem. Process Des. Dev. **25**, 236–241 (1986).

Pant, K.K. and Gupta, R.B., "Fundamentals and Use of Hydrogen as a Fuel", In: Gupta, R.B. (Ed.) "Hydrogen Fuel Production, Transport, and Storage", CRC Press, Boca Raton, 2009.

Parker, D.H., Pettiette-Hall, C.L., Li, Y., McIver, Jr., R.T., Hemminger, J.C., "Kinetic Study of the Initial Stages of Dehydrogenation of Cyclohexane on the Pt(111) Surface", J. Phys. Chem. **96**, 1888–1894 (1992).

Pettiette-Hall, C.L., Land, D.P., McIver, R.T. and Hemminger, J.C., "Identification of Multiple Steps in the Dehydrogenation of Cyclic C$_6$ Hydrocarbons to Benzene on Pt(111)", J. Am. Chem. Soc. **113**, 2755–2756 (1991).

Pereira Daurte, S.I., Barreto, G.F. and Lemcoff, N.O., "Comparison of Two-Dimensional Models for Fixed Bed Catalytic Reactors", Chem. Eng. Sci. **39**, 1017−1024 (1984).

Pinna, F., "Supported Metal Catalysts Preparation", Catal. Today **41**, 129−137 (1998).

Poling, B.E., Prausnitz, J.M. and O´Connell, J.P., "The Properties of Gases and Liquids", 5th ed., McGraw-Hill, New York, 2001.

Pulkrabek, W.W., "Engineering Fundamentals of the Internal Combustion Engines", Prentice Hall, Upper Saddle River, 1997.

Ragwitz, M., Wietschel, M., Hasenauer, U. and Fakolade, O., "Introduction of Alternative Transport Fuels in the European Energy Market: Techno-Economic Barriers and Perspectives", Karlsruhe: Fraunhofer Institute Systemtechnik und Innovationsforschung, 2003.

Rase, H.F., "Chemical Reactor Design for Process Plants", Vol. 1, John Wiley & Sons, Inc., New York, 1977.

Rase, H.F., "Fixed Bed Reactor Design and Diagnostics: Gas-Phase Reactions", Butterworths, Boston, 1990.

Richardson, J.T., "Principles of Catalyst Development", Plenum Press, New York, 1989.

Rimensberger, T.K., "Kinetische Untersuchungen der dehydrierung von methylcyclohexan zu toluol im mikropulsreaktor, im kontinuierlichen mikroreaktor und im laborfestbettreaktor", Ph.D. Thesis, No. 8278, Swiss Federal Institute of technology, Zürich, 1987.

Ritchie, A.W. and Nixon, A.C., "Dehydrogenation of Methylcyclohexane over a Platinum-Alumina Catalyst in Absence of Added Hydrogen", Ind. Eng. Chem. Prod. Res. Dev. **5**, 59−64 (1966).

Ritchie, A.W., Hawthorn, R.D. and Nixon, A.C., "Dehydrogenation of Hydrocarbons over a Chromia-Alumina Catalyst in the Absence of Added Hydrogen", Ind. Eng. Chem. Prod. Res. Dev. **4**, 129−136 (1965).

Rodriguez, J.A. and Campbell, C.T., "Probing Ensemble Effects in Surface Reactions. 3. Cyclohexane Adsorption on Clean and Bismuth-Covered Pt(111)", J. Phys. Chem. **93**, 826−835 (1989).

Rohrer, J.C. and Sinfelt, J.H., "Interaction of Hydrocarbons with Pt-Al$_2$O$_3$ in the Presence of Hydrogen and Helium", J. Phys. Chem. **66**, 1193−1194 (1962).

Sadeghbeigi, R., "Fluid Catalytic Cracking Handbook: Design, Operation, and Troubleshooting of FCC Facilities", 2nd ed., Gulf Professional Publishing, 2000.

Saeys, M., Reyniers, M.-F., Neurock, M. and Marin, G.B., "An Initio Reaction Path Analayis of Benzene Hydrogenation to Cyclohexane on Pt(111)", J. Phys. Chem. B **109**, 2064−2073 (2005a).

Saeys, M., Reyniers, M.-F., Thybaut, J.W., Neurock, M. and Marin, G.B., "First-Principles Based Kinetic Model for the Hydrogenation of Toluene", J. Catal. **236**, 129−138 (2005b).

Satterfield, C.N., "Mass Transfer in Heterogeneous Catalysis", MIT Press, Cambridge, 1970.

Scherer, G.W.H., "Systems and Economic Analysis of the Seasonal Storage of Electricity with Liquid Organic Hydrides", Ph.D. Thesis, ETH No. 12440, Swiss Federal Institute of Technology, Zürich, 1997.

Schildhauer, T.H., Newson, E., Müller, S., "The Equilibrium Constant for Methylcyclohexane-Toluene System", J. Catal. **198**, 355−358 (2001).

Schildhauer, T.H., "Untercuchungen zur Verbesserung des Wärmeübergangs in Katalytischen Festbettreaktoren für Energiespeicheranwendungen", Ph.D. Thesis, ETH No. 14301, Eidgenössischen Technischen Hochschule, Zürich, 2001.

Schlapbach, L. and Züttel, A., "Hydrogen-Storage Materials for Mobile Applications", Nature **414**, 353−358 (2001).

Schutz, R.W., "Stress-Corrosion Cracking of Titanium Alloys", In: Jones, R.H. (Ed.), "Stress-Corrosion Cracking: Materials Performance and Evaluations", ASM International, 1992.

Sehr, R.A., "The Thermal Conductivity of Catalyst Particles", Chem. Eng. Sci. **9**, 145−152 (1958).

Serth, R.W., "Process Heat Transfer: Principles and Applications", Academic Press, 2007.

Sherif, S.A., Barbir, F. and Veziroglu, T.N., "Towards a Hydrogen Economy", Electr. J. **18**, 62−76 (2005).

Shinnar R., "The Hydrogen Economy, Fuel Cells and Electric Cars", Technol. Soc. **25**, 455–476 (2003).

Shyr, Y.-S. and Ernst, W.R., "Preparation of Nonuniformly Active Catalysts", J. Catal. **63**, 425–432 (1980).

Silobreaker, "Hrein Energy Test Drives 1.2 L Vehicle with Retrofitted Organic Hydride System", Available from: http://www.silobreaker.com/Document-Reader.aspx?Item=5_829644044 [Accessed on April 18, 2008].

Sinfelt, J.H., "The Turnover Fequency of Methylcyclohexane Dehydrogenation to Toluene on a Pt Reforming Catalyst", J. Mol. Catal. A: Chem. **163**, 123–128 (2000).

Sinfelt, J.H., Hurwitz, H. and Shulman, R.A., "Kinetics of Methylcyclohexane over Pt-Al_2O_3", J. Phys. Chem. **64**, 1559–1562 (1960).

Sinfelt, J.H. and Rohrer, J.C., "Kinetics of the Catalytic Isomerization-Dehydroisomerization of Methylcyclopentane", J. Phys. Chem. **65**, 978–981 (1961).

Smith, C.E., Biberian, J.P. and Somorjai, G.A., "The Effect of Strogly Bound Oxygen on the Dehydrogenation and Hydrogenation Activity and Selectivity of Platinum Single Crystal Surfaces", J. Catal. **57**, 426–443 (1979).

Smith, J.M., "Chemical Engineering Kinetics", 3rd ed., McGraw-Hill Int. Book Co., Singapore, 1981.

Sonntag, D., Jederberg, W., LeMasters, G., Reutman, S. and Still, K., "Military Personnel" In: Greenberg, M.I., Hamilton, R.J., Phillips, S.D. and McCluskey, G.J. (Eds.), "Occupational, Industrial, and Environmental Toxicology", 2nd ed., Mosby, 2003.

Specchia, V., Baldi, G. and Sicardi, S., "Heat Transfer in Packed Bed Reactors with One Phase flow", Chem. Eng. Commun. **4**, 361–380 (1980).

Steinfeld, A. and Meier, A., "Solar Fuels and Materials", In: Cleveland, C.J. (Ed.), "Encyclopaedia of Energy", Elsevier, Inc., 2004.

Sterba, M.J. and Haensel, V., "Catalytic Reforming", Ind. Eng. Chem. Prod. Res. Dev. **15**, 2–17 (1976).

Sultan, O. and Shaw, M., "Study of Automotive Storage of Hydrogen Using Recyclable Chemical Carriers," TEC-75/003, ERDA. Ann Arbor, MI, 1975.

Tages-Anzeiger, "Umweltfreundlicher Antrieb für Lastwagen und Busse" Technik, May, 1984.

Taube, M. and Taube, P., "A Liquid Organic Carrier of Hydrogen as Fuel for Automobiles", Proc. 3rd World Hydrogen Energy Conf., Tokyo (1980).

Taube, M. Rippin, D.W.T., Cresswell, D.L. and Knecht, W., "A System of Hydrogen-Powered Vehicles with Liquid Organic Hydrides", Int. J. Hydrogen Energy **8**, 213−225 (1983).

Taube, M., Rippin, D.W.T., Knecht, W., Hakimifard, D., Milisavljevic, B. and Grünenfelder, N., "A Prototype Truck Powered by Hydrogen from Organic Liquid Hydrides", Int. J. Hydrogen Energy **10**, 595−599 (1985).

Tech-On, "Organic Hydrides Improve Gasoline Efficiency", Available form: http://techon.nikkeibp.co.jp/english/NEWS_EN/20080228/148164/ [Accessed on April 18, 2008].

Touzani, A., Klvana, D. and Bélanger, G., "A Mathematical Model for the Dehydrogenation of Methylcyclohexane in a Packed Bed Reactor", Can. J. Chem. Eng. **65**, 56−63 (1987).

Touzani, A., Klvana, D. and Bélanger, G., "Dehydrogenation of Methylcyclohexane on the Industrial Catalyst: Kinetic Study", Stud. Surf. Sci. Catal. **19**, 357−364 (1984).

Towler, G. and Sinnot, R., "Chemical Engineering Design: Principles, Practice and Economics of Plant and Process Design", Butterworth-Heinemann, 2008.

Trapnell, B.M.W., "Balandin's Contribution to Heterogeneous Catalysis" Adv. Catal. **3**, 1−25 (1951).

Tsakiris, D.E. "Catalytic Production of Hydrogen from Liquid Organic Hydride", Ph.D. Thesis, The University of Manchester, Manchester, 2007.

Tschudin, S.D., "Wandreaktoren für die Katalytische Dehydrierung von Methylcyclohexan Kinetik und Charakterisierung", Ph.D. Thesis ETH No. 12334, Eidgenössischen Technischen Hochschule, Zürich, 1997.

Tschudin, S.D., Shido, T., Prins, R. and Wokaun, A., "Characterisation of Catalysts Used in Wall Reactors for the Catalytic Dehydrogenation of Methylcyclohexane", J. Catal. **181**, 113−123 (1999).

Tsuji, T., Shinya, Y., Hiaki, T. and Itoh, N., "Hydrogen Solubility in a Chemical Hydrogen Storage Medium, Aromatic Hydrocarbon, Cyclic Hydrocarbon, and Their Mixture for Fuel Cell Systems", Fluid Phase Equilib. **228–229**, 499–503 (2005).

Turner, J., "Sustainable Hydrogen Production", Science **305**, 972–976 (2004).

Van Trimpont, P.A., Marin, G.B. and Froment, G.F., "Activities and Selectivities for Reforming Reactions on Un-Sulfided and Sulfided Commercial Platinum and Platinum-Rhenium Catalysts", Appl. Catal. **17**, 161–173 (1985).

Van Trimpont, P.A., Marin, G.B. and Froment, G.F., "Kinetics of Methylcyclohexane Dehydrogenation on Sulfided Commercial Platinum/Alumina and Platinum-Rhenium/Alumina Catalysts", Ind. Eng. Chem. Fundam. **25**, 544–553 (1986).

Vulcan, Available form: http://www.vulcanfinnedtubes.com/Htm%20Documents/-AreaTable_Longitudinal.htm [Accesssed on 18-July-2010].

Walas, S.M., "Modeling with Differential Equations in Chemical Engineering", Butterworth-Heinemann, Boston, 1991.

Wald, M.L., "Questions about a Hydrogen Economy", Scientific American, May 2004, 68–73.

Weisz, P.B. and Hicks, J.S., "The Behaviour of Porous Catalyst Particles in View of Internal Mass and Heat Diffusion Effects", Chem. Eng. Sci. **17**, 265–275 (1962).

Wen, D. and Ding, Y., "Heat Transfer of Gas Flow through A Packed Bed", Chem. Eng. Sci. **61**, 3532–3542 (2006).

Wolf, E.E. and Petersen, E.E., "Kinetics of Deactivation of a Reforming Catalyst during Methylcyclohexane Dehydrogenation in a Diffusion Reactor", J. Catal. **46**, 190–203 (1977).

Xiaoyun, L., Ding, M. and Xinhe, B., "Dispersion of Pt Catalysts Supported on Activated Carbon and Their Catalytic Performance in Methylcyclohexane Dehydrogenation", Chin. J. Catal. **29**, 259–263 (2008).

Yagi S. and Kunii, D., "Studies on Heat Transfer in Packed Beds", Int. Dev. Heat Transfer, Part IV **750** (1962).

Yi, H.S., Min, K. and Kim, E.S., "The Optimisation Mixture Formation for Hydrogen Fuelled Engines", Int. J. Hydrogen Energy **25**, 685–690 (2000).

Yolcular, S, Olgun, Ö., "Hydrogen Storage in the Form of Methylcyclohexane", Energy Sources **30**, 149−156 (2008).

Zelinskii, N.D., Berchet **44**, 3121 (1911).

Zelinskii, N.D., Berchet **45**, 3678 (1912).
Zengel, A.E., "A Study of Methylcyclohexane Dehydrogenation over a Platinum-on-Alumina Catalyst at 602 °F", Air Force Aero Propulsion Lab Wright-Patterson AFB Ohio, AD0461076, 1968.

Zhou, L., "Progress and Problems in Hydrogen Storage Methods", Renew. Sustain. Energy Rev. **9**, 395−408 (2005).

Züttel, A., "Hydrogen Storage Methods", Naturwissenschaften **91**, 157−172 (2004).

Appendix A

Physical Properties of Methylcyclohexane (MCH), 1-Methylcyclohexene (1-MCHe), Toluene and Isooctane

Table A.1 Physical properties of methylcyclohexane, 1-methylcyclohexene, toluene and isooctane [Lide, 2007; Poling et al. 2001]

Physical properties	MCH	1-MCHe	Toluene	Isooctane	Units
Boiling point@1.013 bar	100.93	110.30	110.63	99.22	°C
Critical molar volume	369		316	468	cm^3/mol
Critical pressure	3.48		4.110	2.57	MPa
Critical temperature	572.1		591.80	543.8	K
Density	0.7694@20°C	0.8102@20°C	0.8668@20°C	0.6878@25°C	g/cm^3
Enthalpy of fusion	6.75		6.64	9.20	kJ/mol
Enthalpy of vaporisation	31.27@100.93°C 35.36@25°C		33.18@110.63 °C 38.01@25°C	30.79@99.22°C 35.14@25°C	kJ/mol
Flammability limits	1.2–6.7		1.1–7.1		%
Flash point	−4		4.0	−12.0	°C
Ignition temperature	250		480	418	°C
Isothermal compressibility			8.96×10^{-4}@20°C		MPa^{-1}
Melting point	−126.6	−120.4	−94.95	−107.3	°C
Molecular weight	98.19	96.17	92.14	114.23	g/mol
Physical state at room conditions	Liquid	Liquid	Liquid	Liquid	—
Refractive index	1.4231@20°C	1.4503@20°C	1.4961@20°C	1.3884@25°C	—
Solubility	i H$_2$O	i H$_2$O	i H$_2$O	i H$_2$O	—
Standard enthalpy of formation (gas)	−154.7		50.5	−224.0	kJ/mol
Standard heat of combustion (NCV)	−4292.5		−3772.0	−5100.4	kJ/mol
Standard sp. heat capacity (Liquid)	184.8		157.3	239.1	J·mol^{-1}·K^{-1}
Surface tension	23.29@25°C		27.73@25°C		mN/m
Thermal conductivity			0.1310@25°C 0.1095@100°C	0.0948@25°C 0.077@100°C	W·m^{-1}·K^{-1}
Thermal expansion (cubic) coefficient			1.05×10^{-3}@20°C		°C^{-1}
Threshold limit value	400		50	300	ppm
Viscosity	0.679@25°C		0.560@25°C		mPa·s

Appendix B

Introduction to RKPES Code and a Simple Illustration

B.1 Introduction to RKPES code

RKPES is a high quality, user friendly code generated in FORTRAN-IV by Technisch-Chemisches Laboratorium E.T.H. Zentrum, Zürich, Switzerland. It can solve a variety of problems with a wide range of experimental data and mathematical models. Based on the modified Marquardt algorithm, the program performs the non-linear regression of the data and the minimisation of the sum of squares of the errors (SSE) is exploited to estimate the regression parameters and to calculate the model values. It provides statistical information on the parameters, such as parameter t-values, 95% confidence limits, standard deviations and correlation matrix. Moreover, an overall sum of square of the errors (SSE) and a residual plot is also shown to observe the goodness of the fit. The user of the program needs only to input the required numerical data and a simple model description in FORTRAN format.

The program may be switched to the following main options:

1-   Explicit algebraic equation model
2-   Explicit ordinary differential equation model-initial value problem
3-   Explicit ordinary differential equation model-boundary value problem
4-   Systems of ordinary differential equations model

The program utilises a 4th order Runge-Kutta routine to solve the ordinary differential equation [Manser Sondrer, 1992].

Rigorous details of the RKPES code may be found in Klaus [1981a, 1981b].

B.2 Illustration

B.2.1 Kinetic model in FORTRAN format — the mthdmodel.f file

For illustration purpose, the kinetic equation for the power law model is
shown below in the FORTRAN format as it is used with RKPES.

```
        SUBROUTINE DMODEL(T,X,Y,PAR,DY)
                implicit real*8 (a-h,o-z)
        DOUBLE PRECISION X(7),Y(2),PAR(4),DY(2),MCH,N2
        DEN=1.0d0+3.0d0*X(1)*Y(1)
        MCH=X(1)*(1.d0-Y(1))/DEN
        TOL=(X(2)+X(1)*Y(1))/DEN
        H2=(X(3)+3.0d0*X(1)*Y(1))/DEN
        N2=X(4)/DEN
        PMCH=MCH*X(5)
        PTOL=TOL*X(5)
        PH2=H2*X(5)
        PN2=N2*X(5)
        TR=617.2
        RK=PAR(1)*EXP(PAR(2)*(1.0d0-TR/X(6)))
        RKE=3.6d3*EXP(-2.6178d4*(1.0d0/X(6)-1.0d0/650.0))
c       A=1.0d0-PTOL*PH2*PH2*PH2/(RKE*PMCH)
        APMCH=PMCH-PTOL*PH2*PH2*PH2/RKE
        if (APMCH) 10,20,30
10      DY(1)=RK*((-APMCH)**PAR(3))*(1.0d0-PAR(4)*X(7))
        go to 40
20      DY(1)=0.d0
        go to 40
30      DY(1)=RK*((APMCH)**PAR(3))*(1.0d0-PAR(4)*X(7))
40      DY(2)=1.0d0
        RETURN
        END
```

B.2.2 Data file in FORTRAN format — the mthdat11.in file

A data file has to be prepared separately and is used with the RKPES software.
The format of a part of the data file for Group-11 (Chapter 4) is shown below.

```
MCH DATA FOR GROUP 1 AT 1 BAR
7
4       4       2       1       1       0
2       1
2       1       0.005   0.001   1.d-07
1
1       0
```

```
100
10.40   0.0001  0.001
0.0d0   1.0d2
10.63   0.0001  0.001
0.0d0   2.0d1
0.993   0.0001  0.001
0.0d0   2.0d0
1.348   0.0001  0.001
0.0d0   1.0d1
1
0.106   0.0     0.893   0.00    1.0     594.8   0.104
0       1.244d0 0.899
1
0.106   0.0     0.893   0.00    1.0     594.9   0.125
0       1.244d0 0.940
1
0.106   0.0     0.893   0.00    1.0     587.2   0.042
0       0.622d0 0.674
1
0.106   0.0     0.893   0.00    1.0     587.6   0.063
0       0.622d0 0.691
1
0.106   0.0     0.893   0.00    1.0     584.4   0.167
0       0.311d0 0.413
.

.

.
```

B.2.3   Results of the execution — FORT.3 and FORT.4 files

At the end of the execution, the program generates two files namely FORT.3 and FORT.4, the contents of which can be exported to a Microsoft® Excel worksheet. The former contains the best-fit values of the parameters of the model, the sum of squares of the errors, the standard deviations of the parameters, the parameter t-values and 95% confidence limits of each parameter. Moreover, it contains the correlation matrix of the parameters and the plot of residuals (the difference between the observed and actual values of the dependent variables). The latter file contains the values of both observed and model predictions of the dependent variables.

Appendix C
Statistical Equations

C.1 The Sum of squares of the errors (SSE)

$$SSE = \sum_{i=1}^{i=N} (X_{obs,i} - X_{mod,i})^2 \qquad \text{(C.1)}$$

where,

N = number of data points

$X_{obs,i}$ = observed fractional conversion

$X_{mod,i}$ = model fractional conversion

$i = ith$ value

C.2 R²

$$R^2 = 1 - \frac{SSE}{SSM} \qquad \text{(C.2)}$$

where, SSM is the sum of squares of the deviations about the mean value and it is defined as

$$SSM = \sum_{i=1}^{i=N} (X_{obs,i} - \overline{X})^2 \qquad \text{(C.3)}$$

where,

$$\overline{X} = \sum_{i=1}^{i=N} \frac{X_{obs,i}}{N} = \text{mean value of the data} \qquad \text{(C.4)}$$

C.3   Adj(R^2)

$$\text{Adj(R}^2) = 1 - \frac{\text{SSE} \cdot (N-1)}{\text{SSM} \cdot (N-m-1)} \qquad \text{(C.5)}$$

where,

m = no. of parameters

C.4   F-value

$$F = \frac{\text{MSR}}{\text{MSE}} \qquad \text{(C.6)}$$

where,

$$\text{MSR} = \frac{\text{SSM} - \text{SSE}}{m-1} \qquad \text{(C.7)}$$

and

$$\text{MSE} = \frac{\text{SSE}}{N-m} \qquad \text{(C.8)}$$

Appendix D

Detailed Results for the Individual Groups Subjected to Power Law Kinetics

Table D.1 Fitted parameters with power law at 1.013 bar

Group	Parameter	Value	Units	Standard deviation	95% confidence interval	
					Lower	Upper
	n	0.993	–	0.040	0.910	1.077
	B	10.63	–	0.744	9.056	12.19
	E	54.55	$kJ \cdot mol^{-1}$			
Group-11	$k_r \times 10^5$	38.40	$mol \cdot g\text{-}cat^{-1} \cdot s^{-1} \cdot bar^{-0.99}$	5.554	26.68	50.12
	$(-r_0) \times 10^5$	4.135	$mol \cdot g\text{-}cat^{-1} \cdot s^{-1}$			
	k_d	1.348	day^{-1}	0.160	1.009	1.686
				$R^2 = 0.993$;	SSE = 0.00519	
	n	0.783	–	0.003	0.777	0.7896
	B	11.46	–	0.969	9.420	13.51
	E	58.83	$(kJ \cdot mol^{-1})$			
Group-21	$k_r \times 10^5$	14.10	$mol \cdot g\text{-}cat^{-1} \cdot s^{-1} \cdot bar^{-0.78}$	1.029	11.93	16.28
	$(-r_0) \times 10^5$	8.001	$mol \cdot g\text{-}cat^{-1} \cdot s^{-1}$			
	k_d	1.679	day^{-1}	0.201	1.254	2.104
				$R^2 = 0.986$;	SSE = 0.00989	
	n	0.710	–	0.007	0.694	0.726
	B	10.63	–	0.855	8.825	12.43
	E	54.55	$(kJ \cdot mol^{-1})$			
Group-31	$k_r \times 10^5$	8.351	$mol \cdot g\text{-}cat^{-1} \cdot s^{-1} \cdot bar^{-0.71}$	0.305	7.707	8.994
	$(-r_0) \times 10^5$	8.292	$mol \cdot g\text{-}cat^{-1} \cdot s^{-1}$			
	k_d	1.751	day^{-1}	0.130	1.477	2.025
				$R^2 = 0.989$;	SSE = 0.00831	
	n	0.695	–	0.0433	0.6034	0.786
	B	10.40	–	0.7546	8.806	11.99
	E	53.37	$(kJ \cdot mol^{-1})$			
Group-41	$k_r \times 10^5$	6.759	$mol \cdot g\text{-}cat^{-1} \cdot s^{-1} \cdot bar^{-0.69}$	0.7387	5.200	8.317
	$(-r_0) \times 10^5$	4.089	$mol \cdot g\text{-}cat^{-1} \cdot s^{-1}$			
	k_d	1.674	day^{-1}	0.1516	1.354	1.994
				$R^2 = 0.993$;	SSE = 0.00648	

Table D.2 Fitted parameters with power law at 5 bar

Group	Parameter	Value	Units	Standard Deviation	95% Confidence Interval	
					Lower	Upper
Group-15	n	1.510	–	0.093	1.314	1.706
	B	27.02	–	1.795	23.23	30.81
	E	138.7	$(kJ \cdot mol^{-1})$			
	$k_r \times 10^5$	8.933	$mol \cdot g\text{-}cat^{-1} \cdot s^{-1} \cdot bar^{-1.51}$	1.554	5.654	12.21
	$(-r_0) \times 10^5$	0.3014	$mol \cdot g\text{-}cat^{-1} \cdot s^{-1}$			
	k_d	0.6871	day^{-1}	0.352	−0.056	1.43
				$R^2 = 0.994;$	SSE = 0.00545	
Group-25	n	1.206	–	0.080	1.037	1.376
	B	22.83	–	1.838	18.95	26.71
	E	117.2	$(kJ \cdot mol^{-1})$			
	$k_r \times 10^5$	1.810	$mol \cdot g\text{-}cat^{-1} \cdot s^{-1} \cdot bar^{-1.21}$	0.153	1.488	2.132
	$(-r_0) \times 10^5$	0.756	$mol \cdot g\text{-}cat^{-1} \cdot s^{-1}$			
	k_d	1.208	day^{-1}	0.318	0.537	1.878
				$R^2 = 0.971;$	SSE = 0.00682	
Group-45	n	0.979	–	0.039	0.896	1.062
	B	16.18	–	0.854	14.38	17.98
	E	83.03	$(kJ \cdot mol^{-1})$			
	$k_r \times 10^5$	2.585	$mol \cdot g\text{-}cat^{-1} \cdot s^{-1} \cdot bar^{-0.98}$	0.127	2.316	2.854
	$(-r_0) \times 10^5$	1.273	$mol \cdot g\text{-}cat^{-1} \cdot s^{-1}$			
	k_d	1.673	day^{-1}	0.140	1.378	1.968
				$R^2 = 0.997;$	SSE = 0.00247	

Table D.3 Fitted parameters with power law at 9 bar

Group	Parameter	Value	Units	Standard Deviation	95% Confidence Interval	
					Lower	Upper
Group-19	n	1.299	–	0.068	1.155	1.442
	B	18.26	–	1.301	15.51	21.00
	E	93.70	$(kJ \cdot mol^{-1})$			
	$k_r \times 10^5$	1.370	$mol \cdot g\text{-}cat^{-1} \cdot s^{-1} \cdot bar^{-1.30}$	0.108	1.143	1.597
	$(-r_0) \times 10^5$	0.076	$mol \cdot g\text{-}cat^{-1} \cdot s^{-1}$			
	k_d	0.806	day^{-1}	0.247	0.2849	1.326
				$R^2 = 0.996$;	SSE = 0.00213	
Group-29	n	1.285	–	0.067	1.143	1.428
	B	23.25	–	1.459	20.17	26.33
	E	119.3	$(kJ \cdot mol^{-1})$			
	$k_r \times 10^5$	0.383	$mol \cdot g\text{-}cat^{-1} \cdot s^{-1} \cdot bar^{-1.29}$	0.018	0.345	0.421
	$(-r_0) \times 10^5$	0.151	$mol \cdot g\text{-}cat^{-1} \cdot s^{-1}$			
	k_d	0.991	day^{-1}	0.271	0.420	1.562
				$R^2 = 0.996$;	SSE = 0.00255	
Group-49	n	1.200	–	0.067	1.059	1.342
	B	16.61	–	1.294	13.88	19.34
	E	85.24	$(kJ \cdot mol^{-1})$			
	$k_r \times 10^5$	0.898	$mol \cdot g\text{-}cat^{-1} \cdot s^{-1} \cdot bar^{-1.20}$	0.044	0.806	0.990
	$(-r_0) \times 10^5$	0.377	$mol \cdot g\text{-}cat^{-1} \cdot s^{-1}$			
	k_d	2.000	day^{-1}	0.221	1.533	2.467
				$R^2 = 0.918$;	SSE = 0.06634	

Appendix E

Derivation of the Kinetic Model Equation Based on Loss of the First Hydrogen (Step-II) in a Dual-Site Langmuir-Hinshelwood-Hougen-Watson (LHHW) Mechanism

E.1   LHHW kinetics dual-site reaction scheme

$$\text{MCH} + \text{s} \rightleftharpoons \text{MCH·s} \tag{E.I}$$

$$\text{MCH·s} + \text{s} \rightleftharpoons \text{MCHe·s} + \text{H}_2\text{·s} \tag{E.II}$$

$$\text{MCHe·s} + \text{s} \rightleftharpoons \text{MCHde·s} + \text{H}_2\text{·s} \tag{E.III}$$

$$\text{MCHde·s} + \text{s} \rightleftharpoons \text{Tol·s} + \text{H}_2\text{·s} \tag{E.IV}$$

$$\text{Tol·s} \rightleftharpoons \text{Tol} + \text{s} \tag{E.V}$$

$$\text{H}_2\text{·s} \rightleftharpoons \text{H}_2 + \text{s} \tag{E.VI}$$
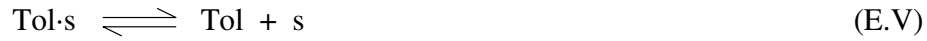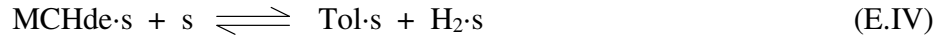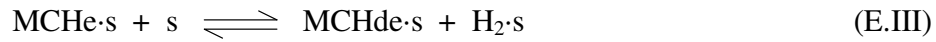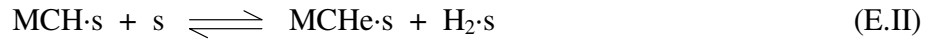
E.2   Derivation

In the following derivation, A, B, C, D and E represent methylcyclohexane (MCH), toluene (Tol), hydrogen (H_2), methylcyclohexene (MCHe) and methylcyclohexadiene (MCHde), respectively. "s" is an empty or available site, C_s is the concentration of the empty sites and $C_{i.s}$ is the concentration of the ith adsorbed species.

For step-E.I, we may write the rate equation as

$$(-r) = k_1 \left(p_A \cdot C_s - \frac{C_{A\cdot s}}{K_1} \right) \tag{E.1}$$

At equilibrium,

$$C_{A\cdot s} = K_1 \cdot p_A \cdot C_s \tag{E.2}$$

For step-E.II which is the rate-controlling step

$$(-r) = k_2 \cdot C_{A \cdot s} \cdot C_s - k_{-2} \cdot C_{D \cdot s} \cdot C_{C \cdot s} \quad \text{(rate-determining step)} \qquad \text{(E.3)}$$

For step-E.III at equilibrium

$$C_{D \cdot s} \cdot C_s = \frac{C_{E \cdot s} \cdot C_{C \cdot s}}{K_3}$$

$$K_3 = \frac{C_{E \cdot s} \cdot C_{C \cdot s}}{C_{D \cdot s} \cdot C_s} \qquad \text{(E.4)}$$

For step-E.IV at equilibrium

$$C_{E \cdot s} \cdot C_s = \frac{C_{B \cdot s} \cdot C_{C \cdot s}}{K_4}$$

$$K_4 = \frac{C_{B \cdot s} \cdot C_{C \cdot s}}{C_{E \cdot s} \cdot C_s} \qquad \text{(E.5)}$$

For step-E.V at equilibrium

$$C_{B \cdot s} = K_5 \cdot p_B \cdot C_s \qquad \text{(E.6)}$$

For step-E.VI at equilibrium

$$C_{C \cdot s} = K_6 \cdot p_C \cdot C_s \qquad \text{(E.7)}$$

From Eq. E.4 and Eq. E.5, respectively

$$C_{D \cdot s} = \frac{C_{E \cdot s} \cdot C_{C \cdot s}}{K_3 \cdot C_s} \tag{E.8}$$

$$C_{E \cdot s} = \frac{C_{B \cdot s} \cdot C_{C \cdot s}}{K_4 \cdot C_s} \tag{E.9}$$

Inserting Eq. E.9 into Eq. E.8, it may be written that

$$C_{D \cdot s} = \frac{\dfrac{C_{B \cdot s} \cdot C_{C \cdot s}}{K_4 \cdot C_s} \cdot C_{C \cdot s}}{K_3 \cdot C_s} \tag{E.10}$$

Using Eq. E.6 and Eq. E.7 in Eq. E.10, it may be shown that

$$C_{D \cdot s} = \frac{\dfrac{K_5 \cdot p_B \cdot C_s \cdot (K_6 \cdot p_C \cdot C_s)}{K_4 \cdot C_s} \cdot (K_6 \cdot p_C \cdot C_s)}{K_3 \cdot C_s}$$

$$C_{D \cdot s} = \frac{K_5 \cdot K_6^2 \cdot C_s \cdot p_B \cdot p_C^2}{K_4 \cdot K_3} \tag{E.11}$$

From Eq. E.9 upon substituting Eq. E.6 and Eq. E.7

$$C_{E \cdot s} = \frac{K_5 \cdot p_B \cdot C_s \cdot K_6 \cdot p_C}{K_4} \tag{E.12}$$

Substituting Eq. E.2 and Eq. E.11 in Eq. E.3, it may be shown that

$$(-r) = k_2 \cdot (K_1 \cdot p_A \cdot C_s) \cdot C_s - k_{-2} \cdot \left(\frac{K_5 \cdot K_6^2 \cdot C_s \cdot p_B \cdot p_C^2}{K_4 \cdot K_3} \right) \cdot (K_6 \cdot p_C \cdot C_s)$$

$$(-r) = k_2 \cdot K_1 \cdot p_A \cdot C_s^2 \left(1 - \frac{k_{-2} \cdot K_5 \cdot K_6^3 \cdot p_B \cdot p_C^3}{k_2 \cdot K_1 \cdot K_3 \cdot K_4 \cdot p_A} \right)$$

$$(-r) = k_2 \cdot K_1 \cdot p_A \cdot C_s^2 \left(1 - \frac{p_B \cdot p_C^3}{K \cdot p_A} \right) \tag{E.13}$$

where,

$$K = \frac{k_2 \cdot K_1 \cdot K_3 \cdot K_4}{k_{-2} \cdot K_5 \cdot K_6^3} \tag{E.14}$$

Total concentration of the sites is the sum of all covered sites and empty sites

$$C_T = C_s + C_{A \cdot s} + C_{B \cdot S} + C_{C \cdot s} + C_{D \cdot s} + C_{E \cdot s} \tag{E.15}$$

$$C_T = C_s + K_1 \cdot p_A \cdot C_s + K_5 \cdot p_B \cdot C_s + K_6 \cdot p_C \cdot C_s + \frac{K_5 \cdot K_6^2 \cdot C_s \cdot p_B \cdot p_C^2}{K_4 \cdot K_3}$$

$$+ \frac{K_5 \cdot p_B \cdot C_s \cdot K_6 \cdot p_C}{K_4}$$

$$C_T = C_s \left(1 + K_1 \cdot p_A + K_5 \cdot p_B + K_6 \cdot p_C + \frac{K_5 \cdot K_6^2 \cdot p_B \cdot p_C^2}{K_4 \cdot K_3} + \frac{K_5 \cdot p_B \cdot K_6 \cdot p_C}{K_4} \right)$$

$$C_T = C_s \left(1 + K_1 \cdot p_A + K_6 \cdot p_C + K_5 \cdot p_B + \frac{K_5 \cdot K_6^2 \cdot p_B \cdot p_C^2}{K_4 \cdot K_3} + \frac{K_5 \cdot p_B \cdot K_6 \cdot p_C}{K_4} \right)$$

Taking $K_5 \cdot p_B$ as common term from the last three terms, it may be written as

$$C_T = C_s \left(1 + K_1 \cdot p_A + K_6 \cdot p_C + K_5 \cdot p_B \left(1 + \frac{K_6^2 \cdot p_C^2}{K_4 \cdot K_3} + \frac{K_6 \cdot p_C}{K_4} \right) \right)$$

$$C_T = C_s \left(1 + K_1 \cdot p_A + K_6 \cdot p_C + K_5 \cdot p_B \left(1 + \frac{K_6 \cdot p_C}{K_4} \left(1 + \frac{K_6 \cdot p_C}{K_3} \right) \right) \right)$$

$$\frac{C_s}{C_T} = \left(1 + K_1 \cdot p_A + K_6 \cdot p_C + K_5 \cdot p_B \left(1 + \frac{K_6 \cdot p_C}{K_4} \left(1 + \frac{K_6 \cdot p_C}{K_3} \right) \right) \right)^{-1}$$

$$C_s = C_T \cdot \left(1 + K_1 \cdot p_A + K_6 \cdot p_C + K_5 \cdot p_B \left(1 + \frac{K_6 \cdot p_C}{K_4} \left(1 + \frac{K_6 \cdot p_C}{K_3} \right) \right) \right)^{-1} \qquad (E.16)$$

Using Eq. E.16 in Eq. E.13, it may be shown that

$$(-r) = \frac{k_2 \cdot K_1 \cdot p_A \cdot C_T^2 \cdot \left(1 - \dfrac{p_B \cdot p_C^3}{K \cdot p_A} \right)}{\left(1 + K_1 \cdot p_A + K_6 \cdot p_C + K_5 \cdot p_B \left(1 + \dfrac{K_6 \cdot p_C}{K_4} \left(1 + \dfrac{K_6 \cdot p_C}{K_3} \right) \right) \right)^2} \qquad (E.17)$$

Defining $k = k_2 \cdot C_T^2$ and representing K_1, K_5 and K_6 as K_A, K_B and K_C, respectively, Eq. E.16 may be written as

$$(-r) = \frac{k \cdot K_A \cdot p_A \cdot \left(1 - \dfrac{p_B \cdot p_C^3}{K \cdot p_A} \right)}{\left(1 + K_A \cdot p_A + K_6 \cdot p_C + K_B \cdot p_B \left(1 + \dfrac{K_C \cdot p_C}{K_4} \left(1 + \dfrac{K_C \cdot p_C}{K_3} \right) \right) \right)^2} \qquad (E.18)$$

Eq. E.18 is the required equation.

Appendix F

Kinetic Models for Adsorption of MCH Rate-Controlling Based on LHHW Dual-Site Surface Reaction Scheme (Scheme-I in Chapter 4)

Table F.1 List of kinetic models for adsorption of MCH rate-controlling based on LHHW dual-site surface reaction scheme (Scheme-I in Chapter 4)

$$(-r) = \frac{k \cdot \left(p_A - \dfrac{p_B \cdot p_C^3}{K} \right)}{1 + K_C \cdot p_C + K_B \cdot p_B + \dfrac{K_B \cdot K_C \cdot p_B \cdot p_C}{K_4} + \dfrac{K_B \cdot K_C^2 \cdot p_B \cdot p_C^2}{K_3 \cdot K_4} + \dfrac{K_B \cdot K_C^3 \cdot p_B \cdot p_C^3}{K_2 \cdot K_3 \cdot K_4}}$$

Model	Model equation	m	Parameters goodness	DOF(R^2)	SSE	F
DSI-1	$(-r) = \dfrac{k \cdot \left(p_A - \dfrac{p_B \cdot p_C^3}{K} \right)}{1 + K_C \cdot p_C}$	4	No parameter C.I. includes zero	0.581	4.83	98.48
DSI-2	$(-r) = \dfrac{k \cdot \left(p_A - \dfrac{p_B \cdot p_C^3}{K} \right)}{1 + K_B \cdot p_B}$	4	No parameter C.I. includes zero	0.818	2.10	315.7
DSI-3	$(-r) = \dfrac{k \cdot \left(p_A - \dfrac{p_B \cdot p_C^3}{K} \right)}{1 + K' \cdot p_B \cdot p_C}, K' = \dfrac{K_B \cdot K_C}{K_4}$	4	No parameter C.I. includes zero	0.908	1.06	690.4

DSI-4	$(-r) = \dfrac{k \cdot \left(p_A - \dfrac{p_B \cdot p_C^3}{K}\right)}{1 + K'' \cdot p_B \cdot p_C^2}, K'' = \dfrac{K_B \cdot K_C^2}{K_3 \cdot K_4}$	4	No parameter C.I. includes zero	0.874	1.45	486.8
DSI-5	$(-r) = \dfrac{k \cdot \left(p_A - \dfrac{p_B \cdot p_C^3}{K}\right)}{1 + K''' \cdot p_B \cdot p_C^3}, K''' = \dfrac{K_B \cdot K_C^3}{K_2 \cdot K_3 \cdot K_4}$	4	No parameter C.I. includes zero	0.833	1.93	349.8
DSI-3a	$(-r) = \dfrac{k \cdot \left(p_A - \dfrac{p_B \cdot p_C^3}{K}\right)}{1 + K' \cdot p_B \cdot p_C}, K' = f(T)$	5	C.I. of "B" includes zero	0.909	1.04	528.4
DSI-4a	$(-r) = \dfrac{k \cdot \left(p_A - \dfrac{p_B \cdot p_C^3}{K}\right)}{1 + K'' \cdot p_B \cdot p_C^2}, K'' = f(T)$	5	No parameter C.I. includes zero	0.886	1.30	411.0
DSI-5a	$(-r) = \dfrac{k \cdot \left(p_A - \dfrac{p_B \cdot p_C^3}{K}\right)}{1 + K''' \cdot p_B \cdot p_C^3}, K''' = f(T)$	5	No parameter C.I. includes zero	0.865	1.55	337.7
DSI-6	$(-r) = \dfrac{k \cdot \left(p_A - \dfrac{p_B \cdot p_C^3}{K}\right)}{1 + K_C \cdot p_C + K_B \cdot p_B}$	5	Three parameters C.I. includes zero	0.836	1.88	269.2
DSI-7	$(-r) = \dfrac{k \cdot \left(p_A - \dfrac{p_B \cdot p_C^3}{K}\right)}{1 + K_C \cdot p_C + K' \cdot p_B \cdot p_C}$	5	K_C goes negative			
DSI-8	$(-r) = \dfrac{k \cdot \left(p_A - \dfrac{p_B \cdot p_C^3}{K}\right)}{1 + K_C \cdot p_C + K'' \cdot p_B \cdot p_C^2}$	5	K_C goes negative			

Model	Equation		Comment			
DSI-9	$(-r) = \dfrac{k \cdot \left(p_A - \dfrac{p_B \cdot p_C^3}{K} \right)}{1 + K_C \cdot p_C + K''' \cdot p_B \cdot p_C^3}$	5	K_C goes negative			
DSI-10	$(-r) = \dfrac{k \cdot \left(p_A - \dfrac{p_B \cdot p_C^3}{K} \right)}{1 + K_B \cdot p_B + K' \cdot p_B \cdot p_C}$	5	No parameter C.I. includes zero	0.921	0.907	613.0
DSI-11	$(-r) = \dfrac{k \cdot \left(p_A - \dfrac{p_B \cdot p_C^3}{K} \right)}{1 + K_B \cdot p_B + K'' \cdot p_B \cdot p_C^2}$	5	No parameter C.I. includes zero	0.936	0.739	764.3
DSI-11a	$(-r) = \dfrac{k \cdot \left(p_A - \dfrac{p_B \cdot p_C^3}{K} \right)}{1 + K_B \cdot p_B + K'' \cdot p_B \cdot p_C^2} \, , \; K_B = f(T)$	6	No parameter C.I. include zero	0.944	0.642	706.4
DSI-11b	$(-r) = \dfrac{k \cdot \left(p_A - \dfrac{p_B \cdot p_C^3}{K} \right)}{1 + K_B \cdot p_B + K'' \cdot p_B \cdot p_C^2} \, , \; K_i = f(T)$	7	B_B goes negative	0.945	0.625	602.5
DSI-11c	$(-r) = \dfrac{k \cdot \left(p_A - \dfrac{p_B \cdot p_C^3}{K} \right)}{1 + K_B \cdot p_B + K'' \cdot p_B \cdot p_C^2} \, , \; K'' = f(T)$	6	No parameter C.I. includes zero	0.945	0.625	726.5
DSI-12	$(-r) = \dfrac{k \cdot \left(p_A - \dfrac{p_B \cdot p_C^3}{K} \right)}{1 + K_B \cdot p_B + K''' \cdot p_B \cdot p_C^3}$	5	No parameter C.I. includes zero	0.924	0.873	638.9
DSI-12a	$(-r) = \dfrac{k \cdot \left(p_A - \dfrac{p_B \cdot p_C^3}{K} \right)}{1 + K_B \cdot p_B + K''' \cdot p_B \cdot p_C^3} \, , \; K_B = f(T)$	6	No parameter C.I. includes zero	0.948	0.588	774.7

DSI-12b	$(-r) = \dfrac{k \cdot \left(p_A - \dfrac{p_B \cdot p_C^3}{K} \right)}{1 + K_B \cdot p_B + K''' \cdot p_B \cdot p_C^3}$, $K_i = f(T)$	7	One parameter C.I. includes zero	0.950	0.572	661.4
DSI-12c	$(-r) = \dfrac{k \cdot \left(p_A - \dfrac{p_B \cdot p_C^3}{K} \right)}{1 + K_B \cdot p_B + K''' \cdot p_B \cdot p_C^3}$, $K''' = f(T)$	6	No parameter C.I. includes zero	0.950	0.574	795.7
DSI-13	$(-r) = \dfrac{k \cdot \left(p_A - \dfrac{p_B \cdot p_C^3}{K} \right)}{1 + K' \cdot p_B \cdot p_C + K'' \cdot p_B \cdot p_C^2}$	5	K'' C.I. includes zero	0.908	1.06	519.1
DSI-14	$(-r) = \dfrac{k \cdot \left(p_A - \dfrac{p_B \cdot p_C^3}{K} \right)}{1 + K' \cdot p_B \cdot p_C + K''' \cdot p_B \cdot p_C^3}$	5	No parameter C.I. includes zero	0.910	1.03	532.3
DSI-15	$(-r) = \dfrac{k \cdot \left(p_A - \dfrac{p_B \cdot p_C^3}{K} \right)}{1 + K'' \cdot p_B \cdot p_C^2 + K''' \cdot p_B \cdot p_C^3}$	5	K''' goes negative			
DSI-16	$(-r) = \dfrac{k \cdot \left(p_A - \dfrac{p_B \cdot p_C^3}{K} \right)}{1 + K_C \cdot p_C + K_B \cdot p_B + K' \cdot p_B \cdot p_C}$	6	K_C goes negative			
DSI-17	$(-r) = \dfrac{k \cdot \left(p_A - \dfrac{p_B \cdot p_C^3}{K} \right)}{1 + K_C \cdot p_C + K_B \cdot p_B + K'' \cdot p_B \cdot p_C^2}$	6	K_C goes negative			
DSI-18	$(-r) = \dfrac{k \cdot \left(p_A - \dfrac{p_B \cdot p_C^3}{K} \right)}{1 + K_C \cdot p_C + K_B \cdot p_B + K''' \cdot p_B \cdot p_C^3}$	6	Four parameters C.I. includes zero	0.924	0.873	508.5

DSI-19	$(-r) = \dfrac{k \cdot \left(p_A - \dfrac{p_B \cdot p_C^3}{K} \right)}{1 + K_C \cdot p_C + K' \cdot p_B \cdot p_C + K'' \cdot p_B \cdot p_C^2}$	6	K_C goes negative			
DSI-20	$(-r) = \dfrac{k \cdot \left(p_A - \dfrac{p_B \cdot p_C^3}{K} \right)}{1 + K_C \cdot p_C + K' \cdot p_B \cdot p_C + K''' \cdot p_B \cdot p_C^3}$	6	K_C goes negative			
DSI-21	$(-r) = \dfrac{k \cdot \left(p_A - \dfrac{p_B \cdot p_C^3}{K} \right)}{1 + K_C \cdot p_C + K'' \cdot p_B \cdot p_C^2 + K''' \cdot p_B \cdot p_C^3}$	6	Two parameters go negative			
DSI-22	$(-r) = \dfrac{k \cdot \left(p_A - \dfrac{p_B \cdot p_C^3}{K} \right)}{1 + K_B \cdot p_B + K' \cdot p_B \cdot p_C + K'' \cdot p_B \cdot p_C^2}$	6	One parameter goes negative			
DSI-23	$(-r) = \dfrac{k \cdot \left(p_A - \dfrac{p_B \cdot p_C^3}{K} \right)}{1 + K_B \cdot p_B + K' \cdot p_B \cdot p_C + K''' \cdot p_B \cdot p_C^3}$	6	No parameter includes zero	0.932	0.782	572.9
DSI-23a	$(-r) = \dfrac{k \cdot \left(p_A - \dfrac{p_B \cdot p_C^3}{K} \right)}{1 + K_B \cdot p_B + K' \cdot p_B \cdot p_C + K''' \cdot p_B \cdot p_C^3} , \; K' = f(T)$	7	One parameter C.I. includes zero	0.932	0.773	481.2
DSI-24	$(-r) = \dfrac{k \cdot \left(p_A - \dfrac{p_B \cdot p_C^3}{K} \right)}{1 + K_B \cdot p_B + K'' \cdot p_B \cdot p_C^2 + K''' \cdot p_B \cdot p_C^3}$	6	One parameter goes negative			
DSI-25	$(-r) = \dfrac{k \cdot \left(p_A - \dfrac{p_B \cdot p_C^3}{K} \right)}{1 + K' \cdot p_B \cdot p_C + K'' \cdot p_B \cdot p_C^2 + K''' \cdot p_B \cdot p_C^3}$	6	One parameter goes negative			

DSI-26	$$(-r) = \frac{k \cdot \left(p_A - \dfrac{p_B \cdot p_C^3}{K} \right)}{1 + K_C \cdot p_C + K_B \cdot p_B + + K' \cdot p_B \cdot p_C + K'' \cdot p_B \cdot p_C^2}$$	7	Two parameters go negative
DSI-27	$$(-r) = \frac{k \cdot \left(p_A - \dfrac{p_B \cdot p_C^3}{K} \right)}{1 + K_C \cdot p_C + K_B \cdot p_B + K' \cdot p_B \cdot p_C + K''' \cdot p_B \cdot p_C^3}$$	7	One parameter goes negative
DSI-28	$$(-r) = \frac{k \cdot \left(p_A - \dfrac{p_B \cdot p_C^3}{K} \right)}{1 + K_C \cdot p_C + K_B \cdot p_B + K'' \cdot p_B \cdot p_C^2 + K''' \cdot p_B \cdot p_C^3}$$	7	Two parameters go negative
DSI-29	$$(-r) = \frac{k \cdot \left(p_A - \dfrac{p_B \cdot p_C^3}{K} \right)}{1 + K_C \cdot p_C + \dfrac{K_B \cdot K_C \cdot p_B \cdot p_C}{K_4} + K'' \cdot p_B \cdot p_C^2 + K''' \cdot p_B \cdot p_C^3}$$	7	Two parameters go negative
DSI-30	$$(-r) = \frac{k \cdot \left(p_A - \dfrac{p_B \cdot p_C^3}{K} \right)}{1 + K_B \cdot p_B + K' \cdot p_B \cdot p_C + K'' \cdot p_B \cdot p_C^2 + K''' \cdot p_B \cdot p_C^3}$$	7	Two parameters go negative
DSI-31	$$(-r) = \frac{k \cdot \left(p_A - \dfrac{p_B \cdot p_C^3}{K} \right)}{1 + K_C \cdot p_C + K_B \cdot p_B + K' \cdot p_B \cdot p_C + K'' \cdot p_B \cdot p_C^2 + K''' \cdot p_B \cdot p_C^3}$$	8	Three parameters go negative

Appendix G

Successful Kinetic Models after First Discrimination (Chapter 4)

Table G.1 List of successful kinetic models after first discrimination

Model	Model type	Mathematical form	m	DOF(R^2)	SSE	F
M-1	SS-II Loss of 1st H$_2$ Negligible coverage of MCHde	$$(-r) = \frac{k \cdot K_A \cdot \left(p_A - \dfrac{p_B \cdot p_C^3}{K} \right)}{\left(1 + K_A \cdot p_A + K_B \cdot p_B + K' \cdot p_B \cdot p_C^2 \right)}$$ $$K' = \frac{K_B}{K_3 \cdot K_4}$$	6	0.950	0.569	801.92
M-2	SS-II Loss of 2nd H$_2$ Negligible coverage of MCH and MCHde	$$(-r) = \frac{k \cdot K' \cdot \left(p_A - \dfrac{p_B \cdot p_C^3}{K} \right)}{\left(p_C + K' \cdot p_A + K_B \cdot p_B \cdot p_C \right)}$$ $$K' = K_A \cdot K_2$$	5	0.938	0.709	798.71
M-3	DS-I Adsorption of MCH Negligible coverage of MCH and MCHde	$$(-r) = \frac{k \cdot \left(p_A - \dfrac{p_B \cdot p_C^3}{K} \right)}{1 + K_B \cdot p_B + K'' \cdot p_B \cdot p_C^2}$$ $$K'' = \frac{K_B \cdot K_C^2}{K_3 \cdot K_4}$$	5	0.936	0.739	764.39

M-4	SS-II Loss of 1st H_2 Negligible coverage of Tol	$$(-r) = \frac{k \cdot K_A \cdot \left(p_A - \frac{p_B \cdot p_C^3}{K} \right)}{\left(1 + K_A \cdot p_A + K' \cdot p_B \cdot p_C^2 + K'' \cdot p_B \cdot p_C \right)}$$ $$K' = \frac{K_B}{K_3 \cdot K_4}$$ $$K'' = \frac{K_B}{K_4}$$	6	0.944	0.642	706.14
M-5	SS-II Loss of 1st H_2 Negligible coverage of MCHe	$$(-r) = \frac{k \cdot K_A \cdot \left(p_A - \frac{p_B \cdot p_C^3}{K} \right)}{\left(1 + K_A \cdot p_A + K_B \cdot p_B + K'' \cdot p_B \cdot p_C \right)}$$ $$K'' = \frac{K_B}{K_4}$$	6	0.941	0.670	675.34
M-6	SS-II Loss of 2nd H_2 Negligible coverage of MCH	$$(-r) = \frac{k \cdot K' \cdot \left(p_A - \frac{p_B \cdot p_C^3}{K} \right)}{\left(p_C + K' \cdot p_A + K_B \cdot p_B \cdot p_C + K'' \cdot p_B \cdot p_C^2 \right)}$$ $$K' = K_A \cdot K_2$$ $$K'' = \frac{K_B}{K_4}$$	6	0.939	0.696	648.91

M-7	SS-II Loss of 2nd H_2 Negligible coverage of MCHde	$(-r) = \dfrac{k \cdot K' \cdot \left(p_A - \dfrac{p_B \cdot p_C^3}{K} \right)}{\left(p_C + K_A \cdot p_A \cdot p_C + K' \cdot p_A + K_B \cdot p_B \cdot p_C \right)}$ $K' = K_A \cdot K_2$	6	0.939	0.696	648.81
M-8	DS-I Adsorption of MCH Negligible coverage of MCHe and MCHde	$(-r) = \dfrac{k \cdot \left(p_A - \dfrac{p_B \cdot p_C^3}{K} \right)}{1 + K_B \cdot p_B + K''' \cdot p_B \cdot p_C^3}$ $K''' = \dfrac{K_B \cdot K_C^3}{K_2 \cdot K_3 \cdot K_4}$	5	0.924	0.873	638.89
M-9	DS-I Adsorption of MCH Negligible coverage of MCH and MCHe	$(-r) = \dfrac{k \cdot \left(p_A - \dfrac{p_B \cdot p_C^3}{K} \right)}{1 + K_B \cdot p_B + K' \cdot p_B \cdot p_C}$ $K' = \dfrac{K_B \cdot K_C}{K_4}$	5	0.921	0.908	612.99

Appendix H
Calculations for Diffusion Limitations

The effectiveness factor η is defined as the ratio of the actual reaction rate to the reaction rate if there is no diffusion limitation (intrinsic reaction rate). An effectiveness factor close to unity ensures negligible diffusion limitations and the actual rate of the reaction is equal to the intrinsic reaction rate. The purpose of this Appendix is to calculate the effectiveness factor for the worst-case conditions (inlet reactor conditions, lowest flowrate, lowest pressure and highest wall temperature) under which the kinetic rate model (Chapter 4) is developed. This is to ensure the reaction rate is intrinsic and is not limited by pore diffusion.

H.1 Calculations for effectiveness factor η

The effectiveness factor is estimated from a relationship between η and a modified Thiele modulus Φ_s as shown in Fig. H.1.
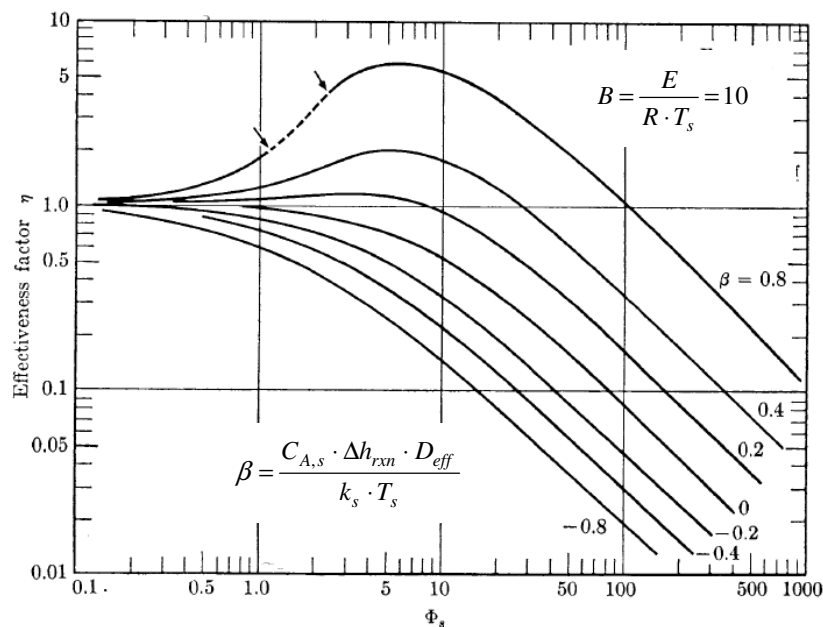

Fig. H.1 Relationship between effectiveness factor η and Φ_s. First order reactions in spheres. The Fig. was originally produced by Weisz and Hicks [1962]. *Source*: [Satterfield, 1970].

Fig. H.1 is applicable for a dimensionless activation energy B equal to 10. For other values of B, the reader may consult Weisz and Hicks [1962] or [Satterfield, 1970]. To use Fig. H.1 for the calculations of η, the values of Φ_s and β are, therefore, required.

H.1.1   Modified Thiele modulus Φ_s

Φ_s is calculated from Eq. H.1 [Satterfield, 1970]

$$\Phi_s = \frac{d_p^2}{4 \cdot D_{eff}} \cdot \left(-\frac{1}{V_c} \frac{dN_A}{dt} \right) \cdot \frac{1}{C_{A,s}} \qquad (H.1)$$

For initial conditions, the term in parentheses, $\left(-\dfrac{1}{V_c} \dfrac{dN_A}{dt} \right)$, in the above equation, may be written as a product of the initial rate of the dehydrogenation reaction and catalyst particle density as $(-r)_0 \cdot \rho_p$ and concentration of MCH at the catalyst surface $C_{A,s}$ as initial concentration of MCH C_{A0}. Therefore, Eq. H.1 may be re-written as Eq. H.2

$$\Phi_s = \frac{d_p^2 \cdot (-r)_0 \cdot \rho_p}{4 \cdot D_{eff} \cdot C_{A0}} \qquad (H.2)$$

In Eqs. H.1 and H.2, d_p is catalyst particle diameter, cm; D_{eff} is effective diffusivity defined in the following section, cm^2/s; V_c is volume of the catalyst, cm^3; N_A is number of moles of MCH, mol; t is time, s; $c_{A,s}$ and c_{A0} are in mol/cm^3; $(-r)_0$ is in mol·g-cat^{-1}·s^{-1} and ρ_p is in g/cm^3.

H.1.1.1 Effective diffusivity D_{eff}

Effective diffusivity is calculated from Eq. H.3 [Satterfield, 1970]

$$D_{eff} = \frac{D_{K,eff} \cdot D_{AC}}{D_{AC} + D_{K,eff}}, \text{cm}^2/\text{s} \qquad (\text{H.3})$$

where, $D_{K,eff}$ is the effective Knudsen diffusivity which may be estimated by Eq. H.4 [Satterfield, 1970] as shown below and D_{AC}, cm^2/s is the bulk molecular diffusivity of MCH in hydrogen and can be estimated as described in Chapter 6 (Eq. 6.29).

$$D_{K,eff} = 19400 \cdot \frac{\varepsilon_p^2}{\tau_m \cdot S_g \cdot \rho_p} \cdot \sqrt{\frac{T_0}{M_A}}, \text{cm}^2/\text{s} \qquad (\text{H.4})$$

where, ε_p is the particle voidage; τ_m is modified tortuosity factor; S_g is the surface area of the catalyst particles, cm^2/g; ρ_p is density of catalyst particle, g/cm^3; T_0 is the inlet absolute temperature, K and M_A is molecular weight of MCH, g/mol.

H.1.2 Heat generation function β

The heat generation function β is estimated by the following expression [Satterfield, 1970]

$$\beta = \frac{C_{A0} \cdot (-\Delta h_{rxn}) \cdot D_{eff}}{k_s \cdot T_0} \qquad (\text{H.5})$$

where, $(-\Delta h_{rxn})$ is the heat of the dehydrogenation reaction in J/mol and k_s is the thermal conductivity of the porous catalyst particle, W·m^{-1}·K^{-1}.

H.1.3 Dimensionless activation energy B

Dimensionless activation energy B is similar to Eq. 4.9 of Chapter 4 but defined at catalyst surface temperature T_0 (T_s) rather than at reference temperature T_r

$$B = \frac{E}{R \cdot T_0} \tag{H.6}$$

where, E is activation energy in J/mol and R is universal gas constant in $\text{J·mol}^{-1}\text{·K}^{-1}$.

H.1.4 Results and discussion

H.1.4.1 Laboratory reactor

Table H.1 shows the dehydrogenation reaction conditions and the results for the calculations of $D_{K,eff}$, Φ_s, β, B and η. The value of $(-r_0)$ in Table H.1 is calculated from the kinetic model developed in Chapter 4 (Table 4.7) for initial conditions.

The results below in Table H.1 are quite encouraging as the effectiveness factor is close to unity at the inlet conditions ($z = 0$ m) of the reactor, where the rate of the reaction is maximum. Down the reactor, the rate will be reduced drastically and the effectiveness factor will be improved accordingly. Moreover, the conditions selected for η in Table H.1 are for pure MCH under atmospheric pressure, lowest flowrate and highest wall temperature used in developing the rate model (Chapter 4) suggest maximum initial rates. Similar calculations for laboratory reactor at 9 bar under same conditions gives $\Phi_s = 0.60$ with effectiveness equal to 1.0.

Table H.1 Reaction conditions and results for the laboratory reactor

Reaction conditions	
$p = 1.013\,\text{bar}$	$d_p = 0.0568\,\text{cm}$ (Table 6.1)
$T_w = 380\,°\text{C}$	$\varepsilon_p = 0.70*$
$T_0 = 630\,\text{K}$	$\tau_m = 3.0$ (guessed [Satterfield, 1970])
	$S_g = 208\,\text{m}^2/\text{g}$ (Table 3.5)
$\dfrac{W}{F_{A0}} = 12.44\times10^{-4}\,\text{s·g-cat}^{-1}/\text{mol MCH}$	$\rho_p = 1.20\,\text{g/cm}^3$ (Table 6.1)
	$k_s = 0.16\,\text{W·m}^{-1}.\text{K}^{-1}$
$C_{A0} = 1.91\times10^{-5}\,\text{mol/cm}^3$ ($y_{A0} = 0.99$)	$(-r)_0 = 4.21\times10^{-5}\,\text{mol·g-cat}^{-1}·\text{K}^{-1}$
	$E = 54.55\,\text{kJ/mol}$ (Table 4.3)

Results
$D_{K,eff} = 0.00322\ \text{cm}^2/\text{s}$ (Eq. H.4)
$D_{AC} = 1.244\,\text{cm}^2/\text{s}$ (Eq. 6.29)
$D_{eff} = 0.00321\,\text{cm}^2/\text{s}$ (Eq. H.3)
$\Phi_s = 2.65$ (Eq. H.2)
$\beta = -0.012$ (Eq. H.5)
$B = 10.41$
From Fig. H.1
$\eta = 0.88$

$* \; \varepsilon_p = 1 - \dfrac{\rho_p}{\rho_s}$, see Table 6.1

H.1.4.1 Prototype reactor

Under essentially same conditions as depicted in Table H.1 for laboratory reactor but with catalyst particle diameter of 1.2 mm, the value of Φ_s is calculated as 13.20 and the effectiveness factor as 0.5. However, for the prototype operation at 9 bar, the modified Thiele modulus is calculated as $\Phi_s = 1.52$ and the corresponding effectiveness factor $\eta > 0.90$.

Appendix I
Regression Results for Group-5159

Table I.1 Results of regression for Group-5159 for the best model based on single-site LHHW

		Kinetic parameters with parameters statistics				
Parameter	Values	Units	t-values	95% confidence intervals		
				Lower	Upper	
$k_r \times 10^5$	2.436±0.12	mol·g-cat^{-1}·s^{-1}	20.20	2.186	2.686	
B	6.616±0.67	—	9.870	5.226	8.007	
(E)	(33.95)	(kJ·mol^{-1})	—	—	—	
K_A	29.41±14.0	—	2.088	0.201	58.62	
K_B	7.014±5.54	bar^{-1}	1.265	−4.484	18.51	
K_r'	14.32±5.63	bar^{-3}	2.544	2.647	25.99	
B'	−30.36±3.69	—	8.238	−38.01	−22.72	
$(\Delta h')$	(−155.82)	(kJ·mol^{-1})	—	—	—	
k_d	1.279±0.23	day^{-1}	5.456	0.793	1.765	
		Overall statistics				
N	m	Adj(R^2)	SSE	F		
29	7	0.992	0.00397	633.48		
Correlation matrix of parameters						

1						
−0.143	1					
−0.695	0.286	1				
−0.160	0.093	0.635	1			
0.618	0.599	−0.314	−0.055	1		
−0.448	0.527	0.913	0.622	−0.016	1	
-0.467	0.479	0.287	-0.493	−0.012	0.294	1

Table I.2 Results of regression for Group-5159 for the best model based on single-site LHHW with one less parameter

Kinetic parameters with parameters statistics					
Parameter	Values	Units	t-values	95% confidence intervals	
				Lower	Upper
$k_r \times 10^5$	2.513±0.14	mol·g-cat^{-1}·s^{-1}	18.00	2.224	2.801
B	5.608±0.58	—	9.694	4.411	6.804
(E)	(28.78)	(kJ·mol^{-1})	—	—	—
K_A	14.89±3.19	—	4.671	8.292	21.48
K_r'	10.55±2.95	bar^{-3}	3.574	4.443	16.66
B'	−32.57±3.45	—	9.450	−39.70	−25.44
$(\Delta h')$	(−167.13)	(kJ·mol^{-1})	—	—	—
k_d	1.201±0.26	day^{-1}	4.696	0.671	1.730

Overall statistics				
N	m	Adj(R^2)	SSE	F
29	6	0.990	0.00541	581.965

Correlation matrix of parameters

1					
−0.154	1				
−0.831	−0.248	1			
0.225	−0.394	0.094	1		
0.659	0.560	−0.717	−0.057	1	
−0.458	0.522	0.173	−0.905	−0.012	1

Table I.3 Results of regression for Group-5159 for the model based on empirical HP model

Kinetic parameters with parameters statistics					
Parameter	Values	Units	t-values	95% confidence intervals	
				Lower	Upper
$k_r \times 10^5$	4.634±0.57	mol·g-cat^{-1}·s^{-1}	8.109	3.514	5.754
B	9.917±0.91	—	10.90	8.134	11.70
(E)	(50.89)	(kJ·mol^{-1})	—	—	—
K'_B	1.016±0.17	bar^{-1}	5.957	0.682	1.350
K^*_{Cr}	0.008±0.002	—	4.533	0.005	0.011
k_d	1.274±0.19	day^{-1}	6.570	0.894	1.655
Overall statistics					
N	m	Adj(R^2)	SSE	F	
29	5	0.990	0.00569	721.435	

Correlation matrix
of parameters

1				
0.713	1			
0.911	0.533	1		
0.780	0.749	0.601	1	
0.721	0.319	0.559	0.377	1

Appendix J

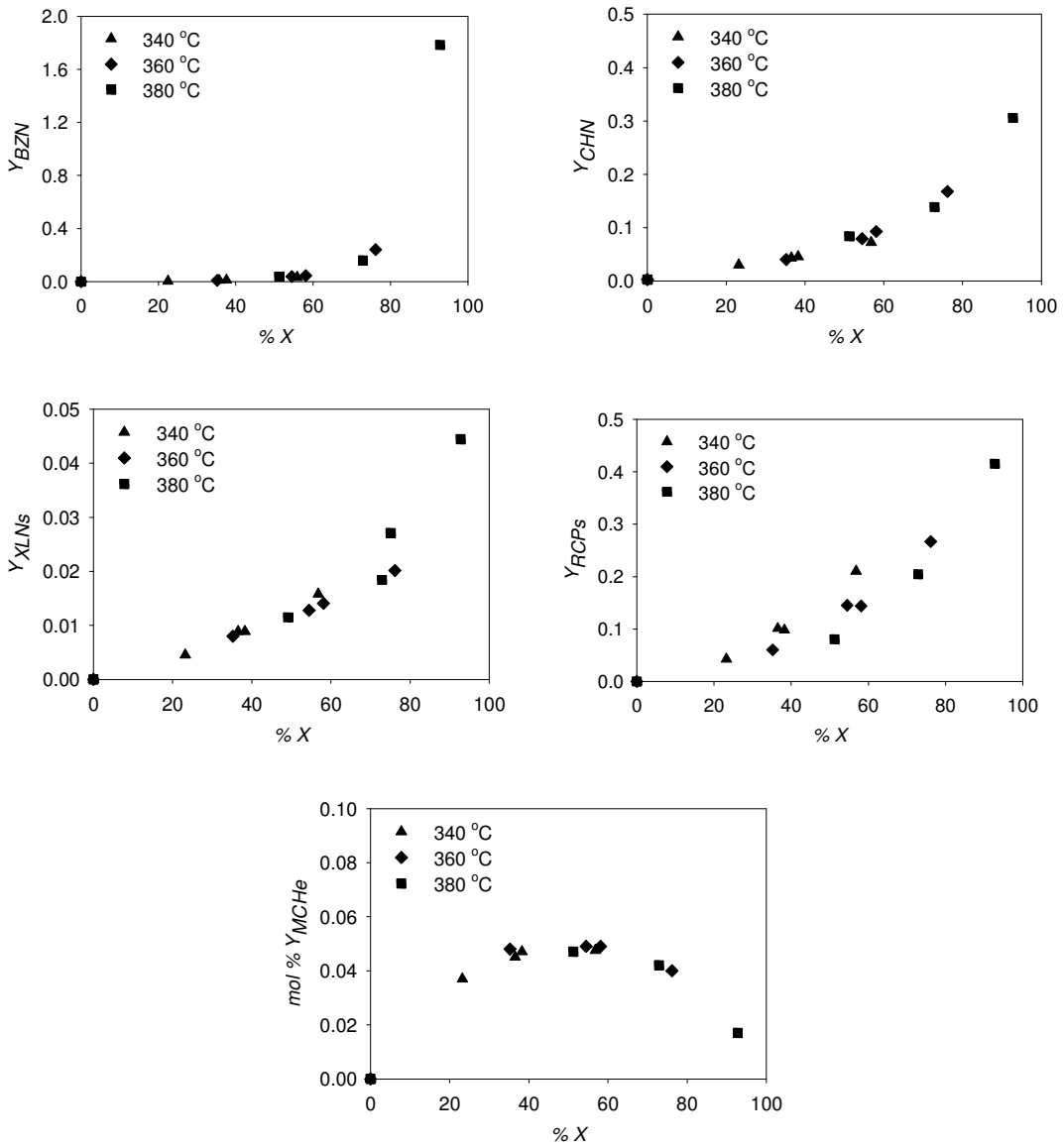# Yields of the By-products at Higher Pressures

Fig. J.1 Yields of the products obtained for Group-15. The temperatures shown are reactor wall temperatures.
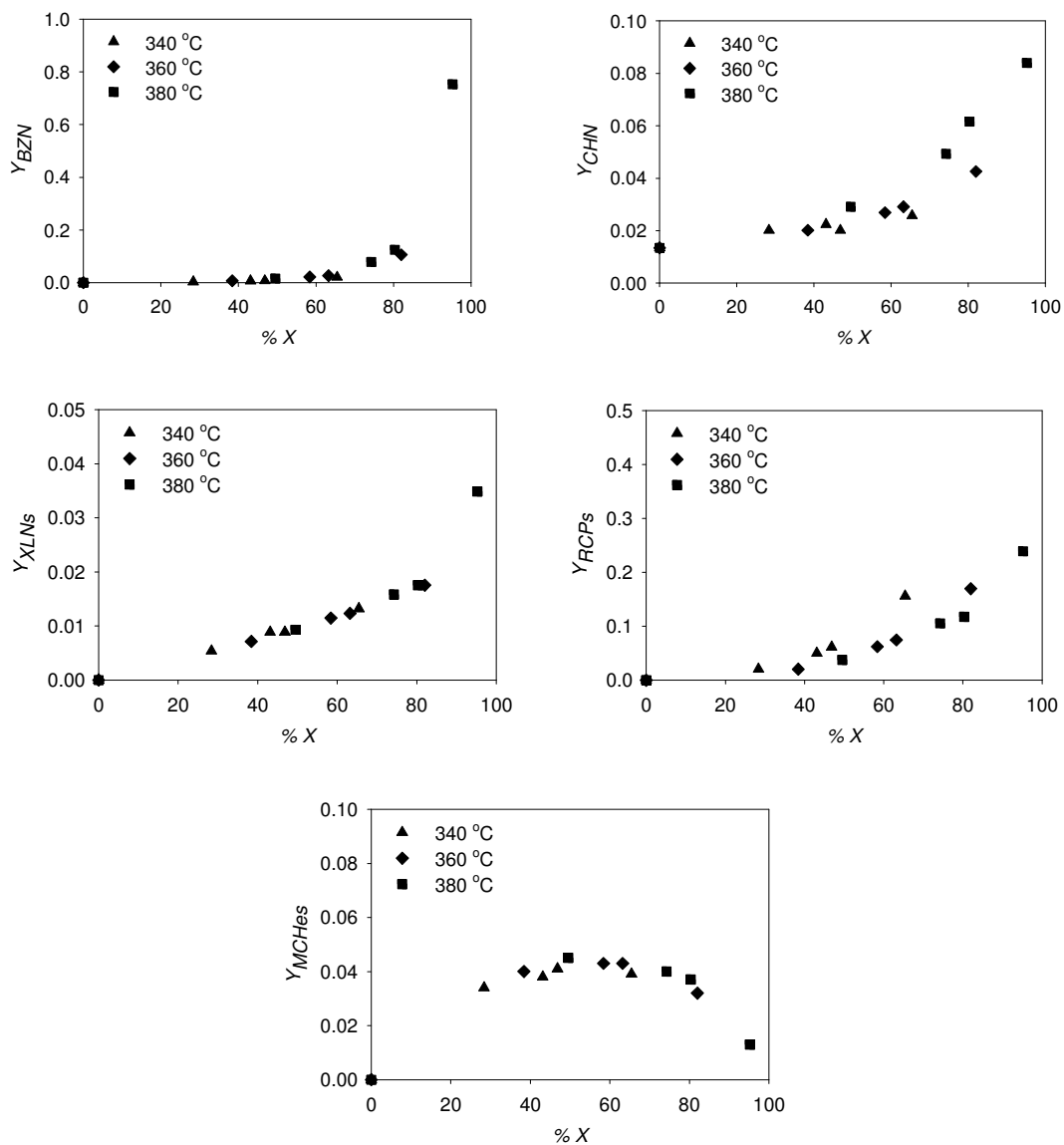
Fig. J.2 Yields of the products obtained for Group-25. The temperatures shown are reactor wall temperatures.

Fig. J.3 Yields of the products obtained for Group-45. The temperatures shown are
reactor wall temperatures.

Fig. J.4 Yields of the products obtained for Group-19. The temperatures shown are reactor wall temperatures.

Fig. J.5 Yields of the products obtained for Group-29. The temperatures shown are reactor wall temperatures.
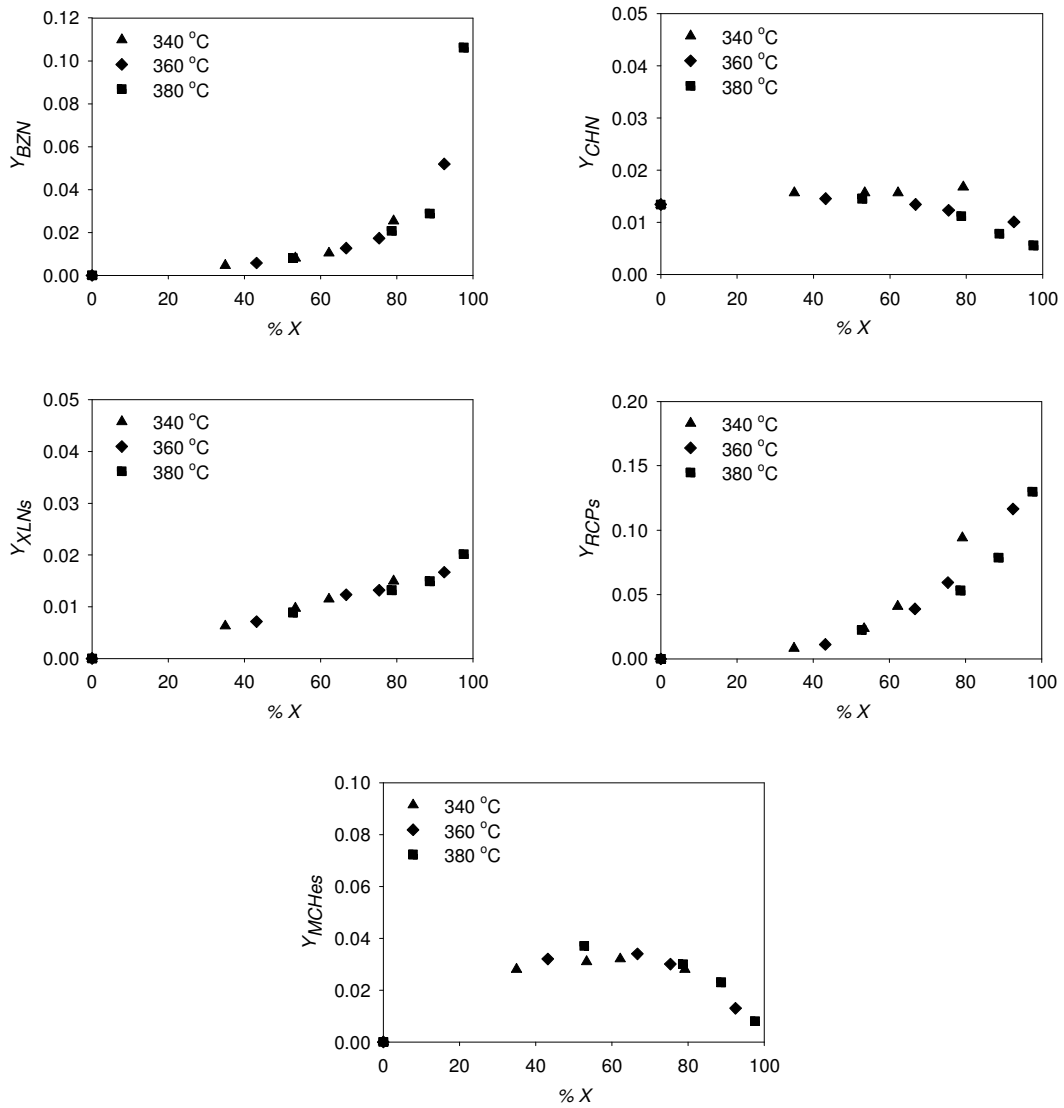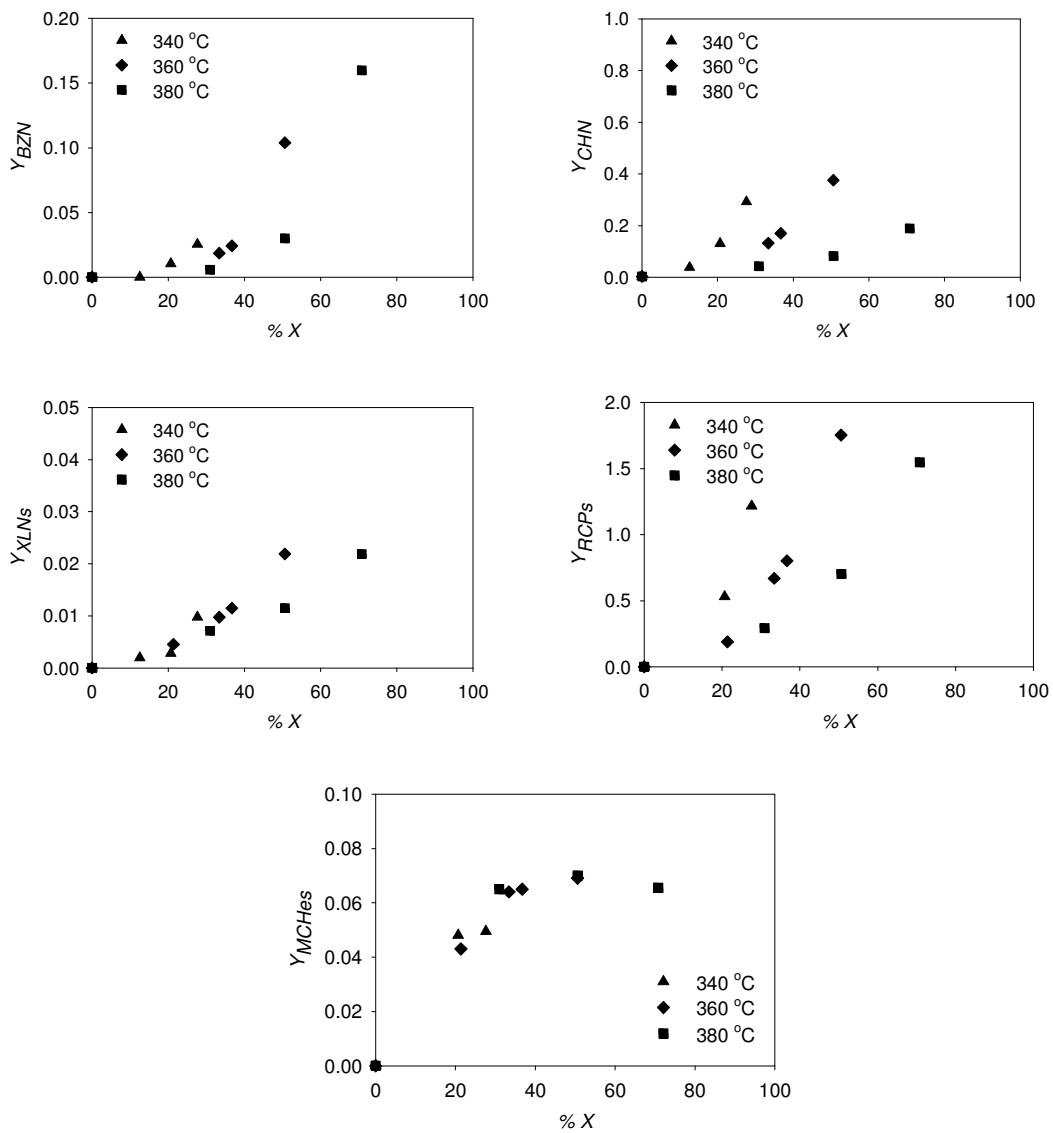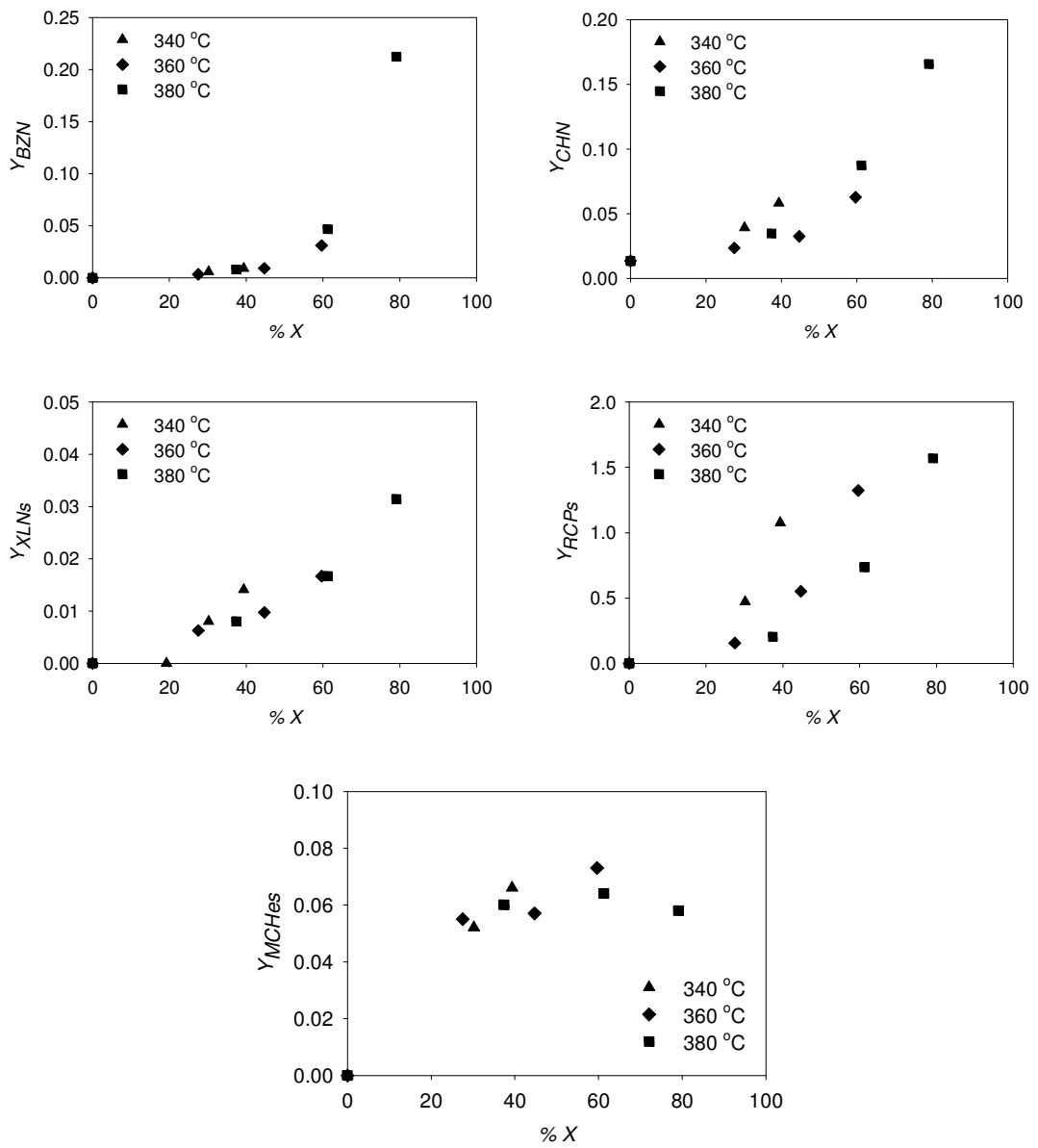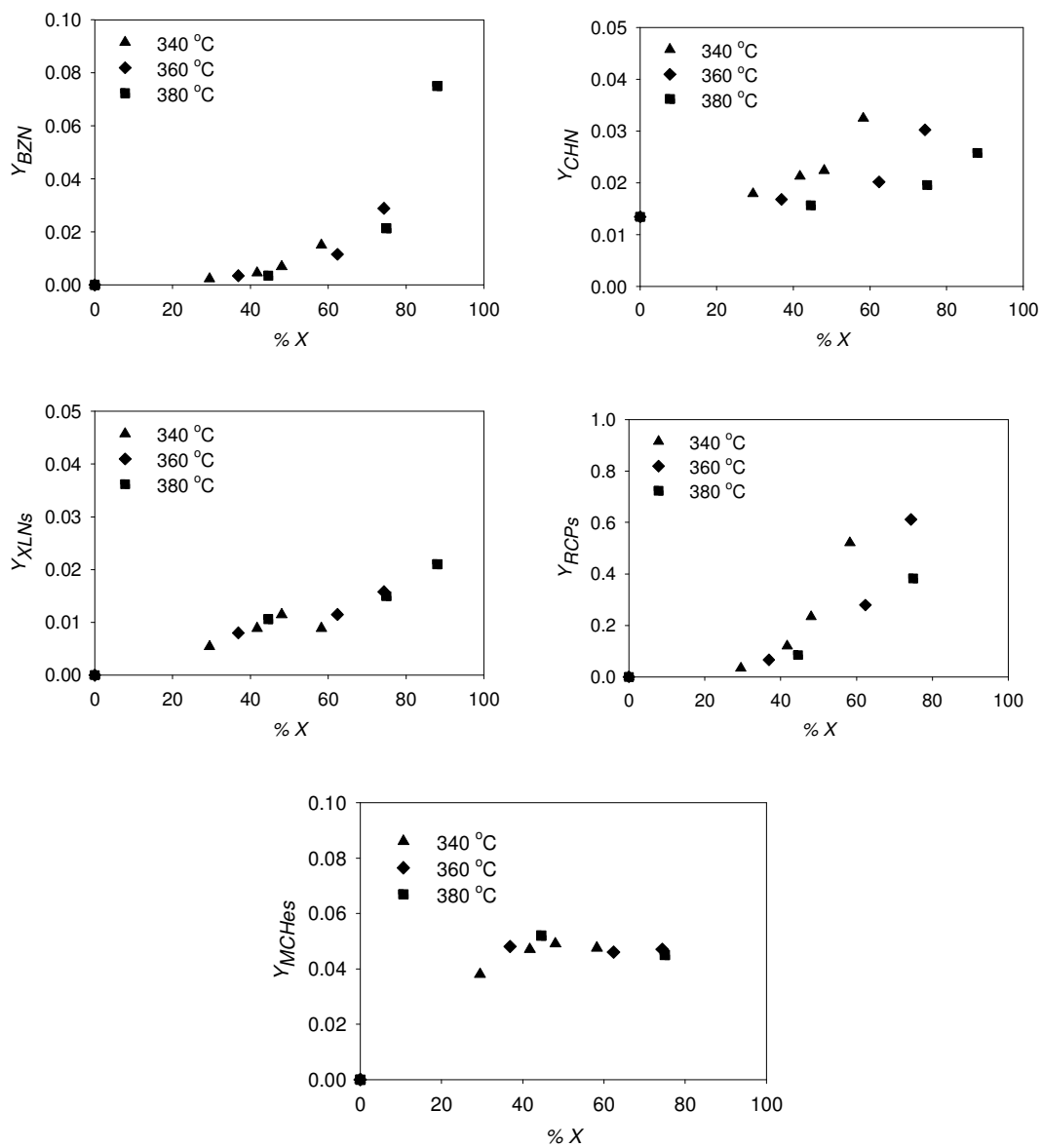
Fig. J.6 Yields of the products obtained for Group-49. The temperatures shown are reactor wall temperatures.

Appendix K
Mathematical Modelling Equations for the Laboratory Fixed Bed Reactor

K.1 Mathematical modelling of the laboratory fixed bed reactors

A two-dimensional pseudo-homogeneous model is used as a basis for mathematical modelling of the laboratory fixed bed reactor.

K.1.1 Control volume

A thin cylindrical shell of the catalyst as shown in Fig. K.1 is selected within the body of the packed bed reactor. This cylindrical shell of the catalyst acts as the control volume for applying mass and energy balances to develop the required model equations.
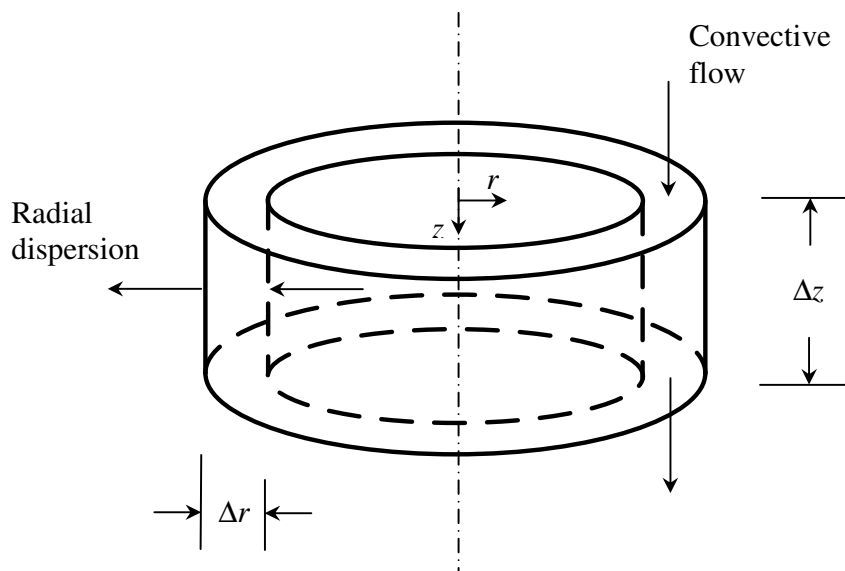

Fig. K.1 Control volume for mass and energy balances.

K.1.2 Mass balance equation

The general mass balance equation for steady-state operation may be written as

$$
\left(\begin{array}{c} \text{Rate of moles of} \\ \text{component ``}A\text{''} \\ \text{into the control} \\ \text{volume} \end{array}\right) - \left(\begin{array}{c} \text{Rate of moles of} \\ \text{component ``}A\text{''} \\ \text{out of the control} \\ \text{volume} \end{array}\right) + \left(\begin{array}{c} \text{Rate of generation} \\ \text{of component ``}A\text{''} \\ \text{within the control} \\ \text{volume} \end{array}\right) = 0
$$

(K.1)

Mass enters or leaves the shell by both convective and molecular (diffusive) flows, therefore

$$
\left((F_A \cdot 2\pi \cdot r \cdot \Delta r)\big|_z + \left(-D_r \cdot 2\pi \cdot r \cdot \Delta z \cdot \frac{\partial C_A}{\partial r}\bigg|_r \right) \right)
$$
$$
- \left((F_A \cdot 2\pi \cdot r \cdot \Delta r)\big|_{z+\Delta z} + \left(-D_r \cdot 2\pi \cdot r \cdot \Delta z \cdot \frac{\partial C_A}{\partial r}\bigg|_{r+\Delta r} \right) \right) - 2\pi \cdot r \cdot \Delta r \cdot \Delta z \cdot \rho_b \cdot (-r) = 0
$$

The negative sign with rate of generation term indicates rate of depletion of the reactant A.

Collecting terms, dividing throughout by $2\pi \cdot r \cdot \Delta r \cdot \Delta z$, taking limit when Δr and Δz tend to zero and introducing the definition of derivative, it may be written as

$$
-\frac{\partial F_A}{\partial z} + D_r \cdot \frac{\partial^2 C_A}{\partial r^2} + D_r \cdot \frac{1}{r} \cdot \frac{\partial C_A}{\partial r} - \rho_b \cdot (-r_A) = 0
$$

(K.2)

But,

$$F_A = F_{A0} \cdot (1 - X) \tag{K.3}$$

which is perfectly general. However, for a constant density system in the radial direction, the following relation is also true

$$C_A = C_{A0} \cdot (1 - X) \tag{K.4}$$

or

$$C_A = \frac{\rho \cdot y_{A0} \cdot (1 - X)}{M_F} \tag{K.5}$$

Defining the radial mass transfer Peclet no. as

$$Pe_{r,m} = \frac{G \cdot d_p}{\rho \cdot D_r} \tag{K.6}$$

and assuming "$\rho \cdot D_r$" to be constant, using Eqs. (K.3), (K.4) and (K.6) in Eq. (K.2), it may be shown that

$$\frac{\partial X_A}{\partial z} = \frac{d_p}{Pe_{r,m}} \left[\frac{\partial^2 X}{\partial r^2} + \frac{1}{r} \cdot \frac{\partial X}{\partial r} \right] + \frac{\rho_b \cdot (-r) \cdot M_F}{G \cdot y_{A0}} \tag{K.7}$$

K.1.3 Energy balance equation

The general energy balance equation for a steady-state operation may be written as:

$$
\begin{pmatrix} \text{Rate of energy} \\ \text{into the control} \\ \text{volume} \end{pmatrix} - \begin{pmatrix} \text{Rate of energy} \\ \text{out of the control} \\ \text{volume} \end{pmatrix} + \begin{pmatrix} \text{Rate of generation} \\ \text{of energy within} \\ \text{the control volume} \end{pmatrix} = 0
$$

$$(K.8)$$

Energy enters or leaves the shell by both convective and molecular (conductive) flows.

$$
\left(G \cdot 2\pi \cdot r \cdot \Delta r \cdot c_p \cdot (T - T_r)\big|_z + \left(-k_r \cdot 2\pi \cdot r \cdot \Delta z \cdot \frac{\partial T}{\partial r}\bigg|_r \right) \right)
$$

$$
- \left(G \cdot 2\pi \cdot r \cdot \Delta r \cdot c_p \cdot (T - T_r)\big|_{z+dz} + \left(-k_r \cdot 2\pi \cdot r \cdot \Delta z \cdot \frac{\partial T}{\partial r}\bigg|_{r+dr} \right) \right)
$$

$$
+ 2\pi \cdot r \cdot \Delta r \cdot \Delta z \cdot \rho_B \cdot (-r) \cdot (-\Delta h_{rxn}) = 0
$$

Following similar steps as above for the derivation of Eq. (K.7) and introducing the definition of the radial Peclet number for heat transfer, Eq. K.9, one may reach at the relation Eq. K10.

$$
Pe_{r,h} = \frac{G \cdot c_p \cdot d_p}{k_r} \tag{K.9}
$$

$$
\frac{\partial T}{\partial z} = \frac{d_p}{Pe_{r,h}} \left(\frac{\partial^2 T}{\partial r^2} + \frac{1}{r} \cdot \frac{\partial T}{\partial r} \right) + \frac{\rho_b \cdot (-r) \cdot (-\Delta h_{rxn})}{G \cdot c_p} \tag{K.10}
$$

K.2 Solution method for the parabolic partial differential equations

Eq. K.7 and K.10 together with the boundary conditions (Section 6.1.3) are numerically solved using the explicit finite-difference approach. First order forward-finite differences are used with the derivatives with respect to variable z (time like

variable) and the second order centred-differences are employed for the derivatives involving spatial gradients (with respect to variable r). A backward-difference approach is applied at the wall of the reactor [Walas, 1991]. Considering axial symmetry, five radial increments are chosen to develop the finite-difference grid as shown in Fig. K.2 and by applying the finite differences, the following difference equations are obtained [Walas, 1991].

K.2.1 Finite-differences for mass balance equation

K.2.1.1 Centre of the reactor

$$X_{0,n+1} = 4 \cdot M \cdot X_{1,n} + X_{0,n} \cdot (1 - 4 \cdot M) + P \cdot (-r)_{0,n} \cdot \Delta z \qquad \text{(K.11)}$$

where,

$$M = \frac{d_p \cdot \Delta z}{Pe_{r.m} \cdot (\Delta r)^2} \qquad \text{(K.12)}$$

$$P = \frac{\rho_b \cdot M_F}{G \cdot y_{A0}} \qquad \text{(K.13)}$$

K.2.1.2 Interior points of the reactor

$$X_{m,n+1} = M \cdot \left(1 + \frac{1}{2 \cdot m}\right) \cdot X_{m+1,n} + (1 - 2 \cdot M) \cdot X_{m,n}$$

$$+ M \cdot \left(1 - \frac{1}{2 \cdot m}\right) \cdot X_{m-1,n} + P \cdot (-r)_{0,n} \cdot \Delta z \qquad \text{(K.14)}$$

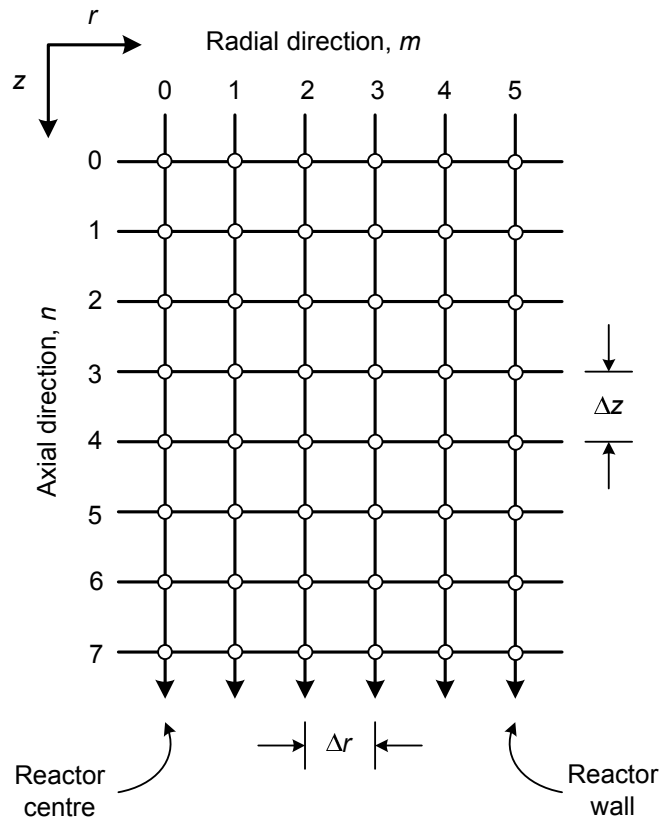Fig. K.2 Finite-difference grid for the laboratory
dehydrogenation reactor taking axial symmetry into
consideration.

K.2.1.3 Wall of the reactor

$$X_{5,n} = X_{4,n} \qquad\qquad (K.15)$$

K.2.2 Finite differences for energy balance equation

K.2.2.1 Centre of the reactor

$$T_{0,n+1} = 4 \cdot M' \cdot T_{1,n} + T_{0,n} \cdot (1 - 4 \cdot M') + Q \cdot (-r)_{0,n} \cdot \Delta z \qquad\qquad (K.16)$$

where,

$$M' = \frac{d_p \cdot \Delta z}{Pe_{r,h} \cdot (\Delta r)^2} \tag{K.17}$$

$$Q = \frac{\rho_b \cdot (\Delta h)_{rxn}}{G \cdot c_p} \tag{K.18}$$

K.2.2.2 Interior points of the reactor

$$T_{m,n+1} = M' \cdot \left(1 + \frac{1}{2 \cdot m}\right) \cdot T_{m+1,n} + (1 - 2 \cdot M') \cdot T_{m,n}$$

$$+ M' \cdot \left(1 - \frac{1}{2 \cdot m}\right) \cdot T_{m-1,n} + Q \cdot (-r)_{m,n} \cdot \Delta z \tag{K.19}$$

K.2.2.3 Wall of the reactor

$$T_{5,n} = \frac{T_{4,n} + (\Delta r \cdot h_w / k_r)}{1 + (\Delta r \cdot h_w / k_r)} \tag{K.20}$$

K.2.3 Validity of the numerical solution method

The analytical solution of Eq. K.10 without the reaction term is available in the literature in the form of Bessel functions of the first kind [Carslaw and Jaeger, 1959; Bejan, 1993]. Fig. K.3 shows a comparison between the analytical solution and the numerical solution obtained by the explicit finite difference method, as proposed above. A long rod of outside diameter of 0.05 m with initial temperature of 200 °C is subjected to a surrounding temperature of 380 °C. There is $< \pm 0.5$ % difference between the results of the two solution methods.
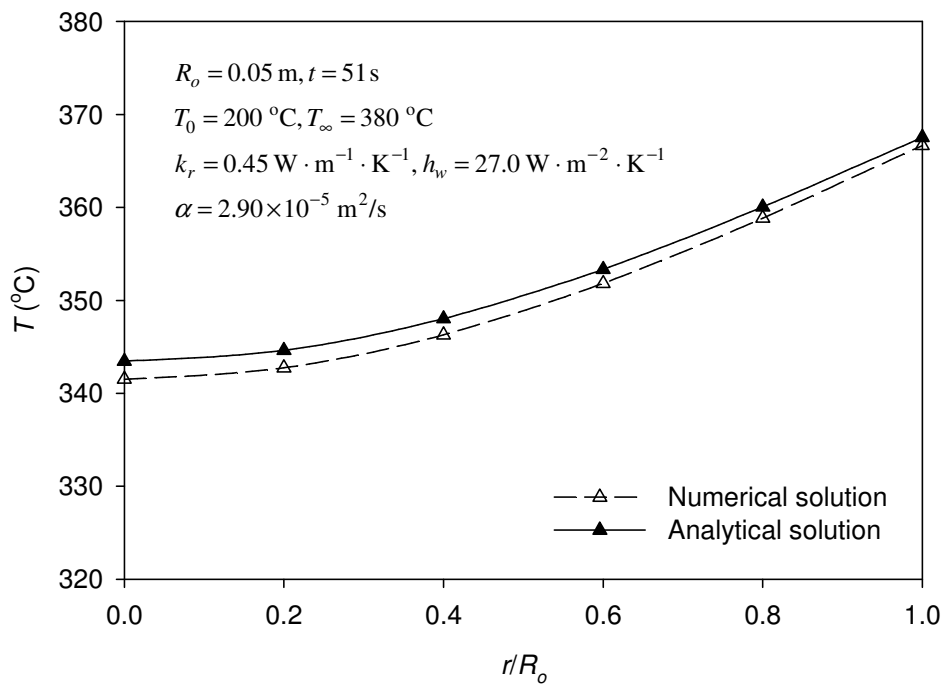
Fig. K.3 Comparison of analytical and numerical solutions.

Appendix L

Thermophysical Properties of the Reaction Mixture

L.1 Heat of the reaction

The standard heat of reaction is calculated from the standard heats of formation of MCH, toluene and hydrogen. Eq. L.1 is used to calculate the standard heat of reaction of MCH dehydrogenation. Table L.1 gives the standard heats of formation of the species involved in the principal reaction.

$$\text{MCH} \rightleftharpoons \text{Tol} + 3\text{H}_2 \tag{4.4}$$

$$\Delta h_{rxn}^o = (\Delta h_{f,B}^o + 3 \cdot \Delta h_{f,C}^o) - (\Delta h_{f,A}^o) \tag{L.1}$$

Table L.1 Standard heats of formation of reacting species [Poling et al., 2001]

Component	Representation	Standard heat of formation, $\Delta h_{f,i}^o$ (kJ/mol)
MCH	A	−154.70
Toluene	B	50.17
Hydrogen	C	0

The calculated value of the standard heat of reaction is −204.87 kJ/mol.

L.2 Specific heat capacity

The specific heat capacity of the gaseous mixture is given by Eq. L.2,

$$c_p = y_A \cdot c_{p,A}(T) + y_B \cdot c_{p,B}(T) + y_C \cdot c_{p,C}(T) + y_I \cdot c_{p,I}(T) \tag{L.2}$$

where, $c_{p,i}$ is the ideal gas specific heat capacity, J·mol^{-1}·K^{-1}.

Ideal gas specific heat capacities at constant pressure are taken as a function of temperature. Eq. L.3 is applied for the calculation of specific heats of the individual components. The coefficients used for the different components are listed in Table L.2.

$$\frac{c_{p,i}}{R \cdot M_i} = a_{0,i} + a_{1,i} \cdot T + a_{2,i} \cdot T^2 + a_{3,i} \cdot T^3 + a_{4,i} \cdot T^4 \quad \text{(L.3)}$$

Table L.2 Coefficients to be used with Eq. L.3 [Poling et al., 2001]

Components	M_i g/mol	Coefficients					
		a_0	$a_1 \times 10^3$	$a_2 \times 10^4$	$a_3 \times 10^7$	$a_4 \times 10^{11}$	Range (K)
MCH	98.19	3.148	18.4	1.36	−1.88	7.36	50−1000
Toluene	92.14	3.866	3.56	1.34	−1.87	7.69	50−1000
H_2	2.016	2.883	3.68	−0.0772	0.0692	−0.213	50−1000
N_2	28.01	3.539	−0.261	0.0007	0.0157	−0.099	50−1000
O_2	32.0	3.63	−1.79	0.0658	−0.0601	0.179	50−1000
CO_2	44.01	3.259	1.36	0.150	−0.237	1.06	50−1000
H_2O	18.02	4.395	−4.19	0.141	−0.156	0.632	50−1000

L.3 Average molecular weight

Similar to the heat capacity, the average molecular weight is given by

$$M_{ave} = y_A \cdot M_A + y_B \cdot M_B + y_C \cdot M_C + y_I \cdot M_I \quad \text{(L.4)}$$

The molecular weight of the impurity present in the feed MCH is assumed the same as the molecular weight of MCH.

L.4   Density of the gas mixture

The density of the gas mixture is calculated assuming that the gases obey ideal gas law under the conditions of experimentation. The ideal gas mass density is then calculated using the following formula

$$\rho = \frac{p \cdot M_{ave}}{R \cdot T} \tag{L.5}$$

L.5   Thermal conductivity of the gaseous mixture

Unlike the heat capacity and the average molecular weight, the thermal conductivity is not an additive property. The thermal conductivity of a mixture is therefore calculated using the empirical formula of Wilke [Bird et al., 2002]. The details of Wilke's formula are given in Section L.5.1 below. To take the thermal conductivity of a mixture as a function of temperature and composition and to use it with the parabolic partial differential equations, a correlation has to be developed for the thermal conductivity of the mixture as a function of temperature and fractional conversion.   The correlation developed is given by Eq. L.6 to Eq. L.8. Different parameters are required for different feed conditions and are provided in Table L.3.

$$k_g = a + \frac{b}{e^X} \tag{L.6}$$

where,

$$a = a_0 + a_1 \cdot T \text{, and} \tag{L.7}$$

$$b = b_0 + b_1 \cdot T \tag{L.8}$$

Table L.3 Coefficients to be used with Eq. L.7 and Eq. L.8

| Feed | | | a_0 | a_1 | b_0 | b_1 |
y_{A0}	y_{C0}	y_{I0}				
0.106	0.893	0.001	0.0349443	3.506×10^{-4}	−0.0162638	-2.254×10^{-5}
0.485	0.511	0.005	0.0142746	0.0003309	−0.0369602	0.0001376
0.990	0	0.010	0.0081138	3.358×10^{-4}	−0.0420007	-2.013×10^{-4}
0.485	0	0.515	0.0109531	0.0002745	−0.0325714	0.0001657

For the thermal conductivity and the viscosity of the individual components, the following equation is employed [DIPPR®, 2010]

$$k_{g,i} = \frac{A \times T^B}{1 + \dfrac{C}{T} + \dfrac{D}{T^2}}, \; \text{W·m}^{-1} \text{·K}^{-1} \tag{L.9}$$

The coefficients to be used with Eq. L.9 are provided in Table L.4.

Table L.4 Coefficients to be used with Eq. L.9 [DIPPR®, 2010]

| Components | Coefficients | | | | Temperature range (K) |
	$A \times 10^5$	B	C	D	
MCH	7.19	1.1274	667	0	374.08−1000
Toluene	2.392	1.2694	537	0	383.78−1000
Hydrogen	265.3	0.7452	12	0	22−1600
Nitrogen	33.143	0.7722	16.323	373.72	63.15−2000

For Wilke's formula to be applied to calculate the thermal conductivity of the gas mixture, the viscosity of the individual components is also required. The viscosity of the individual gases may be calculated by Eq. L.10

$$\mu_i = \frac{A \times T^B}{1 + \dfrac{C}{T} + \dfrac{D}{T^2}}, \; \text{Pa.s} \tag{L.10}$$

The coefficients to be used with Eq. L.10 are provided in Table L.5.

Table L.5 Coefficients to be used with Eq. L.10 [DIPPR®, 2010]

Components	Coefficients				Temperature range (K)
	$A\times10^7$	B	C	D	
MCH	6.5281	0.5294	310.59	0	146.58–1000
Toluene	8.7268	0.49397	323.79	0	178.18–1000
Hydrogen	1.797	0.685	−0.59	140	13.95–3000
Nitrogen	6.5592	0.6081	54.714	0	63.15–1970

L.5.1 Wilke's formula

Wilke's formula for calculating the thermal conductivity of a gas mixture is given by Eq. L.11 and Eq. L.12.

$$k_g = \sum_{i=1}^{i=N} \frac{y_i \cdot k_{g,i}}{\sum_{j=1}^{j=N} y_j \cdot \phi_{ij}} \tag{L.11}$$

where,

$$\phi_{ij} = \frac{1}{\sqrt{8}} \cdot \left(1 + \frac{M_i}{M_j}\right)^{-0.5} \cdot \left(1 + \left(\frac{\mu_i}{\mu_j}\right)^{0.5} \cdot \left(\frac{M_j}{M_i}\right)^{0.25}\right)^2 \tag{L.12}$$

An example problem using Wilke's formula to calculate the mixture viscosity is given in Chapter 1 of the book by Bird et al. [2002].

Appendix M
Equivalent Diameter and Effective External Heat Transfer Surface Calculations for the Outside Finned Surface

M.1 Equivalent diameter

For several pair of longitudinal fins, as shown in Fig. M.1, attached to the outside surface of a circular tube, the mean hydraulic diameter of the annular region can be defined by the following expression

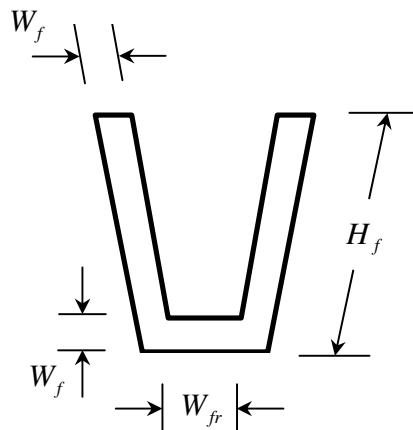$$D_e = \frac{4 \times free\ flow\ area}{wetted\ perimeter} \tag{M.1}$$

Fig. M.1 A single pair of longitudinal fins.

where,

Free flow area = (cross-sectional area of annulus) − (cross-sectional area of the fins including the area of the fin-roots projecting into the annulus)

$$= \frac{\pi \cdot (D_{is}^2 - D_o^2)}{4} - \left(N_f \cdot H_f \cdot W_f + \frac{N_f}{2} \cdot W_f \cdot W_{fr} \right) \tag{M.2}$$

Wetted perimeter = (*perimeter of the annulus*) + (*perimeter of the fins*) − (*perimeter of the fin base*)

$$= \pi (D_{is} + D_o) + N_f \cdot (2H_f) - N_f \cdot W_f \tag{M.3}$$

Substituting Eq. (M.2) and Eq. (M.3) in Eq. (M.1), it may be shown that

$$D_e = \frac{4 \times \left(\frac{\pi (D_{is}^2 - D_o^2)}{4} - \left(N_f \cdot H_f \cdot W_f + \frac{N_f}{2} \cdot W_f \cdot W_{fr} \right) \right)}{\pi (D_{is} + D_o) + N_f \cdot (2H_f) - N_f \cdot W_f}$$

or $\quad D_e = \dfrac{\pi \cdot (D_{is}^2 - D_o^2) - 4 \cdot N_f \cdot W_f \cdot \left(H_f + \dfrac{W_{fr}}{2} \right)}{\pi \cdot (D_{is} + D_o) + N_f \cdot (2H_f - W_f)}$ $\qquad$ (M.4)

Providing the flow is turbulent, the usual equations for friction factor and Nusselt No. derived for pipe flow may be used when the pipe diameter is replaced by D_e.

M.2   Total external heat transfer surface area

The total external heat transfer surface area is equal to the sum of the surface area provided by the fins and the tube surface between the fins. The tips of the fins may be excluded as heat transfer from the tips is negligible.

$$A_T = A_f + A_b \tag{M.5}$$

$$A_T = 2 \cdot N_f \cdot L_f \cdot H_f \tag{M.6}$$

$$A_b = \pi \cdot D_o \cdot L_f - N_f \cdot (L_f \cdot W_f)$$

$$A_b = L_f (\pi \cdot D_o - N_f \cdot W_f) \tag{M.7}$$

M.2.1 Total effective external heat transfer area

Due to a temperature gradient across the fin from the base to the tip, it is necessary to solve the heat conduction equation for this longitudinal heat transfer. The physical situation is depicted in Fig. M.2.
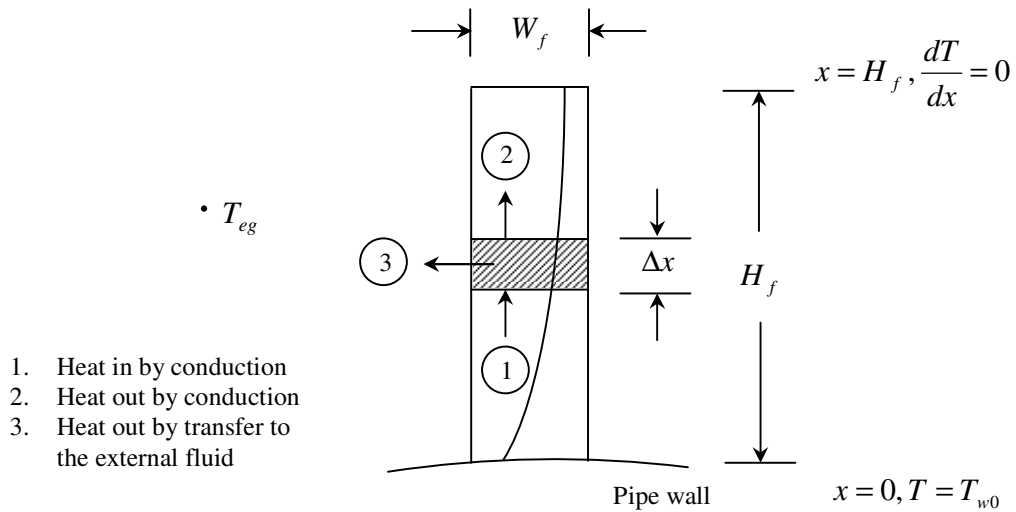

Fig. M.2 Rectangular cooling fin with thickness, $W_f \ll H_f$.

Consider a differential element of height Δx in the body of the fin. A heat balance across the differential element leads to the following thermal conduction equation

$$k_f \cdot \left(\frac{d^2 T}{dx^2} \right) = 2 \cdot \left(\frac{h_o}{W_f} (T - T_{eg}) \right) \tag{M.8}$$

Eq. M.8 is subject to the boundary condition

296

$$T = T_{w0} \qquad \text{at } x = 0 \tag{M.9}$$

where, T_{w0} is the temperature of the outside surface of the reactor tube. If the heat loss from the tip of the fin is neglected, then

$$\frac{dT}{dx} = 0 \qquad \text{at } x = H_f \tag{M.10}$$

Upon integrating Eq. M.8 using boundary conditions in Eq. M.9 and Eq. M.10 and re-arranging gives

$$\frac{T_{eg} - T(x)}{T_{eg} - T_{w0}} = \frac{\cosh\left(M \cdot \left(1 - \frac{x}{H_f}\right)\right)}{\cosh(M)} \tag{M.11}$$

where, M is a dimensionless quantity and is defined by the following expression

$$M = H_f \cdot \sqrt{\frac{2 \cdot h_o}{k_f \cdot W_f}} \tag{M.12}$$

The total rate of heat transfer from fluid to the fin per unit length is given by

$$Q = 2 \cdot h_o \cdot \int_{x=0}^{x=H_f} \left(T_{eg} - T(x)\right) \cdot dx \tag{M.13}$$

From Eq. M.11 and Eq. M.13, it may shown that

$$Q = k_f \cdot \frac{W_f}{H_f} \cdot M \cdot \tanh(M) \cdot (T_{eg} - T_{w0}) \tag{M.14}$$

If the whole surface of the fin were at the base temperature, T_{w0}, the maximum rate of heat transfer would be simply

$$Q_{max} = 2 \cdot H_f \cdot h_o \cdot (T_{eg} - T_{w0}) \qquad \text{(M.15)}$$

It follows from Eq. M.14 and Eq. M.15 that the fin efficiency, defined as the actual rate of heat transfer to the fin divided by the maximum rate of heat transfer, is given by

$$\eta_f = \frac{Q}{Q_{max}} = \frac{\tanh(M)}{M} \qquad \text{(M.16)}$$

The fin efficiency, η_f, approaches unity as M approaches zero. This would be most easily approached by maximising the thermal conductivity of the fin. Copper, rather than stainless steel, would be the preferred material of choice in this regard.

The total effective external heat transfer area, A_e, is less than the total external area, A_T, by virtue of a fin efficiency $\eta_f < 1$. Thus,

$$A_e = \eta_f \cdot A_f + A_b \qquad \text{(M.17)}$$

For a finned tube, an overall heat transfer coefficient, U_i, based on the temperature driving force $T_{eg} - T_{r=Ri}$ and the inside tube wall area per unit length, $2 \cdot \pi \cdot R_i$, may be defined by

$$T_{eg} - T_{r=Ri} = \frac{Q_T}{2 \cdot \pi \cdot R_i \cdot U_i}$$

$$T_{eg} - T_{r=Ri} = \cfrac{Q_T}{2 \cdot \pi \cdot R_i \cdot h_i + \cfrac{\ln(R_o / R_i)}{2 \cdot \pi \cdot k_w} + \cfrac{1}{h_o \cdot (A_b + \eta_f \cdot A_f) / L_f}}$$

$$(\text{M.18})$$

Multiplying both sides of Eq. M.18 by $\dfrac{2 \cdot \pi \cdot R_i}{Q_T}$, it follows that

$$\frac{1}{U_i} = \frac{1}{h_i} + \frac{1}{k_w} \cdot R_i \cdot \ln\left(\frac{R_o}{R_i}\right) + \frac{1}{h_o} \cdot \frac{R_i}{R_o} \cdot \cfrac{1}{\left(1 - \cfrac{N_f \cdot W_f}{2 \cdot \pi \cdot R_o} + \cfrac{N_f \cdot H_f \cdot \eta_f}{\pi \cdot R_o}\right)}$$

$$(\text{M.19})$$

For an un-finned tube, Eq. M.19 reduces to the more familiar form

$$\frac{1}{U_i} = \frac{1}{h_i} + \frac{1}{k_w} \cdot R_i \cdot \ln\left(\frac{R_o}{R_i}\right) + \frac{1}{h_o} \cdot \frac{R_i}{R_o} \qquad\qquad (\text{M.20})$$